

**NASA CONTRACTOR
REPORT**



N73-18022
NASA CR-2167

NASA CR-2167

CASE
COPY
FILE

**FLIGHT TEST MEASUREMENTS AND
ANALYSIS OF SONIC BOOM PHENOMENA
NEAR THE SHOCK WAVE EXTREMITY**

by George T. Haglund and Edward J. Kane

Prepared by

THE BOEING COMPANY

Seattle, Wash. 98124

for Langley Research Center

NATIONAL AERONAUTICS AND SPACE ADMINISTRATION • WASHINGTON, D. C. • FEBRUARY 1973

1. Report No. NASA CR-2167		2. Government Accession No.		3. Recipient's Catalog No.	
4. Title and Subtitle FLIGHT TEST MEASUREMENTS AND ANALYSIS OF SONIC BOOM PHENOMENA NEAR THE SHOCK WAVE EXTREMITY				5. Report Date February 1973	
				6. Performing Organization Code	
7. Author(s) George T. Haglund and Edward J. Kane				8. Performing Organization Report No. D6-40758	
9. Performing Organization Name and Address The Boeing Company Commercial Airplane Group P. O. Box 3707 Seattle, Washington 98124				10. Work Unit No.	
				11. Contract or Grant No. NAS1-10992	
12. Sponsoring Agency Name and Address National Aeronautics and Space Administration Washington, D.C. 20546				13. Type of Report and Period Covered Final Report June 1971 - September 1972	
				14. Sponsoring Agency Code	
15. Supplementary Notes					
16. Abstract The sonic boom flight test program conducted at Jackass Flats, Nevada, during the summer and fall of 1970 consisted of 121 sonic-boom-generating flights over the 457m (1500 ft) instrumented BREN tower. This test program was designed to provide information on several aspects of sonic boom, including caustics produced by longitudinal accelerations, caustics produced by steady flight near the threshold Mach number, sonic boom characteristics near lateral cutoff, and the vertical extent of shock waves attached to near-sonic ($M < 1.0$) airplanes. The measured test data, except for the near-sonic flight data, were analyzed in detail to determine sonic boom characteristics for these flight conditions and to determine the accuracy and the range of validity of linear sonic boom theory. The caustic phenomena observed during the threshold Mach number flights and during the transonic acceleration flights are documented and analyzed in detail. The theory of geometric acoustics is shown to be capable of predicting shock wave-ground intersections, and current methods for calculating sonic boom pressure signatures away from caustics are shown to be reasonably accurate.					
17. Key Words (Suggested by Author(s)) Airplane, caustic, cutoff, flight test, focus, meteorology, noise, pressure, sonic boom, supersonic, transonic				18. Distribution Statement	
19. Security Classif. (of this report) Unclassified		20. Security Classif. (of this page) Unclassified		21. No. of Pages 177	22. Price* \$3.00

CONTENTS

	Page
SUMMARY	1
INTRODUCTION	3
SYMBOLS	7
GENERAL TEST DESCRIPTION	11
THEORETICAL SONIC BOOM CALCULATION INPUTS	13
Flight Conditions	13
Meteorological Conditions	14
Airplane F-Function Data	16
DATA ANALYSIS METHODS	17
Acoustic Propagation Speed	17
Shock Propagation Speed	18
Shock Wave Profiles	18
Ground Reflection Coefficient	19
ANALYSIS OF THE THRESHOLD MACH NUMBER FLIGHT TEST DATA	20
Introduction	20
Shock wave cutoff at low supersonic speeds	20
Threshold Mach number	21
Variability of threshold Mach number	22
Previous flight tests	24
Effect of Terrain Slope	24
Summary of Flight Conditions	25
Mach Number Greater Than Threshold Value	25
Comparison of theory with observation	29
Shock wave profiles and pressure signatures	33
Mach Number Near Threshold Value	34
Precursors	34
Shock wave profiles and pressure signatures	34
Overpressure variation near caustics	36

CONTENTS—Continued

	Page
Mach Number Less Than Threshold Value	37
Ground Reflection Coefficient	40
Analysis of Pressure Signatures	41
Summary of Threshold Mach Number Data	41
ANALYSIS OF LONGITUDINAL ACCELERATION FLIGHT TEST DATA	43
Introduction	43
Caustic-Ground Intersection—Theory and Experiment	44
Comparison of Observed and Theoretical Boom Arrival Times	48
Measurements Uptrack from Caustic-Ground Intersection	49
Measurements Near Caustic-Ground Intersection	49
Measurements Downtrack from Caustic-Ground Intersection	51
Overpressure Variation Near Caustics—Theory and Experiment	52
Ray-Tube Area Limit Near Caustics—Linear Theory	54
Discussion of Observed Phenomena Near Caustics	54
Summary of Longitudinal Acceleration Data	55
ANALYSIS OF LATERAL CUTOFF FLIGHT TEST DATA	57
Introduction	57
Lateral Cutoff Location—Theory and Experiment	59
Ground Reflection Coefficient	62
Overpressure Variation	62
Observed Pressure Signatures and Shock Wave Profiles	64
Measurements before lateral cutoff	65
Measurements near lateral cutoff	65
Measurements past lateral cutoff	66
Summary of Lateral Cutoff Data	66
CONCLUSIONS	68
APPENDIX A—EFFECT OF HUMIDITY ON SHOCK PROPAGATION SPEED	71
APPENDIX B—AIRPLANE F-FUNCTION DATA	77

CONTENTS—Concluded

	Page
APPENDIX C—THEORETICAL RELATIONSHIPS NEAR CUTOFF DURING THRESHOLD MACH NUMBER FLIGHT	81
Threshold Mach Number	81
Theoretical Relationships Near Cutoff During Threshold Mach Number Flight	82
APPENDIX D—THEORETICAL SAFE ALTITUDE FOR SONIC BOOM CUTOFF	84
REFERENCES	85

**FLIGHT TEST MEASUREMENTS AND ANALYSIS OF
SONIC BOOM PHENOMENA NEAR THE SHOCK WAVE EXTREMITY**

George T. Haglund and Edward J. Kane

The Boeing Company

SUMMARY

The sonic boom flight test program conducted at Jackass Flats, Nevada, during the summer and fall of 1970 consisted of 121 sonic-boom-generating flights over the 466 m (1529-ft) BREN tower. This test program was designed to provide information on several aspects of sonic boom, including caustics produced by steady flight near the threshold Mach number, caustics produced by longitudinal accelerations, sonic boom characteristics near lateral cutoff, and the vertical extent of shock waves attached to near-sonic ($M < 1.0$) airplanes. The measured test data (except for the near-sonic flight data) were analyzed in detail to determine sonic boom characteristics for these flight conditions and to determine the accuracy and the range of validity of linear sonic boom theory.

The observations near caustics are of particular value since no methods are currently available for predicting realistic pressure signatures at caustics because of the nonlinear effects that predominate there. Overpressure increases measured at caustics produced during threshold Mach number flight, compared to the overpressure produced during steady, level flight at about Mach 1.2, were relatively low, ranging from about 1.0 to 1.8, except in one case where it appeared that small-scale atmospheric turbulence produced "spikes" on a caustic signature. Caustics were also produced by small inadvertent changes in the airplane speed during several of the "steady," level threshold Mach number flights. These caustics were slightly stronger, with a maximum amplification factor of about 3. Measured overpressures at caustics produced by airplane accelerations beginning from Mach 0.95 ranged from 2 to 5 times those which would be observed during steady, level flight at about Mach 1.2. Pressure signatures were also observed near lateral cutoff which resembled those measured at caustics. These disturbances were of very low intensity, however, less than one-half the intensity beneath the flight path. The caustic phenomena are analyzed and documented in detail. The distinguishing features of pressure signatures near caustics are the "U" shape of the signature, about a 40% longer duration than normal, and the sharp peaks at the bow and tail shocks.

Comparison of theoretical calculations with the observed data showed good agreement in all cases where it was possible to make such calculations. Shock wave intensities, shock wave inclination angles, and sonic boom arrival times were calculated and compared with the observations. The accuracy of the theoretical calculations was limited by the accuracy of the input airplane flight track and meteorological data, particularly for the low supersonic flights where the shock wave travels long distances almost parallel to the ground. Inaccuracies in the upper level wind conditions are also considered to be an important source of error. Caustic locations during transonic acceleration and lateral cutoff locations can be predicted to within ± 1.0 km (3300 ft). Shock wave intensities agree reasonably well, as do signature shapes when the effects of small-scale turbulence are neglected in the observed data. Shock wave arrival times can be predicted to within ± 1.0 sec. Thus, the comparison of theory and experiment has tended to verify the theory and has also indicated its range of validity. The linear theory is invalid within about 100-200 m (330-660 ft) vertically above caustics and where the shock wave is within a few degrees of the cutoff condition.

Analysis of the rumble data produced during flight near the threshold Mach number showed that "low rumbles" occurred when the airplane ground speed was at least 6 m/sec (19.7 ft/sec) lower than the maximum shock propagation speed. This, roughly, is the "safety factor" (or reduction in allowable airplane ground speed to avoid objectionable noise at the ground) that would be required for these flight and meteorological conditions. Comparison of a theoretical "safe altitude" for sonic boom cutoff with the observed data was good considering the assumptions made in deriving it.

INTRODUCTION

During the summer and fall of 1970 a series of sonic boom flight tests were conducted by the NASA at Jackass Flats, Nevada. During this flight test program, 121 sonic-boom-generating flights were made. These flights were designed to provide information on several aspects of sonic boom, including caustics produced by steady flight near the threshold Mach number, caustics produced by longitudinal accelerations, sonic boom characteristics near lateral cutoff, and the vertical extent of shock waves attached to near-sonic ($M < 1.0$) airplanes. By use of the 466 m (1529-ft) BREN tower, sonic boom signature measurements as a function of altitude were obtained for the first time. The primary goal of this test series was to obtain definitive data on caustics produced by accelerations and by atmospheric refraction (threshold Mach number and lateral cutoff). The analysis of these sonic boom data is the subject of this report. The test results and caustic phenomena are presented and described, and wherever possible comparisons are made with the linear sonic boom theory.

The test arrangements for the threshold Mach number flights, the longitudinal accelerations, and the lateral cutoff flights are summarized in table 1 and schematically illustrated in figure 1. The desirability of using a tower to observe the sonic boom pressure field in the vertical plane is illustrated in figure 1, particularly for shock waves near cutoff. For a shock wave angle of incidence of 0.087 rad (5°), a ground array about 5.15 km (3.2 st mi) long would be required to obtain the same data sample as that measured on the 466 m (1529 -ft) BREN tower; at 0.035 rad (2°), a linear array of 13.85 km (8.6 st mi) is required. In addition, the use of a tower gives a much better chance of observing the very localized caustic phenomena. The success of these tests in observing caustics can largely be attributed to the use of the BREN tower.

During the last two decades a large amount of work has been devoted to the development of theoretical methods for predicting sonic boom characteristics. Fundamental contributions were made by Friedrichs, Hayes, Landau, and Whitham (refs. 1 to 6). The current state of the art in sonic boom prediction is represented by the comprehensive analysis and computer program assembled by Hayes, Haefeli, and Kulsrud (ref. 7). Although the basic theory is linear in nature (except for the calculation of pressure signature "aging" and shock locations), a wide range of effects can be accounted for, such as the effects of airplane configuration and lift, nonstandard meteorological conditions, and airplane maneuvers. This basic theory has been verified by wind tunnel tests and flight test data (ref. 8).

During the last few years research efforts have been directed toward extending the basic theory to predict pressure levels in the vicinity of caustics, which can be produced by airplane maneuvers and/or by atmospheric refraction. A caustic is a point in space where ray focusing occurs and the

TABLE 1.—SUMMARY OF 1970 BREN TOWER TESTS

Type of flight	Approximate altitude above ground, km (ft)	Approximate Mach number	Number of flights
Steady, level flight near the threshold Mach number	9.14 (30 000)	1.07 to 1.20	79
Longitudinal acceleration (at constant altitude)	9.14 (30 000)	0.95 to 1.3	19
Lateral cut-off (steady, level flight)	8.84 (29 000)	1.3	9
Near-sonic (steady, level flight)	0.91 (3 000)	0.95 to 1.00	14
			121

ray-tube area of linear sonic boom theory is zero. Linear theory predicts infinite sonic boom intensity at this point. The concept of a ray-tube area, however, is linear and does not account for the nonlinear effects that predominate close to caustics.

The mathematical formulation of the pressure signature behavior near a caustic has been outlined by Guiraud (ref. 9) and Hayes (ref. 10). Théry (ref. 11) has attempted to carry the mathematics to completion, but his results must be viewed as giving only a qualitative indication of the pressure amplification. Seebass (ref. 12) also attempted a mathematical solution for an acoustic disturbance (no shocks) entering a caustic region, while Coakley (ref. 13) has attempted a numerical solution. The calculation of sonic boom pressure signatures and shock intensities in a caustic region has not been accomplished at this time. However, flight test measurements have been most valuable in identifying the phenomena and will, in the future, serve to confirm theories that may be advanced.

During the last decade there have been a number of flight test programs that have contributed substantially to the current understanding of sonic boom phenomena near caustics. One of the earliest was conducted at NASA, Wallops Station, where seven threshold Mach number flights were flown (ref. 14). The tests at Edwards AFB in 1961 consisted of several different airplane maneuvers, including four longitudinal accelerations (refs. 15-17). Another series at Edwards AFB in 1964 included five threshold Mach number flights and five longitudinal accelerations (ref. 18). Other programs have provided information on the variability of sonic boom due to atmospheric effects as a function of lateral displacement from the flight track (refs. 19-23). Reference 24 contains a

general discussion of the variability of sonic boom and some preliminary analysis of the Jackass Flats lateral cutoff data, and reference 25 contains a preliminary analysis of the Jackass Flats threshold Mach number flights.

The French flight tests (ref. 26) demonstrated that the method of linear geometric acoustics is satisfactory for predicting caustic locations. These test results also demonstrated that a dense array of microphones was necessary for observing the caustic phenomena, since they occur over small ground areas.

These early test series, while of excellent quality, did not give definitive measurements on certain aspects of sonic boom phenomena because of the lack of systematic measurements and the lack of the required density of microphones. One aspect that needed further investigation was the sonic boom characteristics near lateral cutoff, since several investigators have postulated large pressure magnifications at lateral cutoff (refs. 27-29). Another was the caustic and acoustic disturbances associated with threshold Mach number flight where a caustic (and cutoff) is produced at some distance above the ground. Finally, the caustic produced by the transonic acceleration of supersonic airplanes is of particular interest since it will be produced by SSTs. These considerations prompted the 1970 test program at the BREN tower.

The data measured by the NASA at the BREN tower represent a unique and valuable set of information on the some of the least well understood aspects of sonic boom propagation. Vertical measurements through the shock waves were made for the first time in any flight test program, and these resulted in the most definitive information available on the formation and nature of caustics. The data acquired during the test program are also valuable because they have application to several future airplane concepts and operations. Among them are:

- Commercial transport operation near the threshold Mach number ($M > 1.0$) to avoid sonic boom noise on the ground
- Commercial transport operation at near-sonic ($M < 1.0$) speeds
- SST operation during the transonic acceleration phase of flight
- Pressure signature characteristics at the outer edge of the sonic boom carpet during normal SST operations

In general, the objectives of the detailed analysis of these test data were: (1) to compare sonic boom theory with observations, and (2) on the basis of these comparisons, to interpret the measurements for each flight condition. The presentation of the test results and analysis in this

report begins with the threshold Mach number data, followed by the longitudinal acceleration and the lateral cutoff data. (The transonic data obtained by flights at 900 m (3000 ft) altitude and Mach numbers less than 1.0 were not analyzed in this study.) A brief discussion of the measurement procedure and the method used to calculate theoretical pressure signatures is given. The appendixes contain an evaluation of the effect of water vapor on shock propagation speed, tabulated airplane F-function data, a discussion of theoretical relationships near cutoff during threshold Mach number flight, and the derivation of a theoretical safe cutoff altitude during threshold Mach number flight.

SYMBOLS

This section defines symbols used in the analysis.

Symbol

A	airplane acceleration
A_h	ray-tube area projection onto horizontal plane
$A(S)$	ray-tube area normal to rays
a	sound speed
a^*	sound speed using virtual temperature, T_v
C_L	lift coefficient
c_o	Snell's law invariant
D	virtual temperature increment, $(T_v - T)$; airplane lateral displacement from tower
F	airplane F-function for pressure signature calculations
F_A	geometry contribution to F-function
F_{A1}	nondimensionalized geometry contribution
F_B	lift contribution to F-function
F_{B1}	nondimensionalized lift contribution
F_i	input F-function, sum of lift and geometry contributions
F_f	F-function conversion factor
g	acceleration of gravity

h	airplane altitude above mean sea level
K_R	ground reflection coefficient
L	distance from airplane nose
L_F	reference F-function length used for nondimensionalizing L
M	airplane Mach number = V/a
M_T	threshold Mach number
\vec{n}	unit vector normal to wave front
n_L	lift (normal) load factor
n_T	thrust (axial) load factor
P	pressure
q	dynamic pressure
r	water vapor mixing ratio
S	separation distance between leading and trailing shocks produced by acceleration
S_{REF}	airplane reference wing area
T	air temperature
t_{REF}	reference time used for shock wave profile calculations
T_v	virtual air temperature
t_o	shock wave arrival time
u	horizontal wind speed
u_n	component of horizontal wind in plane of the normal to the shock wave

- u_t component of horizontal wind in plane tangent to the shock wave
- V airplane velocity relative to atmosphere, Ma_0
- V_G airplane ground speed, $(Ma_0 - u_{n_0})$
- V_p shock propagation velocity, $(a - u_n)$
- $V_{p_{mic}}$ shock propagation speed determined from shock wave arrival times over ground microphone array
- V_{ps} shock propagation speed normal to the shock wave surface
- V_p^* shock propagation velocity with increase because of water vapor, $(a^* - u_n)$
- W airplane weight
- (X,Y,Z) reference coordinate system: east, north, and above ground, respectively
- X_c distance downtrack of acceleration caustic-ground intersection
- Z_c sonic boom cutoff altitude during threshold Mach number flight
- Z_s Theoretical minimum altitude above the ground for which cutoff can occur to obtain low-intensity acoustic-like disturbances at ground during threshold Mach number flight
- α shock wave angle of incidence
- α_G ground slope
- β Prandtl-Glauert parameter, $(M^2 - 1)^{1/2}$
- Δ perturbation from undisturbed value
- ϵ ratio of molecular weight of water vapor to that of dry air
- η direction from which wind blows
- θ inclination angle of wave normal \vec{n} below horizontal

- μ Mach angle, $\sin^{-1} (1/M)$
- ν heading angle of wave normal \vec{n}
- ϕ azimuth angle of wave normal from vertical plane
- ψ airplane heading angle

Subscripts

- G ground level
- max maximum
- REF reference value
- T tower
- o initial value at airplane altitude

GENERAL TEST DESCRIPTION

The unique feature of the Jackass Flats sonic boom tests was the use of the 466-m (1529-ft) BREN tower shown in figure 2. Fifteen microphones were placed at 30.5 m (100-ft) intervals on the tower for observing the sonic boom pressure field. Fourteen microphones were placed on the ground in a line parallel to the nominal flight path. Two additional microphones were placed along a line normal to the flight path. Figure 3 schematically shows the test arrangement and table 2 gives the detailed microphone locations with respect to the tower base. The ground slopes slightly upward by about 0.017 rad (1°) from microphones G-1 to G-14.

TABLE 2.—TOWER AND GROUND MICROPHONE LOCATIONS

Tower microphones			Ground microphones				
Tower microphone number	Altitude above tower base ^a		Ground microphone number	Horizontal distance from tower base		Elevation with respect to tower base	
	m	ft		m	ft	m	ft
Tower Top	466.10	1529.2	G-1	-487.68	-1600	-10.27	-33.7
T-15	458.36	1503.8	G-2	-426.72	-1400	- 8.69	-28.5
T-14	428.09	1404.5	G-3	-365.76	-1200	- 7.32	-24.0
T-13	397.40	1303.8	G-4	-304.80	-1000	- 6.00	-19.7
T-12	366.92	1203.8	G-5	-243.84	- 800	- 4.97	-16.3
T-11	336.47	1103.9	G-6	-182.88	- 600	- 3.72	-12.2
T-10	305.96	1003.8	G-7	-121.92	- 400	- 4.75	-15.6
T-9	275.48	903.8	G-8	121.92	400	2.68	8.8
T-8	245.09	804.1	G-9	182.88	600	3.81	12.5
T-7	214.95	705.2	G-10	243.84	800	4.91	16.1
T-6	184.04	603.8	G-11	304.80	1000	6.16	20.2
T-5	153.65	504.1	G-12	365.76	1200	6.83	22.4
T-4	123.05	403.7	G-13	426.72	1400	7.86	25.8
T-3	92.78	304.4	G-14	487.68	1600	8.14	26.7
T-2	62.24	204.2	G-15 ^b	-544.07	-1785	- 9.42	-30.9
T-1	31.67	103.9	G-16 ^b	536.45	1760	7.16	23.5

^aAltitude of tower base is 1112.5 m (3650 ft) MSL

^bThese microphones were positioned on a line normal to the flight path (see fig. 2).

The BREN tower was also used as a platform for observing the structure of the lower atmosphere while the sonic boom measurements were being made. Anemometers and thermometers were located at eight levels. In addition, low-level measurements were made at two locations on a 30-m (100-ft) mast located 200 m (656 ft) to the south of the BREN tower. This position was selected to avoid distortions caused by the small buildings nearby. The heights of the sensors are given in table 3. Figure 4 shows some of the temperature and wind sensor instrumentation attached to the tower by A-frame supports. The microphone supports can be seen extending from the right side of the tower.

TABLE 3.—LOCATION OF METEOROLOGICAL INSTRUMENTATION
ON THE BREN TOWER

Level no.	Height of wind systems		Height of thermometers	
	m	ft	m	ft
9 ^a	460.3	1510	459.8	1508
8 ^a	303.3	995	300.0	984
7	217.9	715	214.6	704
6	175.3	575	171.6	563
5	132.6	435	129.0	423
4 ^a	89.9	295	86.3	283
3	47.2	155	43.6	143
2	25.9	85	24.4	80
1	15.2	50	14.6	48
0	3.1	10	2.4	8

^aLevels so indicated contained a vertically-orientated propeller anemometer.

A Piper Comanche airplane was used to obtain additional data on the atmospheric conditions above and in the vicinity of the BREN tower. Upper level temperature, wind, humidity, and pressure conditions to about 12.2 km (40 000 ft mean sea level) were obtained by using standard rawinsonde equipment at the Jackass Flats weather station, 4JA, located 3 miles northwest.

Sonic booms were generated by NASA F-104 airplanes. The flight track was nominally on a true heading of 035° in line with the ground microphone array, except for the lateral cutoff flights which were on a 125° heading and displaced to the south by 18.4 to 24.2 km (11.4 to 15.0 st mi). The airplane altitude above mean sea level ranged from 9.78 to 10.30 km (32 100 to 33 800 ft). All flights were controlled by radar and the flight tracks were recorded for later analysis. Each test airplane made three to four consecutive passes over the BREN tower. Voice communication with the pilot provided the capability to change the flight conditions appropriately on the next pass depending on what was observed at the tower.

THEORETICAL SONIC BOOM CALCULATION INPUTS

The primary objectives of the study of the BREN tower measurements included (1) an interpretation of the observed data guided by theoretical study of the test conditions and (2) a determination of the validity and accuracy of current sonic boom calculation methods. To accomplish these the computer method described in references 7 and 30 was used. Several types of data were required as inputs, which include the airplane flight conditions and the meteorological conditions between the airplane and the ground. Accordingly, the necessary data were recorded during the test series for later analysis. In addition, the airplane lift and shape characteristics were required in terms of the airplane F-function. This section contains a discussion of the methods used to obtain each type of input data.

Flight Conditions

Among the important flight conditions measured by tracking radar were the airplane altitude, location with respect to the BREN tower, and airplane velocity as a function of time. These variables were specified as accurately as possible, since relatively small inaccuracies can lead to unrealistic theoretical predictions, particularly for low supersonic Mach number flights.

In most cases it was necessary to smooth the observed radar data, since the radar accuracy tolerance was significant. Figure 5 shows an extreme case of variation of radar-observed airplane ground speed with flight time for one flight. Tolerances in the radar accuracy and a "smoothed" curve are indicated on the figure for reference. The large change in ground speed between 23 and 28 sec corresponds to an axial load factor (longitudinal acceleration) of about 1.7 m/sec^2 (5.5 ft/sec^2) or 0.17 g. This particular flight, however, was a "steady" flight near the threshold Mach number. Since most of the variation observed appears to be due to accuracy tolerance, the maneuver data for each case was smoothed for analysis purposes using a least-squares fit to the data. This smoothing assured reasonable analytical results and reduced the influence of recording accuracy. Similar techniques have been used by the French in analyzing comparable data (see the appendix of reference 26).

In addition to the radar-observed flight conditions, pilot-read altitude, Mach number, and fuel-on-board were also available at both the steady and breakoff points. In general the pilot-read altitudes were used; the pilot-read Mach numbers were not used because of instrument inaccuracies at low supersonic Mach numbers (except in cases where no radar data were available).

For most cases the airplane location and flight time were known, so that the theoretical boom arrival time at the tower could be calculated and compared with actual arrival times. This comparison provided a good test of the accuracy of linear geometric acoustics theory.

Meteorological Conditions

During the flights at low supersonic Mach numbers, the sonic boom traveled a relatively long distance through the atmosphere, so that meteorological conditions had an important effect. In general, sensitivity to atmospheric conditions increases with decreasing Mach number (refs. 31, 32 and 33). Because of this, an effort was made in the BREN tower tests to obtain accurate measurements of the meteorological conditions, particularly in the lowest kilometer. Definitive meteorological measurements were made by using several data-gathering methods. These included at least two rawinsonde observations during the boom-generating periods, two to four Piper Comanche runs, and the BREN tower data at the time of each boom (see ref. 34 for further details). Thus, excellent measurements of the prevailing meteorological conditions in the test area were obtained.

In the theory of references 7 and 30 a horizontally stratified atmosphere is assumed (variations in the vertical direction only). The effects of small-scale turbulence are ignored; only the relatively large-scale variations of temperature, pressure, and wind are taken into account. For each sonic boom overflight it was necessary to construct vertical profiles of temperature, pressure, and wind from the ground to the airplane altitude. This was done by using the BREN tower meteorological data (temperature and wind only), the Piper Comanche airborne turbulence measuring system (ATMS) temperature and pressure data, and the Jackass Flats weather station (4JA) rawinsonde observations of temperature, pressure, humidity, and wind. All of these data are given in reference 34, along with a description of the instrumentation, recording, and analysis methods. Table 4 gives a sample data tabulation of a typical atmospheric sounding constructed from all sources. In compiling these data it was necessary to calculate pressure and humidity at the BREN tower levels based on the nearest rawinsonde observation in time, and to interpolate wind and humidity data at the ATMS significant levels, as noted.

Table 4 also contains a parameter called "virtual" temperature, T_v , which is a corrected temperature used to account for the presence of water vapor. Appendix A contains a discussion of the calculation of the virtual temperature and its effect on shock propagation speed. Normally this effect is negligible, but for shock propagation near cutoff it may become important. Dewpoint temperatures from the rawinsonde observations were used as being representative of the conditions at the BREN tower.

TABLE 4.—TYPICAL METEOROLOGICAL DATA CONSTRUCTED FROM BREN TOWER, ATMS,
AND RAWINSONDE DATA

October 29, Bongo 1-1, Pass 104, 0835 PDT

Altitude, Z		Pressure, P		Temperature, T		Dewpoint temperature, T _d		Virtual temperature, T _v		Horizontal wind velocity, u		Wind direction, η (deg)	Data source	
m	ft	mb	lb/ft ²	°C	°F	°C	°F	°C	°F	m/sec	kn			
1113	3650	897.6	1874.8	14.6	58.3	-10.1	13.8	14.9	58.8	7.2	14.0	90.0	Tower ^a	
1128	3700	896.0	1871.4	14.5	58.1	-8.4	16.9	14.9	58.8	6.7	13.0	80.0		
1138	3735	894.9	1869.0	14.3	57.7	-8.2	17.2	14.7	58.5	8.5	16.5	65.0		
1160	3805	892.6	1864.3	13.9	57.0	-8.2	17.2	14.3	57.7	8.5	16.5	65.0		
1202	3945	888.1	1854.8	14.1	57.4	-8.3	17.1	14.5	58.1	8.0	15.6	20.0		
1245	4085	883.6	1845.5	14.3	57.7	-8.4	16.9	14.7	58.5	4.9	9.5	45.0		
1288	4225	879.1	1836.1	14.0	57.2	-8.5	16.7	14.4	57.9	5.8	11.3	25.0		
1331	4365	874.7	1826.8	13.8	56.8	-8.6	16.5	14.2	57.6	4.9	9.5	30.0		
1416	4645	865.8	1808.3	13.3	55.0	-8.9	16.0	13.7	56.7	2.7	5.2	5.0		
1573	5160	849.8	1774.8	13.3	55.0	-9.5	14.9	13.7	56.7	3.1	6.0	40.0		
2060	6758	800.0	1670.8	11.1	52.0	-11.2	11.8	11.5	52.7	1.7	3.3	45.0		ATMS ^b
2380	7808	770.0	1608.2	11.1	52.0	-12.1	10.2	11.4	52.5	1.6	3.1	42.0		
3100	10171	706.0	1474.5	5.8	42.4	-15.7	3.7	6.1	43.0	1.8	3.5	30.0		Rawin-sonde
3370	11056	683.0	1426.5	5.2	41.4	-16.1	3.0	5.5	41.9	2.0	3.9	10.0		
3770	12369	650.0	1357.6	2.3	35.1	-19.0	-2.2	2.5	36.5	2.4	4.7	346.0		
5970	19586	490.0	1023.4	-15.4	4.3	-30.4	-22.7	-15.3	4.5	1.9	3.7	210.0		
6940	22769	430.0	898.1	-22.8	-9.0	-36.3	-33.3	-22.7	-8.9	5.5	10.7	275.0		
7250	23786	412.0	860.5	-25.1	-13.2	-38.2	-36.8	-25.0	-13.0	5.3	10.3	280.0		
7490	24508	400.0	835.4	-26.8	-16.2	-39.6	-39.3	-26.8	-16.2	4.1	8.0	278.0		
9000	29527	322.0	672.5	-39.7	-39.4	-51.1	-60.0	-39.7	-39.4	9.7	18.9	298.0		
11440	37532	222.0	463.7	-58.3	-72.9	-65.0	-85.0	-58.3	-72.9	15.9	30.9	300.0		

^aDewpoint temperatures and pressures were determined from rawinsonde data

^bDewpoint temperatures and wind data were determined from rawinsonde data

Significant meteorological variations can occur horizontally along the path that the boom travels that would not be measured by vertical soundings. This is particularly true for some of the threshold Mach number flights, when the boom passed within 1.0 km (3300 ft) of the top of Little Skull Mountain (see ref. 34).

Airplane F-Function Data

A basic requirement for calculating theoretical sonic boom pressure signatures is the initial airplane disturbance, which is then propagated through the atmosphere to the ground. This was determined by calculating the F-function from the detailed geometry and lift distribution for the F-104 airplane. A brief description of the method used and tabulations of the resulting data at Mach 1.3 and 1.1 are given in appendix B. The F-104 airplane is about 15 m (50 ft) long, has a reference wing area of 18.21 m^2 (196 ft^2) and, during the tests, had a gross weight between 7300 and 9100 kg (16 000 and 20 000 lb) depending on the fuel consumed. Four different F-104 airplanes from the NASA Edwards Flight Test Center were used.

DATA ANALYSIS METHODS

In this section the methods used in the analysis of the meteorological and sonic boom data are briefly discussed. These include the calculation of the propagation speed from the meteorological observations, the calculation of the shock propagation speed from the shock wave arrival times on the ground microphone array, the calculation of shock wave profiles from the tower shock wave arrival times, and the calculation of the ground reflection coefficient.

Acoustic Propagation Speed

Directly beneath the airplane the propagation speed, V_p , is the speed of sound as determined from the temperature and wind speed in the direction of the normal to the shock wave. It is calculated from the equation:

$$V_p = a - u \cos(\nu - \eta) = a - u_n \quad (1)$$

The term $u \cos(\nu - \eta)$ is the wind component in the direction of flight (tailwind negative), when the ray directly beneath the airplane is being considered. For the threshold Mach number and acceleration flights the airplane heading angle, ψ , was 035° (also $\nu = 035^\circ$). For the lateral cutoff flights, however, ψ was 125° while the shock wave heading angle, ν , was about 90° at the BREN tower. The speed of sound is conveniently calculated from the temperature as follows:

$$a = 20.045 [T(^{\circ}\text{C}) + 273.2]^{1/2} \text{ m/sec} \quad (2)$$

In most cases where V_p is used in this report the sound speed, a , is corrected for the presence of water vapor by replacing the observed temperature, T , with a slightly higher temperature called virtual temperature, T_v . This corrected sound speed is denoted by a^* and the corresponding propagation speed by V_p^* . A discussion of the calculation of the virtual temperature and its effect on the change in propagation speed is contained in appendix A. The propagation speed, V_p^* , is of interest, since it is the speed at which an acoustic disturbance will propagate in the direction of flight. For the threshold Mach number flights and lateral cutoff flights V_p^* is of particular interest, since cutoff will occur at the altitude where it equals the airplane ground speed, V_G . For the lateral cutoff flights it was necessary to account for the fact that the flight path was not parallel to the microphone array.

Shock Propagation Speed

Since a two-dimensional array of microphones was used on the ground, it was possible to compute the velocity of propagation of the shock wave from the shock wave arrival times. For the threshold Mach number and acceleration flights where the flight track was parallel to the microphone array G-1 to G-14, the shock propagation speed is:

$$V_{p_{mic}} = \frac{\Delta X}{[t_o(G-14) - t_o(G-1)]} \quad (3)$$

where:

$$\begin{aligned} \Delta X &= 975.4 \text{ m (3200 ft)} \\ t_o(\quad) &= \text{shock wave arrival time at microphone } (\quad). \end{aligned}$$

For the lateral cutoff flights $V_{p_{mic}}$ was calculated from the arrival times at microphones G-15 and G-16 in an analogous manner.

For cases where discrete shock waves were observed, $V_{p_{mic}}$ is a direct measure of the airplane ground speed, V_G . In many cases this value of the airplane ground speed was more accurate than the ground speed obtained from the tracking radar because of the accuracy tolerances discussed in the previous section. In some cases it was possible to note a change in this calculated propagation speed over the length of the ground microphone array. This was true not only for the longitudinal acceleration flights but also for some of the threshold Mach number flights.

For cases where cutoff occurred above the tower and acoustic disturbances were observed (rather than shock waves), $V_{p_{mic}}$ is approximately equal to the propagation velocity, V_p , determined from the meteorological data. This was to be expected since V_p (or V_p^*) is the propagation velocity of acoustic disturbances, which is dependent on the temperature and wind conditions near the ground. $V_{p_{mic}}$ was calculated for all cases where it was possible to identify pressure signature features from microphones G-1 to G-14. For some rumble cases it was not possible to make this calculation.

Shock Wave Profiles

The sonic boom measurements on the tower provided the capability to calculate the shock wave front shapes and locations at a reference time in the vertical plane. This required a conversion

from time to distance, since the shock wave front swept past the fixed tower at a given velocity, $V_{p_{mic}}$. The shift in distance from the tower, ΔX , corresponding to differences in shock arrival time, t_o from a reference time, t_{REF} , is:

$$\Delta X = (t_{REF} - t_o) \cdot V_{p_{mic}} \quad (4)$$

The reference time was taken as the arrival time at tower microphone T-1. Since the microphones were positioned vertically on the tower, no correction because of microphone offset was necessary. The analysis of shock wave geometries in the vertical plane added significantly to the interpretation of the observations and to comparisons with linear theory.

An associated calculation is the conversion of the observed pressure signatures (overpressure versus time) from the time scale to a distance scale (overpressure versus distance). By making this conversion, shock wave profiles and observed pressure signatures could be placed on the same graph using a common distance scale.

Ground Reflection Coefficient

The ground reflection coefficient, K_R , was of particular interest for the BREN tower flight tests, since shock waves near the cutoff condition were observed. For shock waves near cutoff, incident on the ground, the reflection coefficient was expected to approach 1.0. (For oblique shock waves incident on smooth surfaces, the reflection coefficient is close to 2.0.) In this study K_R was determined by comparing intensities on the tower with those on the ground. The following equation was used:

$$K_R \approx \frac{[\Delta P_{max}(G-7) + \Delta P_{max}(G-8)]}{[\Delta P_{max}(T-1) + \Delta P_{max}(T-2)]} \quad (5)$$

By using two microphones for both tower and ground maximum overpressures, the effects of small-scale atmospheric turbulence were minimized. The specific microphones selected roughly correspond to those that recorded the same portion of the shock wave during and after reflection from the ground. Even with this technique, however, some inaccuracy resulted since large overpressure variations can occur over small distances. In some cases it was necessary to examine pressure signatures in detail.

ANALYSIS OF THE THRESHOLD MACH NUMBER

FLIGHT TEST DATA

This section contains the results of the analysis of the sonic boom characteristics measured during the threshold Mach number flights. The introduction contains background material on the nature of the phenomenon and the definition of the threshold Mach number. A summary table of the flight conditions for the 79 threshold Mach number flights is given. The presentation of the study results has been separated into categories according to what was observed on the BREN tower.

Introduction

Shock wave cutoff at low supersonic speeds.—The criterion for shock wave cutoff above the ground from a supersonic airplane is that the airplane ground speed must be less than the maximum speed of propagation of the shock wave beneath the airplane. This concept is illustrated in figure 6. An airplane with ground speed, V_G flown close to the ground below altitude Z_1 will be flying subsonically, so that no shock wave will form. For flight at a higher altitude, Z_2 , however, with the same ground speed, the airplane will be operating supersonically due to the lower sound speed there, and a shock wave will form. In that case, the shock wave is “bent” or refracted by the shock propagation speed gradient as it travels toward the ground and will be completely refracted at altitude Z_1 where the propagation speed is equal to the airplane ground speed. At the altitude of complete shock wave refraction, the shock wave path is parallel to the ground. As the airplane ground speed or Mach number increases, the initial shock wave angle is less vertical with respect to the ground, so that it takes larger gradients of temperature and wind for the shock wave to become normal to the ground. For an airplane ground speed equal to $V_{p_{max}}$ in figure 6a, the shock wave will be completely refracted at the ground (see fig. 6b). For an airplane ground speed greater than $V_{p_{max}}$, the shock wave and a sonic boom will be observed at the ground (see fig. 6c).

At the altitude of complete shock wave refraction, some interesting phenomena occur. First, a slightly more intense shock wave may occur due to the fact that the energy is focused, producing a caustic. The initial shock wave intensity is relatively low, however, due to the fact it was produced at a Mach number slightly greater than unity. Below the altitude of complete refraction, the shock wave and sonic boom degenerate to acoustic or sound waves which propagate toward the ground. These acoustic waves are perceived as rumbles similar to distant thunder rather than the “bang” of a sonic boom. If the altitude of refraction is high enough above the ground, no noise will be discernible at the ground.

Threshold Mach number.—The threshold Mach number has been defined to be the maximum airplane Mach number for which complete shock wave refraction can occur at or above the ground. For cutoff directly beneath the airplane, the equation defining the threshold Mach number (ref. 32 and appendix C) is:

$$M_T = \frac{1}{a_0} \left\{ [a(Z) - u_n(Z)]_{\max} + u_{n_0} \right\} \quad (6)$$

where:

M_T = threshold Mach number

Z = altitude

$a(Z)$ = speed of sound at altitude Z

$u_n(Z)$ = wind component at altitude Z parallel to flight path (tailwind is negative)

$[a(Z) - u_n(Z)]_{\max}$ = $V_{p_{\max}}$ = maximum shock propagation speed between the airplane and the ground in the direction of flight, with $a(Z)$ and $u(Z)$ taken at the same altitude

a_0 = sound speed at airplane

u_{n_0} = wind speed at airplane (tailwind is negative)

Equation (6) can be rewritten as:

$$V_G = [a(Z) - u_n(Z)]_{\max} = V_{p_{\max}} \quad (7)$$

where:

V_G = airplane ground speed for flight at the threshold Mach number
 = $(M_T)(a_0) - u_{n_0}$

$[a(Z) - u_n(Z)]_{\max}$ = $V_{p_{\max}}$ = maximum shock propagation speed in the direction of flight

Equation (7) simply states that for flight at the threshold Mach number, defined by equation (6), the airplane ground speed, V_G , is equal to the maximum shock propagation in the direction of flight speed, $V_{p_{\max}}$, beneath the airplane. More generally, the shock wave will be completely refracted at the altitude where the shock propagation speed is equal to the airplane ground speed.

For steady, level flight near the threshold Mach number, the following statements can be made:

- The ground speed of the airplane will be equal to the speed of sound at the cutoff altitude plus or minus the wind speed there, depending on whether the wind is a tailwind or headwind.
- Although the allowable airplane speed is determined by the shock propagation speed at the cutoff altitude in the lower atmosphere, the allowable airplane Mach number is dependent on the temperature and wind at the airplane altitude. For a fixed ground speed, a headwind at the airplane gives an increased Mach number, while a tailwind results in a decreased Mach number compared to a case with no wind.

Variability of threshold Mach number.—One of the potential advantages of commercial threshold Mach number operation is that the airplane ground speeds show little variation with direction of flight. Table 5 compares subsonic flight with threshold Mach number operation (where cutoff occurs at a safe altitude above the ground) over the San Francisco to New York City route. For average tailwind and headwind conditions the airplane ground speed varies by only about 7.7 m/sec (15 kn), while for subsonic airplanes the variability is about 46.3 m/sec (90 kn). The low variability of ground speed with flight direction is due to the fact that the ground propagation speeds do not vary appreciably with season or flight direction. Table 6, compiled from the data in reference 35, illustrates average and extreme threshold Mach numbers, ground speeds, and block times over the San Francisco to New York City route. Further data on the variability of the threshold Mach number in time and space are given in reference 35.

TABLE 5.—TYPICAL GROUND SPEEDS AND BLOCK TIMES FOR VARIOUS MACH NUMBER REGIMES OVER THE SAN FRANCISCO TO NEW YORK CITY ROUTE

(Airplane altitude of 13.72 km (45 000 ft))

	Mach 0.95			Mach 0.83			Threshold Mach number operation (Variable Mach number)			
	Ground speed		Block time, hr	Ground speed		Block time, hr	Most probable route mean Mach number	Most probable route mean ground speed		Most probable block time, hr
	m/sec	kn		m/sec	kn			m/sec	kn	
NO WIND	280.4	545	4.6	244.4	475	5.2	1.15	335.9	653	3.94
TAILWIND, 23.1 m/sec (45 kn) ^a	303.5	590	4.3	267.5	520	4.8	1.08	340.0	661	3.90
HEADWIND, 23.1 m/sec (45 kn) ^a	257.2	500	5.0	221.2	430	5.7	1.20	332.3	646	3.98

^a Mean wind component along the route at 13.72 km (45,000 ft) for the data used.

TABLE 6.—MOST PROBABLE AND EXTREME ROUTE MEAN SAFE^a THRESHOLD MACH NUMBERS, GROUND SPEEDS, AND BLOCK TIMES FOR THE SAN FRANCISCO TO NEW YORK CITY ROUTE

Airplane altitude of 13.72 km (45 000 ft)

Data compiled from 5 years of twice-daily meteorological observations at four locations during the seasonal months

[After ref. 35]

	95% probability of being greater than			50% probability of being greater than			5% probability of being greater than		
	Jan.	July	Annual	Jan.	July	Annual	Jan.	July	Annual
WEST BOUND (HEADWIND)									
Safe Threshold Mach Number, M_T	1.140	1.175	1.155	1.185	1.210	1.200	1.250	1.260	1.250
Airplane Ground Speed, m/sec (kn)	317.9 (618)	334.4 (650)	322.0 (626)	324.6 (631)	338.0 (657)	332.3 (646)	330.8 (643)	342.6 (666)	340.0 (661)
Block Time, hr	3.99	3.87	3.90	4.06	3.92	3.98	4.13	3.95	4.09
EAST BOUND (TAILWIND)									
Safe Threshold Mach Number, M_T	1.020	1.060	1.035	1.050	1.110	1.080	1.090	1.155	1.140
Airplane Ground Speed, m/sec (kn)	328.2 (638)	338.5 (658)	331.3 (644)	335.9 (653)	342.6 (666)	340.0 (661)	346.7 (674)	346.7 (674)	347.2 (675)
Block Time, hr	3.83	3.83	3.83	3.94	3.87	3.90	4.02	3.92	3.99

^a A safety factor consisting of a 5.1-m/sec (10-kn) reduction in the maximum airplane ground speed was used, since cutoff must occur above the ground to avoid objectionable sonic boom noise.

Previous flight tests.—There have been two experimental tests during which threshold Mach number flights were conducted. The first experiment (ref. 14) involved seven flights all on one day; the second (ref. 18) involved five flights, also on one day. Both experiments indicated that for airplane Mach numbers less than the threshold Mach number, neither boom nor rumbles were observed at the ground, whereas, for flight at Mach numbers greater than the threshold value, definite shock waves were observed in the pressure signatures. These earlier experiments, however, lacked the required density of microphones and number of flights required to define the shock wave characteristics associated with complete refraction or the cutoff condition.

Effect of Terrain Slope

One of the criteria for determining nearness to complete refraction was the angle of the shock wave front with respect to the ground. Complete refraction occurs when it is normal to the horizontal ground. This angle could be computed from the shock arrival times on the tower. During the analysis of the shock shapes it was noted that the angle of the incident shock wave with respect to the tower was not equal to the angle of the ground-reflected shock wave. Typically, the reflected shock was at a larger angle. This effect is attributed to the sloping terrain uptrack of the tower. Figure 7 illustrates schematically the effect of the sloping terrain. The reflected shock wave is rotated backward $2\alpha_G$ degrees because of the α_G degree ground slope. Two flights were chosen to verify the sloping terrain effect. These flights were at high enough Mach numbers to minimize the effects of changing airplane ground speed and atmospheric variations. In each case the deviation of the reflected shock front from being symmetric with the incident shock was determined with altitude on the tower. These data are given in table 7.

TABLE 7.—CALCULATION OF EFFECT OF GROUND SLOPE ON REFLECTED SHOCK FRONT

Tower mic no.	Altitude above tower base, Z_G		Pass 026; 8-25; bongo 4-2				Pass 082; 10-23; bongo 1-1			
			Deviation of reflected shock from being symmetric, ΔX		Calculated ground slope, $\alpha_G = 1/2 \tan^{-1} (\Delta X/Z)$		Deviation of reflected shock from being symmetric, ΔX		Calculated ground slope, $\alpha_G = 1/2 \tan^{-1} (\Delta X/Z)$	
	m	ft	m	ft	rad	deg	m	ft	rad	deg
15	458.4	1504	18.7	61.4	0.02036	1° 10'	19.6	64.3	0.02123	1° 13'
14	428.1	1405	17.9	58.7	0.02094	1° 12'	16.8	55.1	0.01978	1° 8'
13	397.4	1304	16.4	53.8	0.02065	1° 11'	17.2	56.4	0.02182	1° 14'
12	366.9	1204	14.9	48.9	0.02036	1° 10'	14.3	46.9	0.01949	1° 7'
11	336.5	1104	13.7	44.9	0.02036	1° 10'	13.6	44.6	0.02036	1° 10'
10	306.0	1004	12.1	39.7	0.01978	1° 8'	12.3	40.4	0.02007	1° 9'
9	275.5	904	11.7	38.4	0.02123	1° 13'	10.5	34.4	0.01891	1° 5'
8	245.1	804	9.7	31.8	0.01978	1° 8'	9.0	29.5	0.01832	1° 3'
7	215.0	705	7.8	25.6	0.01803	1° 2'	6.6	21.7	0.01542	0° 53'
6	184.0	604	6.2	20.3	0.01687	0° 58'	5.9	19.4	0.01600	0° 55'
5	153.7	504	—	—	—	—	4.6	15.1	0.01513	0° 52'
4	123.1	404	—	—	—	—	4.0	13.1	0.01629	0° 56'
3	92.8	304	—	—	—	—	3.5	11.5	0.01891	1° 5'

The terrain slope with respect to the tower base between ground microphones G-1 and G-7 uptrack of the tower is about 0.02036 rad (1° 10'). Thus, the ground slope angle, α_G , calculated from the nonsymmetry of the reflected shock, agrees very closely with the actual ground slope to within a small fraction of a degree. As a result of this analysis, the incident shock wave angle was used to determine nearness to cutoff, because of the influence of the sloping terrain on the reflected shock wave angle.

Summary of Flight Conditions

The 79 threshold Mach number flights have been summarized in table 8 for reference and a unique flight number was assigned to each pass for identification. The airplane altitude and Mach number are values read by the pilot at the steady point, and the airplane gross weight was determined from the steady point fuel-on-board. The maximum observed overpressure of all the ground and tower microphones is given, along with subjective observer comments of the boom character. Each pass was also categorized according to the subjective observations of the boom character. These categories are listed below:

THRESHOLD MACH NUMBER CATEGORIES

<u>Category</u>	<u>Reported Subjective Observation</u>	<u>Flight Condition</u>
R1	No Rumble	M < M _T
R2	Low Rumble	
R3	Moderate to Heavy Rumble	
R4	Light Boom	M ≈ M _T
B1	Near Cutoff ($\Theta < 0.01745$ rad (1.0 deg))	M ≈ M _T
B2	Normal Boom ($\Theta > 0.01745$ rad (1.0 deg))	M > M _T
B3	Acceleration Effects	M > M _T

Mach Number Greater Than Threshold Value

Thirty-one threshold Mach number flights were at Mach numbers sufficiently greater than the threshold Mach number to produce well-defined sonic booms on the ground. Hence, the airplane ground speed was greater than the maximum shock propagation speed, $V_{p \max}^*$, between the airplane and the ground. For these cases the airplane ground speed exceeded $V_{p \max}^*$ by a range from about 1 to 36 m/sec (3.3 to 118 ft/sec).

TABLE 8.—SUMMARY OF THRESHOLD MACH NUMBER FLIGHT TEST CONDITIONS

Date	Bongo-pass	Pass	Airplane altitude, h		Airplane weight, W		Pilot-read Mach number	Maximum observed overpressure			Subjective boom character	Category
			km	ft	kg	lb		N/m ²	lb/ft ²	Mic No.		
8-24	1-1	001	10.30	33 800	8437	18 600	1.09	—	—	—	No Boom or Rumble	R1
	1-2	002	10.27	33 700	8029	17 700	1.12	50.75	1.060	T-14	Boom, Near Caustic	B1
	1-3	003	10.27	33 700	7620	16 800	1.10	6.18	0.129	T-15	Very Light Rumble	R2
	2-1	004	10.18	33 400	8392	18 500	1.10	45.05	0.941	G-8	Triple Boom	B3
	2-2	005	9.91	32 500	7893	17 400	1.10	4.50	0.094	T-1	Very Low Rumble	R2
	2-3	006	10.12	33 200	7348	16 200	1.11	67.99	1.42	G-6	Boom, Rumble	B2
	3-1	007	10.18	33 400	8482	18 700	1.11	4.88	0.102	T-15	Long, Low Rumble	R2
	3-2	008	10.15	33 300	8029	17 700	1.115	4.50	0.094	T-15	Long, Low Rumble	R2
	3-3	009	10.18	33 400	7620	16 800	1.12	12.31	0.257	T-10	Moderate Rumble	R3
	3-4	010	10.27	33 700	7212	15 900	1.13	34.37	0.720	T-14	Boom, Rumble	B1, R4
	4-1	011	10.15	33 300	8437	18 600	1.14	35.62	0.744	G-2	Rumble, Boom	B1, R4
	4-2	012	10.15	33 300	7938	17 500	1.15	71.34	1.49	G-4	Double Boom	B3
4-3	013	10.15	33 300	7484	16 500	1.16	30.83	0.644	G-1	Boom, Rumble	B2	
8-25	1-1	014	10.06	33 000	8528	18 800	1.10	18.24	0.381	G-15	Rumble	R3
	1-2	015	10.18	33 400	8074	17 800	1.14	67.03	1.40	G-7	Double Boom	B3
	1-3	016	10.06	33 000	7620	16 800	1.13	45.77	0.956	G-5	Double Boom	B2
	2-1	017	10.07	33 040	8437	18 600	1.12	82.35	1.72	T-14	Near Caustic	B3
	2-2	018	10.09	33 100	7961	17 550	1.11	62.00	1.295	T-8	Double Boom, Rumble	B2
	2-3	019	10.10	33 140	7552	16 650	1.09	9.15	0.191	G-5	Light Rumble	R2
	2-4	020	10.10	33 140	7190	15 850	1.10	57.46	1.20	G-14	Boom, Rumble	B3
	3-1	021	10.06	33 300	8573	18 900	1.10	67.03	1.40	G-1	Rumble, Boom	B2
	3-2	022	10.09	33 100	8119	17 900	1.095	6.99	0.146	G-6	Light Rumble	R2
	3-3	023	10.06	33 000	7711	17 000	1.10	26.05	0.544	T-15	Moderate Rumble	R4
	3-4	024	10.21	33 500	7394	16 300	1.105	63.20	1.32	T-6	Double Boom, Rumble	R2
	4-1	025	10.03	32 900	8414	18 550	1.10	12.74	0.266	G-15	Rumble	R2
4-2	026	9.98	32 750	7938	17 500	1.20	115.87	2.42	G-8	Double Boom, High Peak	B2	
4-3	027	10.03	32 900	7530	16 600	1.115	23.17	0.484	T-15	Mod-Heavy Rumble	R3	
4-4	028	10.03	32 900	7190	15 850	1.12	79.96	1.67	G-14	Triple Boom	B2	
8-31	1-1	051	10.03	32 900	8528	18 800	1.10	58.89	1.23	G-14	Double Boom	B2
	1-2	052	10.06	33 000	8097	17 850	1.09	42.42	0.886	G-8	Double Boom	B2
	1-3	053	10.06	33 000	7643	16 850	1.08	8.91	0.186	G-8	Rumble	R2
	1-4	054	10.06	33 000	7280	16 050	1.07	50.27	1.05	G-16	Double Boom, Rumble	B4

TABLE 8.—Continued

Date	Bong-pass	Pass	Airplane altitude, h		Airplane weight, W		Pilot-read Mach number	Maximum observed overpressure			Subjective boom character	Category	
			km	ft	kg	lb		N/m ²	lb/ft ²	Mic no.			
8-31 (cont)	2-1	055	9.91	32 500	8505	18 750	1.07	12.74	0.266	G-2	Very Slight Boom	R4	
	2-2	056	9.88	32 400	8074	17 800	1.08	21.79	0.455	G-6	Double Boom	R4	
	2-3	057	9.91	32 500	7711	17 000	1.09	64.16	1.34	T-14	Double Boom	B3	
	2-4	058	9.91	32 500	7348	16 200	1.09	66.07	1.38	T-9	Near Caustic Boom	B1	
	3-1	059	10.00	32 800	8573	18 900	1.09	29.40	0.614	G-16	Boom	R4	
	3-2	060	—	—	8165	18 000	1.10	44.67	0.933	G-9	Boom, Rumble	B1	
	3-3	061	10.03	32 900	7757	17 100	1.13	79.00	1.65	G-4	Double Boom	B3	
	3-4	062	10.06	33 000	7348	16 200	1.095	34.81	0.727	G-1	Boom	B1	
	10-23	4-1	063	9.75	32 000	8482	18 700	1.095	135.02	2.82	T-12	Boom (Caustic)	B1
		4-2	064	9.91	32 500	8029	17 700	1.095	33.09	0.691	T-12	Light Rumble, Boom	R4
		4-3	065	9.91	32 500	7666	16 900	1.10	74.21	1.55	G-1	Moderate Double Boom	B3
		4-4	066	9.91	32 500	7280	16 050	1.093	70.38	1.47	T-12	Multi Boom	B3
10-27	1-1	082	10.06	33 000	8437	18 600	1.11	21.59	0.451	G-1	Very Light Boom, Rumble	R4	
	1-2	083	10.21	33 500	8029	17 700	1.09	—	—	—	No Boom or Rumble	R1	
	1-3	084	10.21	33 500	7530	16 600	1.10	—	—	—	No Boom or Rumble	R1	
	1-4	085	9.91	32 500	7122	15 700	1.11	12.11	0.253	G-14	Very Slight Boom, Rumble	R4	
10-27	2-1	089	10.03	32 900	8482	18 700	1.10	25.47	0.532	T-10	Heavy Rumble	R3	
	2-2	090	9.97	32 700	8029	17 700	1.10	19.20	0.401	G-15	Rumble	R2	
	2-3	091	9.75	32 000	7666	16 900	1.11	25.47	0.532	T-3	Very Light Boom	R4	
10-28	1-1	095	10.06	33 000	8092	17 840	1.14	118.65	2.478	G-2	Boom	B3	
	1-2	096	10.06	33 000	7684	16 940	1.12	12.59	0.263	G-13	Rumble	R2	
	1-3	097	10.06	33 000	7321	16 140	1.13	19.82	0.414	T-12	Moderate Rumble	R3	
	2-1	098	10.06	33 000	8408	18 535	1.10	13.65	0.285	G-2	Very Light Rumble	R2	
	2-2	099	9.97	32 700	7977	17 585	1.10	—	—	—	No Boom or Rumble	R1	
	2-3	100	10.06	33 000	7523	16 585	1.10	—	—	—	No Boom or Rumble	R1	
	3-1	101	10.06	33 000	8138	17 940	1.14	49.51	1.034	G-5	Boom, Rumble	B2	
	3-2	102	10.06	33 000	7729	17 040	1.13	38.40	0.802	T-11	Boom, Rumble	B1	
	3-3	103	10.06	33 000	7367	16 240	1.13	37.11	0.775	G-11	Boom, Rumble	B1	

TABLE 8.—Concluded

Date	Bong-pass	Pass	Airplane altitude, h		Airplane weight, W		Pilot-read Mach number	Maximum observed overpressure		Mic no.	Subjective boom character	Category
			km	ft	kg	lb		N/m ²	Lb/ft ²			
10-29	1-1	104	9.81	32 200	8482	18 700	1.12	27.15	0.567	T-5	Mixed, Heavy Rumble	B2
	1-2	105	10.06	33 000	8029	17 700	1.13	39.54	0.805	G-7	Boom, Rumble	B2
	1-3	106	10.06	33 000	7621	16 800	1.125	59.04	1.233	G-8	Boom	B3
	1-4	107	10.06	33 000	7235	15 950	1.12	21.74	0.454	G-6	Rumble, Boom	R4
	2-1	108	9.97	32 700	8863	19 540	1.135	44.29	0.925	G-2	Boom	B2
	2-2	109	9.97	32 700	8455	18 640	1.125	45.10	0.942	G-6	Boom, Rumble	B2
	2-3	110	9.97	32 700	7956	17 540	1.12	45.62	0.732	G-6	Boom	B1
	2-4	111	9.94	32 600	7548	16 640	1.115	12.11	0.253	G-6	Rumble	R2
	2-5	112	9.75	32 000	7185	15 840	1.115	21.21	0.443	T-9	Very Low Boom	R4
	3-1	113	9.75	32 000	8863	19 540	1.13	41.80	0.873	G-13	Triple Boom	B2
	3-2	114	10.03	32 900	8455	18 640	1.12	39.17	0.818	T-15	Boom, Rumble	B1
	3-3	115	10.03	32 900	7911	17 440	1.115	12.98	0.271	T-15	Rumble	R2
10-30	1-1	116	9.78	32 100	8437	18 600	1.12	71.05	1.484	G-8	Boom, Rumble	B2
	1-2	117	9.78	32 100	8029	17 700	1.11	60.14	1.256	G-16	Double Boom	B3
	1-3	118	10.00	32 800	7621	16 800	1.11	17.33	0.362	G-2	Very Light Boom	R4
	1-4	119	10.00	32 800	7258	16 000	1.115	35.57	0.743	T-13,14	Light-Mod. Boom	B3
	2-1	120	10.06	33 000	8573	18 900	1.11	12.93	0.270	G-13	Rumble	R2
	2-2	121	9.91	32 500	8165	18 000	1.12	25.28	0.528	G-3	Muffled Boom, Rumble	R4
	2-3	122	9.91	32 500	7711	17 000	1.12	16.28	0.340	G-6	Very Light Boom, Rumble	R4

A direct measure of nearness to cutoff is the shock wave angle of incidence with respect to the vertical, Θ . This can be calculated from the arrival times of the shock wave at the various tower microphones after a transformation is made from time increments, ΔT , to distance increments, ΔX . This conversion method was previously described in the "Data Analysis Methods" section. For the cases discussed in this section, Θ ranged from 0.01745 to 0.419 rad (1° to 24°). Shock wave profiles and pressure signatures measured on the tower are presented and discussed.

Comparison of theory with observation.—Table 9 summarizes the pertinent observed data for these cases, including the airplane ground speed, V_G the shock propagation speed, V_p^* , the shock wave inclination angle, Θ , the average observed maximum overpressure on the tower, $\Delta P_{T_{max}}$, and the shock wave arrival time, t_o , at microphone T-1. For these cases it is of particular interest to compare the observed data with theoretical results. Theoretical values of Θ , ΔP , and t_o are also given in table 9.

The error of the theoretical arrival time is a good measure of the accuracy of the theoretical calculations. For the August flights this error is about ± 1.0 sec. For the October flights, however, much larger errors were calculated (about ± 5.0 sec). The significantly larger errors during the October flights are due to the meteorological conditions. The gradient of propagation speed in the lower 1 km (3300 ft) was nearly zero or negative during most of the flights. For this condition, small inaccuracies in the flight or atmospheric conditions would lead to large variations in theoretical shock locations and arrival times. Determination of the airplane ground speed is especially sensitive. For example, starting with a ground speed 3.5 m/sec (11.5 ft/sec) greater than $V_{p^*_{max}}$, a 1.5 m/sec (4.9 ft/sec) decrease in the airplane ground speed will change Θ from 8° to 6° , with accompanying changes in ΔP and t_o . An additional 2 m/sec (6.6 ft/sec) decrease in ground speed will change Θ from 6° to 0° . Thus, the accuracy of the theoretical calculations is highly dependent on the accuracy of the measured airplane ground speed, as well as the accuracy of the available meteorological data in representing the conditions along the boom propagation path.

Figure 8 summarizes the comparison between theory and experiment for the shock inclination angle, Θ . The values of $(V_{G_{mic}} - V_{p^*})$ in table 9 and the sound speed, $a(Z)$, near the ground were used to calculate theoretical values of Θ from appendix equation (C8), which is:

$$\Theta = \cos^{-1} \left\{ 1 + \frac{(V_G - V_p)}{a(Z)} \right\}^{-1}$$

A convenient relationship between $(V_{G_{mic}} - V_{p^*_{max}})$ and $(M - M_T)$ is given by appendix equation (C10) as:

$$(M - M_T) = (V_G - V_{p^*_{max}}) / a_o$$

TABLE 9.—SUMMARY OF THRESHOLD MACH NUMBER CASES FOR WHICH $M > M_T$ (CATEGORIES B2 AND B3)
A. (Metric Units)

Date	Bongo-pass	Pass	Airplane ^a ground speed, $V_{G_{mic}}$, ft/sec	Shock ^b propagation speed, V_{p^*} , ft/sec	$(V_{G_{mic}} \cdot V_{p^*})$ ft/sec	Shock inclination angle, Θ , deg	Airplane weight, W , lb	Average tower overpressure ΔP_T , lb/ft ²	Maximum tower overpressure ΔP_T , lb/ft ²	Shock arrival time at Mic T-1 (PDT)	K_R	Theory (radar data)				Category
												Θ_c deg	ΔP_T lb/ft ²	t_o at Mic T-1 (PDT)	t_o error, sec	
8-24	2-1	004	1156.1	1149.9	6.2	6.3	18 500	0.497	0.765	0937: 17.8	1.80	5.7	0.66	0937: 18.2	+0.4	B3
	2-3	006	1187.6	1150.6	37.0	12.9	16 200	0.589	0.875	1001: 01.3	1.90	13.2	0.60	-No. Airplane Time—		B2
	4-2	012	1181.7	1173.5	8.2	6.1	17 500	0.793	1.225	1221: 09.5	1.25	6.6	0.60	1221: 10.1	+0.6	B3
	4-3	013	1212.6	1169.3	43.3	14.4	16 500	0.264	0.351	1232: 00.3	1.50	15.2	0.62	1232: 01.1	+0.8	B2
	1-2	015	1194.5	1168.0	26.5	11.2	17 800	0.817	1.28	0915: 43.8	1.86	12.1	0.62	0915: 44.2	+0.4	B3
	1-3	016	1193.6	1158.1	35.5	12.9	16 800	0.444	0.707	0925: 54.9	1.84	14.4	0.63	0925: 55.0	+0.1	B2
8-25	2-1	017	1175.5	1159.8	15.7	8.7	18 600	0.680	1.22	0937: 36.9	1.52	9.2	0.63	0937: 38.8	+0.1	B2
	2-2	018	1183.0	1167.6	15.4	7.6	17 550	0.620	1.295	0948: 50.4	1.47	9.2	0.87	0948: 50.6	+0.2	B2
	2-4	020	1178.1	1154.2	23.9	9.4	15 850	0.614	0.920	1009: 30.8	1.81	11.3	0.66	1008: 31.1	+0.3	B3
	3-1	021	1185.3	1159.4	25.9	10.0	18 900	0.561	0.748	1044: 19.3	1.71	11.8	0.60	1044: 19.2	-0.1	B2
	3-4	024	1184.4	1169.0	15.4	6.9	16 300	0.694	1.32	1112: 03.0	1.55	9.6	0.76	1112: 03.8	+0.8	B3
	4-2	026	1280.5	1163.4	117.1	23.8	17 500	0.77	1.42	1128: 53.6	2.18	23.0	0.58	1128: 52.9	-0.7	B2
	4-4	028	1172.9	1169.3	3.6	2.7	15 850	1.007	1.65	1148: 56.2	1.43	4.5	0.71	1148: 55.5	-0.7	B2
	1-1	051	1167.0	1152.5	14.5	8.0	18 800	0.502	0.575	0839: 48.4	1.36	9.0	0.55	0839: 47.8	-0.6	B2
	1-2	052	1166.7	1154.2	12.5	6.4	17 850	0.454	0.525	0850: 06.2	1.72	6.9	0.65	0850: 05.9	-0.3	B2
	1-4	064	1162.1	1157.1	5.0	3.9	16 050	0.346	0.350	0910: 32.6	1.47	4.8	0.63	0910: 32.1	-0.5	B2
	2-3	057	1168.6	1157.8	10.8	6.9	17 000	0.670	1.342	0937: 18.8	1.38	7.5	0.62	0937: 18.4	-0.4	B3
	3-3	061	1215.5	1165.3	50.2	15.3	17 100	0.842	1.183	1053: 28.6	1.13	16.3	0.61	1053: 27.4	-1.2	B3
4-3	065	1192.2	1160.7	31.5	12.5	16 900	0.852	1.352	1133: 42.6	1.34	13.1	0.50	1133: 42.5	-0.1	B3	
4-4	066	1181.1	1162.7	18.4	9.1	16 050	0.628	1.471	1143: 57.2	1.51	10.0	0.64	1143: 57.1	-0.1	B3	
10-28	1-1	095	1113.5	1080.4	33.1	13.0	17 840	0.620	1.097	0832: 08.8	1.70	14.0	0.59	0832: 04.2	-4.6	B3
10-29	3-1	101	1107.6	1096.4	11.2	5.6	17 940	0.521	0.819	1013: 28.3	1.03	8.2	0.72	0813: 23.2	-5.1	B2
	1-1	104	1118.1	1100.4	17.7	10.8	18 700	0.432	0.567	0835: 18.3	1.29	10.2	0.36	0835: 20.2	+1.9	B2
	1-2	105	1110.9	1099.7	11.2	10.4	17 700	0.445	0.789	0845: 49.6	1.00	8.2	0.50	0845: 52.1	+2.5	B2
	1-3	106	1132.9	1100.1	32.8	14.1	16 800	0.647	0.847	0856: 36.9	1.80	14.0	0.42	0856: 39.2	+2.3	B3
	2-1	108	1138.4	1132.9	5.5	3.9	19 540	0.391	0.763	1137: 26.9	0.95	5.6	0.65	0937: 24.5	-2.4	B2
2-2	109	1130.6	1128.3	2.3	1.2	18 640	0.421	0.765	1147: 59.7	1.14	11.4	0.65	0937: 24.5	-2.4	B2	
3-1	113	1152.9	1140.3	12.5	9.5	19 640	0.580	0.775	1351: 25.6	1.64	10.4	0.31	cutoff at 4500 ft—		B2	
10-30	1-1	116	1139.1	1124.3	14.8	11.1	18 600	0.535	0.981	0908: 23.6	1.71	10.4	0.51	0908: 36.0	+6.4	B2
1-2	117	1135.2	1124.4	10.8	6.7	17 700	0.662	0.782	0919: 09.2	1.51	8.0	0.51	0919: 11.8	+2.6	B3	
	1-4	119	1147.0	1128.3	18.7	9.2	16 000	0.408	0.743	0939: 30.4	1.80	10.5	0.24	0939: 33.1	+2.7	B3

^aCalculated from shock wave arrival times at ground microphones

^bAverage value between 100 and 500 ft on tower

^cEquation (C8) was used with $(V_{G_{mic}} \cdot V_{p^*})$ values

TABLE 9.—SUMMARY OF THRESHOLD MACH NUMBER CASES FOR WHICH $M > M_T$ (CATEGORIES B2 AND B3)

B. (English Units)

Date	Bongo-pass	Pass	Airplane ^a ground speed, V_G , mic m/sec	Shock ^b propagation speed, V_p m/sec	$(V_G \cdot V_p)$, mic m/sec	Shock inclination angle, Θ , rad	Airplane weight, W, kg	Average tower overpressure ΔP_T , N/m ²	Maximum tower overpressure ΔP , N/m ²	Shock arrival time at Mic T-1 (PDT)	K_R	Theory (radar data)				Category
												Θ_c rad	ΔP_T N/m ²	t_0 at Mic T-1	t_0 error, sec	
8-24	2-1	004	352.4	350.5	1.9	0.1105	8392	23.80	36.63	0937: 17.8	1.80	0.099	30.9	0937: 18.2	+0.4	B3
	2-3	006	362.0	350.7	11.3	0.225	7348	28.20	41.90	1001: 01.3	1.90	0.230	28.4	-No Airplane Time-		B2
	4-2	012	360.2	357.7	2.5	0.106	7938	37.97	58.65	1221: 09.5	1.25	0.115	35.3	1221: 10.1	+0.6	B3
	4-3	013	369.6	356.4	13.2	0.252	7484	12.64	16.81	1232: 00.3	1.50	0.265	29.0	1232: 01.1	+0.8	B2
	1-2	015	364.1	356.0	8.1	0.195	8074	39.12	61.29	0915: 43.8	1.86	0.210	29.4	0915: 44.2	+0.4	B3
	1-3	016	363.8	353.0	10.8	0.225	7620	21.26	33.85	0925: 54.9	1.84	0.251	29.9	0925: 55.0	+0.1	B2
8-25	2-1	017	358.3	353.5	4.8	0.152	8437	29.11	82.35	0937: 38.9	1.52	0.161	29.8	0937: 38.8	+0.1	B3
	2-2	018	360.6	355.9	4.7	0.133	7961	29.69	62.00	0948: 50.4	1.47	0.161	40.8	0948: 50.6	+0.2	B2
	2-4	020	359.1	351.8	7.3	0.164	7190	29.40	44.05	1009: 30.8	1.81	0.197	31.1	1008: 31.1	+0.3	B3
	3-1	021	361.3	353.4	7.9	0.1745	8573	26.86	37.83	1044: 19.3	1.71	0.206	28.3	1044: 19.2	-0.1	B2
	3-4	024	361.0	356.3	4.7	0.121	7394	33.23	63.20	1112: 03.0	1.55	0.167	35.8	1112: 03.8	+0.8	B3
	4-2	026	390.3	354.6	35.7	0.415	7938	48.22	67.99	1128: 53.6	2.18	0.401	27.4	1128: 52.9	-0.7	B2
	4-4	028	357.5	356.4	1.1	0.047	7190	24.04	79.00	1148: 56.2	1.43	0.079	33.4	1148: 55.5	-0.7	B2
	1-1	051	355.7	351.3	4.4	0.140	8528	24.04	27.53	0839: 48.4	1.36	0.157	25.8	0839: 47.8	-0.6	B2
	1-2	052	355.6	351.8	3.8	0.112	8097	21.74	25.14	0850: 06.2	1.72	0.120	30.7	0850: 05.9	-0.3	B2
	1-4	054	354.2	352.7	1.5	0.068	7280	16.57	31.12	0910: 32.6	1.47	0.084	29.9	0910: 32.1	-0.5	B2
	2-3	057	356.2	352.9	3.3	0.121	7711	32.08	64.26	0937: 18.8	1.38	0.131	29.4	0937: 18.4	-0.4	B3
	3-3	061	370.5	355.2	15.3	0.267	7757	40.32	56.64	1053: 28.6	1.13	0.285	28.9	1053: 27.4	-1.2	B3
4-3	065	363.4	353.8	9.6	0.218	7666	40.79	64.73	1133: 42.6	1.34	0.229	23.7	1133: 42.5	-0.1	B3	
4-4	066	360.0	354.4	5.6	0.158	7280	30.07	70.43	1143: 57.2	1.51	0.175	30.0	1143: 57.1	-0.1	B3	
10-28	1-1	095	339.4	329.3	10.1	0.227	8092	29.69	52.52	0832: 08.8	1.70	0.244	27.7	0832: 04.2	-4.6	B3
	3-1	101	337.6	334.2	3.4	0.097	8138	24.95	39.21	1013: 28.3	1.03	0.143	34.0	0813: 23.2	-5.1	B2
	1-1	104	340.8	335.4	5.4	0.188	8482	20.68	27.15	0835: 18.3	1.29	0.178	16.9	0835: 20.2	+1.9	B2
10-29	1-2	105	338.6	335.2	3.4	0.181	8029	21.31	37.78	0845: 49.6	1.00	0.143	23.6	0845: 52.1	+2.5	B2
	1-3	106	345.3	335.3	10.0	0.246	7621	30.98	40.55	0856: 36.9	1.80	0.247	19.7	0856: 39.2	+2.3	B3
	2-1	108	347.0	345.3	1.7	0.068	8863	18.72	36.53	1137: 26.9	0.95	0.097	30.6	0937: 24.5	-2.4	B2
	2-2	109	344.6	343.9	0.7	0.021	8455	20.16	36.63	1147: 59.7	1.14	0.114	30.6	1147: 59.7	-1.14	B2
	3-1	113	351.4	347.6	3.8	0.166	8863	27.77	37.11	1351: 25.6	1.64	0.181	14.6	0908: 36.0	+6.4	B2
	1-1	116	347.2	342.7	4.5	0.193	8437	25.62	46.97	0908: 23.6	1.71	0.140	23.8	0919: 11.8	+2.6	B2
10-30	1-2	117	346.0	342.7	3.3	0.193	8029	37.44	37.44	0919: 09.2	1.51	0.140	23.8	0919: 11.8	+2.6	B3
	1-4	119	349.6	343.9	5.7	0.161	7258	19.54	35.58	0939: 30.4	1.80	0.183	11.25	0939: 33.1	+2.7	B3

^aCalculated from shock wave arrival times at ground microphones

^bAverage value between 100 and 500 ft on tower

^cEquation (CB) was used with $(V_G \cdot V_p)$ values

Thus, an $(M - M_T)$ scale is also given in figure 8. The observed $(V_G - V_{p^* \max})$ versus Θ values agree reasonably well with theory.

Examination of the overpressure data in table 9 shows that in many cases relatively high values occurred for flight at Mach numbers well above the threshold value. These cases typically exhibited caustic-like pressure signatures, which were apparently produced by relatively low-magnitude airplane accelerations rather than by ray focusing due to the cutoff condition. These cases have been placed in a separate category, B3. Relatively low-magnitude accelerations from below the threshold Mach number could produce caustics similar to accelerations begun at subsonic Mach numbers. Variations of 5 m/sec (16.4 ft/sec) or more in the airplane ground speed were noted from the radar data, and these would be sufficient to produce caustics. In some cases the theoretical calculations are influenced by changes in the radar-observed airplane ground speed. In general, an acceleration results in overpressures higher than steady flight, while a deceleration results in lower overpressures. During steady flight at about Mach 1.2 the nominal theoretical maximum overpressure is about 28.7 N/m^2 (0.60 lb/ft^2) for shock waves observed on the tower (this value is approximately doubled at the ground due to reflection).

Figure 9 shows the variation of maximum overpressure measured on the tower near the cutoff condition. The cases where caustics were produced by accelerations are indicated by triangular data points. The cases for which cutoff occurred on the tower are plotted at zero $(V_G - V_{p^*})$ and are discussed in detail in a later section. These data indicate that the linear theory is fairly accurate to within $(M - M_T) = 0.01$ and $(V_G - V_{p^*}) = 2.0 \text{ m/sec}$ (6.6 ft/sec). In addition, these data indicate that accelerations can have an important effect near cutoff.

In general, the agreement between the theoretical calculations and the experimental data given in table 9 is good. The range of differences between the theoretical calculations and the observations for Θ , ΔP , and t_o is as follows:

$$\begin{aligned} \Theta & \approx \pm 0.0436 \text{ rad } (2.5^\circ) \\ \Delta P \text{ (with respect to } \overline{\Delta P_T}) & \approx \pm 17.0 \text{ N/m}^2 \text{ (} 0.35 \text{ lb/ft}^2 \text{)} \\ t_o & \approx \pm 1.0 \text{ sec (except } \pm 5.0 \text{ sec for cases with inversions)} \end{aligned}$$

In view of the sensitivity of the theoretical calculations to the airplane ground speed, the airplane ground speed as determined from the shock propagation speed over the ground microphones, $V_{G_{mic}}$, was used instead of the ground speed measured by the tracking radar for several cases. These results are given in table 10 for passes 015, 054, and 109. For these three cases use of $V_{G_{mic}}$ gives substantially better agreement.

TABLE 10.—EFFECT ON THEORETICAL BOOM ARRIVAL TIME OF USING $V_{G_{mic}}$ INSTEAD OF RADAR GROUND SPEED

Date	Bongo-pass	Pass	$V_{G_{mic}}$		t_o error using $V_{G_{mic}}$, sec	t_o error from table 9, sec
			m/sec	ft/sec		
8-25	1-2	015	364.1	1194.5	0.0	+0.4
8-31	1-4	054	354.2	1162.1	-0.1	-0.5
10-29	2-2	109	344.6	1130.6	—	-2.4

Shock wave profiles and pressure signatures.—The shock wave profiles and tower pressure signatures are shown in figures 10 through 13 for passes 101, 106, 117, and 028, respectively. The incident and reflected shock waves (onset of each) are plotted to scale so that Θ values can be read directly. In addition, the pressure signatures were converted to the same distance scale and are given along with the shock wave profiles. A time scale and overpressure scale are also shown for the pressure signatures.

The data for pass 101, given in figure 10, is a case where acceleration effects were not of great importance. The angle Θ for this case is about 0.105 rad (6°). A theoretical pressure signature is superimposed on the observed pressure signature at microphone T-13; the agreement in this case is very good. The incident N-wave at the lower tower levels appears to have been distorted by small-scale atmospheric turbulence.

As noted in the previous section, in several cases accelerations produced caustics for cases where the incident shock wave was not near cutoff. Two such cases are shown in figures 11 and 12 (passes 106 and 117, respectively). In both these cases a decayed pressure wave or pressure pulse precedes the basic caustic-like pressure signature. The angle of the incident shock front with the vertical, Θ , is about 0.1745 rad (10°).

Pass 028, shown in figure 13, is a particularly interesting case since Θ at the ground is about 0.01745 rad (1.0°). Here again, however, it appears that acceleration effects have produced the caustic-like pressure signatures rather than focusing due to the cutoff condition alone.

In several cases a series of pressure signatures were observed. In one case (pass 004) at the ground a "triple boom" was observed. Changes in airplane ground speed (decelerations as well as

accelerations) can produce such effects, since the propagation path is very dependent on the airplane Mach number, and shock waves emitted from different portions of the flight path may reach the same point at the ground at about the same time (see fig. 5).

Mach Number Near Threshold Value

Eleven flights produced shock waves that were cut off on the tower. The shock wave inclination angle for these cases was between 0 and 0.01745 rad (0 and 1°). The airplane ground speed was thus within 0.1 m/sec (0.3 ft/sec) of the shock propagation speed on the tower, and the airplane Mach number was within 0.0005 of the threshold Mach number. For these cases it was not possible to perform theoretical calculations, since the shock waves were too near cutoff. Table 11 contains a summary of the observed data for these cases.

It is interesting that the overpressure intensities on the tower for the cutoff cases are not appreciably greater than would be produced during steady flight at higher Mach numbers (about 28.7 N/m²; 0.60 lb/ft²), with the exception of pass 063 (see table 11). Thus, it would appear that accelerations through the threshold Mach number can produce caustics stronger than those produced by the cutoff phenomena.

Precursors.—A characteristic of pressure signatures near the cutoff condition is that pressure pulses or “precursors” are frequently evident propagating ahead of well-defined shock waves in the pressure signature. Precursors appear to be associated with near-sonic conditions, where disturbances generated by the shock wave can propagate ahead of it. In some cases several precursors could be seen. Henderson (ref. 36) has presented some theoretical work on this aspect of the cutoff phenomena. He shows that precursors can be stationary with respect to the shock wave (“bound”) or nonstationary (“free”). Bound precursors may be thought of as a detached shock moving ahead of a blunt body. The author shows that free precursors may be produced before actual cutoff. Postcursor waves propagating in the downstream direction also occur, but these were difficult to differentiate in the experimental data from acoustic-like disturbances that normally trail behind the main part of the pressure signature. In Figures 14 through 20 the onset of precursors is indicated by dashed lines and the onset of shock waves by solid lines.

Shock wave profiles and pressure signatures.—Figures 14 through 20 contain shock wave profiles and pressure signatures for the most interesting cases, where cutoff occurred on the tower. The pressure signatures are given to the same distance scale as the shock wave profiles; a time scale is also given for the pressure signatures.

TABLE 11.—SUMMARY OF CASES FOR WHICH CUTOFF OCCURRED NEAR THE GROUND (CATEGORY B1)

Date	Bongo-pass	Pass	Approximate cutoff altitude above ground, Z _c		Airplane ^a ground speed, V _G		Shock arrival time at mic T-1, PDT	Average tower maximum overpressure, ΔP _T max		Maximum tower overpressure		Tower mic no.	Ground reflection coefficient, K _R
			ft	m	m/sec	ft/sec		N/m ²	lb/ft ²	N/m ²	lb/ft ²		
8-24	1-2	002	1300	400	348.0	1141.7	0918:12.2	23.46	0.490	50.75	1.060	14	1.07
	3-4	010	1000	300	356.9	1170.9	1141:33.9	17.09	0.357	34.47	0.720	14	1.26
	4-1	011	0	0	360.2	1181.7	1210:02.5	17.33	0.362	25.28	0.528	2	1.18
8-31	2-4	058	600	180	351.0	1151.6	0947:44.8	30.64	0.640	46.01	^b 0.961	8	1.51
	3-2	060	1500+	460+	355.5	1166.3	1043:45.4	19.30	0.403	27.53	0.575	4	1.72
	3-4	062	1500	460	354.0	1161.4	1103:27.6	19.34	0.404	31.84	0.665	12	1.27
	4-1	063	900	275	353.0	1158.1	1112:34.0	54.82	1.145	134.93	2.818	12	1.25
10-28	3-2	102	800	245	332.0	1089.2	1025:49.2	24.99	0.522	38.40	0.802	11	0.74
	3-3	103	500	150	335.6	1101.0	1037:27.3	23.89	0.499	35.91	0.750	5	1.02
10-29	2-3	110	1500+	460+	340.0	1115.5	1157:55.5	16.28	0.340	21.83	0.456	1	1.52
	3-2	114	1500	460	341.4	1120.1	1401:12.7	27.82	0.581	39.17	0.818	9	0.89

^aFrom propagation speed, V_p, at cutoff altitude.

^bFor this case the observed maximum overpressure at microphone T-9 was 66.3 N/m² (1.385 lb/ft²); however, this value is in doubt since this microphone was not calibrated.

Passes 002 and 114, shown in figures 14 and 15, respectively, are two cases where cutoff apparently occurred very near the top of the tower. In both cases caustic-like pressure signatures occurred at the tower top preceded by a pressure rise, coincident with the shock wave becoming vertical to the ground ($\Theta = 0$). The shock waves decay rapidly with distance below the cutoff altitude, with acoustic-like disturbances occurring at the ground (but still identifiable as decayed pressure signatures).

For three cases cutoff occurred near midtower. These are shown in figures 16, 17, and 18. In each case caustic-like pressure signatures occur simultaneously with the shock wave becoming vertical ($\Theta = 0$). Pressure pulses propagating ahead of the basic signatures are evident. Passes 063 and 102 (figs. 17 and 18) are particularly interesting, since the incident and refracted shock waves that form the caustic at the cutoff altitude are evident. The pressure signature observed at microphone T-11 during pass 063 had the largest overpressure measured during the threshold Mach number flights. This maximum value was 135.0 N/m^2 (2.82 lb/ft^2). This pressure signature, however, appears to have been influenced by microscale turbulence.

Pass 103 (fig. 19) shows the effect of the varying propagation speed on the shock front orientation. In this case cutoff may have occurred above the tower because of an inversion in the propagation speed gradient, since Θ is negative at the tower top. Caustic-like pressure signatures are evident near the tower base where a second complete refraction occurred.

Overpressure variation near caustics.—The variation of shock wave strength in the vicinity of the caustic was determined from the data. Figure 21 gives the observed maximum overpressures with distance from the caustic for several cases where caustics associated with the cutoff condition ($\Theta = 0$) were observed on the tower. Amplified intensities occur only within about 100 to 200 m (330 to 660 ft) above and below the caustic. This suggests that linear theory is capable of predicting intensities to about 100 m (330 ft) above the caustic with reasonable accuracy, since the nonlinear effects that predominate at caustics become important at that distance.

The maximum overpressure observed on the tower was 135.0 N/m^2 (2.82 lb/ft^2) during pass 063. This signature, however, appears to have been influenced by microscale turbulence, with the high overpressure due to "spikes" superimposed on the front and rear shocks (see fig. 17). The next highest overpressure on the tower for these cases was about 51 N/m^2 (1.06 lb/ft^2), and is more representative of the caustic intensity produced by threshold Mach number flight. Compared to steady, level flight at about Mach 1.2 (which gives an intensity of about 28.7 N/m^2 (0.60 lb/ft^2) on the tower), the caustic amplification is about 1.8.

A fundamental consideration is whether the caustic intensity is related to the gradient of the shock propagation speed. A stronger caustic intensity would be expected where a large gradient in

propagation speed existed, and focusing would occur over a small altitude range. In this case there would be a rapid decay of intensity below the caustic. Passes 063 and 102 (figs. 17 and 18) can be considered to represent this situation. When the propagation speed gradient is small, however, the focusing would occur over a larger depth of the atmosphere, and only moderate amplification would be expected. In addition, caustic-like pressure disturbances may propagate a considerable distance below the actual caustic, particularly if an inversion exists in the propagation speed profile below the cutoff altitude. Figure 20 shows the data for pass 112, where cutoff occurred above the tower but caustic-like signatures of moderate intensity are observed on the tower. Thus, the meteorological conditions which produce the cutoff shock wave and associated caustic have a fundamental influence on the nature of the observed pressure signatures in the vicinity of the caustic.

Mach Number Less Than Threshold Value

Of the 79 threshold Mach number flights, 37 produced shock waves which were cut off above the tower. Relatively low-intensity acoustic disturbances were recorded on the tower and the ground, with overpressure levels less than 24.0 N/m^2 (0.5 lb/ft^2). In general, observers subjectively rated the disturbances for these 37 flights as rumbles (low, moderate, or heavy). In a few cases, however, they were rated as "low" or "very slight" booms, and in five cases cutoff occurred at an altitude high enough above the ground so that no booms or rumbles were observed. These 37 "rumble cases" provide information on the predictability of the cutoff altitude and on the nature of the acoustic noise that occurs below the cutoff altitude in terms of the known meteorological conditions. To aid in this analysis a number of measured and calculated parameters were determined and compared. These are shown in table 12.

The first of these parameters is the calculated propagation speed of the disturbance over the ground microphone array determined from the arrival times at the microphone locations. An average value over the length of the ground array was used. This propagation velocity is called $V_{p\text{mic}}$. The second parameter is the propagation speed, $V_p^*_{\text{max}}$, determined from the observed meteorological conditions in the vicinity of the tower. The effect of the presence of water vapor was taken into account (see appendix A). The maximum value of V_p^* from the tower meteorological measurements was used. In some cases, however, a significant inversion occurred in the V_p profile (on October 23 and October 30) so that the maximum value above the tower was noted in the table instead, since it determines the cutoff condition. The airplane ground speed, V_G , was obtained from the radar data. Since the exact portion of the flight path which produced the cutoff shock wave above the tower was not known, the accuracy of this speed is about $\pm 2 \text{ m/sec}$ ($\pm 6.6 \text{ ft/sec}$). Other parameters in table 12 include the theoretical cutoff altitude, Z_C , the average

TABLE 12.—SUMMARY OF RUMBLE CASES—THRESHOLD MACH NUMBER FLIGHT

Date	Bongo-pass	Pass	Calculated propagation speed, V_{pmic}		Observed V_{pmax} near ground		Airplane ground speed, V_G		$(V_{pmax} - V_G)$		Predicted cutoff altitude, Z_c		Safe altitude, Z_s		$\overline{\Delta P_G}_{max}$		Cate. gory ^a	Ground reflection coefficient, K_R
			m/sec	ft/sec	m/sec	ft/sec	m/sec	ft/sec	m/sec	ft/sec	m	ft	m	ft	N/m ²	lb/sq ft		
8-24	1-1	001	No Data	No Data	348.5	1143.4	341.1	1119.1	7.4	24.3	2225	7300	1550	5100	0.0	0.0	R1	—
	1-3	003	353.4	1159.4	351.2	1152.2	345.0	1131.9	6.2	20.3	2000	6600	1450	4800	2.82	0.059	R2	0.98
	2-2	005	352.0	1154.8	350.9	1151.2	341.4	1120.1	9.5	31.2	2225	7300	1650	5400	3.26	0.068	R2	0.88
	3-1	007	352.0	1154.8	352.5	1156.5	348.4	1143.0	4.1	13.5	1000	3300	750	2500	3.40	0.071	R2	1.35
8-25	3-2	008	353.0	1158.1	353.0	1158.1	347.5	1140.1	5.5	18.0	1300	4300	750	2500	2.97	0.062	R2	0.90
	3-3	009	353.1	1158.5	352.5	1156.5	349.0	1145.0	3.5	11.5	500	1600	450	1500	6.03	0.126	R3	1.28
	1-1	014	354.7	1163.7	355.0	1164.7	350.5	1149.9	4.5	14.8	350	1100	450	1500	9.67	0.202	R3	1.25
	2-3	019	(b)	(b)	353.5	1159.8	346.3	1136.1	7.2	23.6	1300	4300	600	2000	7.13	0.149	R2	1.88
8-31	3-2	023	356.0	1168.0	355.0	1164.7	348.4	1143.0	6.6	21.7	880	2900	700	2300	5.22	0.109	R2	1.87
	3-3	023	356.1	1168.3	356.5	1169.6	351.1	1151.9	5.4	17.7	400	1300	600	2000	10.61	0.225	R4	1.41
	4-1	025	355.2	1165.3	357.2	1171.9	349.6	1147.0	7.6	24.9	1000	3300	825	2700	9.58	0.200	R2	1.15
	4-3	027	353.1	1158.5	356.2	1168.6	356.6	1169.9	0.4	1.3	—	—	850	2800	16.61	0.347	R3	1.03
	1-3	053	353.0	1158.1	352.3	1155.8	349.0	1145.0	3.3	10.8	950	3100	600	2000	6.94	0.147	R2	1.58
	2-1	055	353.9	1161.1	352.9	1157.8	350.5	1148.3	2.9	9.5	580	1900	700	2300	10.66	0.226	R4	1.59
10-23	2-2	056	354.8	1164.0	352.9	1157.8	350.5	1149.9	2.4	7.9	300	1000	600	2000	18.75	0.398	R4	1.24
	3-1	059	354.2	1162.1	353.6	1160.1	353.6	1160.1	0.0	0.0	0	0	500	1600	7.42	0.158	R4	1.41
	4-2	064	357.5	1172.9	357.2	1171.9	354.0	1161.4	3.2	10.5	450	1500	700	2300	14.48	0.308	R4	1.45
	1-1	082	349.2	1145.7	350.0	1148.3	349.6	1147.0	0.4	1.3	—	—	?	?	19.73	0.419	R4	1.66
10-27	1-2	083	(b)	(b)	342.0	1122.0	342.0	1122.0	8.0	26.2	~2200	~7200	?	?	~0.0	~0.0	R1	—
	1-3	084	(b)	(b)	345.2	1132.5	345.2	1132.5	4.8	15.7	~2000	~6600	?	?	~0.0	~0.0	R1	—
	1-4	085	349.7	1147.3	349.0	1145.0	349.0	1145.0	1.0	3.3	—	—	?	?	9.11	0.193	R3	1.41
	2-1	089	327.5	1074.5	329.8	1082.0	325.2	1066.9	4.6	15.1	330	1100	400	1300	8.38	0.175	R3	0.87
10-28	2-2	090	329.6	1081.4	330.0	1082.7	321.6	1055.1	8.4	27.6	730	2400	600	2000	13.55	0.283	R2	1.02
	2-3	091	329.1	1079.7	330.4	1084.0	328.0	1076.1	2.4	7.9	250	800	450	1500	18.98	0.403	R4	0.87
	1-2	096	(b)	(b)	332.7	1091.5	327.4	1074.1	5.3	17.4	2070	6800	1500	4900	7.80	0.163	R2	0.92
	1-3	097	335.3	1100.1	333.3	1093.5	328.9	1079.1	4.4	14.4	1700	5600	1600	5200	10.68	0.223	R3	0.63
10-29	2-1	098	335.9	1102.0	334.5	1097.4	324.0	1063.0	10.5	34.4	2745	9000	2000	6600	8.57	0.179	R2	0.77
	2-2	099	No Data	No Data	334.6	1097.8	321.6	1055.1	13.0	42.7	3050	10000	1600	5200	~0.0	~0.0	R1	—
	2-3	100	No Data	No Data	336.3	1103.3	323.1	1060.0	13.2	43.3	2800	9200	1600	5200	~0.0	~0.0	R1	—
	1-4	107	336.0	1102.3	337.7	1107.9	335.3	1100.1	2.4	7.9	1500	4900	1750	5700	13.33	0.283	R4	1.71
10-30	2-4	111	346.3	1136.1	347.0	1138.4	339.5	1113.8	7.5	24.6	600	2000	450	1500	10.49	0.219	R2	1.48
	2-5	112	344.1	1128.9	344.4	1129.9	339.5	1113.8	4.9	16.1	850	2800	800	2600	7.52	0.160	R4	0.84
	3-3	115	348.5	1143.4	347.3	1139.4	339.2	1112.8	8.1	26.6	550	1800	450	1500	6.66	0.139	R2	0.85
	1-3	118	348.4	1143.0	345.6	1133.8	344.4	1129.9	d4.0	d13.1	1500	4900	1900	6200	12.50	0.261	R4	1.54
10-30	2-1	120	350.7	1150.6	c348.6	c1143.7	346.0	1135.2	d4.7	d15.4	~2500	~8200	2200	7200	7.57	0.158	R2	1.65
	2-2	121	351.1	1151.9	c348.6	c1143.7	349.0	1145.0	d2.1	d6.9	—	—	2200	7200	21.80	0.463	R4	1.53
	2-3	122	353.7	1160.4	c349.0	c1145.0	349.0	1145.0	d4.7	d15.4	—	—	2200	7200	13.74	0.292	R4	1.72

^aCategories: R1 = no rumble; R2 = low rumble; R3 = moderate-heavy rumble; R4 = light boom.

^bDiscrete signature features could not be traced to determine time increment over microphone array.

^cFor these passes an inversion existed in the V_p profile, therefore V_{pmax} was used instead of V_{pmin} on tower.

^d V_{pmic} was used instead of V_{pmax} .

observed maximum overpressure of all 16 ground microphones, $\overline{\Delta P_{G_{\max}}}$, the subjective category of the disturbance, and the ground reflection coefficient, K_R as determined from several of the ground and tower maximum overpressures.

The theoretical "safe" altitude, Z_s is also given in table 12. A discussion of this parameter is given in appendix D. The safe altitude is defined to be the minimum altitude above the ground where cutoff can occur so that the disturbances which reach the ground will be acoustic in nature with significantly reduced overpressure intensity. The safe altitude is a strong function of the prevailing meteorological conditions. During the BREN tower tests it ranged from 400 m to about 2200 m (1300 to 7200 ft) above the ground.

Figure 22 shows the comparison between the airplane ground speed, V_G , and the shock propagation speed, $V_{p^*_{\max}}$. In theory, cutoff should occur where these two are equal. For cutoff above the ground, the airplane ground speed must be less than $V_{p^*_{\max}}$. The data indicate this to be true for these rumble cases. As the airplane ground speed approaches $V_{p^*_{\max}}$, the moderate-to-heavy rumble and light boom cases predominated. For $(V_{p^*_{\max}} - V_G) > 6.0$ m/sec (>19.7 ft/sec), low rumbles occurred.

Figure 23 shows the comparison between the observed shock propagation speed determined from arrival times at the ground microphones, $V_{p_{\text{mic}}}$, and the propagation speed as determined from the meteorological conditions, $V_{p^*_{\max}}$. The two agree very well, which indicates that these disturbances are propagating at the local speed of sound, V_{p^*} , rather than at the slower airplane ground speed, V_G (see fig. 22). The range of $(V_{p_{\text{mic}}} - V_{p^*_{\max}})$ is from -3.1 m/sec to +4.7 m/sec (-10.2 to +15.4 ft/sec), with all but five cases within ± 2.0 m/sec (± 6.6 ft/sec).

The variation of the overpressure with cutoff altitude was also determined. This type of analysis would be required to determine an empirical ground speed "safety factor" for commercial threshold Mach number operations to avoid objectionable noise on the ground. Figure 24 shows the variation of the average overpressure of all 16 ground microphones, with the speed increment $(V_{p^*_{\max}} - V_G)$. A ground speed increment or "safety factor" of about 6 m/sec (19.7 ft/sec) is indicated if low rumbles are to be permitted, while a safety of over 10 m/sec (33 ft/sec) would be necessary for these test conditions if it were desired to produce no noise at the ground.

It is interesting that some of the low rumble cases for $(V_{p^*_{\max}} - V_G)$ between 5 and 10 m/sec (16 and 33 ft/sec) have a higher average overpressure at the ground than the heavy rumble and low boom cases. This is most likely due to differences in rise times of the observed pressure signatures, with the more subjectively objectionable noise associated with the shorter rise times. Typical pressure signatures for these cases are sketched on figure 24.

A theoretical safe altitude, Z_s was computed for each rumble-producing flight and was correlated with the subjective observations. The theoretical safe altitude computed is strictly valid only in the case of constant lapse rate of V_p^* , so only order of magnitude comparisons could be expected. In general, the lapse rates observed during the tests varied considerably with altitude above the ground. Safe altitudes are given in table 12 for each flight. Figure 25 shows the variation of the overpressure on the ground with the difference between the theoretical cutoff altitude and safe altitude, $(Z_c - Z_s)$. For positive $(Z_c - Z_s)$ values, cutoff is higher than the safe altitude and low rumbles would be expected at the ground. When cutoff occurred below the theoretical safe altitude, heavy rumbles or low booms would be expected. Figure 25 shows that the transition to low rumbles for these data occurs at a value of $(Z_c - Z_s)$ of about +120 m (+400 ft). Thus, the safe altitude was underestimated for these data. The correlation indicated by these results is encouraging and indicates that the concept of a safe altitude may be of operational value.

Ground Reflection Coefficient

Reflection of shock waves from the ground influences the observed overpressure magnitude. For regular reflection of weak oblique shock waves, K_R is close to 2.0 (i.e., the observed overpressure is twice the incident overpressure). At the cutoff condition there is no reflection, so K_R should be near 1.0. The manner in which K_R varies close to cutoff was studied by Thomas (ref. 37) and Thery (ref. 38). These authors used the one-dimensional flow relationships to show that irregular reflection may occur close to cutoff where K_R may increase to 3.0 before decreasing to 1.0 at cutoff.

The method described in an earlier section was used to estimate K_R for the threshold Mach number flights. The resulting data were given in tables 9 and 11 of earlier sections. These data for categories B1, B2, and B3 have been plotted in figure 26. In general, there is a large scatter in the results, which is to be expected since the method used to determine K_R from the measurements is somewhat crude. The K_R values for cases well before cutoff vary from the 0.95 to 2.2. There does not appear to be any increase in K_R near cutoff, but rather a gradual decrease is suggested, beginning at about 0.175 rad (10°) from cutoff. This result suggests that the one-dimensional analysis by Thomas (ref. 37) and Thery (ref. 38) is not realistic. A two-dimensional analysis taking into account the axisymmetric nature of the actual flow may give better agreement with this experimental data. For the cases categorized as rumbles or low booms (table 12) K_R varied from 0.63 to 1.88, with an average value of 1.27. For some of these cases, however, the angle of incidence, θ , was appreciable due to an inversion in the V_p profile. This condition existed on October 23 and October 30, and K_R averaged 1.59 with a range of 1.41 to 1.72 for these six cases. The remaining rumble cases then average 1.20.

Analysis of Pressure Signatures

The pressure signatures observed in the vicinity of caustics produced by threshold Mach number flight are significantly different from pressure signatures produced at higher Mach numbers. Nonlinear effects predominate at caustics, and the linear theory is not valid. Analysis of these caustic pressure signatures may be helpful in isolating these important nonlinear effects.

Figure 27 shows the six "best" caustic pressure signatures observed, together with the linear theory steady, level pressure signatures at a slightly higher Mach number ($\Delta P_{\max} = 28.7 \text{ N/m}^2$ (0.59 lb/ft²)). Compared to the theoretical signatures these caustic signatures are of stronger intensity, longer duration, and exhibit the U-shape characteristic of caustics (rather than the well-known N-wave shape). The increase in overpressure for these six cases from the linear theory overpressure away from caustics ranges from 29% to 76%. It appears that small-scale turbulence may have produced spikes on the caustic pressure signature measured for pass 063 which resulted in an overpressure increase of 478%. Suspicion of this type of interaction stems from the sharpness of the spike (i.e., very small time duration) and the time delay between the initial pressure rise and the spike. Signatures of this nature are common for the temperature and wind conditions present near the ground during this series of flights.

The duration of the theoretical pressure signature away from caustics is about 0.10 sec. The duration of the observed caustic pressure signatures, however, ranges from about 0.135 to 0.140 sec, an increase of about 40% from linear theory. This increase in duration of the caustic pressure signatures can be caused by two effects—the aging caused by the long propagation path for the cutoff rays and nonlinear effects that become important very close to the caustic.

Summary of Threshold Mach Number Data

The analysis of the threshold Mach number data has provided valuable definitive information on the nature of shock waves produced by flight at speeds slightly greater than the threshold value, at the threshold value, and below the threshold value. At speeds greater than the threshold value, regular sonic booms are observed and linear sonic boom theory agrees very well with observed data. During several of the flights at speeds well above the threshold Mach number, however, caustics were observed. These caustics apparently were not produced by the cutoff condition but rather by relatively low-magnitude changes in the airplane speed. The maximum observed caustic intensity for these cases was 82.4 N/m^2 (1.72 lb/ft²), which gives an amplification factor of about 3 (compared to steady, level flight at slightly higher Mach numbers).

Several flights produced caustics on the tower associated with the cutoff condition. These cases have helped to define the caustic phenomena more clearly. Significant increases in overpressure occur within about 100 m (330 ft) above and below the caustic. However, for these flights the caustic intensities were only about 25 to 50 N/m² (0.5 to 1.1 lb/ft²). This is an amplification of 1 to 1.8 compared to steady, level flight. For one case, however, an overpressure of 135.02 N/m² (2.82 lb/ft²) was measured where very sharp peaks characteristic of signature distortions due to microscale turbulence in the pressure signature occurred. Observed pressure signatures in the vicinity of caustics have a duration that is about 40% greater than pressure signatures produced at higher Mach numbers.

Almost half of the threshold Mach number flights produced rumbles or low booms at the ground, since cutoff occurred above the tower. Analysis of the propagation speed of these disturbances at the ground showed that they propagate at the local sound speed, which was faster than the airplane ground speed. When low rumbles were produced on the ground, the airplane ground speed was at least 6 m/sec (19.7 ft/sec) lower than the maximum shock propagation speed. Comparison of a theoretical "safe altitude" for sonic boom cutoff (for which no objectionable noise would reach the ground) with the observed data was good considering the assumptions made in deriving it.

The analysis of the ground reflection coefficient indicates a gradual decrease in K_R from 2.0 to about 1.0 beginning at a shock wave angle of about 0.175 rad (10°) with respect to the vertical.

ANALYSIS OF LONGITUDINAL ACCELERATION FLIGHT TEST DATA

This section contains a discussion and presentation of the results of the analysis of the sonic boom measurements obtained from the 19 longitudinal acceleration flights. A brief description is given of the generation of the acceleration caustic, followed by presentation of the test measurements and their comparison with linear sonic boom theory.

Introduction

The caustic produced by a longitudinal acceleration will be produced by SSTs during the acceleration from subsonic to supersonic flight. In terms of sonic boom, a caustic is a cusp or fold that exists in a shock surface. During longitudinal accelerations through Mach 1, a cusp is formed because the Mach number increases with time along the flight path. Figure 28 illustrates the development of shock waves and the caustic formation during acceleration from subsonic to supersonic Mach numbers. A single magnified sonic boom signature is observed at the caustic. As the acceleration continues, the caustic eventually reaches the ground, and is the first part of the shock wave to reach the ground.

The caustic locus is the line which defines the progressive intersection of the caustic with the ground (see fig. 28) as it forms at progressively greater lateral distances from the flight path. In the region immediately surrounding the caustic locus, two or more pressure signatures are observed, one of which is somewhat stronger than the steady-flight signature but has nearly the same shape. At the caustic these two signatures are merged, forming a U-shaped signature. As the acceleration progresses, the caustic is reflected from the ground and the leading shock travels progressively farther ahead of the trailing shock until finally the trailing shock is completely refracted, so that only one pressure signature is observed.

Two other U.S. flight test programs designed to provide measurements near caustics produced by longitudinal accelerations have been conducted prior to the 1970 BREN tower tests. The first tests were done in September and October 1961 at Edwards AFB (ref. 17). A total of seven longitudinal acceleration flights were performed; four of these cases are discussed in more detail in reference 16. A second test series consisting of five acceleration flights were conducted at Edwards AFB during October 1964 (ref. 18). These early tests, while of good quality, did not have the required microphone density to obtain definitive measurements near caustics.

“Operation Jericho-Virage,” conducted by the French, provided the first definitive measurements of caustics. The resulting test data are documented in reference 26. These tests showed the necessity for using a dense network of microphones to observe the acceleration caustic. In addition, the theory of geometric acoustics was shown to be adequate for predicting caustic occurrences on the ground.

Table 13 summarizes the 19 longitudinal acceleration flights conducted during the 1970 BREN tower tests. The nominal flight conditions for these flights were:

Airplane altitude—10.3 km (33 700 ft)

Initial Mach number—0.95

Final Mach number—1.3

Airplane heading—035° (true North)

Acceleration magnitude—about 1.1 to 1.6 m/sec² (3.7 to 5.1 ft/sec²)

Table 13 contains the airplane weight, the maximum observed overpressure, boom time at microphone T-1, and an indication of the type of boom observed for each flight. About half the flights placed the acceleration caustic on or near the microphone array.

In the next section the results of the comparison between theoretical and observed caustic locations are given. Then the sonic boom measurements are presented in three sections, according to nearness of the tower to the caustic-ground intersection. In the last section, sonic boom intensities predicted by the linear theory are compared with observed intensities near the caustic, and the nature of the caustic pressure signature is discussed.

Caustic-Ground Intersection—Theory and Experiment

A relatively simple method for calculating caustic locations numerically is described in appendix B of reference 33. Appendix C of reference 33 contains a comparison of the predicted caustic locations with observed caustic locations for five longitudinal acceleration flights from the French “Jericho-Virage” tests (ref. 26). The error of the predicted caustic locations ranged from -1.37 to +0.69 km (-0.85 to +0.43 st mi). The error quoted in reference 26 for the French computer program “STROUM” for the same flights ranged from -2.0 to +2.4 km (-1.24 to +1.49 st mi). Both the method described in reference 33 and computer program “STROUM” are based on the linear theory of geometric acoustics, but the numerical calculation procedures are considerably different.

In the calculation of theoretical caustic locations for the 19 BREN tower acceleration flights, the method of references 7 and 30 was used. This required the calculation of ray trajectories at

TABLE 13.—SUMMARY OF LONGITUDINAL ACCELERATION FLIGHT TEST CONDITIONS^a

Date	Bongo-pass	Pass	Airplane altitude, h		Airplane weight, W		Boom time at tower base, PDT	Maximum observed overpressure			Subjective boom character	
			m	ft	Kg	lb		N/m ²	lb/ft ²	Mic no.		
8-28	1-1	b038	10.27	33 700	8525	18 800	—	—	—	—	No Boom	
	1-2	039	→	→	8025	17 700	0848:48.380	16.18	0.338	—	Rumble	
	1-3	040	→	→	7575	16 700	0857:28.661	93.94	1.962	G-9	Sharp Double Boom	
	2-1	041	→	→	8400	18 500	—	No Data - Recorder	Not On	—	—	
	2-2	042	→	→	8000	17 600	—	~0.0	~0.0	—	Rumble	
	2-3	043	→	→	7575	16 700	0957:19.874	137.32	2.868	G-1	Near Superboom	
	3-1	044	→	→	8575	18 900	1033:40.392	31.22	0.652	T-14	Near Superboom	
	3-2	045	→	→	8075	17 800	1043:48.723	197.12	4.117	G-9	Superboom	
	3-3	046	→	→	7575	16 700	1055:28.108	240.36	5.020	G-8	Superboom	
	3-4	047	→	→	7150	15 800	1106:19.141	139.14	2.906	G-12	Superboom	
	4-1	048	→	→	8525	18 800	—	~0.0	~0.0	—	Rumble	
	4-2	049	→	→	8125	17 900	1214:19.633	44.05	0.920	T-14	Boom-Rumble	
	4-3	050	→	→	7650	16 900	—	~0.0	~0.0	—	Rumble	
	10-27	1-1	086	10.21	33 500	8000	17 650	0843:47.242	41.42	0.865	G-7	Double Boom
		1-2	087	→	→	7650	16 850	0853:31.931	62.20	1.299	G-8	Boom-Rumble
1-3		088	→	→	7325	16 150	0904:13.744	140.82	2.941	G-9	Superboom	
3-1		092	10.06	33 000	8000	17 650	1146:58.628	137.32	2.868	G-1	Superboom	
3-2		093	→	→	7650	16 850	1158:34.954	169.35	3.537	G-14	Superboom	
3-3		094	→	→	7275	16 050	1210:49.308	128.99	2.694	G11	Superboom	

^aAirplane heading = 035°; Airplane Mach number ~ 0.95 to 1.3.

^bOn this flight the acceleration was terminated at M = 1.07.

small flight time increments. These theoretical caustic locations were then referenced with respect to the tower. Figure 29 shows calculated caustic locations for pass 045. Three calculated caustic locations are shown. One was calculated using rawinsonde data alone (S), another using all available meteorological data including the BREN tower and ATMS data (T), and the third using virtual temperature in place of ambient temperature for the T data (T_v). The three different meteorological conditions change the caustic location slightly, but it should be remembered that T and T_v differ from S in the lowest 2 km (1.24 st mi) only. Thus, it would appear the upper level meteorological conditions are more important, particularly the wind conditions near the airplane altitude. In this case the wind was from the SSE, so that the ray directly beneath the airplane ($\phi = 0$) was displaced slightly to the NW.

Figure 30 shows the calculated and observed caustic locations for pass 093. For this case there was very good agreement between theory and experiment. The wind was generally from a northerly direction, so that the $\phi = 0$ ray was displaced to the SE.

Table 14 gives the theoretical and observed caustic locations with respect to the tower for the remainder of these flights. The flights have been separated into categories according to nearness to the caustic. For seven flights the caustic passed over the tower and intersected the ground downtrack, so that only rumbles or low booms were observed at the tower. For three flights the caustic occurred well before the tower, so that regular sonic booms were observed. For eight of the flights, however, the acceleration caustic occurred on or near the microphone array. For these cases it is possible to make a more accurate comparison of theoretical and observed caustic locations. The errors in the theoretical caustic locations are summarized in table 14. The error ranges from -1.6 to +0.5 km (-1.0 to +0.3 st mi). A histogram of the errors is given in figure 31. The errors for passes 044, 045, 046, 047, and 049 are all negative, suggesting that the rawinsonde wind data near the airplane altitude are not quite accurate (the same rawinsonde observation was used for all of these cases). For these flight conditions a *decrease* of only 3.7 m/sec (12 ft/sec) in the tailwind component is required to cause the caustic to occur 1.0 km (3300 ft) farther downtrack. From the rawinsonde observation the tailwind component at the airplane altitude is about 18 m/sec (60 ft/sec), so that a slight change in wind direction and/or magnitude could have produced such a change.

The error in the theoretical caustic locations (for the seven cases when the caustic occurred on or near the microphone array) ranged from -1.6 to +0.6 km (-1.0 to +0.4 st mi). The range of error is very similar to the error for the five acceleration caustics of the Jericho-Virage tests referenced earlier (-1.4 to +0.7 km, -0.9 to +0.4 st mi).

TABLE 14.—COMPARISON OF THEORETICAL GROUND CAUSTIC LOCATIONS WITH OBSERVED SHOCK WAVE CHARACTERISTICS—LONGITUDINAL ACCELERATION

Date	Bongo-pass	Theoretical caustic location from tower		Actual caustic location from tower		Error		Maximum overpressure observed		Comments
		km	ft	km	ft	km	ft	N/m ²	lb/ft ²	
A) Rumble or Low Boom Cases (Caustic Occurred Downtrack From Tower)										
8-28	1-1	—	—	—	—	—	—	—	—	No boom since acceleration terminated at Mach 1.07
	1-2	+1.4	+4600	>+1.6	>+5200	<-0.2	<-600	16.2	0.338	Rumble
	2-2	+0.2	+650	>+1.5	>+4900	<-1.3	<-4250	~0.0	~0.0	Light rumble
	3-1	+0.3	+1000	~+1.5	~+4900	~+1.2	~-3900	31.2	0.652	Moderate rumble, max ΔP near tower top
	4-1	+2.3	+7500	>+1.5	>+4900	<+0.8	<+2600	~0.0	~0.0	Light rumble
	4-2	+0.8	+2600	~+1.4	~+4600	~+0.6	~-2000	44.05	0.92	Low boom, max ΔP near tower top
	4-3	+1.9	+6200	>+1.5	>+4900	<+0.4	<+1300	~0.0	~0.0	Low rumble
B) Caustic Near Tower										
8-28	2-3	—	—	~+0.7	~+2300	—	—	137.3	2.868	Caustic prior to G-1
	3-2	-0.7	-2300	+0.1	+300	-0.8	-2600	197.1	4.117	
	3-3	-1.5	-5000	+0.1	+300	-1.6	-5300	240.4	5.020	
	3-4	-1.0	-3300	+0.2	+650	-1.2	-3950	139.1	2.906	
10-27	1-3	-0.8	-2600	+0.1	+300	-0.9	-2900	140.8	2.941	Caustic location could be +0.1 to +0.2
	3-1	0.0	0	-0.6	-2000	+0.6	+2000	137.3	2.868	Double boom
	3-2	+0.4	+1300	+0.4	+1300	0.0	0	169.4	3.537	Caustic just prior to first microphone
	3-3	+0.6	+2000	+0.4	+1300	+0.2	+700	129.0	2.694	
C) Double Boom Observed at Tower (Caustic Occurred Before Tower)										
8-28	1-3	-4.6	-15 000	—	—	—	—	93.9	1.962	High peak (spike), second boom weak
10-27	1-1	-5.2	-17 000	—	—	—	—	41.4	0.865	Second boom weak, well behind
10-27	1-2	-2.6	-8 500	—	—	—	—	62.2	1.299	Second boom weak

^aFor passes 041 and 043 no airplane radar data are available, and for pass 041 there are no sonic boom data.

Comparison of Observed and Theoretical Boom Arrival Times

For cases when sonic booms were observed on the tower, a comparison between theoretical and observed boom arrival times can be made. Theoretical arrival times can be calculated since the airplane position with time is known and since the sonic boom propagation time can be calculated for the ray trajectory which intercepts the tower base. The accuracy of the airplane position with time (i.e., radar accuracy), when translated to boom arrival time, is about ± 0.2 sec. Errors of this magnitude can be attributed to the radar tolerance in the airplane position. Table 15 shows the comparison between observed and theoretical boom times. For two cases the arrival times at microphone G-14 were used, since the caustic (which is the first part of the sonic boom to occur on the ground) occurred past the tower and thus no theoretical arrival time at the tower base was predicted. The maximum error in the predicted arrival times for the 10 cases shown in table 15 is ± 1.0 sec. It may be significant that for *all* flights on August 28 the theoretical arrival times were too early, while for *all* flights on October 27 the theoretical arrival times were too late. This is consistent with the predicted caustic location errors shown in table 14. When an early arrival time was predicted, an "early" caustic location was also predicted (farther uptrack). The wind on August 28 was a tailwind, while on October 28 a headwind prevailed at the airplane altitude.

TABLE 15.—COMPARISON OF OBSERVED AND THEORETICAL BOOM ARRIVAL TIMES

Date	Pass	Bongo-pass	Observed boom arrival time, PDT (mic. T-1)	Theoretical boom arrival time at tower base, PDT	Error, sec
8-28	040	1-3	0857:28.7	0857:27.7	-1.0
	045	3-2	1043:48.7	1043:48.6	-0.1
	046	3-3	1055:28.1	1055:27.9	-0.2
	047	3-4	1106:19.1	1106:18.6	-0.5
10-27	086	1-1	0843:47.2	0843:47.7	+0.5
	087	1-2	0853:31.9	0853:32.7	+0.8
	088	1-3	0904:13.7	0904:14.3	+0.6
	092	3-1	1146:53.6	1146:54.4	+0.8
	093	3-2	^a 1158:36.4 (G 14)	^a 1158:36.6 (G-14)	+0.2
	094	3-3	^a 1210:51.0 (G-14 +122 m 400 ft)	^a 1210:52.0 (G-14 + 122m 400 ft)	+1.0

^aFor these cases the caustic occurred downtrack of tower so arrival times at microphone G-14 were used.

Measurements Uptrack from Caustic-Ground Intersection

Seven of the 19 acceleration flights produced caustics which passed over the tower, so that only rumbles and acoustic disturbances were observed (see table 13). For several of these cases it was possible to compute profiles of the acoustic fronts from measurements obtained on the BREN tower. Figure 32 shows the acoustic front locations (indicated by dashed lines) at the given reference times for passes 039, 044, and 049. The arrival time at microphone T-1 was used as the reference. In all cases the onset of the waves was used as a reference point to determine arrival times.

The predicted and extrapolated caustic paths are indicated in figure 32. The caustic paths were estimated from the approximate caustic-ground intersections downtrack of the tower. Figure 32 shows that the acoustic waves were oriented like a shock wave, and reflections from the ground are evident. The observed acoustic waves appear to be extensions of the caustic, which has a finite limit but produces acoustic disturbances that extend several thousand feet below it. Since the caustic is a moving source of disturbances, the acoustic wave would be oriented like a shock wave. For these cases it propagated over the ground (parallel to it) at a speed about 7% faster 20 m/sec (65.6 ft/sec) than the local sound speed near the ground.

Figure 33 shows the pressure signatures observed on the tower for pass 049. While the signature looks very much like a typical N-wave, its time duration is about 20% greater than normal and it decays rapidly to an acoustic-type wave near midtower.

Measurements Near Caustic-Ground Intersection

Eight of the accelerations produced caustics on or near the microphone array. These measurements represent unique and valuable information on the nature of the caustic phenomena. Shock wave profiles are presented in this section for all of these cases, and observed pressure signatures on the tower and ground arrays are presented and discussed for most of them.

Figure 34 shows the shock wave profiles for passes 043 and 092. For both of these cases the caustic intercepted the ground slightly uptrack of the ground microphone array. The observed pressure signatures on the ground during pass 043 are given in figure 35, while the tower data are given in figure 36. The caustic intersected the ground uptrack of microphone G-1, and the leading and trailing shock waves separated as the shock wave system propagated from microphone G-1 to G-14. On the tower (fig. 36) the incident leading shock is well defined, while the incident trailing shock is weak. The reflected shocks merge just above the tower top to produce the caustic. Some portions of pressure signatures have been omitted in figure 36 to fit them on a single page.

Figure 37 shows the tower pressure signatures for pass 092. The incident trailing shock is somewhat better defined in this case and shows the typical U-shape characteristic of shock waves that have passed through the caustic. A moderate-intensity caustic can be seen at microphones T-9 and T-10 where the reflected shocks have merged.

Five of the caustic cases (passes 045, 046, 047, 093, and 094) are basically similar in character, since in each case the caustic was incident on the lower half of the tower. Shock wave profiles and observed pressure signatures are given in figures 38 through 46. In all of these cases the ground pressure signatures show acoustic-like disturbances occurring uptrack from the caustic-ground intersection. In most cases there is a rapid increase in overpressure within a few hundred feet of the caustic. Downtrack from the caustic the overpressure decreases with distance as the leading and trailing shock waves progressively separate.

The tower pressure signatures and shock wave profiles for these five cases reveal a number of significant features. Above the caustic location on the tower the leading and trailing shocks are separated by a relatively small distance, which progressively decreases until they are merged at the caustic. Below the caustic, significant disturbances can occur for several hundred feet, but generally within 150 to 300 m (500 to 1000 ft) below the caustic (or after reflection from the ground), these disturbances are of relatively low magnitude and acoustic-like in nature. The pressure signatures near caustics exhibit the typical U-shape noted in previous flight tests. There is considerable variation in the maximum overpressures, however, and in signature shapes.

Pass 046 is of particular interest since it produced the most intense caustic measured. The maximum overpressure at microphone G-8 was 240.4 N/m^2 (5.02 lb/ft^2), and at microphone T-2 a maximum overpressure of 134.3 N/m^2 (2.805 lb/ft^2) was recorded (for a ground reflection coefficient of 2.0 this becomes 268.6 N/m^2 (5.61 lb/ft^2)). A distinguishing feature of pass 046 is that the distance between the leading and trailing shocks just above the caustic is significantly greater than for the other cases. The separation distance between the leading and trailing shocks increases with increasing airplane acceleration magnitude. This suggests that the acceleration may have been greater for pass 046, which resulted in the stronger caustic.

To determine the effect of airplane acceleration on the caustic strength, airplane acceleration magnitudes were determined from the unsmoothed radar observations. A 7-sec flight time interval over which the shock waves near the caustic were generated by the airplane was used to calculate the average instantaneous acceleration. The distance between the leading and trailing shock waves is also related to the airplane acceleration. An arbitrary distance of 300 m (1000 ft) above the approximate caustic altitude was selected for measuring the shock wave separation, which was read directly from the shock wave profiles and is plotted in the upper half of figure 47. The maximum observed tower overpressures and shock separation distances are tabulated in table 16 and plotted in

figure 47. The data indicate a trend toward increasing caustic intensity with increasing acceleration magnitude.

TABLE 16.—EFFECT OF ACCELERATION ON CAUSTIC STRENGTH

Date	Bongo-pass	Pass	Maximum overpressure observed on tower			Shock separation at 300 m, (984 ft)		Airplane acceleration from radar, A	
			N/m ²	lb/ft ²	Mic no.	m	ft	m/sec ²	ft/sec ²
8-28	3-2	045	109.6	2.29	T-2	25	82	1.27	4.2
	3-3	046	134.5	2.81	T-2	92	300	1.48	4.9
	3-4	047	93.4	1.95	T-4	35	115	^a 1.25	4.1
10-27	1-3	088	112.0	2.34	T-2	50	164	1.34	4.4
	3-2	093	107.3	2.24	T-7	60	197	^a 1.36	4.5
	3-3	094	80.0	1.67	T-5	20	66	1.26	4.1

^aFor these flights the detailed radar data are suspect over the flight path interval of interest; therefore a longer averaging period was used.

The last case (pass 088) is particularly interesting since it is anomalous when compared with other acceleration caustic cases. The shock profile for pass 088 is shown in figure 48 and indicates the nature of the anomaly. It appears that a caustic was produced uptrack of the tower (similar to pass 043, fig. 34). A second caustic, however, and leading-trailing shock wave system, also occur where in previous cases a trailing shock wave alone occurs. The measured pressure signatures for this flight are shown in figure 49.

The presentation of the observed pressure signatures on the tower and ground, along with the calculated shock wave profiles, has shown that the caustic is formed at the cusp in the shock front where the leading and trailing shocks merge. The observed pressure signatures exhibit the characteristic U-shape, with sharp peaks at the bow and tail shocks. The maximum observed intensity was 240.4 N/m² (5.02 lb/ft²). There is some evidence to suggest that acceleration magnitude may affect the caustic intensity.

Measurements Downtrack from Caustic-Ground Intersection

For three of the acceleration flights (passes 040, 086, and 087) the caustic occurred well before the tower (about 2 to 5 km (1.2 to 3.1 st mi) from tower) so that a leading shock wave was observed, with a weak trailing shock wave following well behind the first shock wave. Figure 50 shows the shock wave geometry system for pass 040 constructed from the tower arrival times. The leading and trailing shocks were separated by about 150 m (500 ft) at the ground. For this reference time the caustic occurred on the ground uptrack and passed above the tower, since it had been reflected earlier from the ground. The estimated caustic path is indicated.

Figure 51 is a reproduction of the pressure signatures observed on the ground for pass 040. The occurrence of "spikes" on many of the leading pressure signatures was believed to be due to the effects of small-scale atmospheric turbulence rather than airplane acceleration (refs. 20-22). The trailing signatures are much lower in magnitude and exhibit the U-shape characteristic of pressure signatures near caustics or those that have passed through it. The trailing signatures have thus been influenced by nonlinear effects.

Figures 52 and 54 illustrate the shock wave profiles for passes 086 and 087, respectively. As in pass 040, the trailing shock wave is well behind the leading shock wave, with the caustic occurring well above the tower after reflection from the ground. Observed ground pressure signatures are given in figures 53 and 55.

For these three passes it is possible to compute theoretical pressure signatures for the leading shock waves. The linear theory is not valid in the case of the trailing shock waves, since these have passed through the caustic and have been influenced by nonlinear effects. Figure 56 gives a comparison between calculated pressure signatures ($K_R = 1.0$) and observed tower pressure signatures for passes 040, 086, and 087. In each case two tower signatures are given. The comparison between theory and experiment is reasonably good. In general, the calculated signature lengths and intensities agree fairly well. Considerable variation in the observed pressure signatures can be seen. These variations are believed to be caused by the effects of small-scale atmospheric turbulence not accounted for in the linear theory. The small-scale turbulence causes spikes and rounded signatures to occur alternately over small distances (refs. 20-22).

Overpressure Variation Near Caustics--Theory and Experiment

The linear theory of sonic boom propagation is not valid near caustics since, in the concept of ray-tube area from geometric acoustics theory, higher order effects have been ignored. The ray-tube area, A , is related to the sonic boom overpressure, ΔP , in the following manner:

$$\Delta P \propto (A)^{-1/2} \quad (8)$$

Thus, near caustics where the ray-tube area becomes small, the overpressure becomes correspondingly large. At a caustic, where it is zero, an infinitely large overpressure is predicted, and the linear concept of ray-tube area is no longer valid. A fundamental consideration, then, is how close to caustics the linear theory is valid. A comparison with the experimental data is made in this section to empirically determine this limit.

Passes 045, 046, and 092 were selected for comparison with linear theory since for these cases caustics were produced before or near the BREN tower. Thus, overpressure data were available just downtrack of the caustic where the theory could be compared. Figures 57 through 59 give the overpressure variations near caustics for these cases. Two maximum overpressures are given, one for the leading shock, ΔP_1 , and one for the trailing, caustic-like shock wave, ΔP_2 . At the caustic these are superimposed. The linear theory applies only to the leading shock wave. The data have been referenced to the caustic location on the ground for convenience. The accuracy of this location, however, is about 60 m (200 ft). Figures 57 through 59 also give a typical linear theory variation of overpressure close to the caustic. In addition, a steady, level flight reference intensity is given for comparison. For a ground reflection coefficient of 2.0 this reference intensity is about 56.5 N/m^2 (1.18 lb/ft^2). Ground microphone numbers are indicated for the observed data.

The overpressure variation for passes 045 and 046 (figs. 57 and 58, respectively) indicate that at about 400 m (1300 ft) from the caustic the nonlinear effects (ΔP_2) are more important than the linear effects (ΔP_1). That is, at 400 m (1300 ft) from the caustic ΔP_1 is equal to or greater than ΔP_2 and thus the trailing, caustic-like signature begins to dominate. For pass 046 the linear theory predicts ΔP_1 fairly accurately within 100 m (330 ft) of the caustic. During pass 092 (fig. 59) a caustic was produced on the ground just uptrack of microphone G-1, and overpressure measurements farther downtrack of the caustic were obtained. Overpressure levels comparable to those produced during steady, level flight occurred at 400 to 500 m (1300 to 1600 ft) from the caustic. These data indicate that the theory gives reasonable results to within a horizontal distance of about 400 m (1300 ft) downtrack of the caustic-ground intersection. An examination of the tower pressure signatures (for example, fig. 42) shows that at a vertical distance of about 150 m (500 ft) above the caustic the linear and nonlinear effects are about equal. At distances closer to the caustic than these (within 400 m (1300 ft) horizontally downtrack of the caustic-ground intersection and within 150 m (500 ft) vertically) the nonlinear effects are important and the linear theory alone cannot be expected to give realistic results. These distances are somewhat dependent on the acceleration magnitude, generally increasing as the airplane acceleration magnitude decreases.

In the analysis of the Jericho-Virage acceleration caustic data (ref. 26), a caustic "amplification factor" is given for the maximum observed amplification compared to a reference intensity measured away from the caustic. For the five longitudinal accelerations of the Jericho-Virage tests, this coefficient of amplification was found to be about 5. During the BREN tower acceleration tests the maximum observed overpressure was 240.4 N/m^2 (5.02 lb/ft^2) at microphone G-8 on pass 046. The observed maximum overpressure at microphone T-2 for that same case, however, was 134.3 N/m^2 (2.805 lb/ft^2). For a reflection coefficient of 2.0 this becomes 268.6 N/m^2 (5.61 lb/ft^2). The maximum caustic amplification observed, then, is this maximum overpressure divided by the reference steady, level overpressure value of 56.5 N/m^2 (1.18 lb/ft^2). The resulting caustic amplification factor is 4.75, which agrees very well with the results of the Jericho-Virage acceleration tests.

Ray-Tube Area Limit Near Caustics—Linear Theory

As shown in the previous section, at a distance of about 400 m (1300 ft) from the caustic the nonlinear effects are of the same order of magnitude as the linear effects. At this distance from the caustic the linear theory should still be valid, since the nonlinear effects do not predominate. Figure 60 gives the variation of the ray-tube area with maximum overpressure and distance downtrack from the caustic-ground intersection. From figure 60 the ray-tube area at 400 m (1300 ft) is about 2000 m (7000 ft) and the linear theory maximum overpressure is about 91.0 N/m^2 (1.9 lb/ft^2). Figure 61 compares the linear theory pressure signature 400 m (1300 ft) from the caustic with observed pressure signatures at that distance from the caustic. The linear theory predicts the leading shock wave intensity fairly well. Based on these data, a limiting value of the ray-tube area, $A(S)$, of about 2000 m (7000 ft) is indicated. The area $A(S)$ is the area normal to the ray, and is significantly different from the horizontal projection of the ray-tube area, A_h , used in the basic theory. The two are related by the expression:

$$\begin{aligned} A(S) &= \left(\frac{a}{a + u_n} \right) (\sin \Theta) A_h \\ &\approx (\sin \Theta) A_h \text{ for small } u_n \end{aligned} \quad (9)$$

Theoretical calculations at lower ray-tube area values than 2000 m (7000 ft) will give unrealistic results.

By placing an empirically-determined limit on the ray-tube area it is possible to obtain realistic theoretical intensities at caustics. From figure 60 and using the caustic amplification coefficient of 5, the ray-tube area limit would be about 300 m (1000 ft). A linear theory pressure signature was calculated using this ray-tube area limit. The maximum overpressure of this pressure signature is, as expected, 237.8 N/m^2 (5.05 lb/ft^2). This linear theory "caustic" pressure signature is given in figure 62, along with two observed caustic signatures for comparison. By using the ray-tube area limit the intensities compare favorably. The linear theory signature shape, however, does not agree since no nonlinear effects have been considered. This comparison shows that the nonlinear effects at caustics must be considered if realistic theoretical pressure signatures are desired.

Discussion of Observed Phenomena Near Caustics

A fundamental consideration is the nature of the nonlinear effects that transform the leading, incoming N-wave pressure signature into the U-shaped trailing pressure signature. The distance from the caustic where this process occurs is also of interest. In an effort to determine these the measured pressure signatures near caustics were analyzed in detail by subtracting out the theoretical N-wave

part of the measured signatures, leaving the nonlinear, caustic-like portion. When the leading and trailing shocks first begin to interact, they are superimposed in a linear manner. At the caustic, however, the superposition is nonlinear, since the N-wave is transformed to a U-wave. By decomposing the measured signatures into N-wave and U-wave components it may be possible to determine the nature and importance of the nonlinear effects with distance from the caustic.

Figures 63 and 64 show typical results of this analysis for passes 045 and 046, respectively. In each case several signatures are analyzed at various distances from the caustic. The observed pressure signatures, the linear theory N-wave, and the nonlinear residual after subtraction of the N-wave from the observed signature are given for each signature. The N-wave is the calculated theoretical signature at about 400 m (1300 ft) from the caustic ($A(S) = 2000$ m (7000 ft)).

The analysis in figure 63 for pass 045 shows the results for three signatures measured on the ground at about 50, 175, and 370 m (165, 575, and 1200 ft) downtrack from the caustic-ground intersection and for one tower signature. Close to the caustic, the nonlinear residual consists of highly spiked shocks, with a nearly constant but slightly negative overpressure between the two shocks. The relatively large negative overpressure just prior to the tail shock is caused by the fact that the N-wave is of shorter duration than the observed signatures. The trailing U-wave generally has about a 10% to 20% longer duration than the incident N-wave.

Figure 64 shows the analysis of the tower-observed signatures measured above the caustic during pass 046. These measurements in the vertical plane clearly show the merging of the leading N-wave and trailing U-wave. The observed pressure signature at microphone T-13 is well above the caustic where the N-wave and U-wave are separated and not interacting. At closer distances to the caustic the N-wave and U-wave are superimposed. As in the previous case, the nonlinear residuals exhibit the highly spiked shocks, and in all cases the nonlinear residual is well-behaved and reasonable. From this analysis it must be concluded that the N-wave and U-wave are superimposed in a linear manner up to very close to the caustic (within a vertical distance of about 30 m (100 ft)). Thus, the transformation of the incoming N-wave to the U-wave must also occur within this distance. This analysis method may prove to be useful for future investigators.

Summary of Longitudinal Acceleration Data

The analysis of the longitudinal acceleration data has shown that the method of linear geometric acoustics is capable of predicting caustic-ground intersections to an accuracy of about ± 1.0 km (± 3300 ft). This accuracy is about the same as that obtained for the Jericho-Virage data, which suggests that inaccuracies in the upper level meteorological conditions are responsible for most of the error. A comparison of observed and theoretical shock wave arrival times at the tower

showed that they agreed to within ± 1.0 sec. Most of this error is probably also due to lack of detailed knowledge of the meteorological conditions along the boom propagation path. These results indicate that linear geometric acoustics can be used with good accuracy when the airplane flight path and meteorological conditions are known.

The analysis of shock wave profiles, airplane acceleration magnitude, and caustic intensity has shown that the caustic intensity may increase with increasing acceleration magnitude. Shock wave profiles are helpful in visualizing the phenomena, and it is clear that the caustic occurs where the leading and trailing shock waves merge, forming a cusp. Significant disturbances can occur below the actual caustic, since low-magnitude acoustic disturbances propagate several thousand feet below the caustic.

The analysis of pressure signature intensities in the vicinity of caustics has shown that amplified intensities occur within about 400 m (1300 ft) downtrack of the caustic-ground intersection and within 150 m (500 ft) vertically above the caustic. Nonlinear effects become progressively more important as the caustic is approached. The maximum observed caustic overpressure for these accelerations was about 264 N/m^2 (5.6 lb/ft^2). This is about five times the intensity that would be produced during comparable level flight at constant Mach number. Sonic boom pressure signatures calculated with linear sonic boom theory give reasonable agreement with the observations, but become unrealistic at distances closer than about 150 m (500 ft) vertically from the caustic. The separation of the observed pressure signatures near the acceleration caustic into linear and nonlinear components has shown that the transformation from the N-wave to the U-wave must have occurred within a vertical distance of about 30 m (100 ft) from the caustic for the case analyzed.

ANALYSIS OF LATERAL CUTOFF

FLIGHT TEST DATA

In this section the results of the analysis of the data for the nine lateral cutoff flights are discussed. Comparisons with theoretical results are shown for several cases.

Introduction

Lateral cutoff is similar to the threshold Mach number phenomenon; in each case the shock wave is completely refracted by atmospheric temperature and wind gradients. Lateral cutoff, however, occurs at all supersonic Mach numbers at the lateral extremity of the sonic boom carpet. The top part of figure 65 illustrates the lateral cutoff phenomenon.

During the last decade there have been several experimental programs where sonic booms were observed at the side of the flight path (refs. 18-24). These pressure signature measurements have indicated that near the lateral extremities of the boom carpet, large variations in overpressure occur. These large variations are caused by atmospheric inhomogeneities that distort the shape of the signature as it travels long distances near the ground where atmospheric turbulence is most prevalent. Although large variations in overpressure occur near lateral cutoff, a general trend toward lower overpressure levels has been observed at the outer edges of the sonic boom carpet.

The 1970 BREN tower sonic boom flight tests included nine flights designed to determine more exactly the characteristics of sonic boom near lateral cutoff. An illustration of the test arrangement is shown in figure 65. For the nine flights the nominal airplane flight conditions were: Mach number 1.3; altitude 10.0 km MSL (32 700 ft); and heading 125° true. The airplane lateral displacement from the BREN tower varied from 18.4 to 24.2 km (11.4 to 15.0 st mi). All nine of the passes were made on August 27, 1970 over a 3-hr period. Three flights were made, each consisting of three passes about 10 minutes apart. Table 17 summarizes the airplane flight conditions and observed sonic boom characteristics. The airplane weight was determined from pilot-observed fuel on-board at the "steady" and "breakoff" points. The boom time at tower microphone T-1 is also given in table 17, along with the maximum observed overpressure recorded by any of the tower or ground microphones.

The meteorological conditions during these lateral cutoff tests were important, since a fairly strong sidewind was present. At the airplane altitude the wind was from the SSW at a speed of about 15.2 m/sec (50 ft/sec), almost directly perpendicular to the flight path. This sidewind

TABLE 17.—SUMMARY OF LATERAL CUTOFF FLIGHT TEST CONDITIONS, AUGUST 27, 1970

Bongo-pass	Pass	Airplane altitude, h		Airplane Mach number	Airplane weight, W		Boom time at tower base, PDT	Maximum observed overpressure			Subjective boom character
		m	ft		kg	lb		N/m ²	lb/ft ²	Mic no.	
1-1	029	9 940	32 600	1.3	8 250	18 200	1006:36.7	14.9	0.312	G-6	Low boom-rumble
1-2	030	9 940	32 600	1.3	7 625	16 800	1019:19.3	16.23	0.339	T-5	Very light double boom-rumble
1-3	031	9 940	32 600	1.3	7 100	15 650	1029:03.0	3.93	0.082	G-7	Rumble
2-1	032	10 000	32 800	1.3	8 200	18 100	1103:19.15	11.49	0.240	G-1	Very low boom-rumble
2-2	033	10 030	32 900	1.3	7 575	16 700	1114:02.2	23.80	0.497	G-9	Low boom-rumble
2-3	034	9 970	32 700	1.3	7 125	15 700	1124:49.8	6.42	0.134	G-6	Rumble
3-1	035	9 955	32 650	1.3	8 250	18 200	1248:01.9	20.11	0.420	T-7	Light boom-rumble
3-2	036	10 000	32 800	1.3	7 675	16 900	1259:32.2	6.18	0.129	G-7	Rumble
3-3	037	9 980	32 750	1.3	7 125	15 700	1310:57.3	6.42	0.134	G-6	Rumble

produces an asymmetric shock pattern on the ground with respect to the flight path, as shown in figure 65; the shock-ground pattern is shifted to the NNW. The BREN tower was on the downwind side and thus in an area where lateral cutoff was extended due to the sidewind.

Another important meteorological effect is the location of the maximum shock propagation speed, V_p . Normally this occurs at the ground. Occasionally, however, the maximum value occurs above the ground, so that an "inversion" exists in the V_p profile. When this is the case, lateral cutoff will occur at or above the maximum V_p altitude, which is above the ground. This condition can exist when there is a strong temperature inversion and/or when moderately strong tailwinds occur near the ground. During several of the BREN tower lateral cutoff flights an inversion did exist which somewhat complicated the data analysis.

Lateral Cutoff Location—Theory and Experiment

The actual location of lateral cutoff is somewhat difficult to determine from measured data. However, an excellent measure of how close the shock wave at the tower was to cutoff is the observed shock inclination angle relative to the vertical. Before cutoff a shock wave will be observed with a positive angle, Θ , while after cutoff an acoustic front will be observed propagating faster at the lower levels (due to the normally higher temperatures and sound speed at the ground) so that the inclination angle, Θ , is negative. Thus, Θ is a direct measure of closeness to lateral cutoff, and is useful for correlating measured data with theoretical calculations.

The computation of the theoretical lateral cutoff location, Y_{\max} , was performed as follows:

- The computer method of reference 30 was used to calculate lateral cutoff to within about 0.0175 rad (1.0°) of actual cutoff
- The additional displacement to actual lateral cutoff ($\Theta = 0$) was calculated by using the approximation (ref. 7):

$$\Delta r = \frac{\Theta(\text{deg})}{57.3} \frac{a(Z)}{\partial V_p / \partial z}$$

- For cases when an inversion in the V_p profile existed, lateral cutoff was defined to be the location where $\Theta = 0$ occurred *anywhere* on the tower.
- To reduce inaccuracies caused by the boom-time-only meteorological observations at the tower, the Y_{\max} values calculated for the three passes of each flight were averaged to obtain a more representative Y_{\max} .

Table 18 contains the theoretical lateral cutoff locations, Y_{\max} , the airplane lateral displacement from the tower, D , the observed shock inclination angle, Θ , the ground reflection coefficient, K_R , and the average ΔP_{\max} of all the ground microphones for each flight.

Figure 66 gives an indication of the accuracy of the theoretical lateral cutoff location, Y_{\max} , compared to nearness to actual cutoff, Θ . The parameter $(D - Y_{\max})$ is plotted versus Θ . $(D - Y_{\max})$ is the theoretical lateral cutoff location with respect to the BREN tower. The agreement between theory and experiment is fairly good, and these calculations are accurate to about ± 1.0 km (± 3300 ft). It does not appear possible to achieve better accuracy than indicated in figure 66, since the meteorological conditions along the ray paths associated with boom at the tower are not known precisely. Thus, the accuracy indicated in figure 66 is probably an upper limit for these kinds of calculations.

Another measure of the nearness of lateral cutoff is the shock propagation speed, V_{ps} (parallel to the flight path as determined from the propagation speed of the shock front normal to itself) compared to the airplane ground speed, V_G . In theory, lateral cutoff should occur when these two are equal. By analysis of the shock arrival times on the two-dimensional ground microphone array, it is possible to determine both of these parameters. Since microphones G-15 and G-16 were parallel to the airplane ground track, the shock arrival times, t_o , can be used to obtain the airplane ground speed directly, as:

$$V_{G_{mic}} = \frac{[t_o(G-16) - t_o(G-15)]}{\Delta X}$$

where $\Delta X = 1081$ m (3545 ft) = the distance between microphones G-15 and G-16.

To obtain the propagation speed normal to the shock wave requires that the angle of the direction of shock propagation with respect to the line of microphones G-15 to G-16 be known. This can be calculated from:

$$\cos \alpha = \frac{V_{G_{mic}}}{[t_o(G-14) - t_o(G-1)]/\Delta X}$$

where $\Delta X = 975.4$ m (3200 ft) = the distance between microphones G-1 and G-14.

The propagation speed, V_{ps} , is then:

$$V_{ps} = V_p / \cos \alpha$$

where $V_p = a - u_n$; $u_n = u \cos(\nu - \eta)$; $\nu \cong 90^\circ$.

TABLE 18.-SUMMARY OF LATERAL CUTOFF FLIGHT TEST DATA ANALYSIS, AUGUST 27, 1970

Bongo-pass	Pass	Airplane displacement, D		Theoretical lateral cutoff location Y _{max}		Lateral cutoff (D-Y _{max})		Observed Θ at tower		Average ΔP max of ground mics		Comments
		km	st mi	km	st mi	km	st mi	rad	deg	lb/ft ²	N/m ²	
A) Cutoff past tower												
1-1	029	18.4	11.4	20.0	12.4	-1.6	-1.0	+0.070	+4.0	0.23	11.01	Observed ΔP max on tower is 12.0 N/m ² (0.25 lb/ft ²); calculated is 17.7 N/m ² (0.37 lb/ft ²)
B) Cutoff near tower												
1-2	030	22.5	14.0	20.0	12.4	+2.5	+1.55	-0.035	a-2.0	0.86	6.70	Cutoff at midtower with caustic-like signals
2-2	033	20.6	12.8	19.5	12.1	+1.1	+0.7	+0.003	+0.2	1.26	16.76	Reflected signals stronger than incident ones
3-1	035	19.8	12.3	18.5	11.5	+1.3	+0.8	-0.0175	-1.0	1.21	16.28	Caustic-like signals on lower half of tower
C) Cutoff before tower (acoustic disturbances at tower)												
1-3	031	24.2	15.0	20.0	12.4	+4.2	+2.6	-0.070	-4.0	0.87	2.39	Large decrease in ΔP max from G-1 to G-7.
2-1	032	21.9	13.6	19.5	12.1	+2.4	+1.5	-0.061	-3.5	1.15	5.75	
2-3	034	21.1	13.1	19.5	12.1	+1.6	+1.0	-0.087	-5.0	1.08	4.79	
3-2	036	20.8	12.9	18.5	11.5	+2.3	+1.4	-0.044	-2.5	0.90	4.31	
3-3	037	20.4	12.7	18.5	11.5	+1.9	+1.2	-0.087	-5.0	0.97	3.83	

^aLateral cutoff occurred at midtower; therefore Θ is negative and estimated to be -0.034 rad (-2.0°).

Table 19 presents these data and figure 67 is a plot of $V_{G_{mic}}$ versus V_{ps} for six of the lateral cutoff flights (for three flights the disturbances were too weak to determine shock arrival times with accuracy). Also shown on figure 67 is V_{ps}^* , the normal shock propagation speed with the effect of the presence of water vapor taken into account (see appendix A). The accuracy shown by these calculations is amazingly good, particularly for the V_{ps}^* data. The values of Θ , which indicate nearness to lateral cutoff obtained by an independent analysis, are also shown. The above indicate that for shock waves near lateral cutoff shock propagation speed is affected by water vapor and that linear geometric acoustics can be used to accurately predict the location of cutoff.

Ground Reflection Coefficient

A parameter of interest near lateral cutoff is the ground reflection coefficient, K_R . A doubling of shock wave intensity occurs for oblique shock waves incident on smooth surfaces, so that $K_R = 2.0$. Measurements of K_R for most natural ground surfaces have been between 1.8 and 1.9. As discussed in a previous section, however, K_R should approach 1.0 near lateral cutoff where the shock wave is almost perpendicular to the ground. To provide further insight into this variation near lateral cutoff, the experimental data were analyzed to determine K_R . A direct measurement of K_R was not made, so the observed intensities on the tower and on the nearest ground microphones were used. The procedure was previously defined in the "Data Analysis Methods" section.

Figure 68 shows the variation of K_R with Θ . Before and close to lateral cutoff the data indicate that a K_R of about 1.2 is representative, while past cutoff K_R varied from 0.86 to 1.08. Pass 030 is anomalous because cutoff and caustic-like signatures occurred near midtower, while lower intensity signatures occurred on the ground, giving a K_R value less than 1.0. As with the threshold Mach number measurements, these data do not indicate a significant increase in reflection coefficient near lateral cutoff.

Overpressure Variation

The variation of overpressure near lateral cutoff was studied using both theoretical predictions and the measurements. The theoretical variation is shown in figure 69. Directly beneath the airplane an overpressure of 57.0 N/m^2 (1.21 lb/ft^2) is predicted, gradually decreasing with increasing lateral distance, and then increasing rapidly just prior to cutoff. The linear theory incorrectly predicts an infinite intensity at cutoff due to ray focusing.

The data are plotted in figure 70. The average and extreme maximum overpressure, ΔP_{max} , of the pressure signatures observed on the ground are given for all nine flights. The shock wave

TABLE 19.—CALCULATION OF OBSERVED SHOCK PROPAGATION SPEED
(NORMAL TO SHOCK) AND COMPARISON WITH OBSERVED AIRPLANE
GROUND SPEED

Bongo-pass	Pass	$V_{p \max \text{ tower}}$		$V_{p \max \text{ tower}}^*$		$\cos \alpha$	V_{ps}		V_{ps}^*		V_{Gmic}	
		m/sec	ft/sec	m/sec	ft/sec		m/sec	ft/sec	m/sec	ft/sec	m/sec	ft/sec
1-1	029	345.1	1132	346.2	1136	0.8685	397.4	1304	398.5	1307	401.5	1317
1-2	030	346.3	1136	347.4	1140	0.8656	400.1	1312.6	401.2	1316	400.3	1313
2-1	032	346.0	1135	347.1	1139	0.8854	390.8	1282	391.9	1286	391.8	1285
2-2	033	345.7	1134	346.8	1138	0.8730	396.0	1299	397.1	1303	397.8	1305
2-3	034	346.8	1138	347.8	1141	0.8860	391.5	1284	392.6	1288	390.8	1282
3-1	035	346.1	1135.5	347.2	1139	0.8785	394.0	1292.6	395.1	1296	395.8	1298.5

inclination angle, Θ , was used as a measure of nearness to lateral cutoff. For each pass (except 034 and 037) microphones G-1 through G-7 and G-8 through G-14 have been separated to give an indication of the overpressure variation along the microphone array. Microphone G-1 was closest to the airplane.

The theoretical variation of overpressure with Θ near lateral cutoff is also shown in figure 70 for two cases. The data for pass 030 are representative of the normal theoretical variation where an inversion in the V_p profile does not exist. The minimum overpressure calculated was about 43.1 N/m^2 (0.90 lb/ft^2) at the location where Θ was about 0.175 rad (10°). The theoretical variation of overpressure with Θ for pass 029, however, also shown in figure 70, shows a continued decrease in overpressure to much lower Θ angles. This is due to the effect of the inversion in the V_p profile that existed for pass 029. In plotting the data for 029 the minimum Θ was used rather than Θ at the ground, since this value is more indicative of nearness to cutoff. It occurred at about 120 m (400 ft) above the ground. The better agreement of linear theory with the experimental data for pass 029 is significant, since it implies that the method is capable of calculating results to within 0.035 rad (2.0°) of lateral cutoff for some combinations of meteorological conditions.

Figure 70 indicates an interesting variation of overpressure near lateral cutoff. Relatively stronger intensities were measured very near lateral cutoff, and the pressure signatures for these passes (033 and 035) are caustic-like in nature. However, the highest overpressure measured was about 24.0 N/m^2 (0.5 lb/ft^2). The average intensity for passes 033 and 035 was about 15.8 N/m^2 (0.33 lb/ft^2). These relatively low-magnitude disturbances were perceived as low booms or rumbles.

These results are much more definitive than an early study of overpressure variation near lateral cut off for these data, given in figure 9 of reference 24. The detailed analysis of nearness to lateral cutoff has added significantly to the interpretation of the results.

Observed Pressure Signatures and Shock Wave Profiles

The observed pressure signatures and shock front shapes are presented in this section. The results are separated into discussions of measurements obtained before, near, and beyond lateral cutoff. The shock wave profiles and tower pressure signatures have been presented on the same plots to the same distance scale. This required a transformation of the pressure signatures from the time coordinate to a distance coordinate by using the airplane ground speed (see "Data Analysis Methods" section). The pressure signatures observed on the ground are presented as observed (overpressure versus time).

Measurements before lateral cutoff.—Only one of the nine lateral cutoff flights (pass 029) was performed with the airplane positioned so that lateral cutoff occurred past the tower. Figure 71 shows the shock wave orientation in the vertical plane, along with several representative pressure signatures observed on the tower. Although the disturbance is of low magnitude (about 12.0 N/m^2 , 0.25 lb/ft^2), a reflected shock wave is evident and the incident shock wave angle with the vertical, Θ , is about 0.070 rad (4°). The incident shock wave is very weak and ill-defined, while the reflected shock wave near the tower top has a well-defined signature shape. The reflected shock wave has significant curvature, since it was reflected from the ground earlier and well before cutoff at a larger angle, Θ .

For this case it was possible to calculate a theoretical pressure signature. The calculated signature is given in figure 71; it has a maximum overpressure 17.72 N/m^2 (0.37 lb/ft^2). It was also possible to calculate a theoretical shock front shape, which is also indicated.

The pressure signatures observed at the 16 ground microphones are given in figure 72. There is considerable variation in the signature shape and intensity observed at each microphone. In addition, acoustic disturbances occur for a significant duration after the initial signatures.

Measurements near lateral cutoff.—Three of the flights (passes 030, 033, and 035) produced shock waves at the BREN tower that were very close to lateral cutoff and exhibited caustic-like pressure signatures. Figures 73 through 78 show shock front profiles and observed pressure signatures on the tower and ground for these cases.

The tower data for pass 033 in figure 73 show a weak incident pressure wave, which may be the remnants of the incident shock wave, followed by the reflected shock wave. Since the incident wave is almost vertical, it is very near lateral cutoff. The pressure signatures on the ground in figure 74 show one basic signature, followed by acoustic-like pressure disturbances. In general, the disturbances are acoustic in nature since the signatures are rounded, without shocks.

Pass 035 shown in figures 75 and 76 is similar to pass 033 except that the incident wave is even weaker and occurs near the top of the tower only (indicated by the dashed line in fig. 75). The reflected pressure signature is caustic-like and is almost vertical at the ground. Both the pressure signatures on the bottom half of the tower and on the ground are caustic-like, but rounded and of relatively low intensity. Ground microphones G-8, G-9, and G-10 show an extra intermediate peak in the observed pressure signatures.

Pass 030 is another case for which cutoff was near the tower. Figure 77 shows the shock front to be perpendicular to the ground from the middle of the tower to the tower top. Several pressure pulses can be seen ahead of the main part of the signature, and the signature itself is caustic-like

with sharp peaks. Further evidence that lateral cutoff was just uptrack of the tower can be seen in the ground pressure signatures, shown in figure 78. These signatures have mostly random acoustic pressure variations, particularly microphones G-10 through G-14. Again an extra intermediate peak was observed at microphones G-8 and G-9, which suggests some effect caused by the small buildings at the tower base.

Because cutoff occurred near the middle of the tower, pass 030 is somewhat anomalous when compared with other cases. For example, the ground reflection coefficient as calculated from the tower and ground overpressure intensities is less than one, since the tower intensities are greater than those on the ground. Also, the value of Θ at the ground was not obvious. It should have been negative since cutoff has already occurred at the ground. Thus, a Θ of -0.035 rad (-2.0°) was used for this case, based on the acoustic disturbances measured near the tower base.

Measurements past lateral cutoff.—Five of the nine flights produced disturbances at the tower that were well past cutoff, so that acoustic signals were observed. To observers on the ground, these flights (passes 031, 032, 034, 036, and 037) produced signals that were generally perceived as rumbles. The maximum overpressure of all these cases was 11.5 N/m^2 (0.24 lb/ft^2); generally the overpressures were about 4.8 N/m^2 (0.10 lb/ft^2).

The data for pass 032 are given in figures 79 and 80. The acoustic front shown in figure 79 propagates fastest at the ground, giving a negative Θ . From the tower pressure measurements, it is difficult to distinguish a pressure signature as such. The ground pressure measurements show a rapid decrease of overpressure from microphone G-1 to microphone G-5. This case is anomalous in that respect, although it illustrates the large variations that can occur near lateral cutoff. The pressure measurements of microphones G-6 through G-14 are representative of the measurements of the remainder of these passes.

Summary of Lateral Cutoff Data

The nine lateral cutoff flights during the 1970 BREN tower tests have provided some interesting and valuable information about sonic boom characteristics near lateral cutoff. The most significant observation was the caustic-like signatures produced by ray focusing very close to the lateral cutoff location. The measured overpressure increases, however, were only about 50% higher than those observed just prior to cutoff and were much lower than those experienced directly beneath the airplane. The maximum overpressure observed for all the passes was about 24.0 N/m^2 (0.50 lb/ft^2). Near lateral cutoff the incident shock waves were found to be very weak, while the reflected shock waves recorded on the tower in all cases were stronger. The ground reflection coefficient prior to lateral cutoff appears to be about 1.2, while past lateral cutoff it is nearer to 1.0 but showed large variations.

Theoretical calculations of the lateral cutoff location using linear geometric acoustics are accurate to about ± 1.0 km (± 3300 ft) for these cases, even though the exact meteorological conditions along the ray path were not precisely known. For the one case where it was possible to calculate a theoretical pressure signature, the agreement with the observed signature was reasonably good (the theoretical ΔP_{\max} was 17.7 N/m^2 (0.37 lb/ft^2) compared with the observed value of about 12.0 N/m^2 (0.25 lb/ft^2). Figure 81 is a summary of the shock front profiles and typical pressure signatures.

CONCLUSIONS

The 1970 sonic boom tests conducted at Jackass Flats, Nevada, have helped to define more exactly sonic boom phenomena associated with (1) flight near the threshold Mach number, (2) transonic acceleration, and (3) lateral cutoff. The use of the BREN tower was indispensable for measuring these test data, because it enabled vertical observations through the shock waves. Hence, it was not necessary to place caustics precisely at a point on the ground to obtain a dense sampling of measured pressure signatures. These vertical measurements also allowed the calculation of shock wave profiles and angles of incidence, which added substantially to the overall value of the data and to the interpretation of the test results.

The observations near caustics are of particular value, since no methods are currently available for predicting realistic pressure signatures at caustics, because of the nonlinear effects that predominate there. Overpressure increases measured at caustics produced during threshold Mach number flight were relatively low, ranging from about 1.0 to 1.8 times those predicted for flight at a slightly higher Mach number. In one case where it appeared that small-scale atmospheric turbulence produced "spikes" on a caustic signature, the increase was higher. There is some evidence to suggest that the caustic intensity during threshold Mach number flight is affected by the shock propagation speed gradient. Caustics were also produced by small, inadvertent changes in the airplane speed during several of the "steady," level threshold Mach number flights. These caustics were slightly stronger, with a maximum amplification of about 3. Measured overpressures at caustics produced by airplane accelerations ranged from 2 to 5 times those which would be observed during steady, level flight at about Mach 1.2. For these caustics, acceleration magnitude appeared to affect the intensity, with the strongest produced by the greatest acceleration. This conclusion is also supported by the data measured for some threshold Mach number flights, where small magnitude accelerations produced lower intensity caustics.

Pressure signatures were also observed near lateral cutoff which resembled those measured at caustics. These disturbances were of very low intensity, however—less than one-half the intensity beneath the flight path. The meteorological conditions during the lateral cutoff flights were significant, since a relatively strong sidewind component prevailed and in several cases an inversion in the shock propagation speed profile existed at the tower. In theory, these conditions would be expected to have a strong effect on the measured overpressures.

The maximum intensities and amplifications compared to the overpressures predicted directly beneath the airplane during steady, level flight are summarized in table 20.

TABLE 20—SUMMARY OF MAXIMUM INTENSITIES AND AMPLIFICATIONS PRODUCED BY VARIOUS FLIGHT CONDITIONS

Type of caustic	Maximum tower overpressure observed		Approximate maximum amplification factor ^a
	N/m ²	lb/ft ²	
Steady Threshold Mach Number Flight	^b 50.8	^b 1.06	1.8
Low-Magnitude Acceleration Through Threshold Mach Number	82.4	1.72	3
Transonic Acceleration	134.5	2.81	5
Lateral cutoff	^c 23.9	^c 0.5	^c 1

^aA theoretical reference overpressure of 28.7 N/m² (0.60 lb/ft²) was used as a reference for determining caustic amplification (steady flight, M = 1.2, K_R = 1.0).

^bFor one case small-scale atmospheric turbulence appears to have produced "spikes" on a caustic signature. This maximum overpressure was 135.0 N/m² (2.82 lb/ft²).

^cSince K_R ~ 1.0, the amplification factor in terms of ground-observed boom is ~ 0.5.

Analysis of pressure signatures near caustics and comparison with linear theory showed that nonlinear effects predominate at caustics. Nonlinear effects become important within about 150 m (500 ft) vertically above the acceleration caustic (or about 400 m (1300 ft) horizontally from the caustic-ground intersection) and within 100 m (330 ft) above and below the threshold Mach number caustic. Caustic pressure signatures are quite different in shape from normal sonic booms, since they typically exhibit a U-shape rather than an N-wave shape and the intermediate shock wave (for the F-104) is generally not present. In addition, caustic pressure signatures have a significantly longer duration than normal N-wave pressure signatures. These measurements of sonic boom characteristics at caustics produced by several different flight conditions should prove to be of great value in extending theoretical methods to include calculations near caustics.

During the threshold Mach number flights and the lateral cutoff flights, considerable information was obtained on the acoustic disturbances that occur past the cutoff condition. Generally, these disturbances propagate at the local speed of sound rather than the airplane ground speed. By detailed analysis of these data it was possible to isolate the effect of the presence of water vapor on the propagation speed. An increase was noted, in agreement with theory. For low supersonic flight and when the increase in propagation speed is 1.0 m/sec (3.3 ft/sec) or more, this effect should be taken into account.

Additional analysis of the rumble data produced during flight near the threshold Mach number showed that "low rumbles" occurred when the airplane ground speed was at least 6 m/sec (19.7 ft/sec) lower than the maximum shock propagation speed. This, roughly, is the "safety factor" (or reduction in allowable airplane ground speed to avoid objectionable noise at the ground) that would be required for these flight and meteorological conditions. Comparison of a theoretical "safe altitude" for sonic boom cutoff with the observed data was good considering the assumptions made in deriving it.

A characteristic of sonic boom disturbances near the cutoff condition is the presence of "precursors" or pressure pulses that propagate ahead of the basic pressure signature. Precursors were produced during the threshold Mach number flights and the lateral cutoff flights when shock waves were near the cutoff condition, and thus propagating at speeds close to the local propagation speed parallel to the ground.

The ground reflection coefficient was calculated for a number of cases, and the data indicate a gradual decrease from about 2.0 to 1.0 near the cutoff condition. This is in direct contrast to several theoretical studies which predict an increase to 3.0 near cutoff.

Comparison of theoretical calculations with the observed data showed good agreement in all cases where it was possible to perform such calculations. Shock wave intensities, inclination angles, and arrival times were calculated and compared with the observations. The accuracy of the theoretical calculations was limited by the accuracy of the input airplane flight path and meteorological data, particularly for the low supersonic flights where the shock wave travels long distances almost parallel to the ground. Inaccuracies in the upper level wind conditions are considered to be an important source of error. Caustic locations during transonic acceleration and lateral cutoff locations can be predicted to within ± 1.0 km (3300 ft). Shock wave intensities agree reasonably well, as do signature shapes when the effects of small-scale turbulence are neglected in the observed data. Shock wave arrival times can be predicted to within ± 1.0 sec. Thus, the comparison of theory and experiment has tended to verify the theory and has also indicated its range of validity.

APPENDIX A

EFFECT OF HUMIDITY ON SHOCK PROPAGATION SPEED

The presence of water vapor has a second-order effect on the speed of sound and the shock wave propagation speed. Normally in sonic boom studies this effect can be neglected. For shock wave propagation near cutoff, however, where shock waves are deteriorating to acoustic waves, this effect may be important. The small change in velocity caused by humidity acting over relatively large propagation distances for cutoff rays can result in significant alteration in the direction of sound waves or low-magnitude sonic boom waves.

The effect of humidity on sound velocity is attributed to the fact that the density of water vapor is approximately 60% of the density of dry air. Thus, humid air is slightly less dense and has a slightly higher speed of sound than dry air at the same temperature and pressure. The normal method for accounting for the effect of humidity is to use a "corrected" temperature called the virtual temperature.

The virtual temperature, T_v of moist air is given by the expression:

$$T_v = T \frac{(1 + r/\epsilon)}{(1 + r)} \quad (A1)$$

where:

- T = temperature of moist air
- r = mixing ratio of moist air (ratio of mass of water vapor to the mass of dry air with which the water vapor is associated)
- ϵ = ratio of molecular weight of water vapor to that of dry air (0.62198)
- T_v = temperature which dry air must have at the given pressure in order to have the same density as moist air when the densities of both dry and moist air are deduced from the equation of state for ideal gas

Tables for the calculation of T_v are given in reference 39 for various pressure, temperature, and humidity conditions.

A useful form of equation (A1) is:

$$D = (T_v - T) = \left[\frac{1}{\epsilon} - 1 \right] \left[\frac{r}{1+r} \right] T \quad (\text{A2})$$

or:

$$D = (0.60777) \left[\frac{r}{(1+r)} \right] T$$

where T is expressed in °K and D is expressed in °K or °C.

Some of the results given in earlier sections have indicated that it may be possible to use the experimental data to determine the increase in sound speed because of the presence of water vapor. The lateral cutoff and threshold Mach number flight data for cases where acoustic propagation was occurring would appear to be useful for this purpose. Table 21 is a comparison of the shock propagation speed as determined from the arrival times at the ground microphones, $V_{p_{mic}}$ and the maximum shock propagation speed calculated from the meteorological conditions on the tower, $V_{p_{max}}$. Both of these calculations have been discussed earlier. The only cases considered were those for which it was possible to calculate a reasonable accurate propagation speed from identifiable pressure signature features. In addition, only cases for which acoustic signals were observed were used in this analysis. On two days (October 23 and 30), significant inversions existed in the V_p profile well above the tower, so that it was not possible to determine accurately a representative shock propagation speed. In most cases the maximum occurred within 30 m (100 ft) of the ground. Reference 34 contains V_p data for each pass.

The difference between $V_{p_{mic}}$ and $V_{p_{max}}$ on the tower is a measure of the increase in shock propagation speed caused by water vapor. The data in table 21 show considerable variation for individual passes. This is to be expected, since the accuracy of both $V_{p_{mic}}$ and $V_{p_{max}}$ are the same order of magnitude as their difference. (The increase in shock propagation to be isolated is less than 1.0 m/sec (3.3 ft/sec) or about 0.3% of the propagation velocity itself.) Daily averages of the data are also given in table 21; these indicate less variability since for only one day is ($V_{p_{mic}} - V_{p_{max}}$) negative. Combining all August measurements and all October measurements by a second averaging gives an increase of 1.1 m/sec (3.6 ft/sec) for the August data and 0.25 m/sec (0.8 ft/sec) for the October data.

The theoretical increase in shock propagation speed for the observed atmospheric conditions is given in table 22. Average humidity and temperature conditions were used. An average increase during the August period was 1.0 m/sec (3.3 ft/sec) and during October 0.20 m/sec (0.7 ft/sec). The lower temperatures and humidity during October give a much lower increase in shock propagation

TABLE 21.—COMPARISON OF OBSERVED SHOCK PROPAGATION SPEED OVER GROUND WITH PROPAGATION SPEED FROM METEOROLOGICAL OBSERVATIONS
(Acoustic Non-Inversion Cases Only^a)

Date	Bongo-pass	Pass	V _p max tower		V _p mic		V _p mic - V _p max					
			m/sec	ft/sec	m/sec	ft/sec	Individual passes		Daily average		Seasonal average	
							m/sec	ft/sec	m/sec	ft/sec		m/sec
8-24 (M _T)	1-3	003	350.5	1149.9	353.4	1159.4	2.9	9.5				
	2-2	005	350.2	1148.9	352.0	1154.8	1.8	5.9				
	3-1	007	351.8	1154.2	352.0	1154.8	0.2	0.7	1.4	4.6		
	3-2	008	352.3	1155.8	353.0	1158.1	0.7	2.3				
	3-3	009	351.7	1153.9	353.1	1158.5	1.4	4.6				
8-25 (M _T)	1-1	014	354.1	1161.7	354.7	1163.7	0.6	2.0				
	3-2	022	353.9	1161.0	356.0	1167.8	2.1	6.9				
	3-3	023	355.4	1166.0	356.1	1168.3	0.7	2.3	0.5	1.6	1.1	3.6
	4-1	025	354.2	1162.1	355.2	1165.3	1.0	3.3				
	4-3	027	355.1	1165.0	353.1	1158.5	-2.0	-6.6				
8-27 (Lateral Cut- off)	1-2	030	b 400.1	1312.6	400.3	1313.3	0.2	0.7				
	2-1	032	b 390.8	1282.1	391.8	1285.4	1.0	3.3				
	2-2	033	b 396.0	1299.2	397.8	1305.1	1.8	5.9	0.8	2.6		
	2-3	034	b 391.5	1284.4	390.8	1282.1	-0.7	-2.3				
	3-1	035	b 394.0	1292.6	395.8	1298.5	1.8	5.9				
8-31 (M _T)	1-3	053	351.4	1152.9	353.0	1158.1	1.6	5.2				
	2-1	055	352.0	1154.8	353.9	1161.1	1.9	6.2				
	2-2	056	352.0	1154.8	354.8	1164.0	2.8	9.2	1.8	5.9		
10-27 (M _T)	3-1	059	352.7	1157.1	354.2	1162.1	1.5	4.9				
	4-2	064	356.3	1168.9	357.5	1172.9	1.2	3.9				
	2-1	089	329.6	1081.4	327.5	1074.5	-2.1	-6.9				
10-28 (M _T)	2-2	090	329.8	1082.0	329.6	1081.4	-0.2	-0.7				
	2-3	091	330.2	1083.3	329.1	1079.7	-1.1	-3.6				
	1-3	097	333.1	1092.8	335.3	1100.0	2.2	7.2				
10-29 (M _T)	2-1	098	334.3	1096.8	335.9	1102.0	1.6	5.2	1.9	6.2	0.25	0.8
	1-1	104	336.1	1102.7	338.8	1111.5	2.7	8.9				
	1-4	107	337.5	1107.3	336.0	1102.3	-1.5	-4.9				
2-5	2-4	111	346.8	1137.8	346.3	1136.1	-0.5	-1.6	0.4	1.3		
	2-5	112	344.2	1129.3	344.1	1128.9	-0.1	-0.3				
	3-3	115	347.0	1138.4	348.5	1143.4	1.5	4.9				

^aOn October 23 and 30 significant inversions existed in the V_p profiles so that V_pmic > V_ptower by about 2%.

^bFor these cases V_{ps} = V_p/cos α since the flight path was not parallel to the microphone array. (see "Analysis of Lateral Cutoff Flight Test Data" section).

TABLE 22.—AVERAGE HUMIDITY CONDITIONS AND THEORETICAL INCREASE
IN PROPAGATION SPEED

Date	Mixing ratio, r	Relative humidity, %	Temperature				D		$(V_p^* - V_p)$				
			°C		°F		°K	°F	Daily average		Seasonal average		
			°C	°F	°K	°F	m/sec	ft/sec	m/sec	ft/sec			
8-24	0.007	23	30	86	303	1.28	2.3	0.74	2.4	2.4			
8-25	0.010	33	29	84	302	1.82	3.3	1.05	3.4	3.4			
8-27	0.012	43	27	80.6	300	2.16	3.9	1.25	4.1	4.1			
8-31	0.0085	29	29	84	302	1.55	2.8	0.89	2.9	2.9			3.2
10-27	0.0018	25	8	46.4	281	0.31	0.6	0.19	0.6	0.6			
10-28	0.0016	17	11	52	284	0.28	0.5	0.17	0.6	0.6			
10-29	0.0020	15	17	62.6	290	0.35	0.6	0.21	0.7	0.7			0.7
8-28	0.013	51	27	80.6	300	2.34	4.2	1.35	4.4	4.4			
10-23	0.0045	35	16	61	289	0.79	1.4	0.47	1.5	1.5			
10-30	0.0020	13	18	64.4	291	0.35	0.6	0.21	0.7	0.7			
Standard Con- ditions	0.00725	50	20.0	68.0	293.2	1.283	2.31	0.75	2.5	2.5			

speed than during August. The experimental data averaged over August and October agree very closely with the predicted shock propagation speed increase. Figure 82 shows the comparison between theory and experiment. While considerable scatter is evident in the data, the averaged experimental data agree surprisingly well with theory. These data indicate that the observed change in shock propagation speed due to water vapor ($V_{P_{mic}} - V_{P_{max}}$) is approximately equal to the theoretical increase in shock propagation speed.

In view of these results, it would be desirable to account for the increase in shock propagation speed due to water vapor during low supersonic Mach number flight when the water vapor content is high enough to cause an increase of more than 1.0 m/sec (3.3 ft/sec) in the shock propagation speed. For supersonic flight at speeds appreciably higher than the threshold Mach number and for low-temperature, low-humidity conditions the effect need not be considered. Figure 83 shows the theoretical increase with relative humidity for an atmospheric pressure condition of 1000 mb (2088.5 lb/ft²) and several temperatures. For the propagation speed to change by more than 1.0 m/sec (3.3 ft/sec), temperatures in excess of about 12.0°C (53.6°F) are required with high relative humidity. At a temperature of 30.0°C (86.0°F) a relative humidity of only 35% is required since the air is capable of holding much more water vapor before saturation.

Harris (ref. 40) has presented the results of some interesting laboratory work on the effects of humidity on the velocity of sound in air, obtained at two frequencies in the lower audio range. His results indicate that as moisture is added to dry air the velocity of sound at first decreases until the minimum velocity is reached at 14% relative humidity. Above about 30% relative humidity the velocity increases linearly with increasing moisture content. The initial decrease in sound speed with increasing relative humidity is attributed to the effect of molecular relaxation. As humidity is first added to dry air, the decrease in velocity because of molecular relaxation is larger than the increase in velocity because of density changes. His measurements were performed in air at a constant temperature of 20.00°C (68.0°F) and at normal atmospheric pressure. The estimated accuracy of the sound speed increase is ±0.05 m/sec (±0.16 ft/sec).

Harris' work raises an important question with regard to sonic boom waves propagating at near-sonic speeds. It is generally acknowledged that the humidity at which the molecular absorption is maximum (a decrease in sound speed) increases with increasing frequency. This suggests two things when sonic boom signals (consisting of a wide range of frequencies) are considered. First, the higher frequencies would tend to have slower propagation speeds because of higher molecular absorption, while the lower frequencies would tend to have higher speeds because of lower molecular absorption. Thus, the higher frequencies would tend to lag behind the lower frequencies, after propagation over large distances. Secondly, for low-frequency signals the molecular absorption is at a minimum, so that the full increase in propagation speed predicted by theory would be expected.

Harris has also done some experimental work on the attenuation of sound (ref. 41). In this study he found that a 2000-Hz sound wave was attenuated to 0.3 its original amplitude after traveling 400 m (1300 ft). A 300-Hz signal, however, is attenuated the same amount after traveling 4 km (2.5 st mi). Thus, the higher frequency waves are attenuated much more rapidly with distance. This attenuation (and slowing) of higher frequency sound waves suggests that past sonic boom cutoff where acoustic disturbances occur, the higher frequency components would be lost, leading to rounded, smooth signatures.

Hodgson and Johannesen (ref. 42) give an approximate expression for the thickness (rise time) of weak, fully dispersed shock waves. They found that humidity has a large effect on the shock thickness. For an overpressure of 24.0 N/m^2 (0.5 lb/ft^2) the thickness is calculated to be between 6 m (19.7 ft) (dry air) and 6 mm (0.24 in.) (hot humid conditions) at 300° K (80.3° F) and between 3 m (9.8 ft) and 30 mm (1.18 in.) at 270° K (26.3° F). Thus, even before cutoff where shock waves exist, shock thickening may occur producing rounded pressure signatures (see fig. 71).

APPENDIX B

AIRPLANE F-FUNCTION DATA

To obtain accurate theoretical sonic boom pressure signatures, it is necessary to compute the airplane F-function. The F-function specifies the initial conditions for the sonic boom propagation and is calculated from the detailed geometry and lift distribution of the airplane. The F-function was derived by Whitham (ref. 43), and references 8, 44, and 45 describe methods for computing it. To facilitate the computation of the effects of airplane Mach number, load factor, weight, and the ray azimuth angle, the format developed by NASA Langley Research Center was used, where the geometry and lift components are nondimensionalized. In general, the F-function varies most significantly with airplane station, L , Mach number, M , ray azimuth angle, ϕ_r , and lift coefficient, C_L . It is represented as:

$$\begin{aligned} F &= F_f (F_A + F_B \cos \phi_r) \\ &= F_f F_i \end{aligned} \tag{B1}$$

where F_f is that part that varies significantly with Mach number, F_A is the volume contribution, and F_B is the lift contribution. Mathematically they are:

$$\begin{aligned} F_f &= M^2 / (2\beta)^{1/2} \\ F_A &= F_{A1} (L_F)^{1/2} \\ F_B &= F_{B1} \left(\frac{(\beta/2) (n_L W/q)}{(L_F)^{3/2}} \right) \end{aligned} \tag{B2}$$

The parameters F_{A1} and F_{B1} are the nondimensionalized volume and lift contributions, respectively. The other parameters are:

L_F = a basic length used to nondimensionalize the F-function

M = Mach number

n_L = lift load factor

P_O = atmospheric pressure at the airplane altitude

- $q = 1/2 P_0 \gamma M^2 = \text{dynamic pressure}$
 $W = \text{airplane weight}$
 $\beta = (M^2 - 1)^{1/2}$
 $\gamma = 1.4 = \text{ratio of specific heats for air}$
 $\phi_r = \text{ray azimuth angle}$

Tables 23 and 24 give the nondimensionalized geometry and lift components of the F-function, F_{A1} and F_{B1} , for Mach numbers of 1.1 and 1.3 for the F-104 airplane. Since the parameters F_{A1} and F_{B1} vary slowly with Mach number (most of the Mach number dependence is contained in the F_f factor), they may be used over a fairly wide range of Mach numbers. In the computer method (refs. 7 and 30) used to calculate the sonic boom pressure signatures the parameter F_f is calculated for each flight time and Mach number. The Mach 1.1 F-function data were used for the threshold Mach number pressure signature calculations and the Mach 1.3 F-function data were used for the acceleration and lateral cutoff pressure signature calculations.

The data in tables 23 and 24 are given at various airplane stations, L/L_F , beginning at the nose and extending past the tail. The F-function reference length is 0.3048 m (1.0 ft). The units of F_A and F_B are $(\text{ft})^{1/2}$. The airplane reference wing area, S_{REF} , was 18.708 m² (196.0 ft²). The airplane weight, W , determines the lift contribution to the F-function.

Typical F-function data are given in figures 84 and 85 for the particular flight conditions noted on the figures. The contributions of various airplane components to the F-function are indicated in figure 85.

TABLE 23.—F-FUNCTION DATA FOR F-104 AT MACH 1.10

^aL_F = 0.3048 m (1.0 ft); S_{REF} = 18.208 m² (196.0 ft²)

L, ft	F _{A1}	F _{B1}	L, ft	F _{A1}	F _{B1}
0.0	0.0	0.0	36.0	- 0.314922	0.0083620
0.5	0.0325166	0.0	37.5	- 0.243227	0.0060987
1.0	0.0568285	0.0	38.5	- 0.091745	0.0039997
1.5	0.0753496	0.0	39.0	0.001296	0.0020510
2.0	0.0895217	0.0	40.0	0.2136	- 0.0029230
3.0	0.1082570	0.0	40.5	0.0872	- 0.0058339
3.5	0.1139427	0.0	41.0	0.0585	- 0.0097013
4.5	0.1209745	0.0	41.5	0.0522	- 0.0151971
5.5	0.1303826	0.0	42.0	0.0271	- 0.0110773
7.5	0.1571810	0.0	42.5	0.0086	- 0.0078617
8.5	0.1731034	0.0	43.0	- 0.0031	- 0.0062546
9.0	0.1782168	0.0	43.5	- 0.0114	- 0.0052313
9.5	0.1733862	0.0	44.0	- 0.01755	- 0.004504
10.0	0.1586302	0.0	44.5	- 0.02157	- 0.003952
10.5	0.1350020	0.0	45.0	- 0.00785	- 0.003517
11.5	0.0672169	0.0	45.5	- 0.00269	- 0.003165
12.0	0.0256514	0.0	46.0	- 0.00125	- 0.002873
12.5	- 0.0142418	0.0	46.5	- 0.00187	- 0.002627
13.0	- 0.0459985	0.0	47.0	- 0.01911	- 0.002417
14.0	- 0.0900011	0.0	47.5	- 0.00714	- 0.002236
15.0	- 0.1143158	0.0	48.0	- 0.01119	- 0.002077
17.0	- 0.1402204	0.0	48.5	- 0.01630	- 0.001937
18.0	- 0.1520094	0.0	49.5	- 0.02972	- 0.001703
18.5	- 0.1575704	0.0	50.5	- 0.04805	- 0.001513
19.0	- 0.0976976	0.0	51.1	0.14020	- 0.001428
19.5	- 0.0103902	0.0	52.5	0.05361	- 0.001228
20.5	- 0.0158538	0.0	53.15	- 0.00702	- 0.001156
21.5	- 0.0179638	0.0	54.0	0.12815	- 0.001070
22.0	0.0248128	0.0	54.5	0.15800	- 0.001025
22.5	0.0592704	0.0	54.9	0.17490	- 0.000996
23.0	0.0341000	0.0	55.5	0.02278	- 0.000944
23.5	0.0131156	0.0	56.0	- 0.14983	- 0.000907
24.0	- 0.0066519	0.0	56.5	- 0.25893	- 0.000867
25.0	- 0.0416093	0.0	56.9	- 0.19683	- 0.000850
26.5	- 0.0721385	0.0	57.15	- 0.21905	- 0.000833
27.0	- 0.0751240	0.0	58.0	- 0.02270	- 0.000782
27.5	- 0.0748659	0.0	58.5	0.03222	- 0.000755
28.0	- 0.0724169	0.0	59.0	0.05335	- 0.000730
28.5	- 0.0677570	0.0030731	59.45	0.14208	- 0.000706
29.0	0.1054490	0.0052179	60.0	0.06701	- 0.000684
29.5	0.2103205	0.0066011	60.5	0.04495	- 0.000663
30.0	0.2679040	0.0076445	61.5	0.02953	- 0.000623
30.5	0.2422265	0.0084255	62.5	0.02153	- 0.000588
31.0	0.1714775	0.0090480	63.5	0.01753	- 0.000555
32.0	0.0091100	0.0124630	64.5	0.01485	- 0.000526
32.5	- 0.0749998	0.0131268	65.0	0.01391	- 0.000512
33.0	- 0.135454	0.0132260	67.5	0.01003	- 0.000452
34.0	- 0.211430	0.0123497	70.0	0.00719	- 0.000402
35.0	- 0.269263	0.0104246	72.0	0.00600	- 0.000369
35.5	- 0.296427	0.0092520	75.0	0.00426	- 0.000327

^aFor L_F = 1.0, F_A = F_{A1} and F_B = F_{B1} $\left[\frac{\beta}{2} \left(\frac{n_L W}{q} \right) \right]$

TABLE 24.—F-FUNCTION DATA FOR F-104 AT MACH 1.30

^aL_F = 0.3048 m (1.0 ft); S_{REF} = 18.288 m² (196.0 ft²)

L, ft	F _{A1}	F _{B1}	L, ft	F _{A1}	F _{B1}
0.0	0.0	0.0	35.0	-0.282686	0.0102549
0.5	0.025489	0.0	36.0	-0.350166	0.0082707
1.0	0.046537	0.0	36.5	-0.352058	0.0074282
1.5	0.063821	0.0	37.0	-0.329608	0.0066129
2.0	0.077941	0.0	37.5	-0.283138	0.0058070
3.0	0.098322	0.0	38.0	-0.202292	0.0043933
4.0	0.110278	0.0	38.5	-0.099395	0.0022456
5.0	0.120083	0.0	39.0	0.017605	-0.000349
6.0	0.132273	0.0	39.5	0.147210	-0.003303
7.0	0.146507	0.0	40.0	0.290607	-0.006570
8.0	0.162150	0.0	40.5	0.039094	-0.011211
8.5	0.189494	0.0	41.0	0.018795	-0.017391
9.0	0.171036	0.0	41.5	0.003757	-0.010724
9.5	0.163363	0.0	42.0	-0.006566	-0.007794
10.0	0.147299	0.0	42.5	-0.013909	-0.006257
11.0	0.093184	0.0	43.5	-0.024085	-0.004527
12.0	0.021022	0.0	44.5	-0.031073	-0.003540
13.0	-0.035122	0.0	45.0	-0.033937	-0.003186
14.0	-0.071911	0.0	46.0	-0.038558	-0.002644
15.0	-0.094154	0.0	47.0	-0.042389	-0.002290
16.0	-0.110615	0.0	48.0	-0.045358	-0.001982
17.0	-0.125486	0.0	50.0	-0.049865	-0.001564
18.0	-0.138975	0.0	50.5	-0.050753	-0.001478
18.5	-0.076983	0.0	51.0	-0.012266	-0.001400
19.0	-0.028085	0.0	51.5	0.086256	-0.001329
20.0	-0.026429	0.0	52.0	0.073575	-0.001263
21.0	-0.025551	0.0	52.5	0.063988	-0.001203
21.5	0.026107	0.0	53.0	0.057613	-0.001148
22.0	0.040255	0.0	53.5	0.050119	-0.001097
22.5	0.024784	0.0	54.0	0.044532	-0.001050
23.0	0.009648	0.0	55.0	0.036273	-0.000965
23.5	-0.005522	0.0	56.0	0.029772	-0.000891
24.0	-0.020072	0.0	57.0	0.025192	-0.000827
24.5	-0.034020	0.0	58.0	0.021930	-0.000770
25.0	-0.046156	0.0	59.0	0.018686	-0.000719
26.0	-0.062328	0.0	60.0	0.015523	-0.000674
27.0	-0.067120	0.0	61.0	0.013558	-0.000633
28.32	-0.062800	0.0	62.0	0.011948	-0.000596
28.5	-0.060170	0.0033474	63.0	0.018012	-0.000563
29.0	-0.055389	0.0056780	64.0	0.009658	-0.000533
29.5	0.022966	0.0071764	65.0	0.008575	-0.000505
30.0	0.195671	0.0082951	66.0	0.007879	-0.000480
30.5	0.304881	0.0091224	68.0	0.006461	-0.000435
31.0	0.306149	0.0099622	69.0	0.005985	-0.000416
31.5	0.232487	0.0119982	69.5	0.005630	-0.000406
32.0	0.126461	0.0136219	70.0	0.005535	-0.000397
32.5	0.026559	0.0140847	71.0	0.005053	-0.000380
33.0	-0.070748	0.0139967	72.5	0.004599	-0.000357
33.5	-0.154147	0.0135073	74.0	0.004105	-0.000336
34.0	-0.206160	0.0126914	75.0	0.003798	-0.000323

^aFor L_F = 1.0, F_A = F_{A1} and F_B = F_{B1} $\left[\frac{\beta}{2} \left(\frac{n_L W}{q} \right) \right]$

APPENDIX C

THEORETICAL RELATIONSHIPS NEAR

CUTOFF DURING THRESHOLD MACH NUMBER FLIGHT

A number of useful relationships can be derived relating various parameters near the cutoff condition. For reference, several of these are presented in this section.

Threshold Mach Number

The threshold Mach number has been defined to be the maximum airplane Mach number for which complete shock wave refraction will occur above the ground. Since the refraction is caused by gradients of temperature and wind, the threshold Mach number is dependent on the sound and wind speeds at the airplane altitude and at the cutoff altitude. It can be derived from the equation describing the change of the wave normal direction with altitude. This relationship directly beneath the airplane for steady, level flight is given by equation (17) of reference 7 as:

$$\cos \Theta = \frac{a(Z)}{c_o + u_n(Z)} \quad (C1)$$

where:

Θ = inclination angle of wave normal below the horizontal

$a(Z)$ = sound speed at altitude Z

$u_n(Z)$ = wind component at altitude Z parallel to flight path (tailwind is negative)

$$c_o = \left(\frac{a_o}{\sin \mu_o} - u_{n_o} \right) = (M a_o - u_{n_o}) = V_G \quad (C2)$$

The subscript o indicates initial values at the airplane altitude.

The condition for cutoff or complete refraction is that $\Theta = 0$ or $\cos \Theta = 1.0$. Then we have

$$\cos \Theta = 1.0 = \frac{a(Z)}{[M_T a_o - u_{n_o}] + u_n(Z)} \quad (C3)$$

Solving for M_T gives

$$M_T = \frac{1}{a_0} \left[\{a(Z) - u_n(Z)\}_{\max} + u_{n_0} \right] \quad (C4)$$

The parameter $\{a(Z) - u_n(Z)\}_{\max}$ is the maximum shock propagation speed, $V_{p\max}$, that occurs between the airplane and the ground.

Nicholls (ref. 46) has stated that the above equation for M_T (and the equivalent equation in ref. 32) is incorrect since no sidewind effect has been taken into account. In reality, however, Nicholls' equation agrees with previous results when the differences between coordinate systems for the wind terms are considered. Nicholls failed to realize that the wind component u_n is the horizontal wind component in the vertical plane of the wave normal. Nicholls' equation (12) of reference 46 which was used for comparison between his and previous results is in error since u_n is not equal to his wind term u . The wind component u_n is defined as $u \cos(\nu - \eta)$. For $\phi = 0$ this becomes $u \cos(\psi - \eta)$ where:

- u = horizontal wind speed
- ψ = airplane heading (true North)
- η = direction from which wind blows (true North)
- ν = heading angle of wave normal (true North)

Theoretical Relationships Near Cutoff During Threshold Mach Number Flight

In deriving relationships for propagation near cutoff it is useful to start with the basic relationship describing the inclination of the wave normal below the horizontal, Θ , with sound and wind speed differences between the airplane and a particular altitude. This is given by equation (C1). Two other parameters of interest are the airplane ground speed, V_G , and the shock wave propagation speed, V_p . These are given by

$$V_G = M a_0 - u_{n_0} \quad (C5)$$

$$V_p = a(Z) - u_n(Z) \quad (C6)$$

Also:

$$\cos \Theta = \frac{a(Z)}{(M a_o - u_{n_o}) + u_n(Z)} = \frac{a(Z)}{V_G + u_n(Z)}$$

$$M_T = \frac{1}{a_o} \{V_{p_{\max}} + u_{n_o}\}$$

By algebraic manipulation of the above equations it can be shown that the following relationships exist as long as Θ is greater than 0° . This means that cutoff has not occurred.

$$\cos \Theta = \frac{\{V_p + u_n(Z)\}}{\{V_G + u_n(Z)\}} \approx \frac{V_p}{V_G} \text{ for small } u_n(Z) \quad (C7)$$

$$\cos \Theta = \left[1 + \left(\frac{V_G - V_p}{a(Z)} \right) \right]^{-1} \quad (C8)$$

$$(V_G - V_p) = a(Z) \left[\frac{(1 - \cos \Theta)}{\cos \Theta} \right] \quad (C9)$$

$$(M - M_T) = (V_G - V_{p_{\max}}) / a_o \quad (C10)$$

$$V_G = \{a(Z) / \cos \Theta\} - u_n(Z) \quad (C11)$$

Other forms of the above relationships could be derived, but in this study these were found to be useful. For example, since $\cos \Theta$ was available from the tower shock arrival times and $a(Z)$ and $u_n(Z)$ were known from the tower meteorological observations, the airplane ground speed, V_G , could be calculated from equation (C11). The value of $(M - M_T)$ is a useful parameter, as is $(V_G - V_p)$. They apply only as long as cutoff has not occurred, however. In general, for Θ greater than 0° the following will be true:

$$\cos \Theta \leq 1.0; (M - M_T) > 0.0; V_p / V_G \leq 1.0.$$

APPENDIX D

THEORETICAL SAFE ALTITUDE FOR SONIC BOOM CUTOFF

Below the caustic produced by threshold Mach number flight the signal decreases in amplitude. Several years ago Dr. Wallace D. Hayes determined a theoretical distance below the cutoff altitude where the signal will be reduced to an acoustic disturbance of relatively small intensity. Dr. Hayes based his analysis on the theory of reference 10. Two parameters are required which include the signal length, L , and a relative radius of curvature, R , of the caustic (relative to the ray). The ratio L/R must be small.

According to the theory the safe altitude, Z_s , is

$$Z_s = (R)^{1/3} (L)^{2/3} \quad (D1)$$

where R depends on the meteorological conditions.

$$R = \frac{a}{\partial(a - u_n)/\partial Z} \quad (D2)$$

It should be noted that in this analysis R should be approximately constant with altitude and always positive. R can be negative under certain atmospheric conditions such as in very stable lapse rate conditions or with a tailwind increasing with altitude (negative u_n). In physical terms, a negative R means that cutoff cannot occur.

It is of interest to calculate a typical safe altitude for the F-104 airplane used in the BREN tower tests. A typical pressure signature length is about 39.6 m (130.0 ft) at the ground for the flight test conditions. For standard no-wind conditions, R is calculated to be about 87 600 m (288 000 ft). Thus, the safe altitude is 517 m (1700 ft). For the atmospheric conditions during the BREN tower tests the safe altitude calculated from the local meteorological conditions using equation (D1) ranged from about 400 m (1300 ft) to over 2000 m (6600 ft) above the ground.

REFERENCES

1. Friedrichs, K. L.: Formation and Decay of Shock Waves. *Commun. Pure Appl. Math.*, vol. 1, 1948, pp. 211-245.
2. Hayes, W. D.: Linearized Supersonic Flow. Ph. D. Thesis, Cal. Inst. Tech., 1947. Also available as AMS Rept. 052, Princeton Univ.
3. Hayes, W. D.: Pseudotransonic Similitude and First-Order Wave Structure. *J. Aeronaut. Sci.*, vol. 21, 1954, pp. 721-720.
4. Landau, L. D.: On Shock Waves at Large Distances From the Place of Their Origin. *Prik. Mat. Mekh.*, vol. 9, 1945, pp. 286-292.
5. Whitham, G. B.: The Behavior of Supersonic Flow Past a Body of Revolution Far From the Axis. *Proc. Roy. Soc., Ser. A*, vol. 201, 1950, pp. 89-109.
6. Whitham, G. B.: On the Propagation of Weak Shock Waves. *J. Fluid Mech.*, vol. 1, 1956, pp. 290-318.
7. Hayes, W. D.; Haefeli, R. C.; and Kulsrud, H. E.: Sonic Boom Propagation in a Stratified Atmosphere with Computer Program. NASA CR-1299, 1969. Also Hayes, W. D.; and Haefeli, R. C.: The ARAP Sonic Boom Computer Program. Second Conference on Sonic Boom Research, NASA SP-180, 1968, pp. 151-158.
8. Carlson, H. W.: Correlation of Sonic Boom Theory With Wind Tunnel and Flight Measurements. NASA TR R-213, 1964.
9. Guiraud, J. P.: Acoustique Géométrique, Bruit Ballistique des Avions Supersonic et Focalisation. *J. Méc.*, vol. 4, 1965, pp. 215-267.
10. Hayes, W. D.: Similarity Rules for Nonlinear Acoustic Propagation Through a Caustic. Second Conference on Sonic Boom Research, NASA SP-180, 1969, pp. 165-171.
11. Théry, C.: Réfraction Atmosphérique et Réflexion en Sol des Bangs. Aircraft Noise and the Sonic Boom, AGARD Conf. Proc., May 1969.

12. Seebass, R.: Nonlinear Acoustic Behavior at a Caustic. Third Conference on Sonic Boom Research, NASA SP-255, 1971, pp. 87-120.
13. Coakley, T. J.: Preliminary Numerical Investigation of Sonic Boom at Threshold Mach Numbers. Third Conference on Sonic Boom Research, NASA SP-255, 1971, pp. 181-191.
14. Lina, L. J.; and Maglieri, D. J.: Ground Measurements of Airplane Shock-Wave Noise at Mach Numbers to 2.0 and at Altitudes to 60,000 Feet. NASA TN D-235, 1960.
15. Hubbard, H.; Maglieri, D. J.; Huckel, V.; and Hilton, D. A.: Ground Measurements of Sonic-Boom Pressures for the Altitude Range of 10,000 to 75,000 Feet. NASA TR R-198, 1964.
16. Maglieri, D. J.; and Lansing, D. L.: Sonic Booms from Aircraft in Maneuvers. NASA TN D-2370, 1964.
17. Lansing, D. L.; and Maglieri, D. J.: Comparison of Measured and Calculated Sonic-Boom Ground Patterns Due to Several Different Aircraft Maneuvers. NASA TN D-2730, 1965.
18. Maglieri, D. J.; Hilton, D. A.; and McLeod, N. J.: Experiments on the Effects of Atmospheric Refraction and Airplane Accelerations on Sonic-Boom Ground-Pressure Patterns. NASA TN D-3520, 1966.
19. Hilton, D. A.; Huckel, V.; Steiner, R.; and Maglieri, D. J.: Sonic-Boom Exposures During FAA Community-Response Studies Over a 6-Month Period in the Oklahoma City Area. NASA TN D-2539, 1964.
20. Stanford Res. Inst.: Sonic Boom Experiments at Edwards Air Force Base. Rept. NSBEO-1-67. National Sonic Boom Evaluation Office, ASTIA no. AD 655 310, 1967.
21. Maglieri, D. J.: Sonic Boom Flight Research—Some Effects of Airplane Operations and the Atmosphere on Sonic Boom Signatures. Sonic Boom Research, NASA SP-147, 1967, pp. 25-49.
22. Garrick, I. E.; and Maglieri, D. J.: A Summary of Results on Sonic-Boom Pressure-Signature Variations Associated With Atmospheric Conditions. NASA TN D-4588, 1968.

23. Maglieri, D. J.: Sonic Boom Ground Pressure Measurements for Flights at Altitudes in Excess of 70,000 Feet and at Mach Numbers up to 3.0. Second Conference on Sonic Boom Research, NASA SP-180, 1968, pp. 19-27.
24. Hubbard, H. H.; Maglieri, D. J.; and Huckel, V.: Variability of Sonic Boom Signatures with Emphasis on the Extremities of the Ground Exposure Patterns. Third Conference on Sonic Boom Research, NASA SP-255, 1971, pp. 351-359.
25. Maglieri, D. J.; Hilton, D. A.; Huckel, V.; Henderson, H. R.; and McLeod, N. J.: Measurements of Sonic Boom Signatures From Flights at Cut-off Mach Number. Third Conference on Sonic Boom Research, NASA SP-255, 1971 pp. 243-254.
26. Vallée, J.: Operation Jericho-Virage. Rapport d'Etude no. 277, Centre d'Essais en Vol Annexe d'Istres, 1969.
27. Dressler, R. F.: Sonic-Boom Waves in Strong Winds. FFA Rept. 97, Aeronaut. Res. Inst. Swed., 1964.
28. Dressler, R. F.; and Fredholm, N.: Statistical Magnifications of Sonic Booms by the Atmosphere. FFA Rept. 104, Aeronaut. Res. Inst. Swed., 1966.
29. Lundberg, B. K.; Dressler, R. F.; and Lagman, S.: Atmospheric Magnification of Sonic Booms in the Oklahoma Tests. FFA Rept. 112, Aeronaut. Res. Inst. Swed., June 1967.
30. Haglund, G. T.; and Olson, D. L.: Study Covering Calculations and Analysis of Sonic Boom During Operational Maneuvers, vol. III—Description of Computer Program. FAA Report EQ. 71-2, Feb. 1971.
31. Randall, D. G.: Methods for Estimating Distributions and Intensities of Sonic Bangs. R.&M. No. 3113, British A.R.C., 1959.
32. Kane, E. J.; and Palmer, T. Y.: Meteorological Aspects of the Sonic Boom. SRDS Report No. RD 64-160, Federal Aviation Agency, ASTIA No. AD 610463, 1964.
33. Haglund, G. T.; and Kane, E. J.: Study Covering Calculations and Analysis of Sonic Boom During Operational Maneuvers, Vol. I—Analysis and Computation of Maneuver Effects. FAA Report EQ. 71-2, Feb. 1971.

34. Herbert, G. A.; and Giarrusso, A.: Meteorological Measurements in Support of the NASA Grazing Sonic Boom Experiment at Jackass Flats, Nevada. NOAA Tech. Memo. ERL ARL-35, 1971.
35. Haglund, G. T.: A Preliminary Climatology of the Threshold Mach Number. Paper Presented at the Fourth Conference on Aerospace Meteorology, Am. Meteorol. Soc. and AIAA (Las Vegas, Nevada) May 1970, pp. 399-413.
36. Henderson, L. F.: On Shock Impedance. J. Fluid Mech., vol. 40, part 4, 1970, pp. 719-735.
37. Thomas, C. L.: Sonic Boom Reflection Factors for Flight near the Threshold Mach Number. J. Aircraft, vol. 8, no. 6, p. 490, 1971.
38. Théry, C.: Atmospheric Refraction and Reflection in Sonic Booms. NASA TT F-13, 409, 1970.
39. Letestu, S., ed.: International Meteorological Tables. World Meteorol. Organ., Geneva, Switzerland, 1966, pp. 4.11-1 - 4.11-3.
40. Harris, C. M.: Effects of Humidity on the Velocity of Sound. J. Acoust. Soc. Am., vol. 49, no. 3, 1971, pp. 890-893.
41. Harris, C. M.: Absorption of Sound in Air Versus Humidity and Temperature. NASA CR-647, 1967.
42. Hodgson, J. P.; and Johannesen, N. H.: Real-Gas Effects in Very Weak Shock Waves in the Atmosphere and the Structure of Sonic Bangs. J. Fluid Mech., vol. 50, part 1, 15 Nov. 1971, pp. 17-20.
43. Whitham, G. B.: The Flow Pattern of a Supersonic Projectile. Commun. Pure Appl. Math., vol. 5, 1952, pp. 301-348.
44. Carlson, H. W.: Experimental and Analytic Research on Sonic Boom Generation at NASA. Sonic Boom Research, NASA SP-147, 1967, pp. 9-23.
45. Middleton, W. D.; and Carlson, H. W.: A Numerical Method of Calculating Near-Field Sonic-Boom Pressure Signatures. NASA TN D-3082, 1965.
46. Nicholls, J. M.: A Note on the Calculation of "Cut-Off" Mach Number. The Meteorological Magazine, vol. 100, Feb. 1971, pp. 33-46.

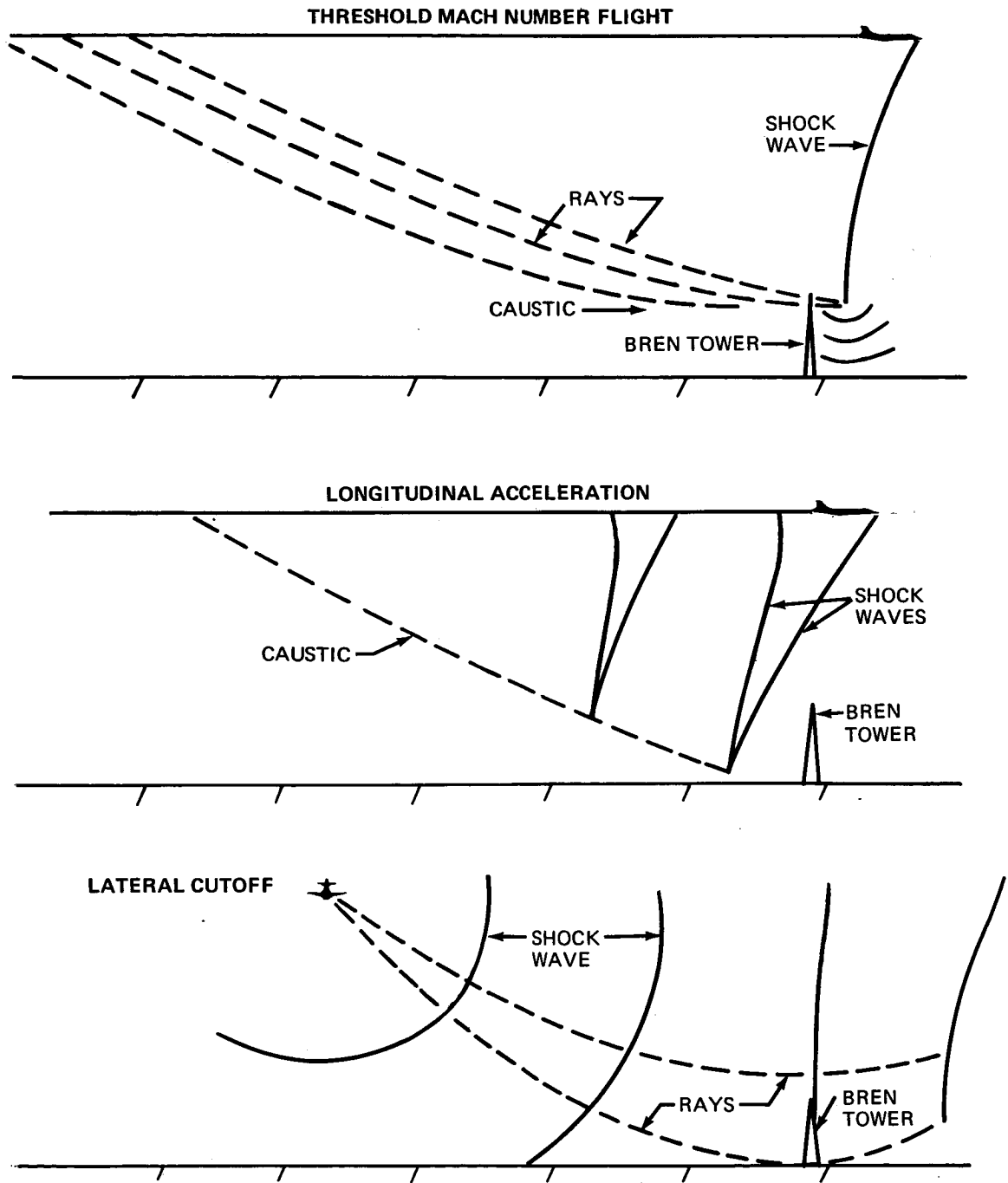


FIGURE 1.—TEST SET UP DURING BREN TOWER TESTS

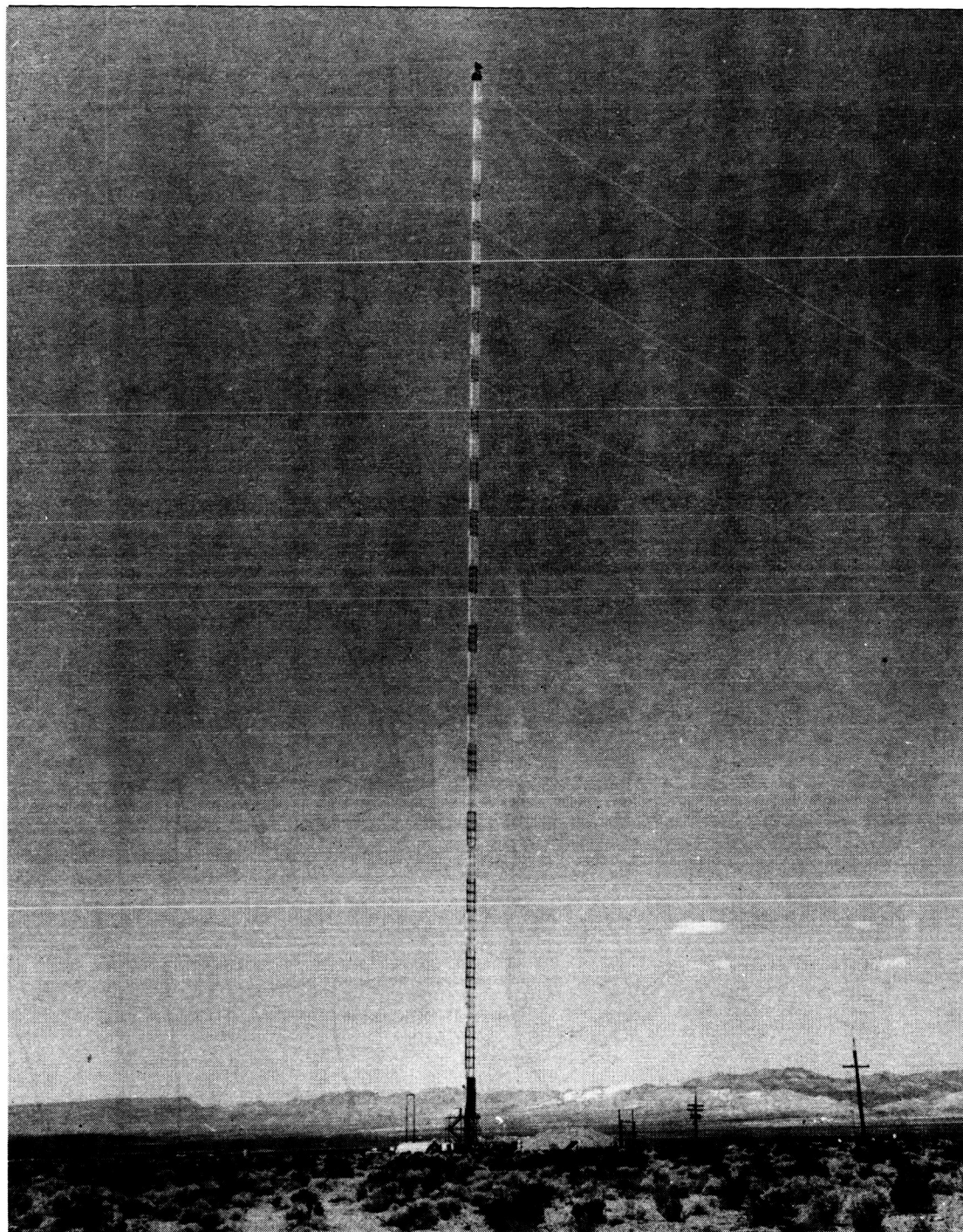


FIGURE 2.—BREN TOWER AT JACKASS FLATS, NEVADA

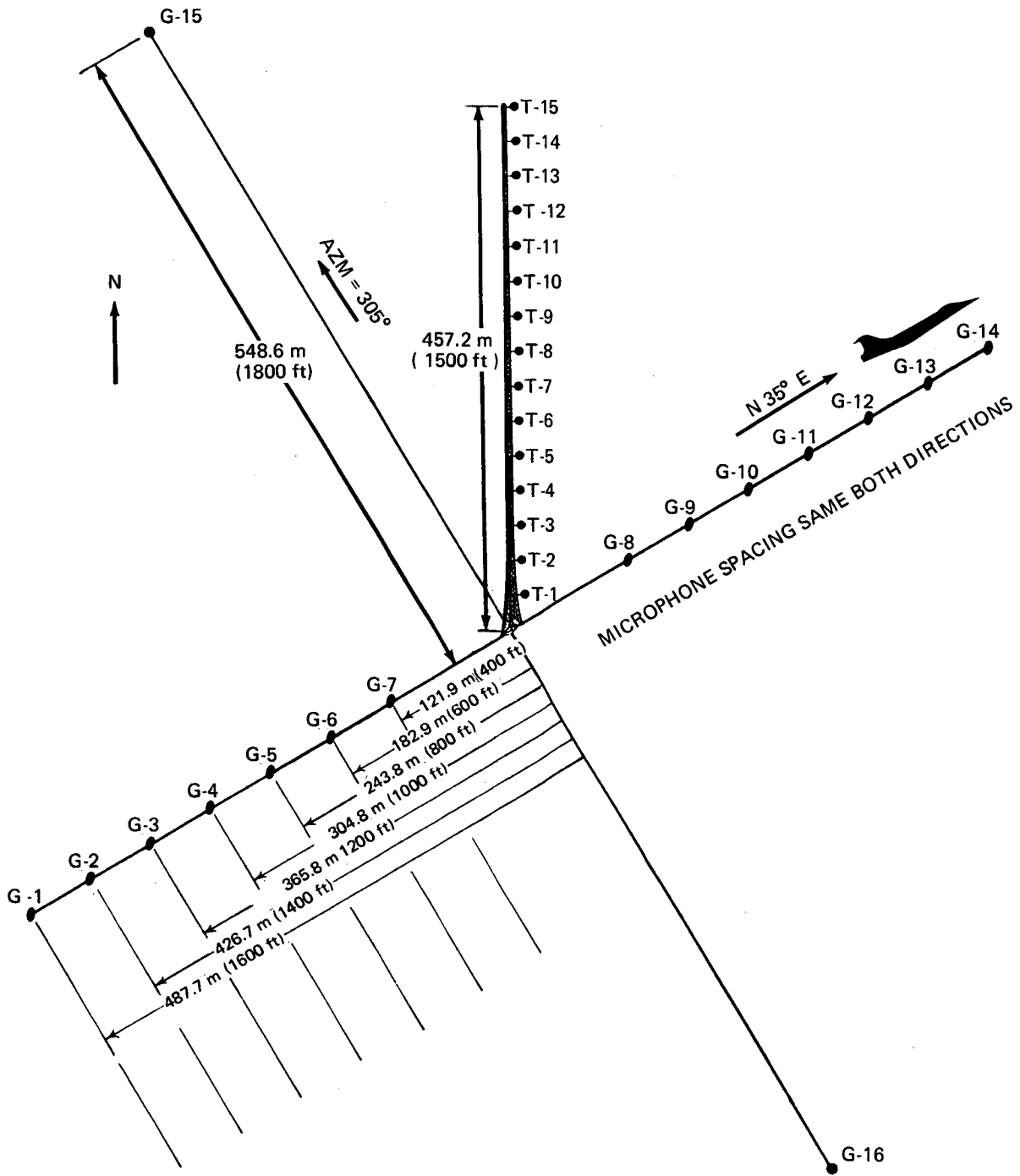


FIGURE 3.—BREN TOWER MICROPHONE ARRAY

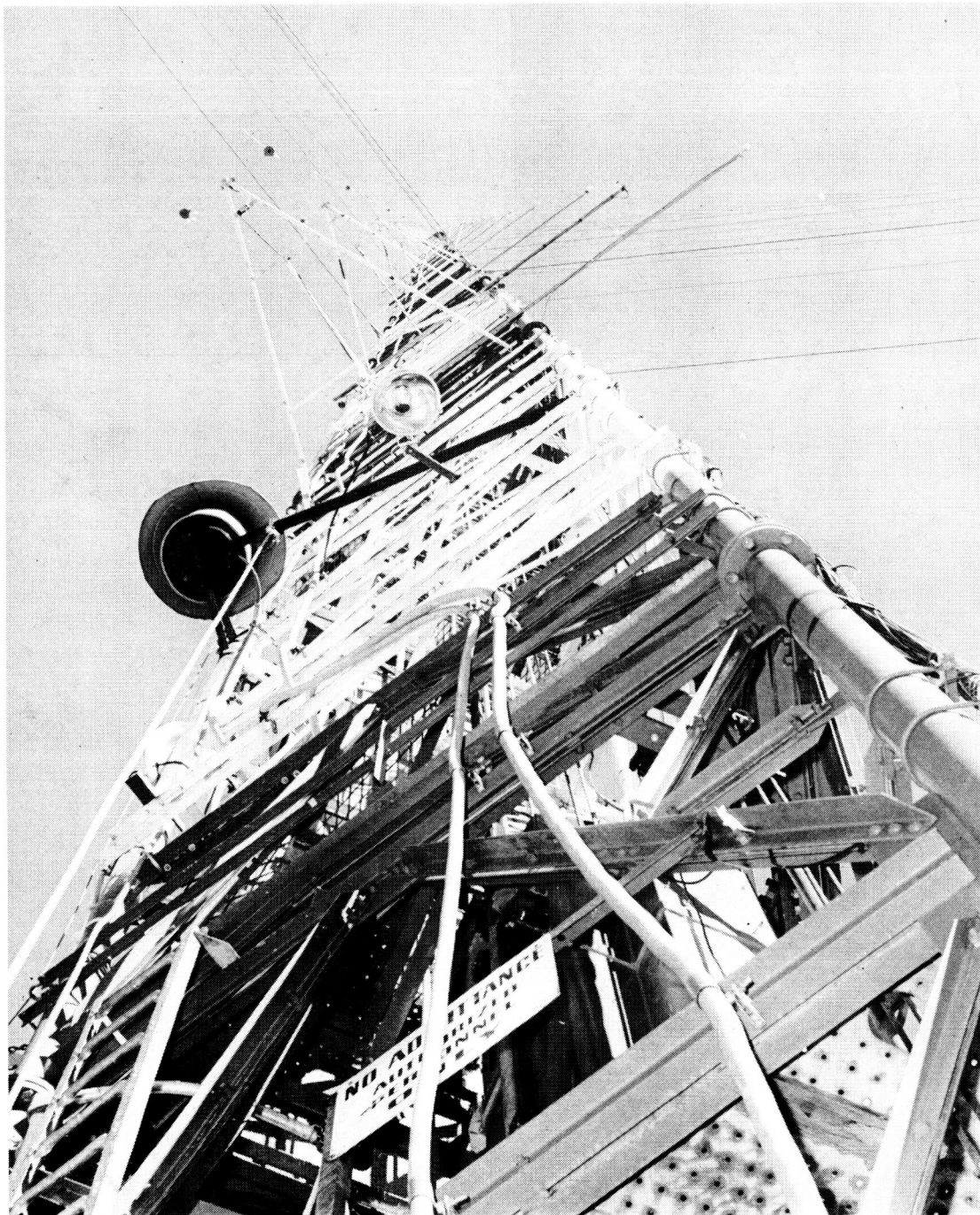


FIGURE 4.—CLOSEUP VIEW OF TOWER. ANEMOMETER SUPPORTS ARE ON THE LEFT AND MICROPHONES ON THE RIGHT

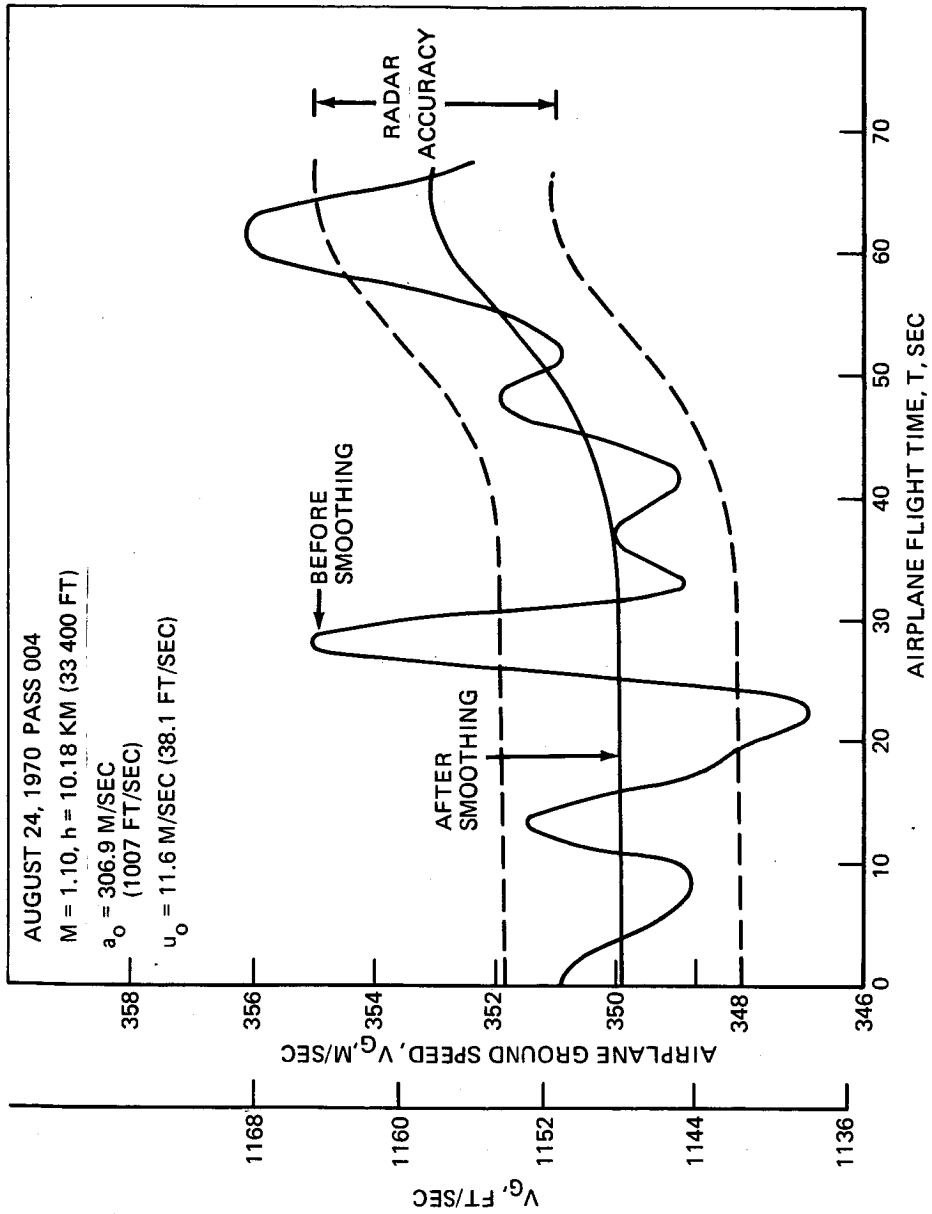
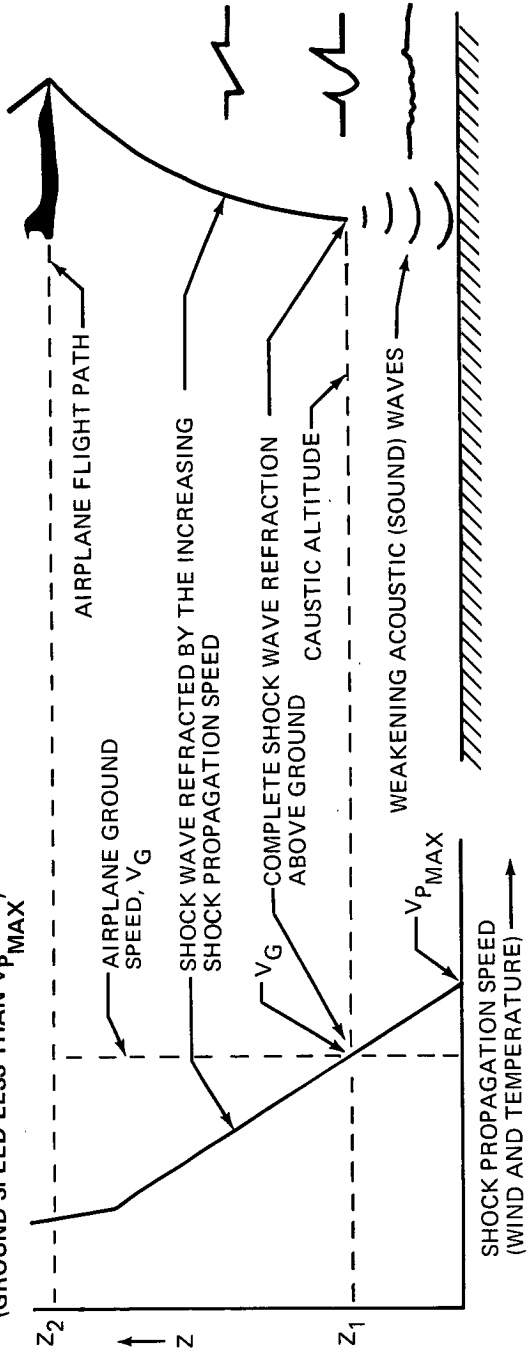
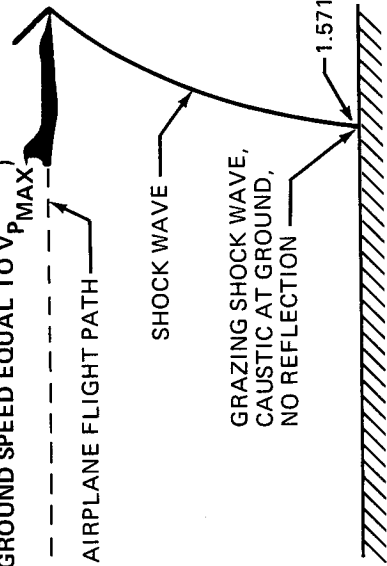


FIGURE 5.—AIRPLANE GROUND SPEED VS FLIGHT TIME—PASS 004

a) MACH NUMBER LESS THAN THRESHOLD MACH NUMBER
(GROUND SPEED LESS THAN $V_{P\text{MAX}}$)



b) MACH NUMBER EQUAL TO THRESHOLD MACH NUMBER
(GROUND SPEED EQUAL TO $V_{P\text{MAX}}$)



c) MACH NUMBER GREATER THAN THRESHOLD MACH NUMBER
(GROUND SPEED GREATER THAN $V_{P\text{MAX}}$)

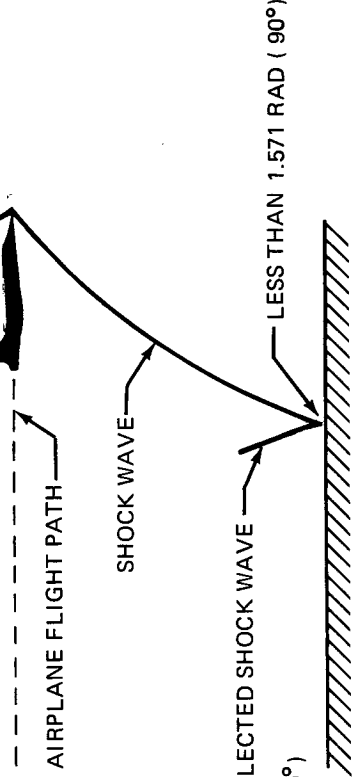


FIGURE 6.—REFRACTION OF SONIC BOOM SHOCK WAVE FOR FLIGHT NEAR THE THRESHOLD MACH NUMBER

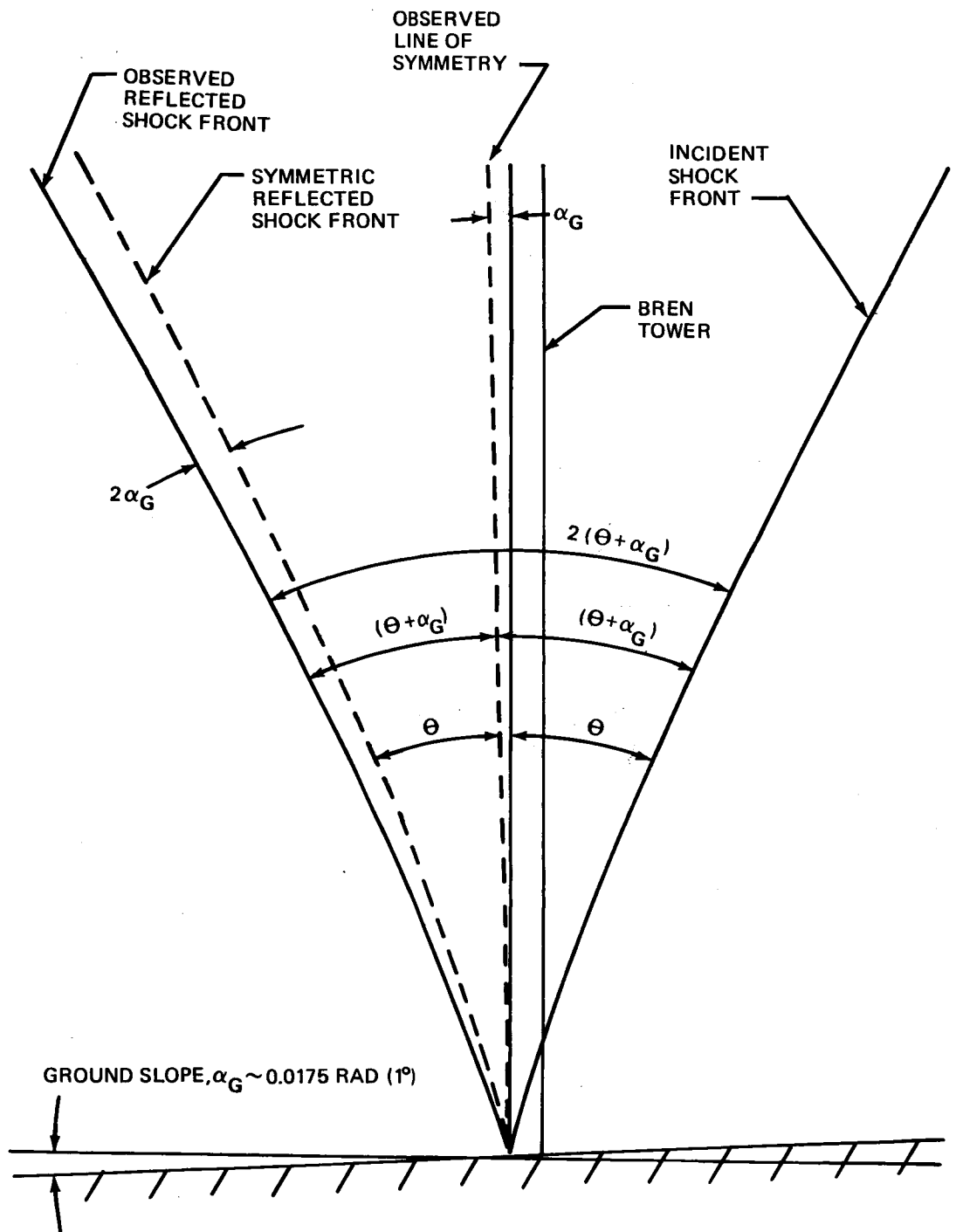


FIGURE 7.—EFFECT OF GROUND SLOPE ON REFLECTED SHOCK FRONT ORIENTATION

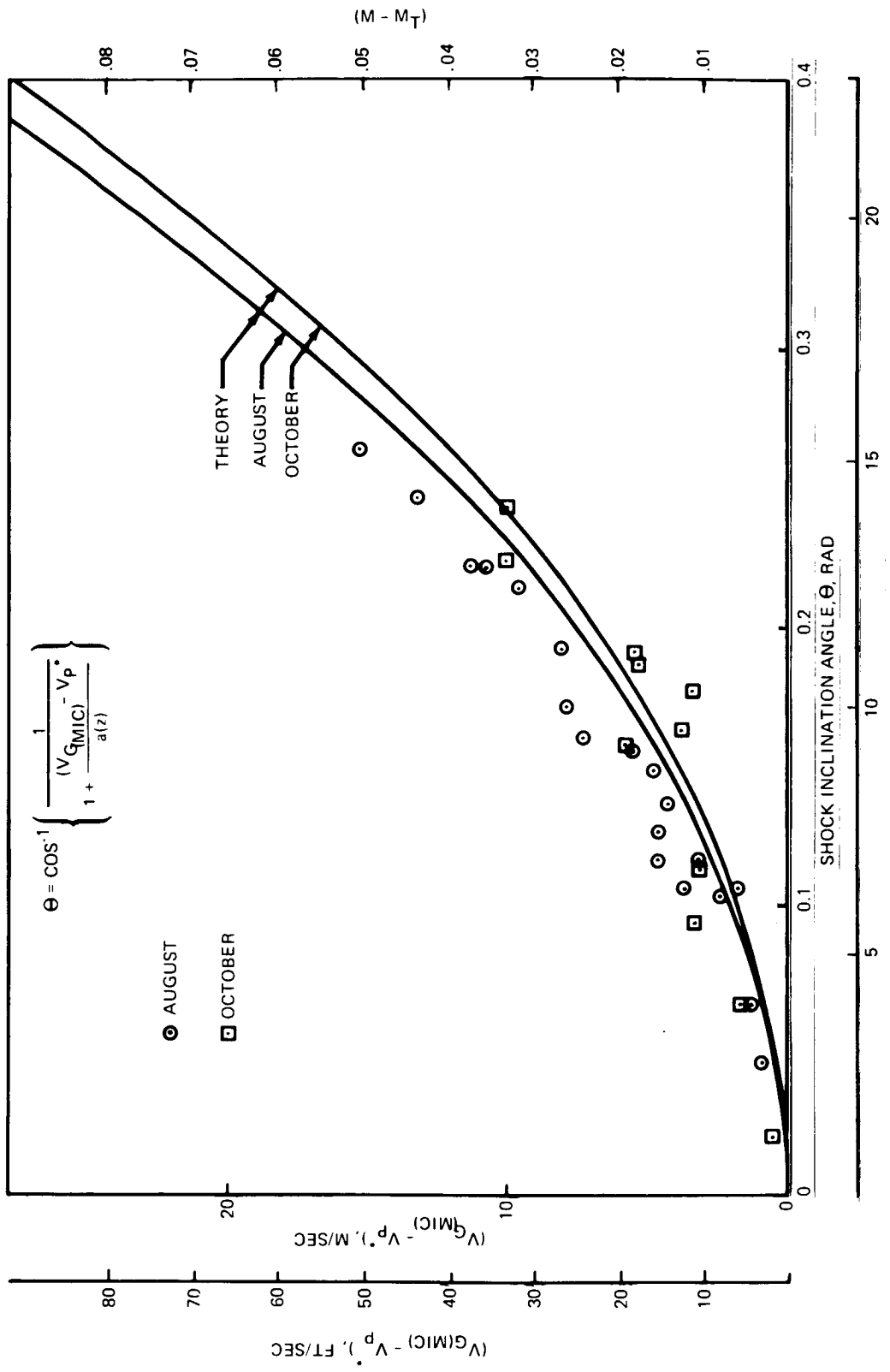


FIGURE 8.—COMPARISON BETWEEN THEORY AND EXPERIMENT—θ

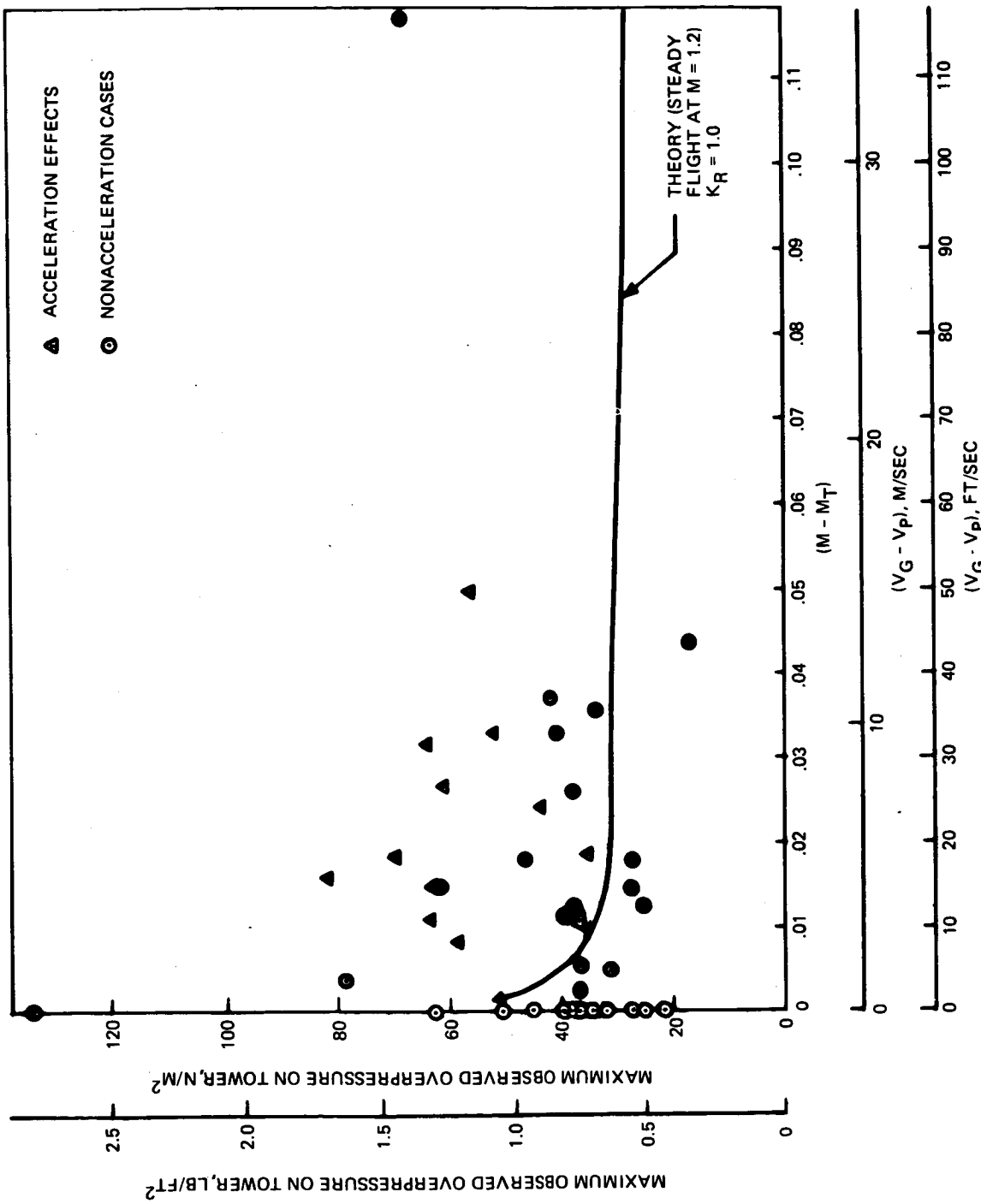


FIGURE 9.—VARIATION OF OVERPRESSURE NEAR THE CUTOFF CONDITION

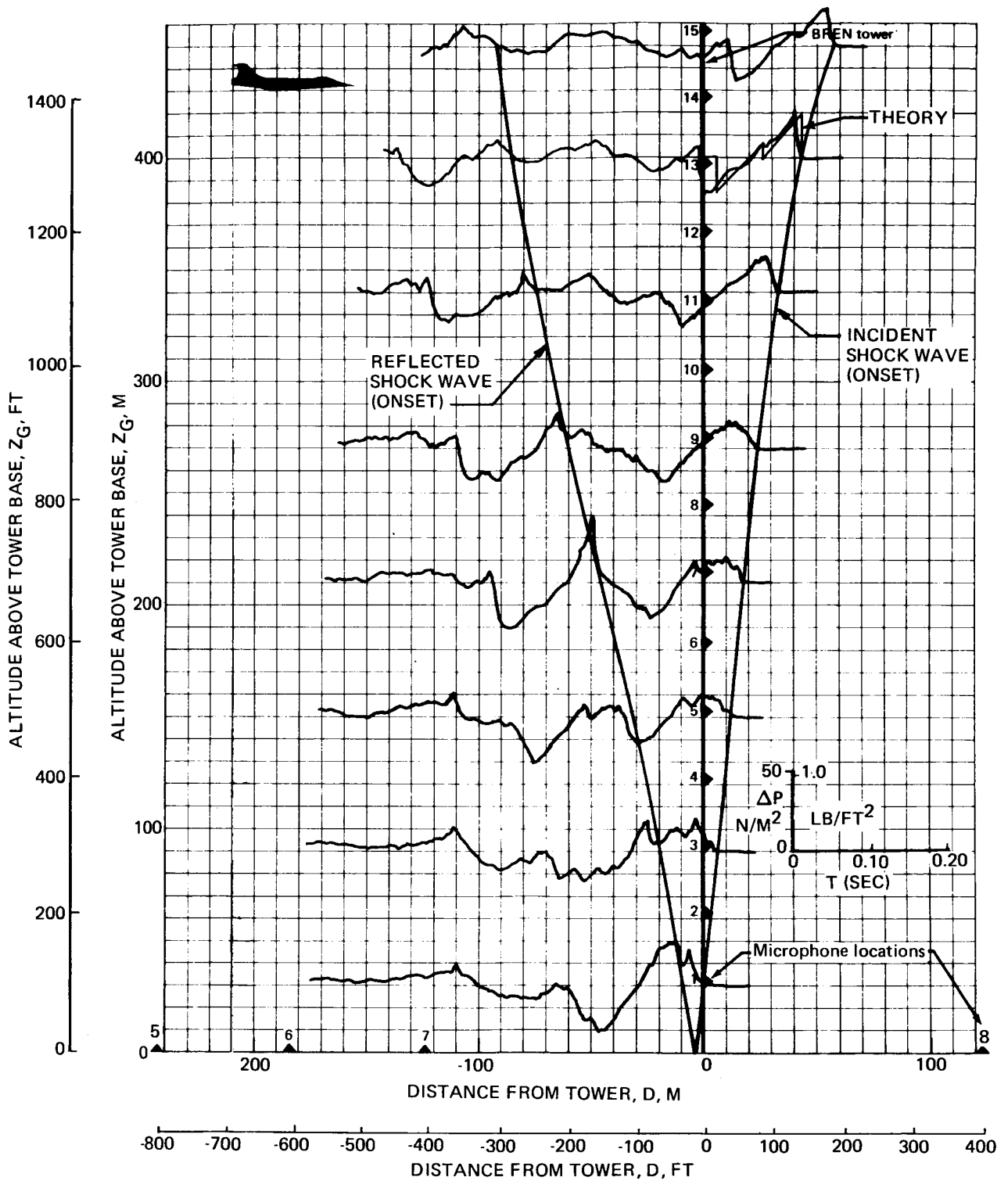


FIGURE 10.—SHOCK WAVE PROFILE AND TOWER PRESSURE SIGNATURES, $M > M_T$ —PASS 101, OCTOBER 28, 3-1

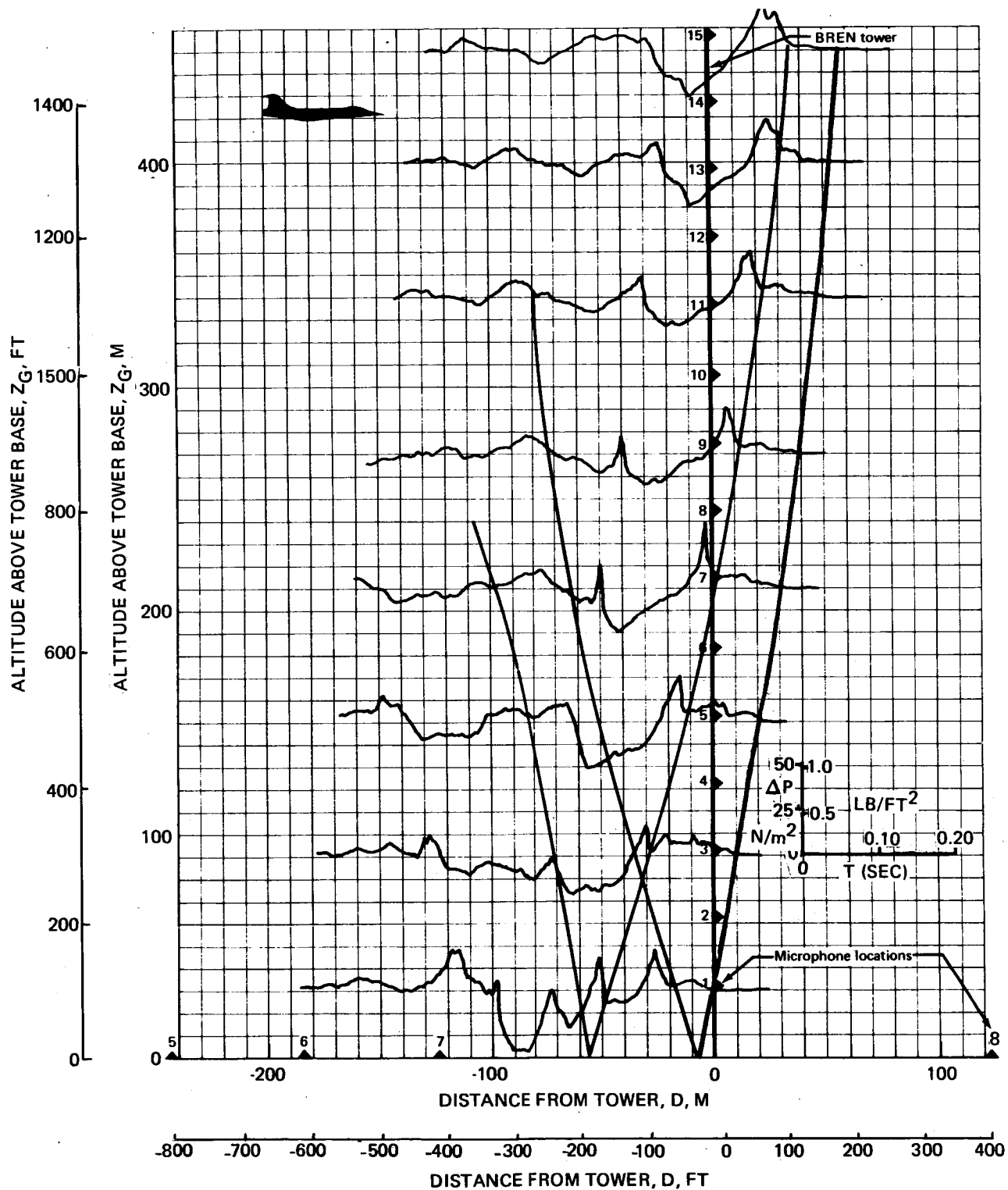


FIGURE 11.—SHOCK WAVE PROFILE AND TOWER PRESSURE SIGNATURES,
 $M > M_T$ —PASS 106, OCTOBER 29, 1-3

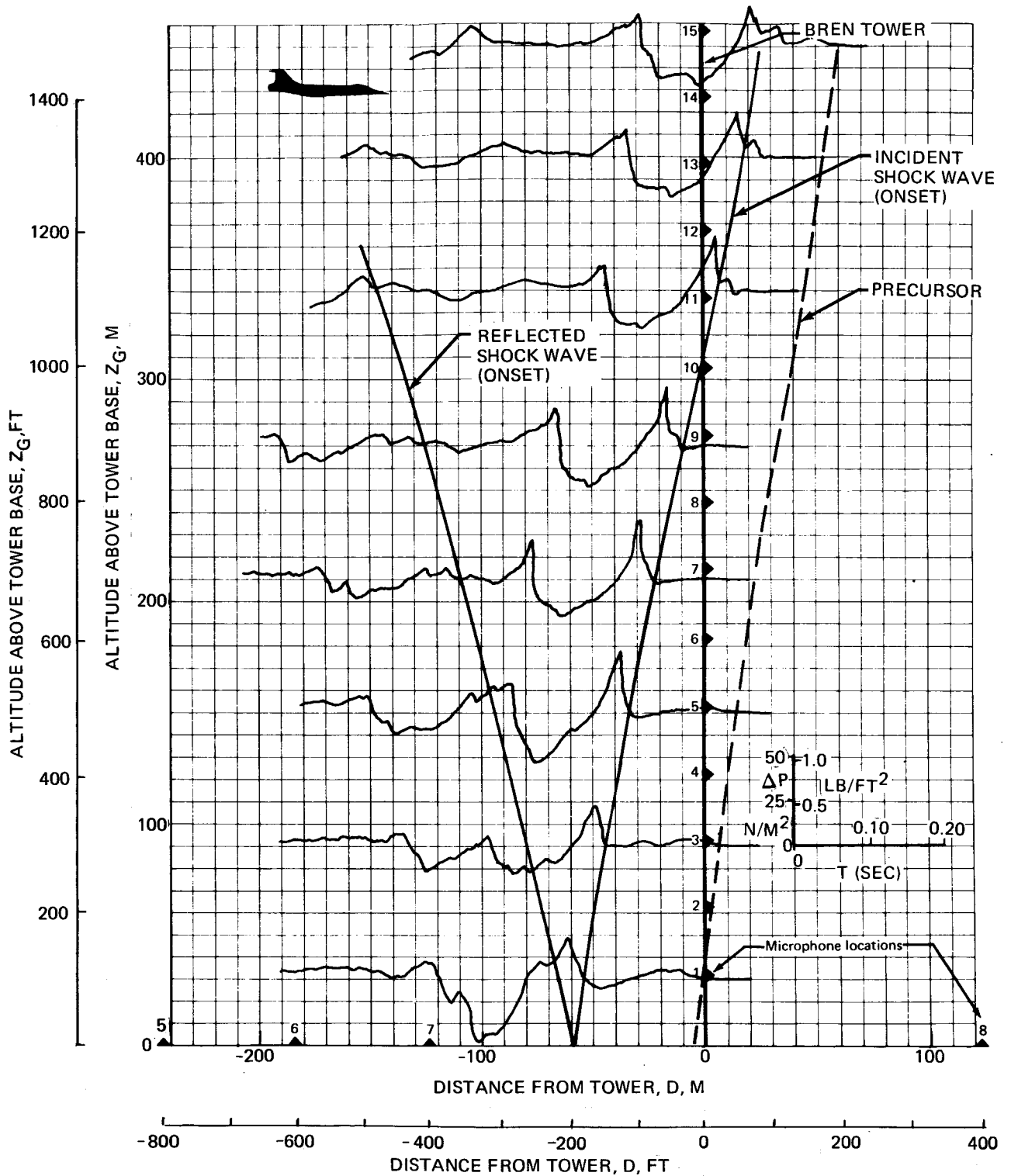


FIGURE 12.—SHOCK WAVE PROFILE AND TOWER PRESSURE SIGNATURES,
 $M > M_T$ —PASS 117, OCTOBER 30, 1-2

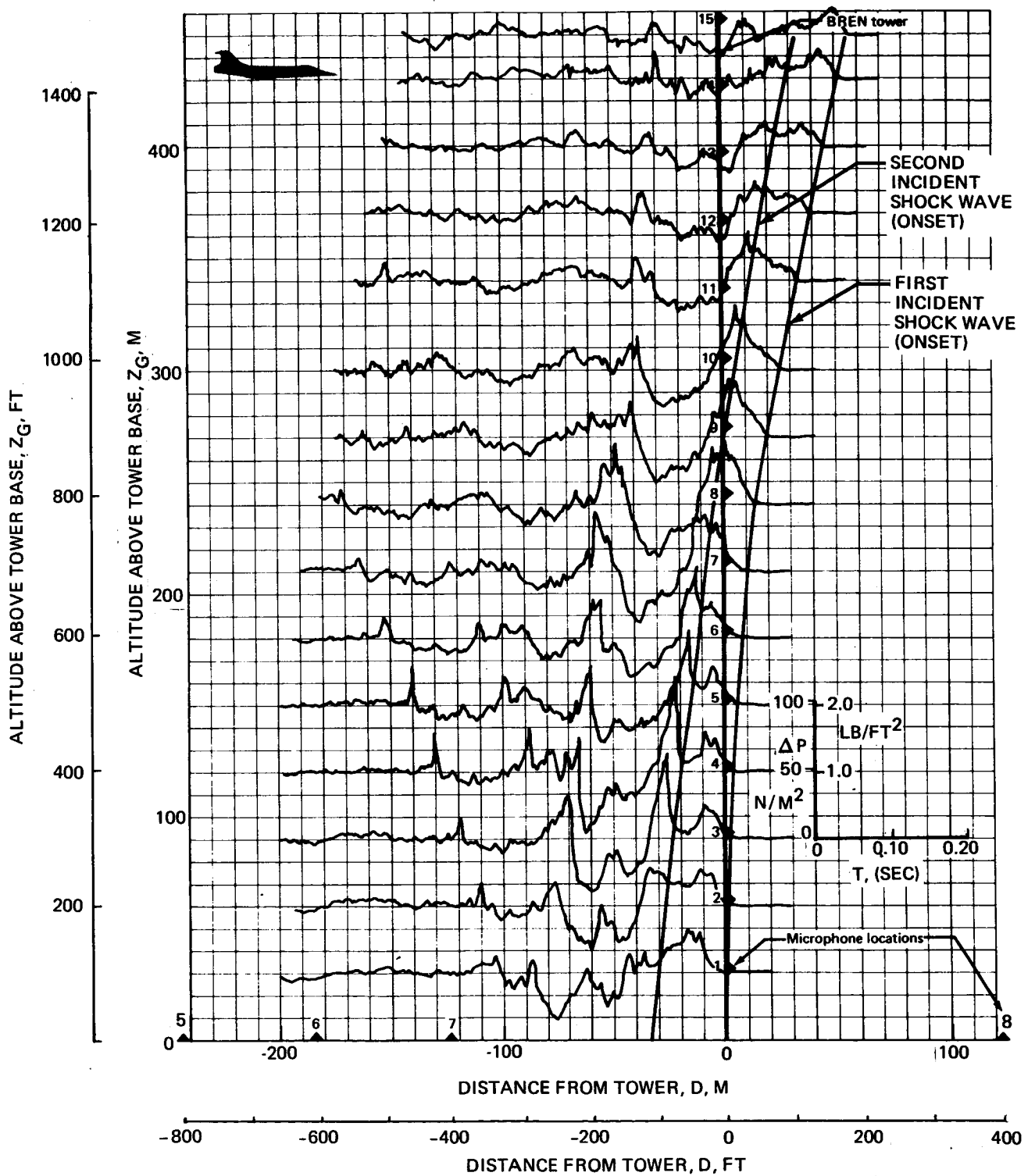


FIGURE 13.—SHOCK WAVE PROFILE AND TOWER PRESSURE SIGNATURES,—PASS 028, AUGUST 25, 4-4

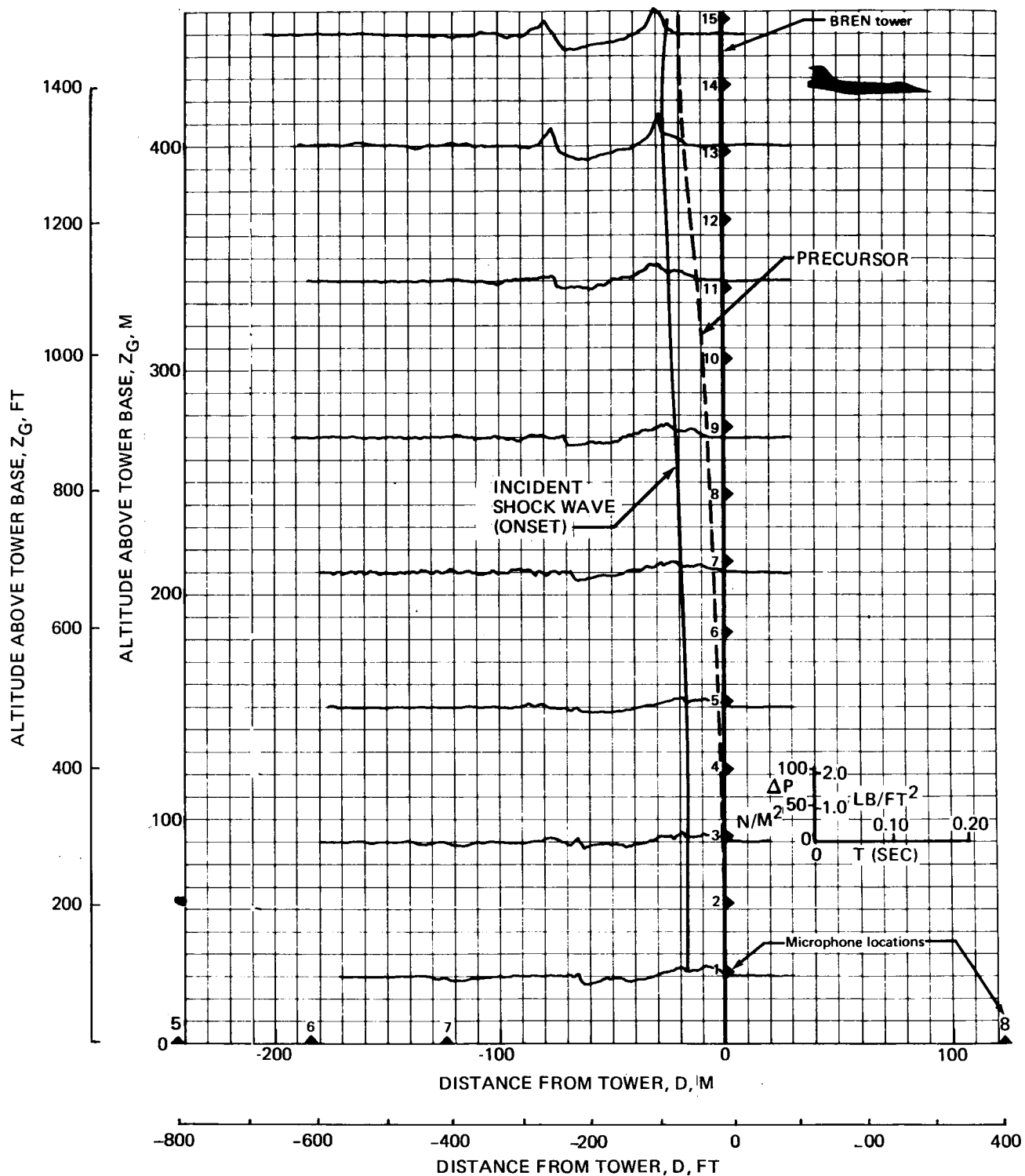


FIGURE 14.—SHOCK WAVE PROFILE AND TOWER PRESSURE SIGNATURES, M ~ M_T—PASS 002, AUGUST 24, 1-2

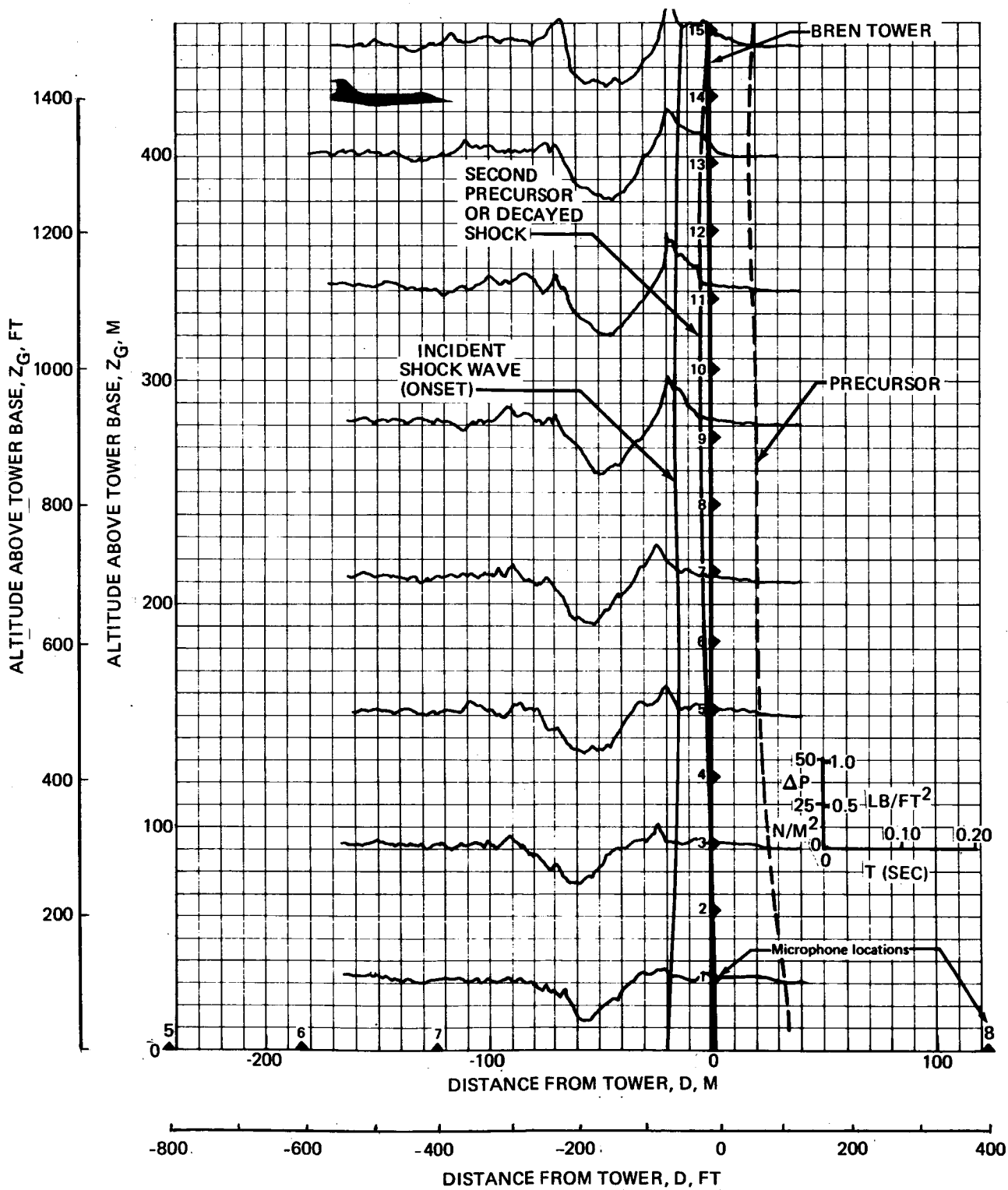


FIGURE 15.—SHOCK WAVE PROFILE AND TOWER PRESSURE SIGNATURES,
 $M \sim M_T$ —PASS 114, OCTOBER 29, 3-2

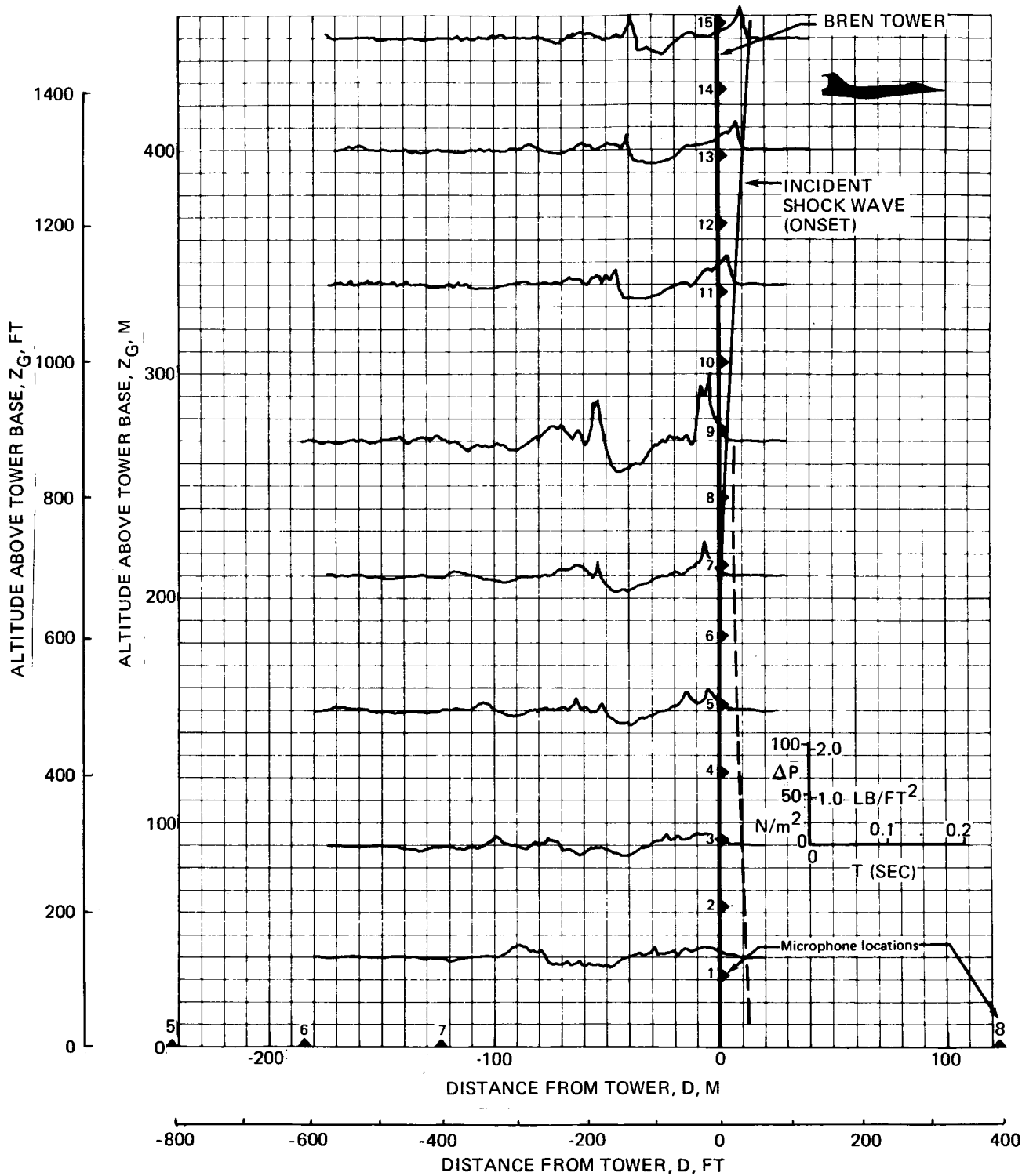


FIGURE 16.—SHOCK WAVE PROFILE AND TOWER PRESSURE SIGNATURES,
 $M \sim M_T$ —PASS 058, AUGUST 31, 2-4

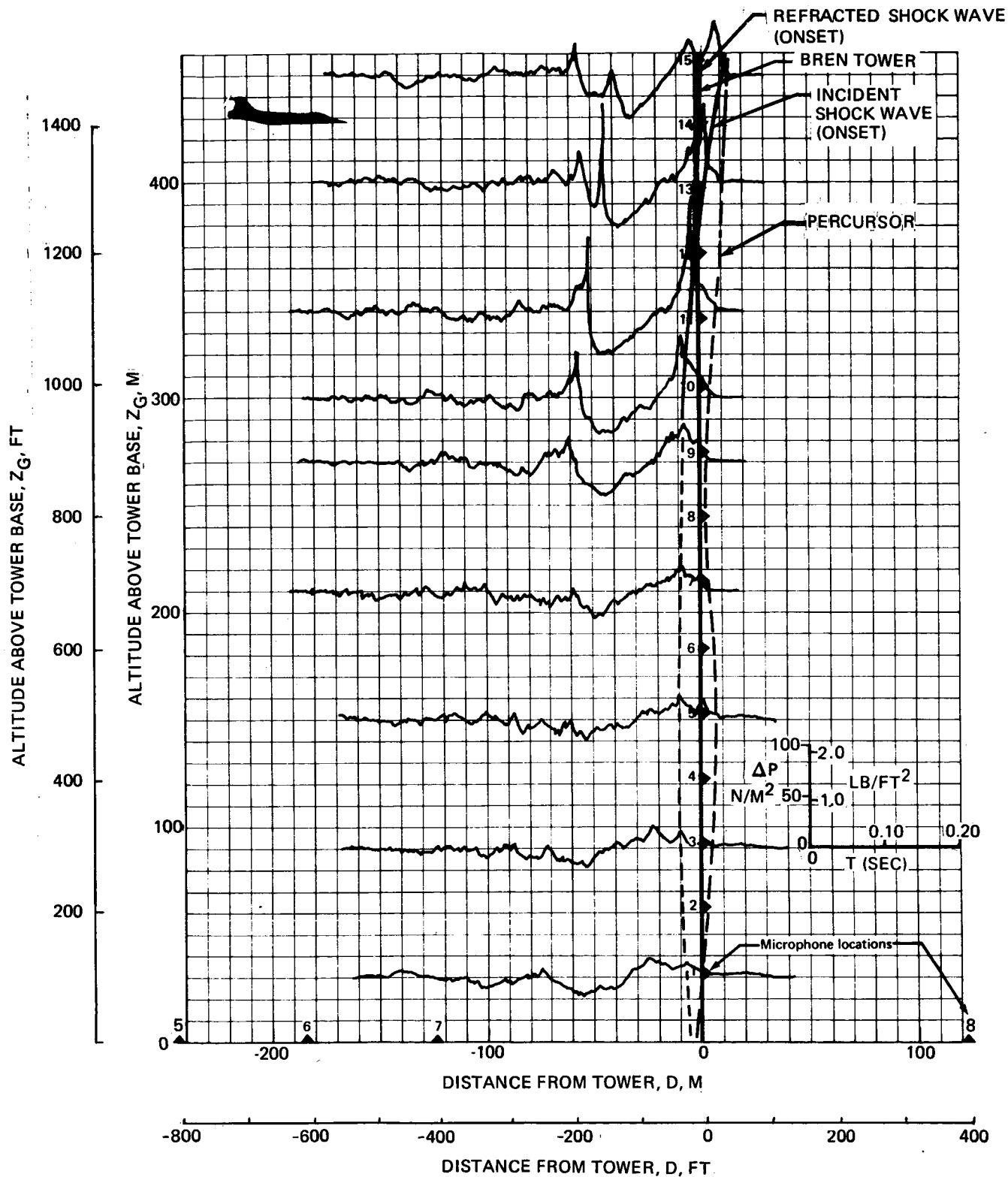


FIGURE 17.—SHOCK WAVE PROFILE AND TOWER PRESSURE SIGNATURES, $M \sim M_T$ —PASS 063, AUGUST 31, 4-1

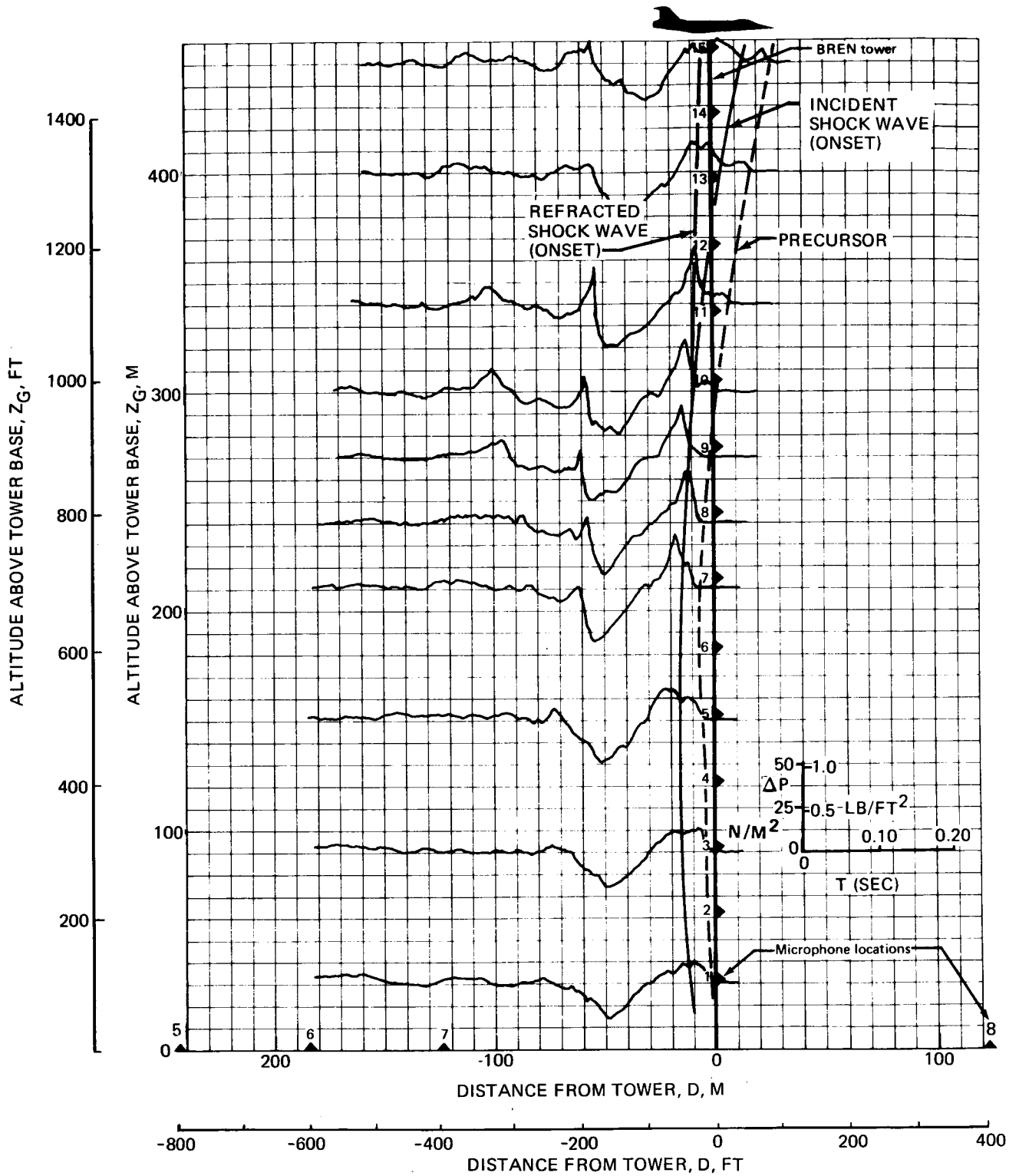


FIGURE 18.—SHOCK WAVE PROFILE AND TOWER PRESSURE SIGNATURES, M~M_T—
PASS 102, OCTOBER 28, 3-2

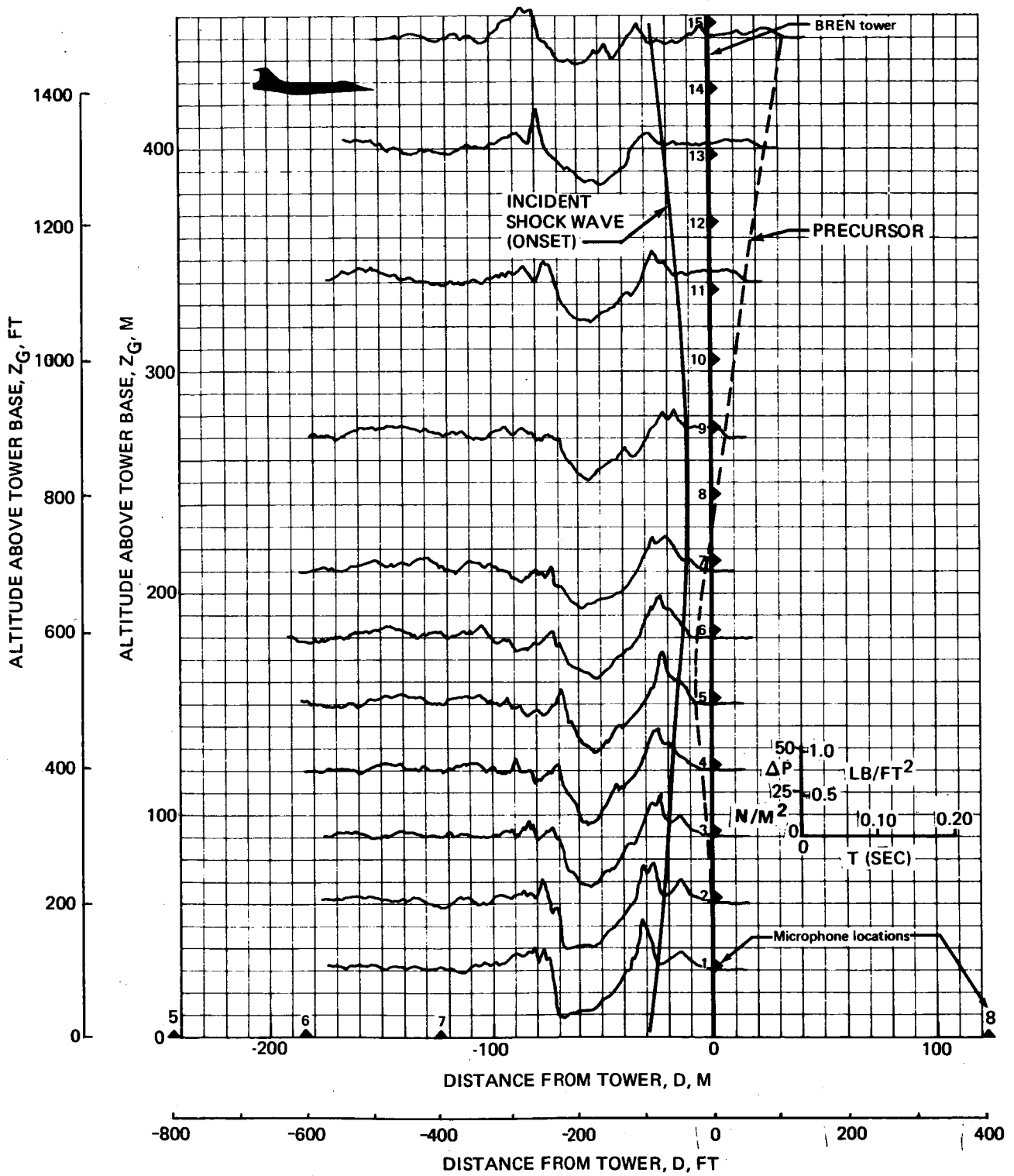


FIGURE 19.—SHOCK WAVE PROFILE AND TOWER PRESSURE SIGNATURES, M ~ MT
 —PASS 103, OCTOBER 28, 3-3

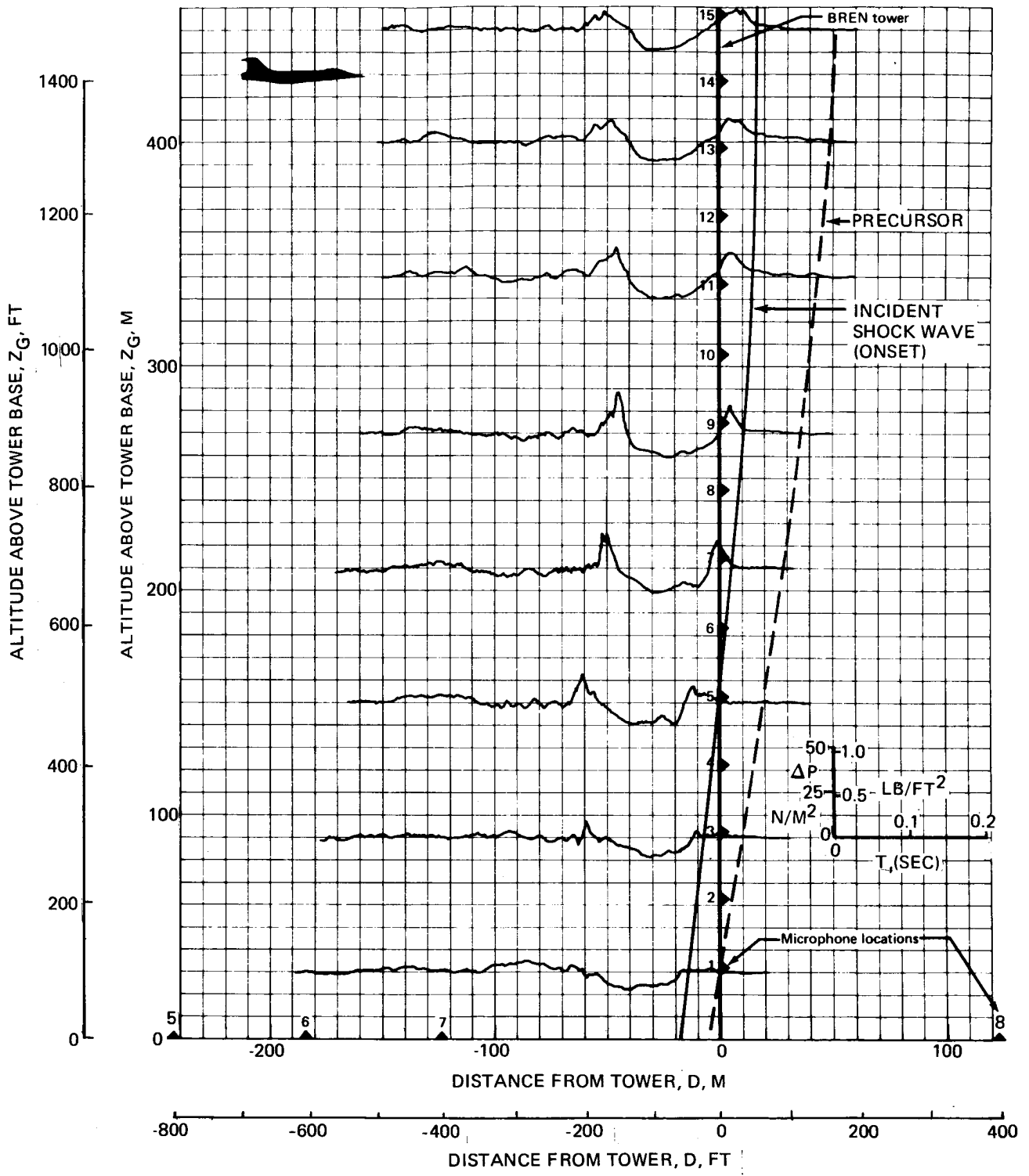


FIGURE 20.—SHOCK WAVE PROFILE AND TOWER PRESSURE SIGNATURES, $M < M_T$ —PASS 112, OCTOBER 29, 2-5

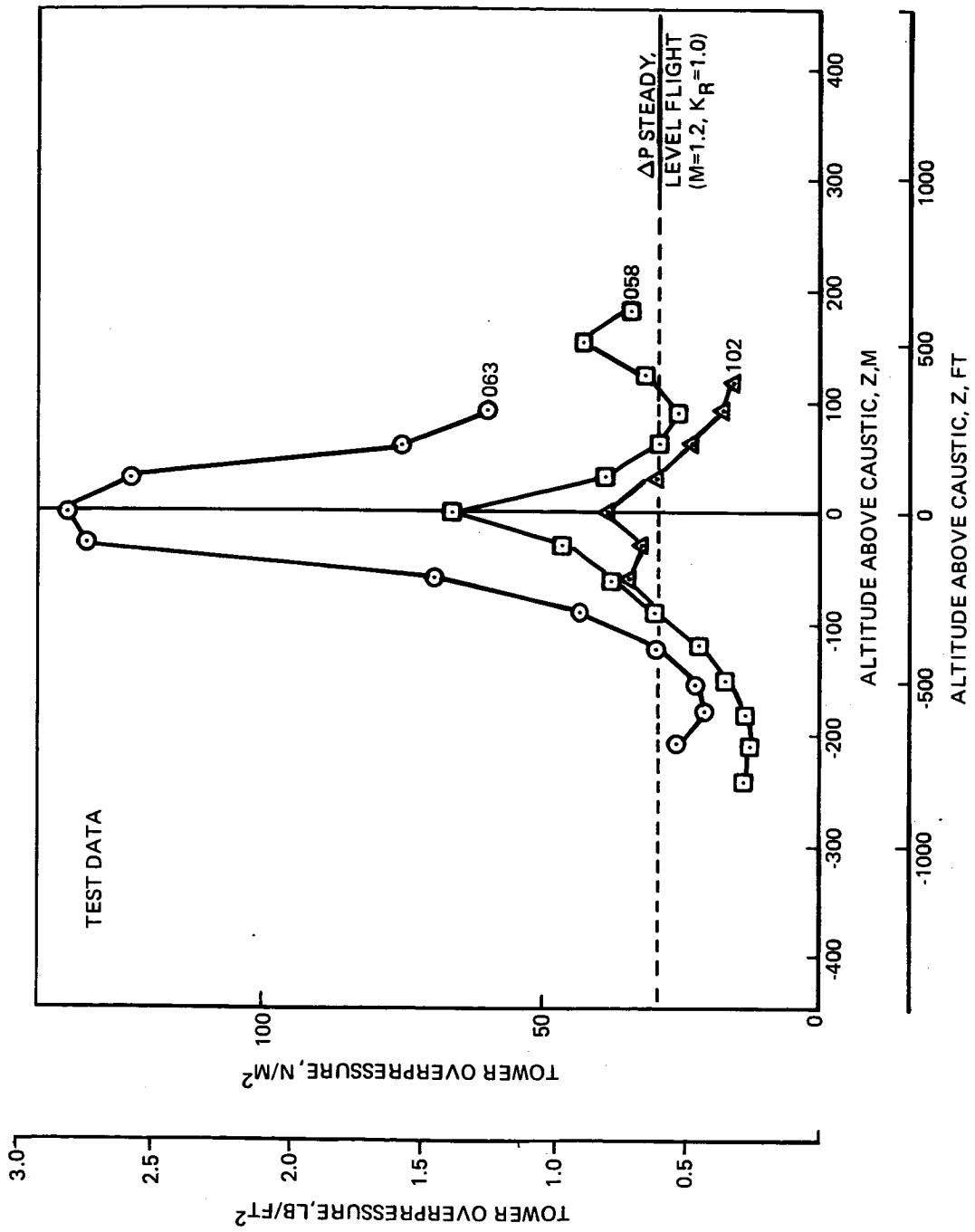


FIGURE 21.--VARIATION OF OVER PRESSURE NEAR CAUSTIC
--THRESHOLD MACH NUMBER FLIGHT

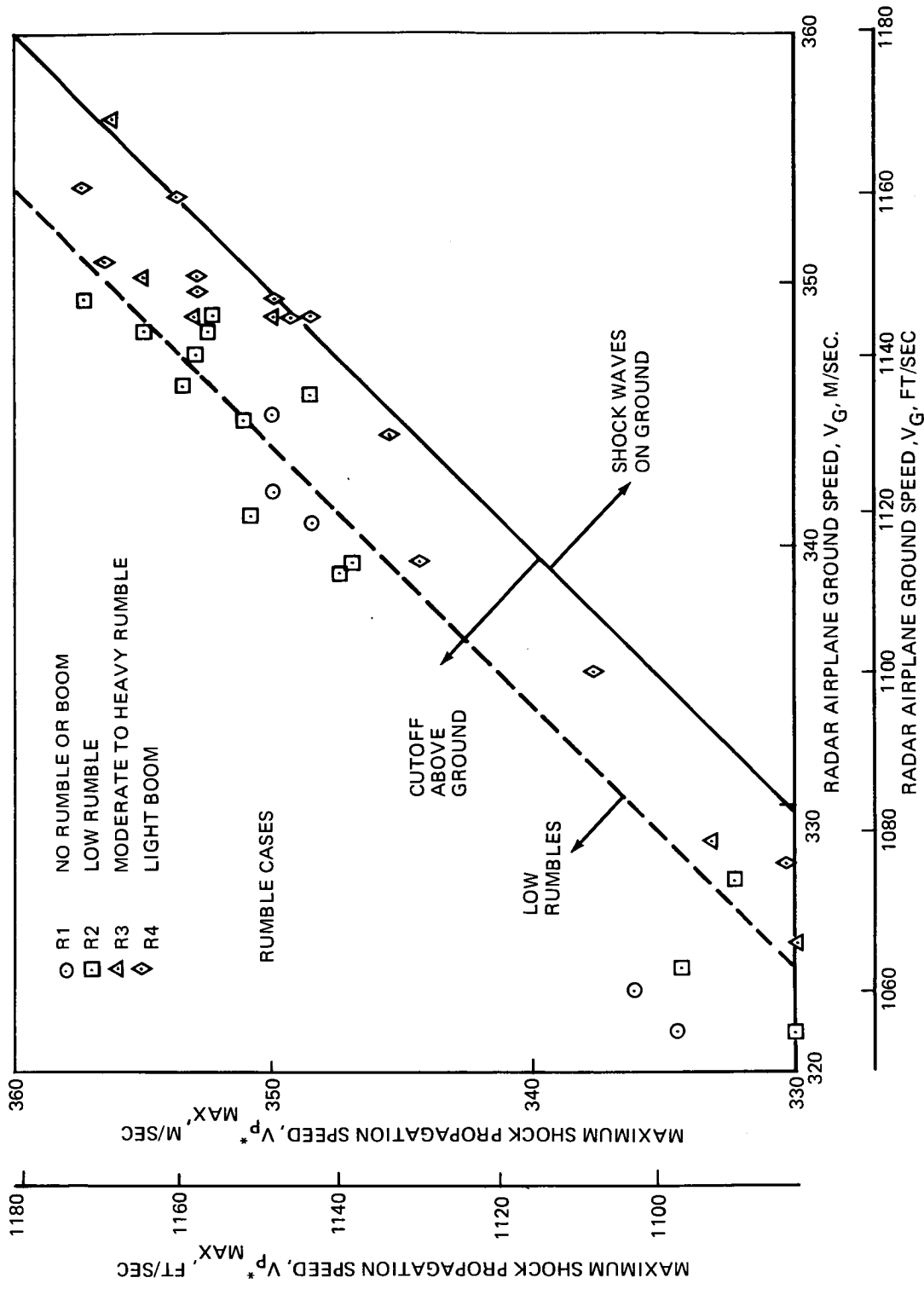


FIGURE 22.—COMPARISON OF AIRPLANE GROUND SPEED AND SHOCK PROPAGATION SPEED

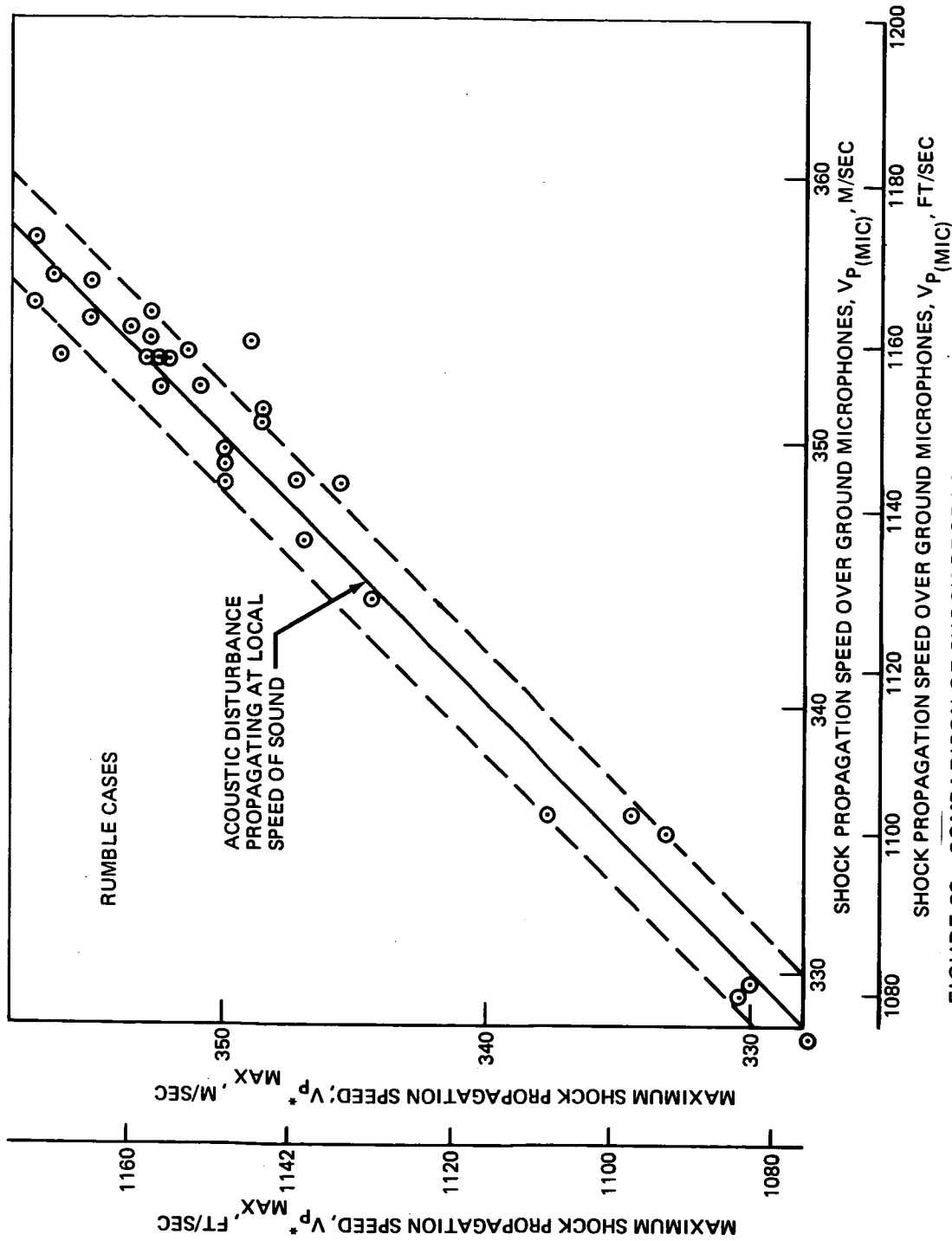


FIGURE 23.—COMPARISON OF SHOCK PROPAGATION SPEEDS

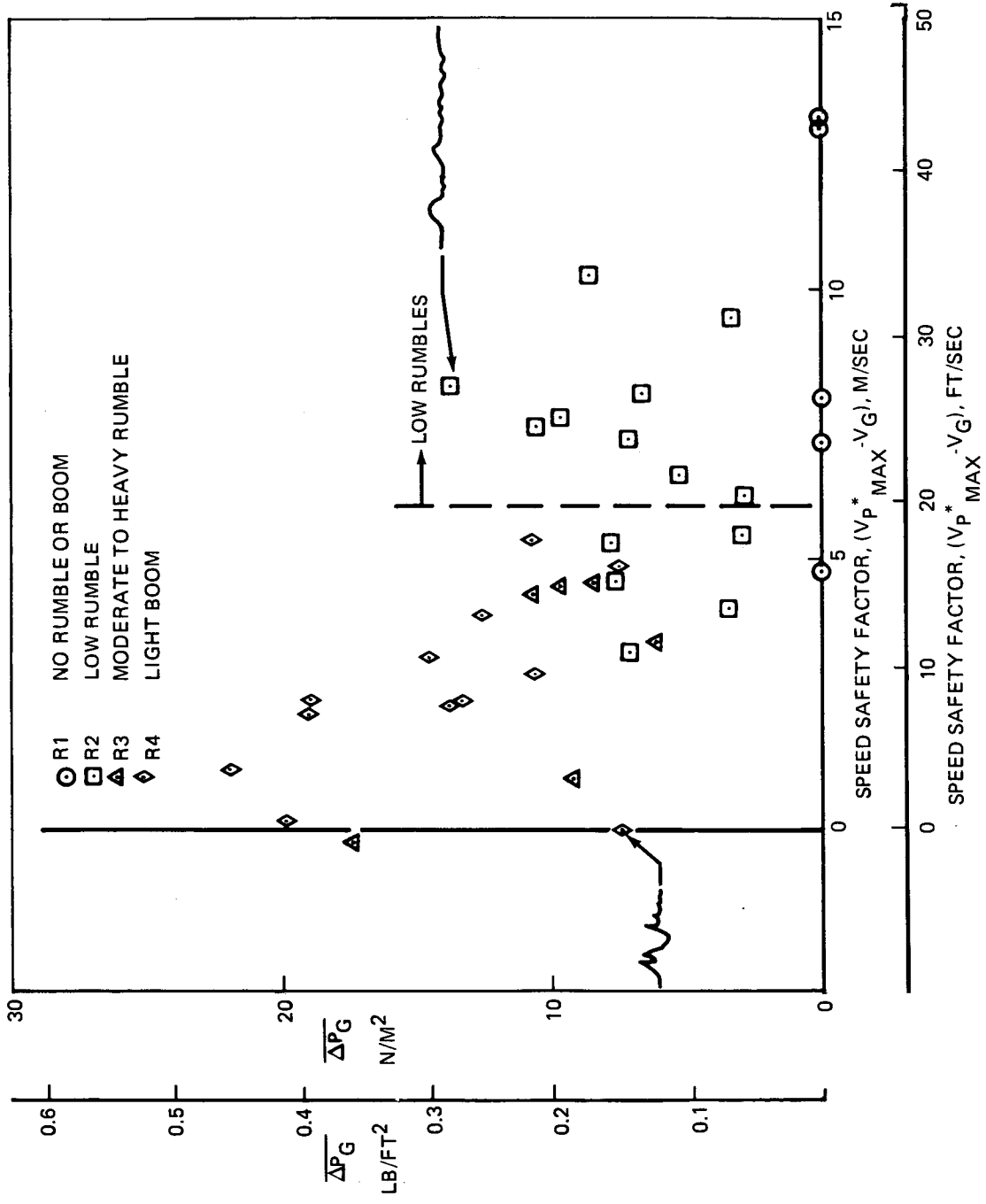


FIGURE 24.—VARIATION OF OVERPRESSURE WITH SPEED SAFETY FACTOR

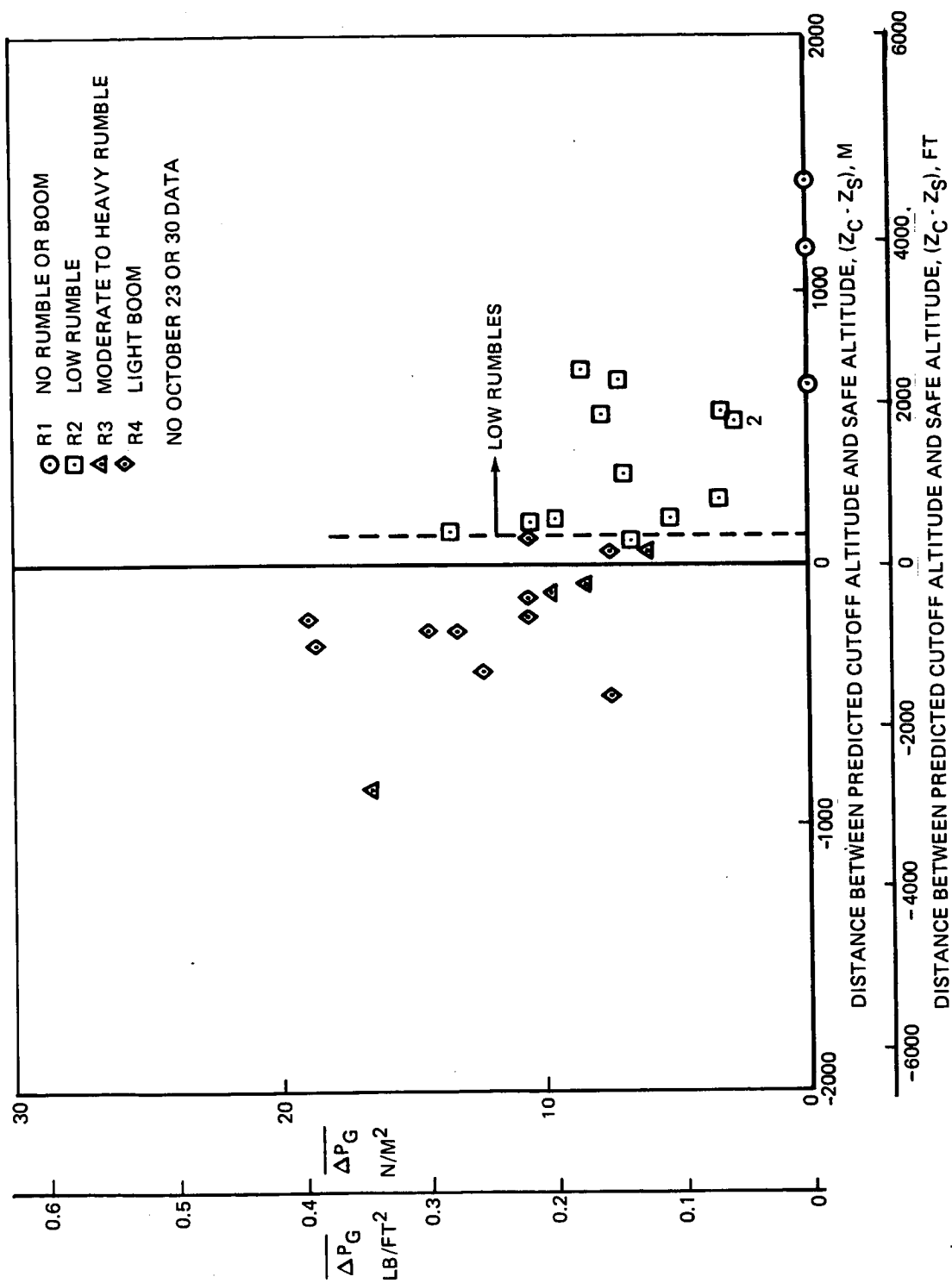


FIGURE 25.—VARIATION OF OVERPRESSURE WITH DISTANCE BETWEEN CUTOFF AND THE SAFE ALTITUDE

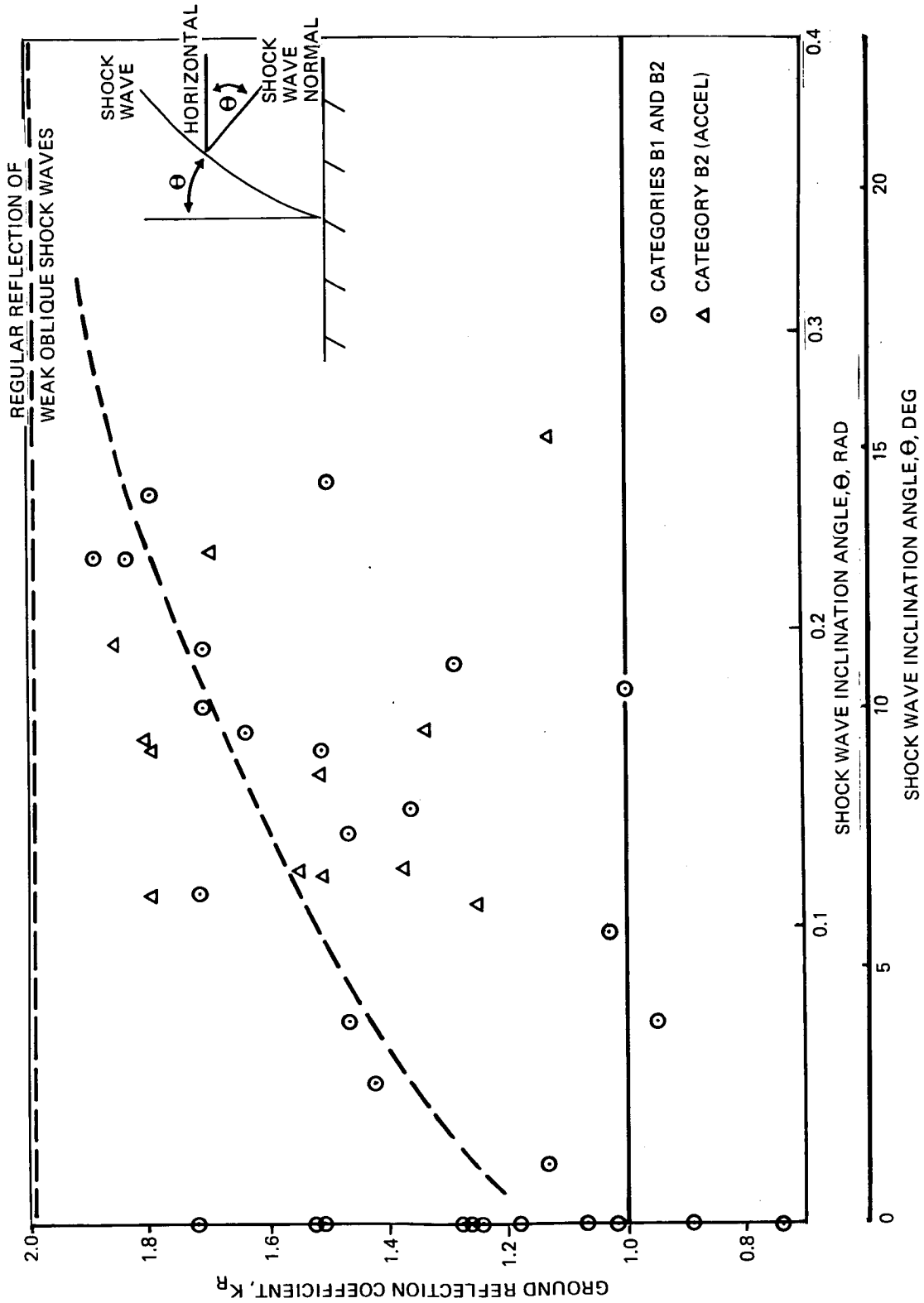


FIGURE 26.—VARIATION OF GROUND REFLECTION COEFFICIENT NEAR CUTOFF—THRESHOLD MACH NUMBER FLIGHT, $M \geq M_T$

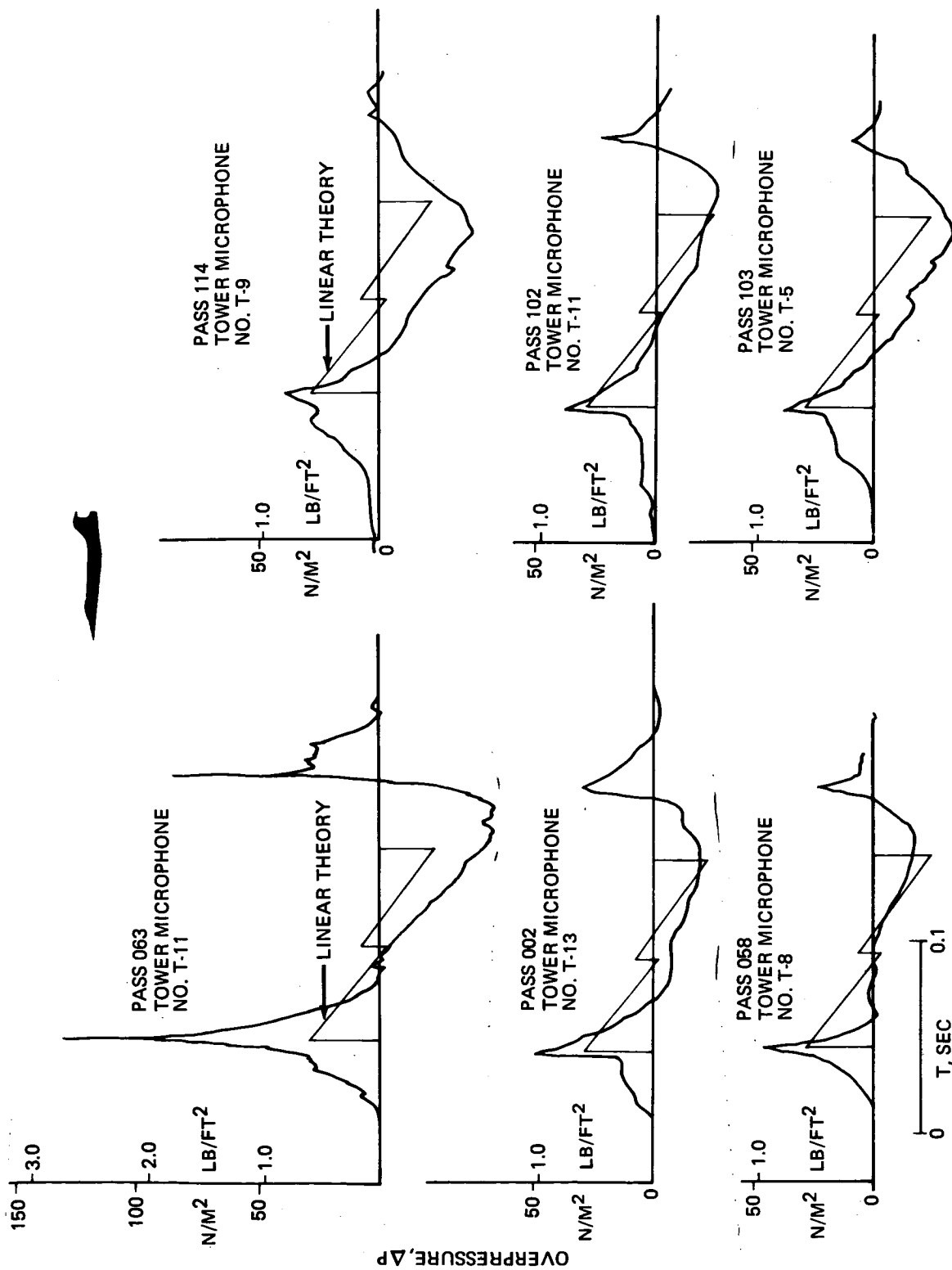


FIGURE 27.--OBSERVED CAUSTIC SIGNATURES PRODUCED BY THRESHOLD MACH NUMBER FLIGHT COMPARED WITH LINEAR THEORY SIGNATURES AT SLIGHTLY HIGHER MACH NUMBER

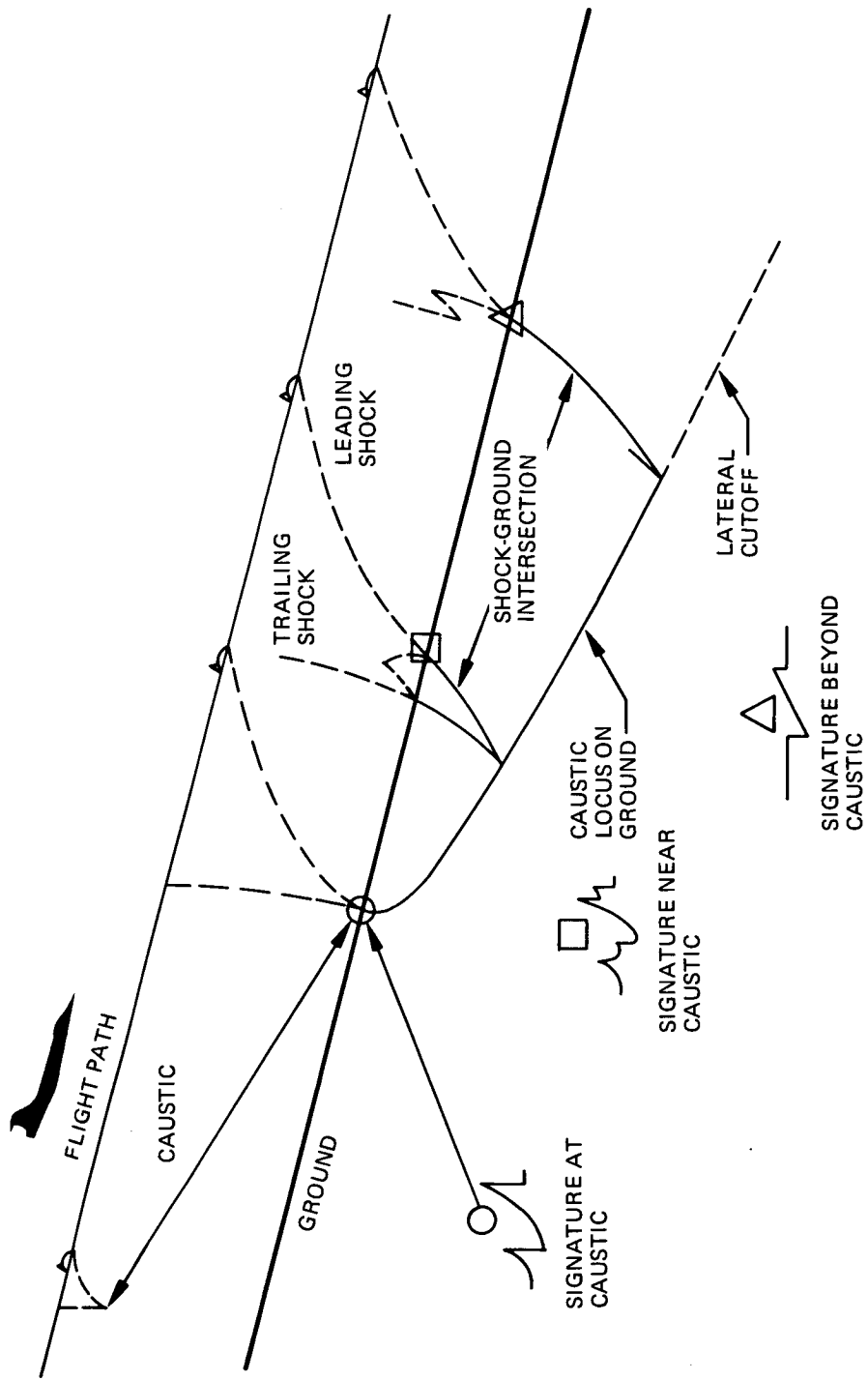


FIGURE 28.—DEVELOPMENT OF SHOCK WAVES DURING ACCELERATION FROM SUBSONIC MACH NUMBER

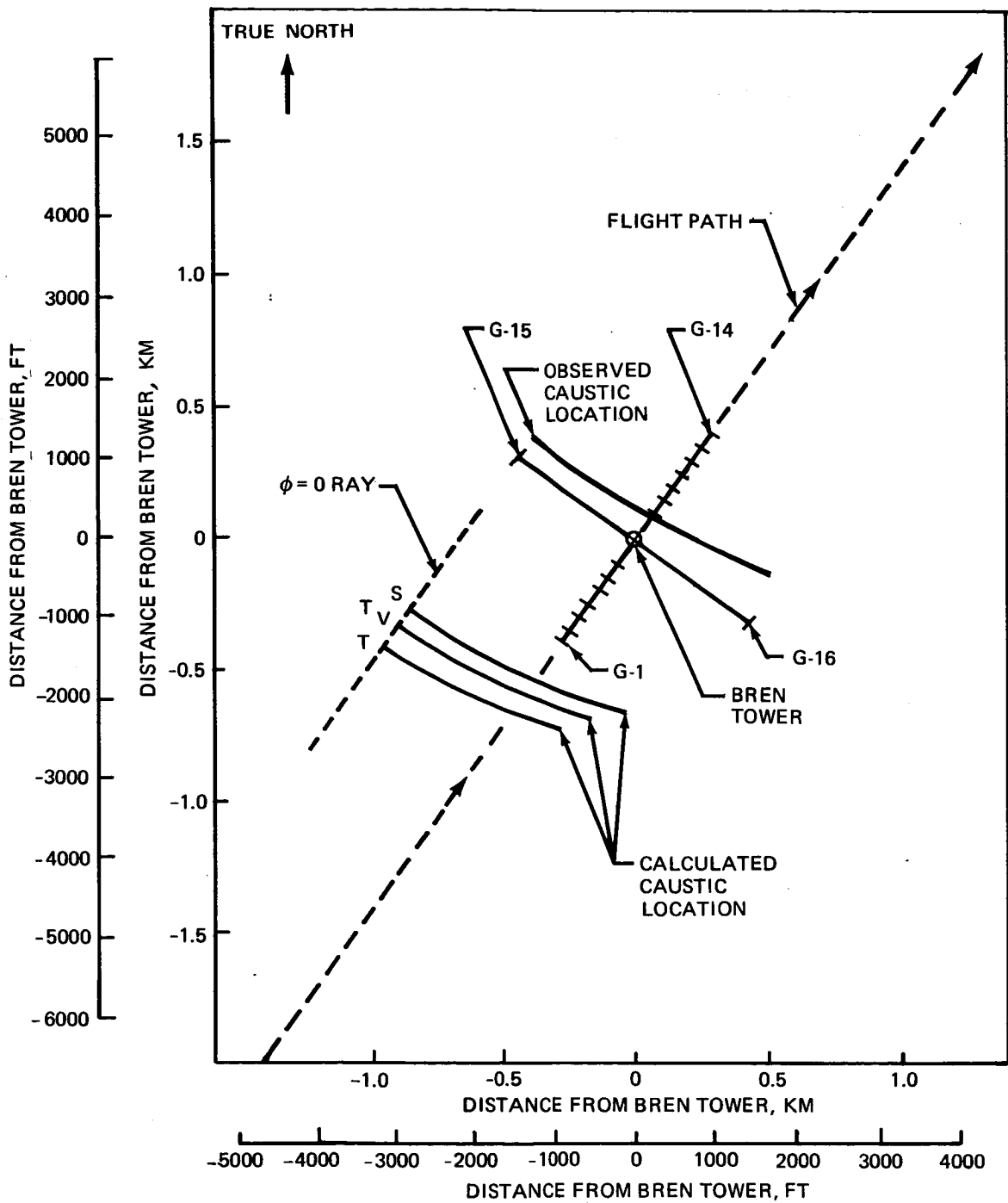


FIGURE 29.—COMPARISON OF THEORETICAL AND OBSERVED CAUSTIC LOCATIONS—PASS 045

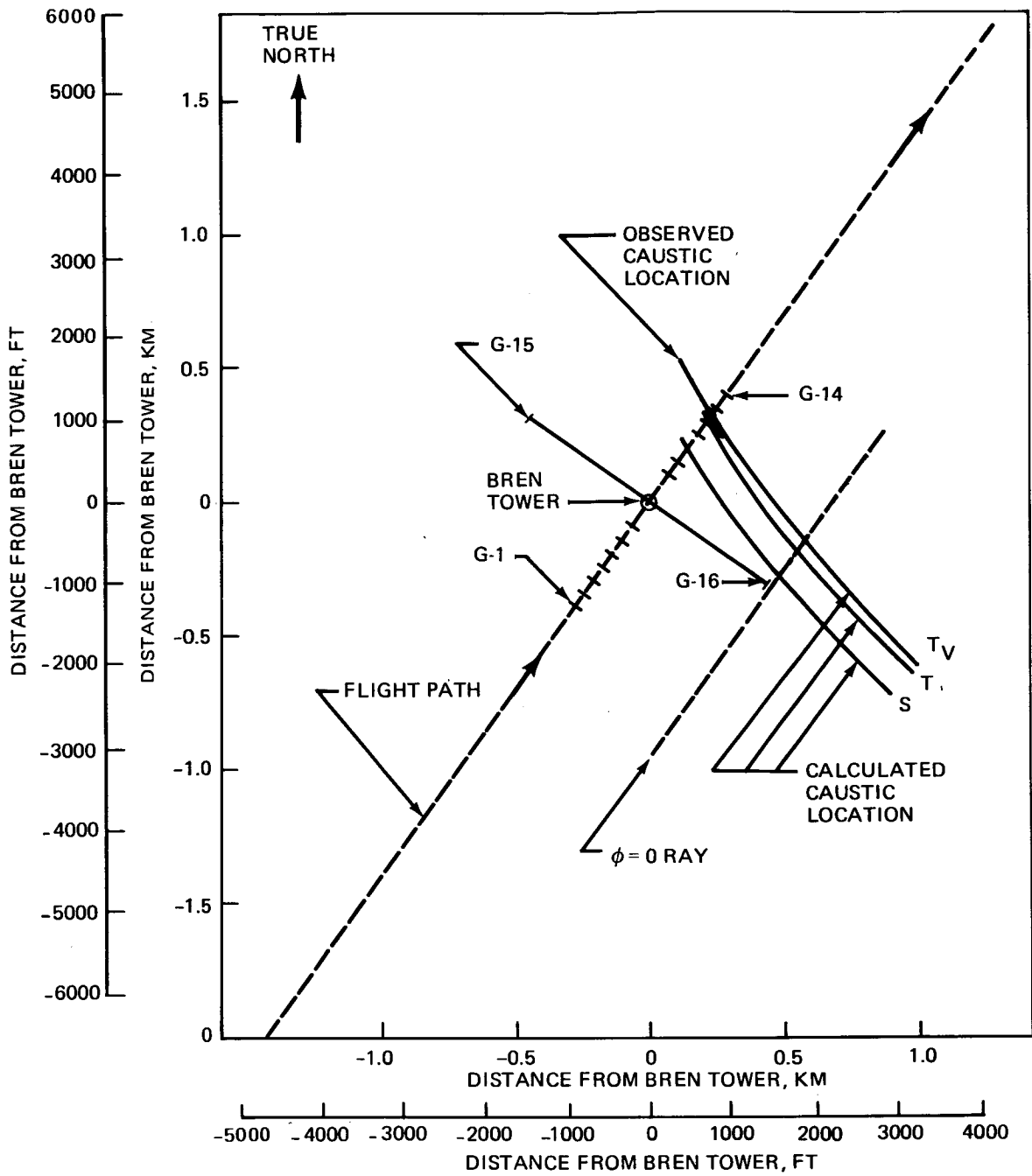


FIGURE 30.—COMPARISON OF THEORETICAL AND OBSERVED CAUSTIC LOCATIONS—PASS 093

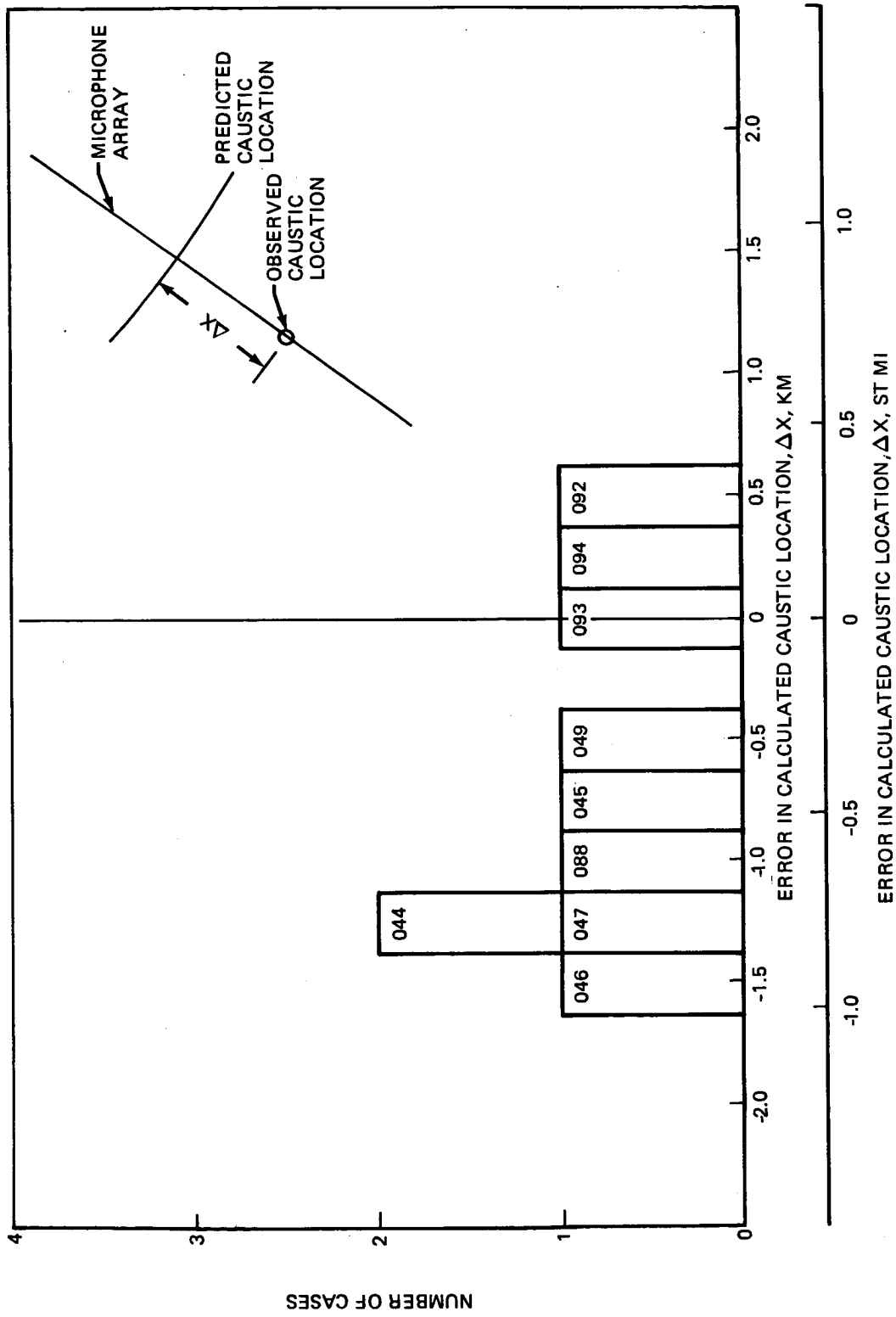


FIGURE 31.—HISTOGRAM OF DIFFERENCES BETWEEN THEORETICAL AND OBSERVED CAUSTIC-GROUND INTERSECTIONS

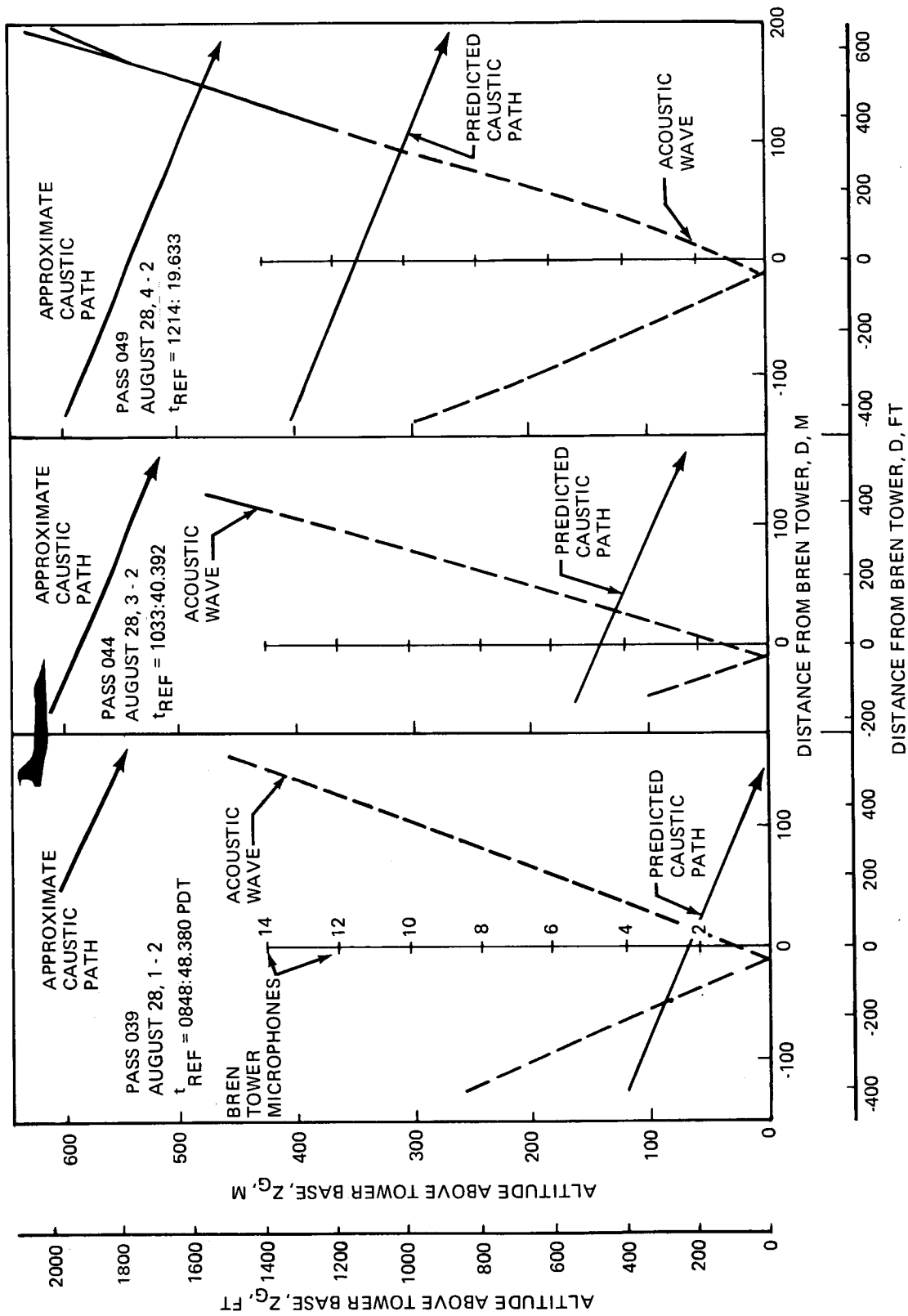


FIGURE 32.—SHOCK WAVE SYSTEM PROFILES FOR PASSES 039, 044, 049

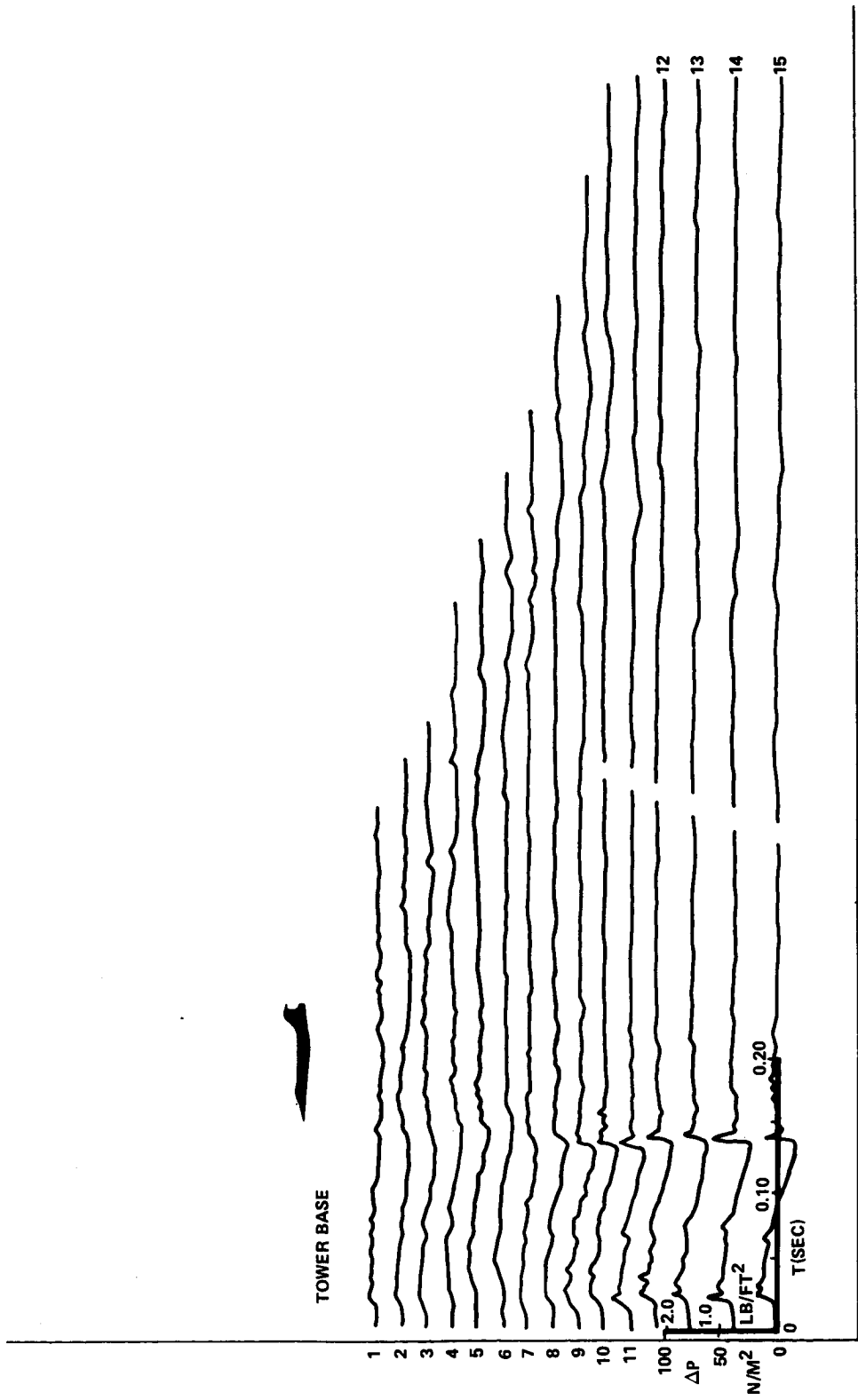


FIGURE 33.—TOWER PRESSURE SIGNATURES UPTRACK FROM CAUSTIC-GROUND INTERSECTION
PASS 049, AUGUST 28, 4-2

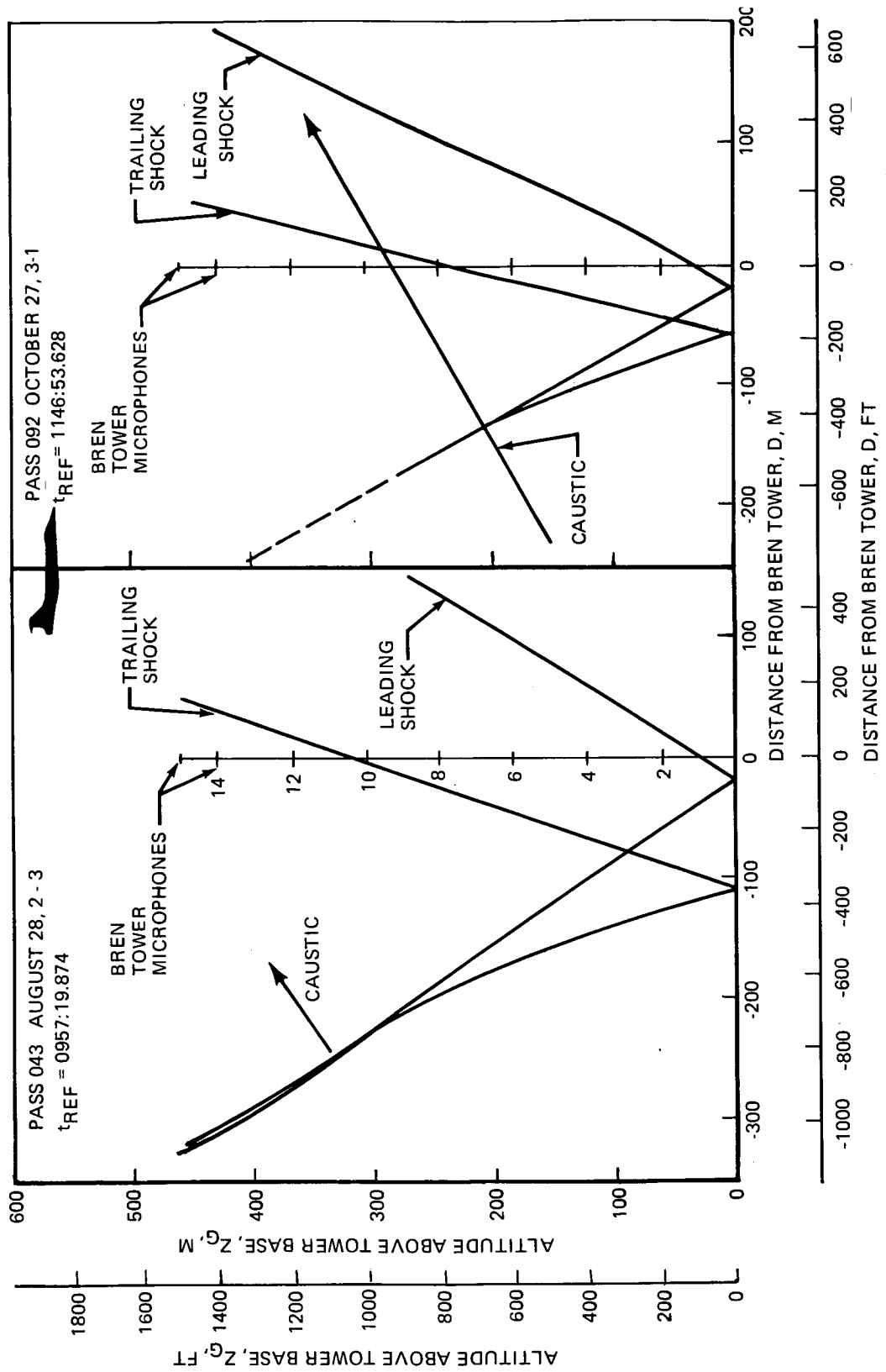


FIGURE 34.-SHOCK WAVE SYSTEM PROFILES FOR PASSES 043 AND 092

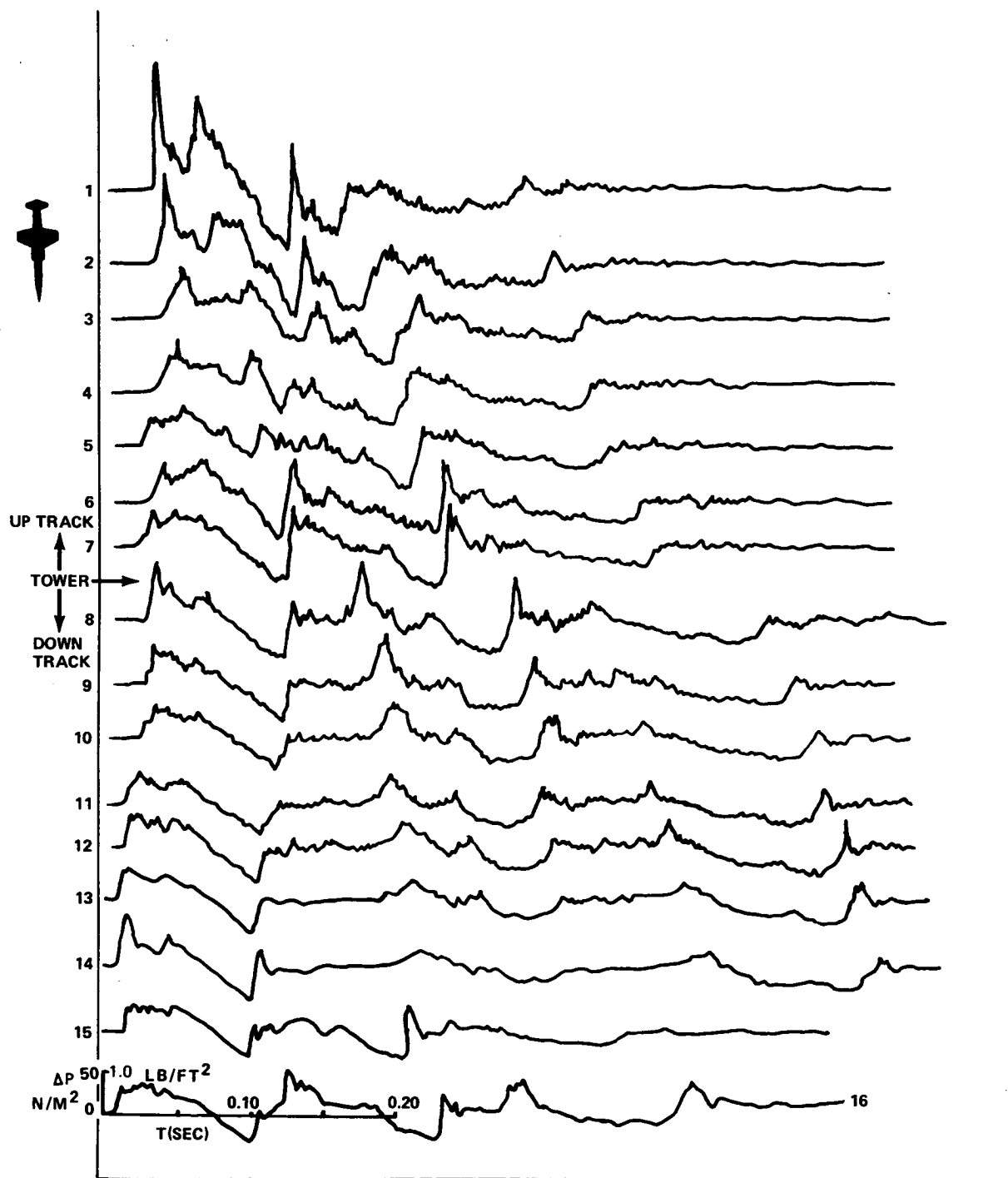


FIGURE 35.—GROUND PRESSURE SIGNATURES JUST DOWNTRACK OF CAUSTIC-GROUND INTERSECTION—PASS 043, AUGUST 28, 2-3

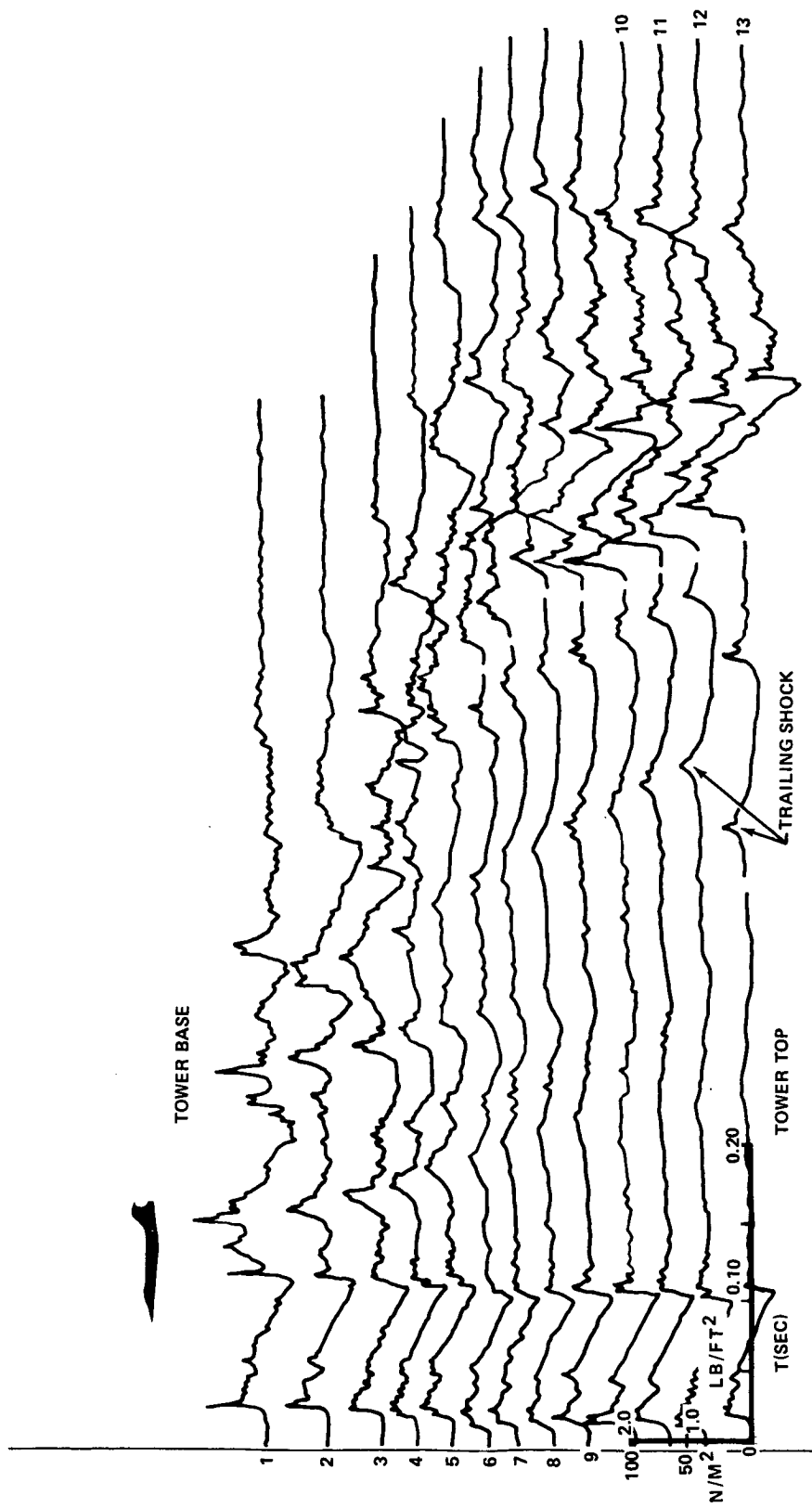


FIGURE 36.—TOWER PRESSURE SIGNATURES JUST DOWNTRACK OF CAUSTIC-GROUND INTERSECTION—PASS 043, AUGUST 28, 2-3

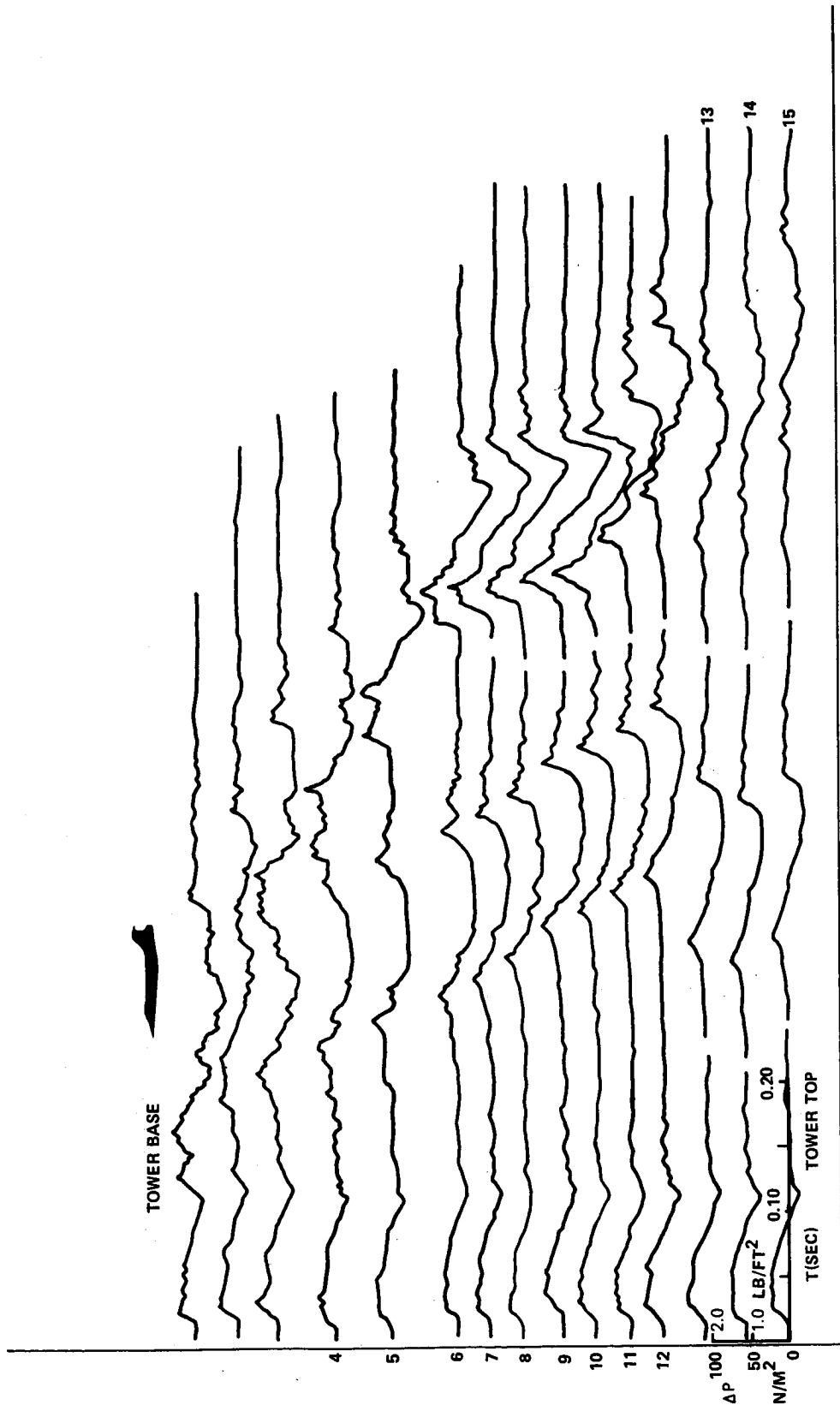


FIGURE 37.—TOWER PRESSURE SIGNATURES DOWNTRACK FROM CAUSTIC-GROUND INTERSECTION—PASS 092, OCTOBER 27, 3-1

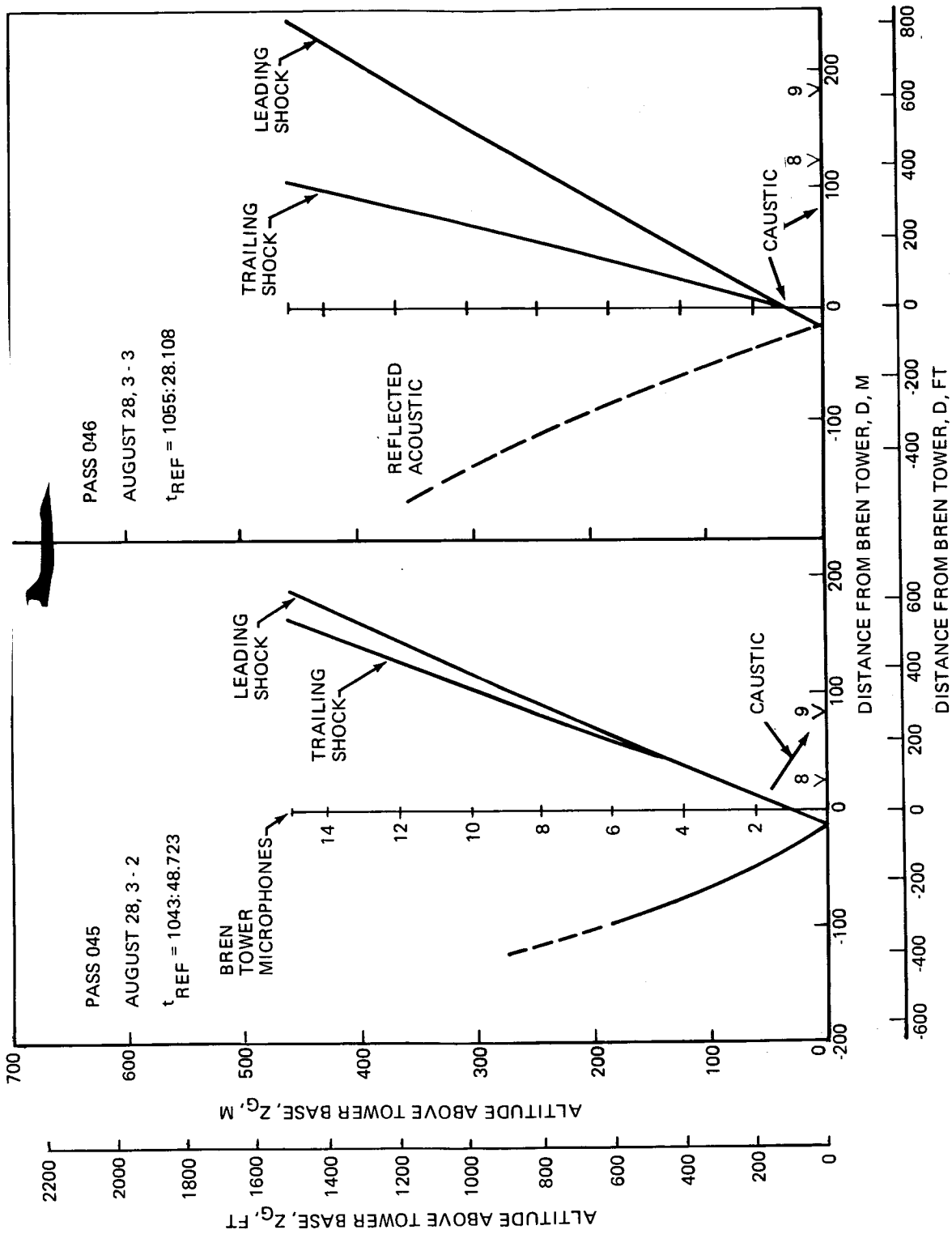


FIGURE 38.—SHOCK WAVE SYSTEM PROFILE FOR PASSES 045 AND 046

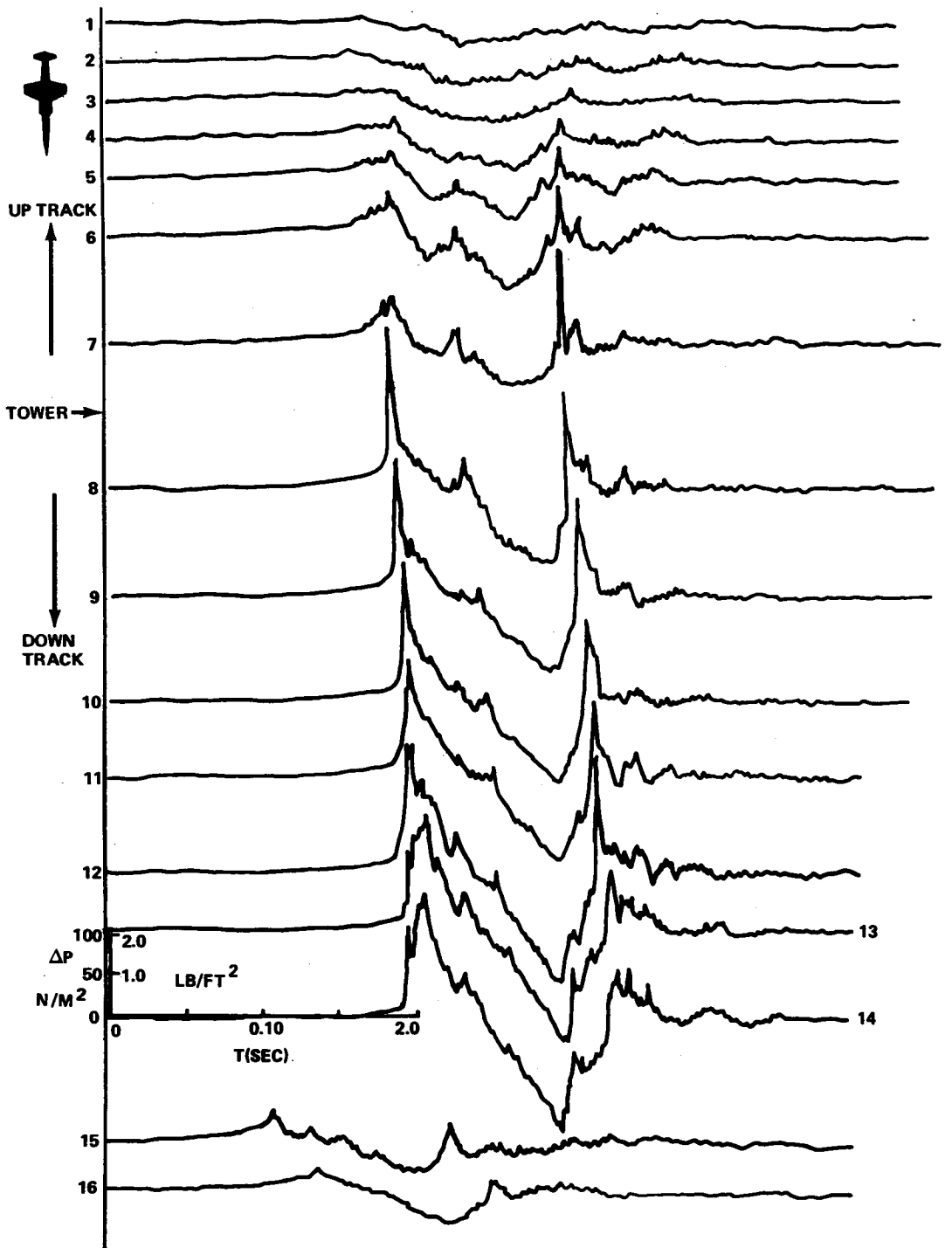


FIGURE 39.—GROUND PRESSURE SIGNATURES NEAR CAUSTIC-GROUND INTERSECTION—PASS 045, AUGUST 28, 3-2

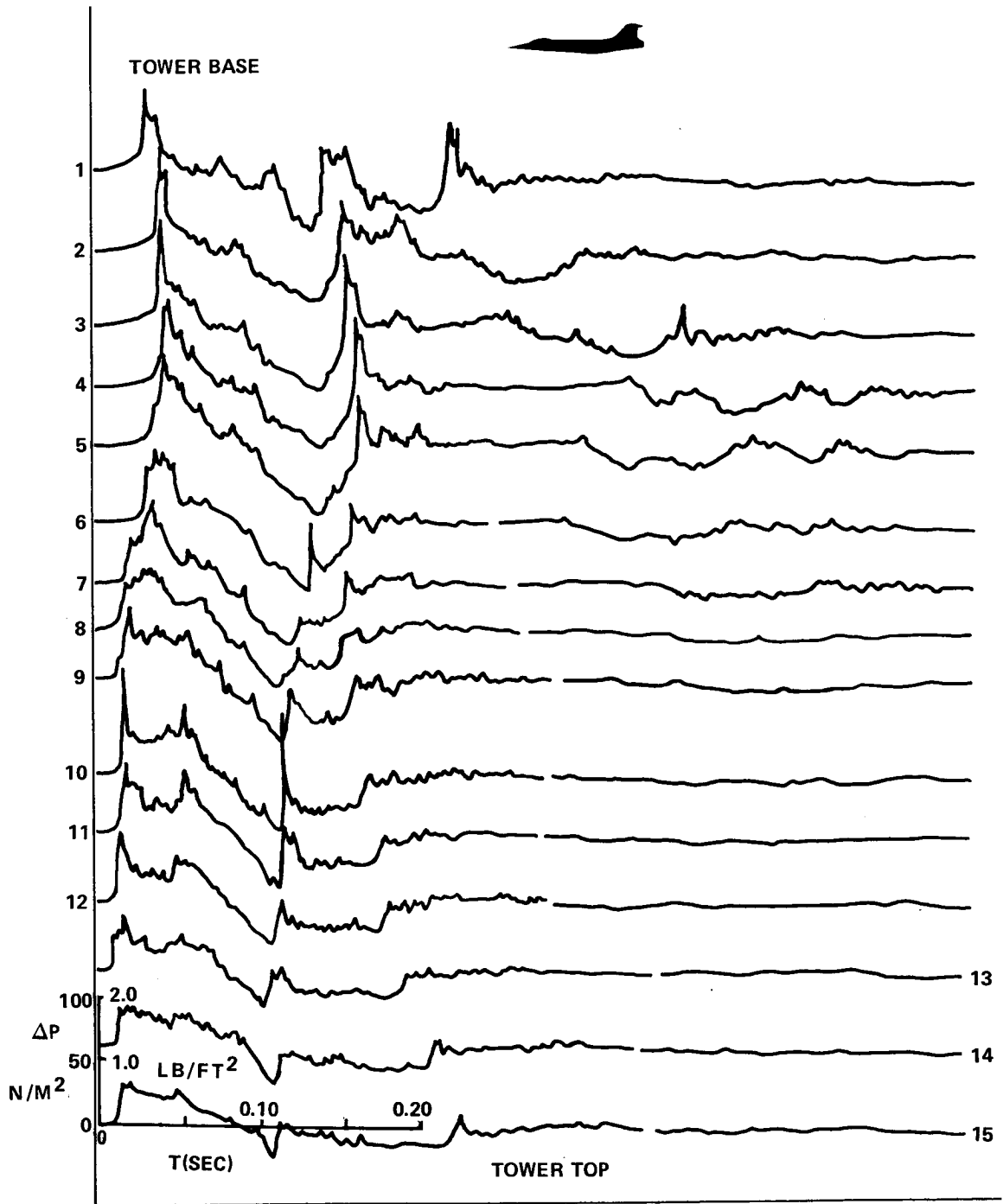


FIGURE 40.—TOWER PRESSURE SIGNATURES NEAR CAUSTIC-GROUND INTERSECTION—PASS 045, AUGUST 28, 3-2

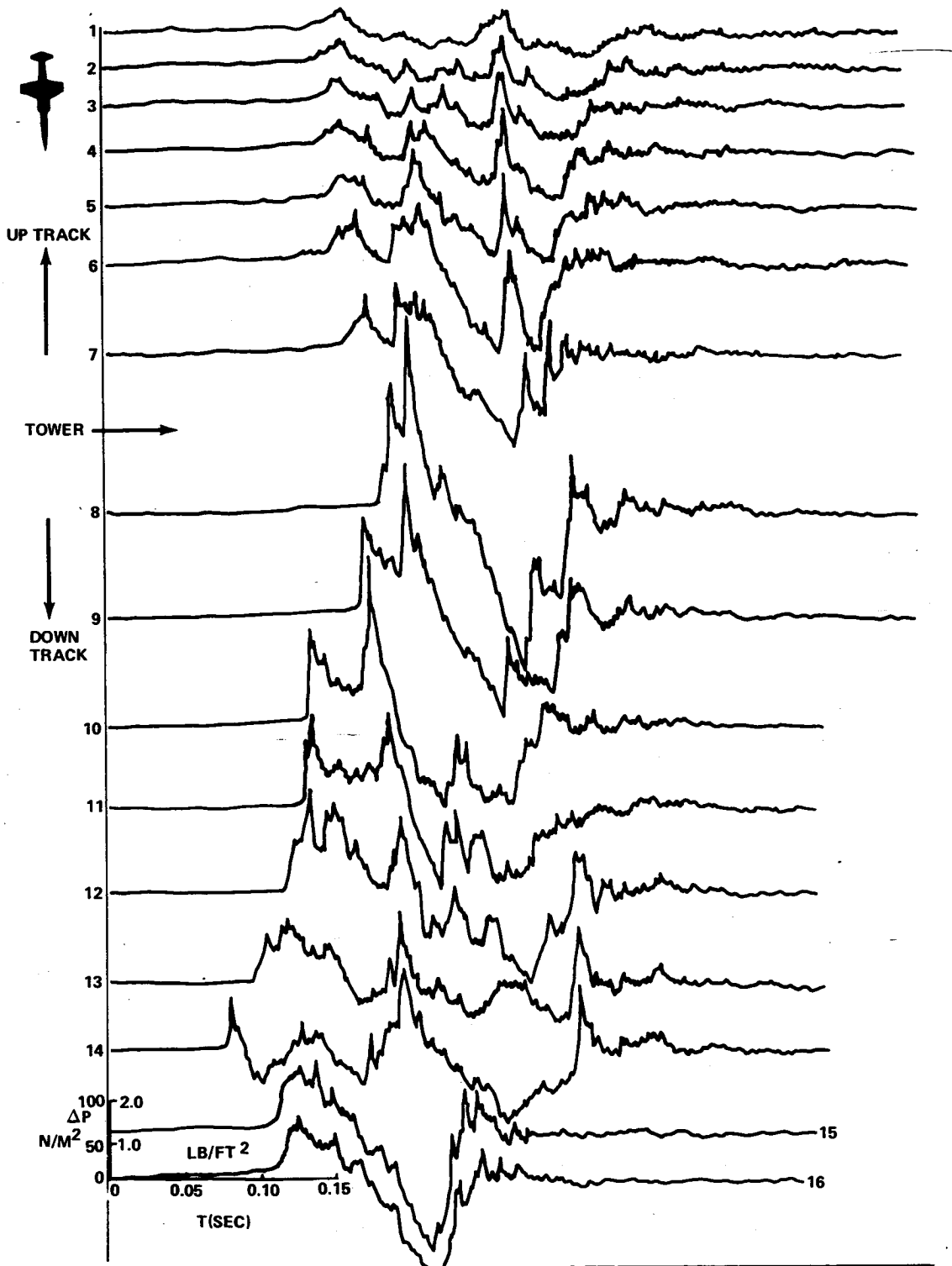


FIGURE 41.—GROUND PRESSURE SIGNATURES NEAR CAUSTIC-GROUND INTERSECTION—PASS 046, AUGUST 28, 3-3

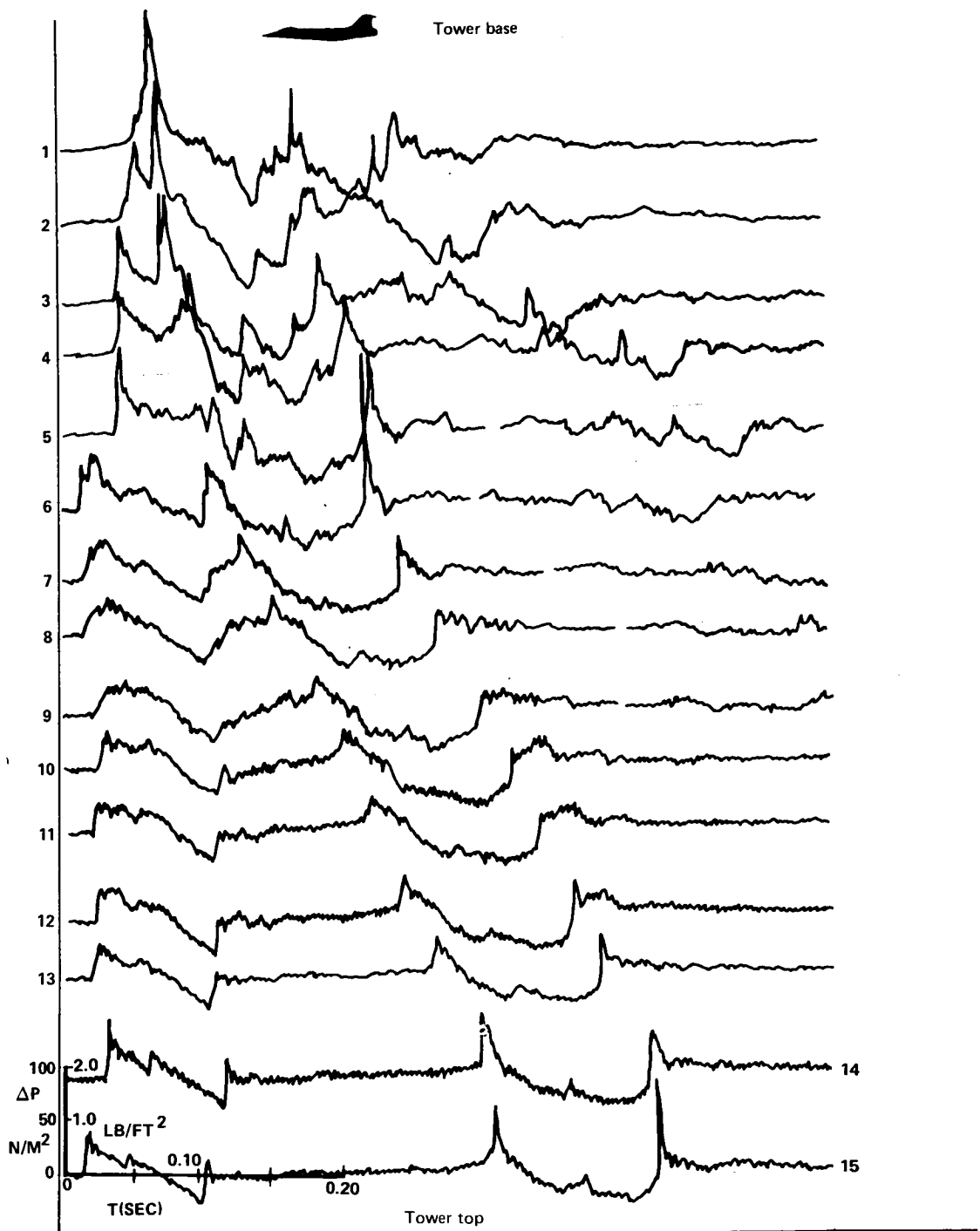


FIGURE 42.—TOWER PRESSURE SIGNATURES NEAR CAUSTIC-GROUND INTERSECTION—PASS 046, AUGUST 28, 3-3

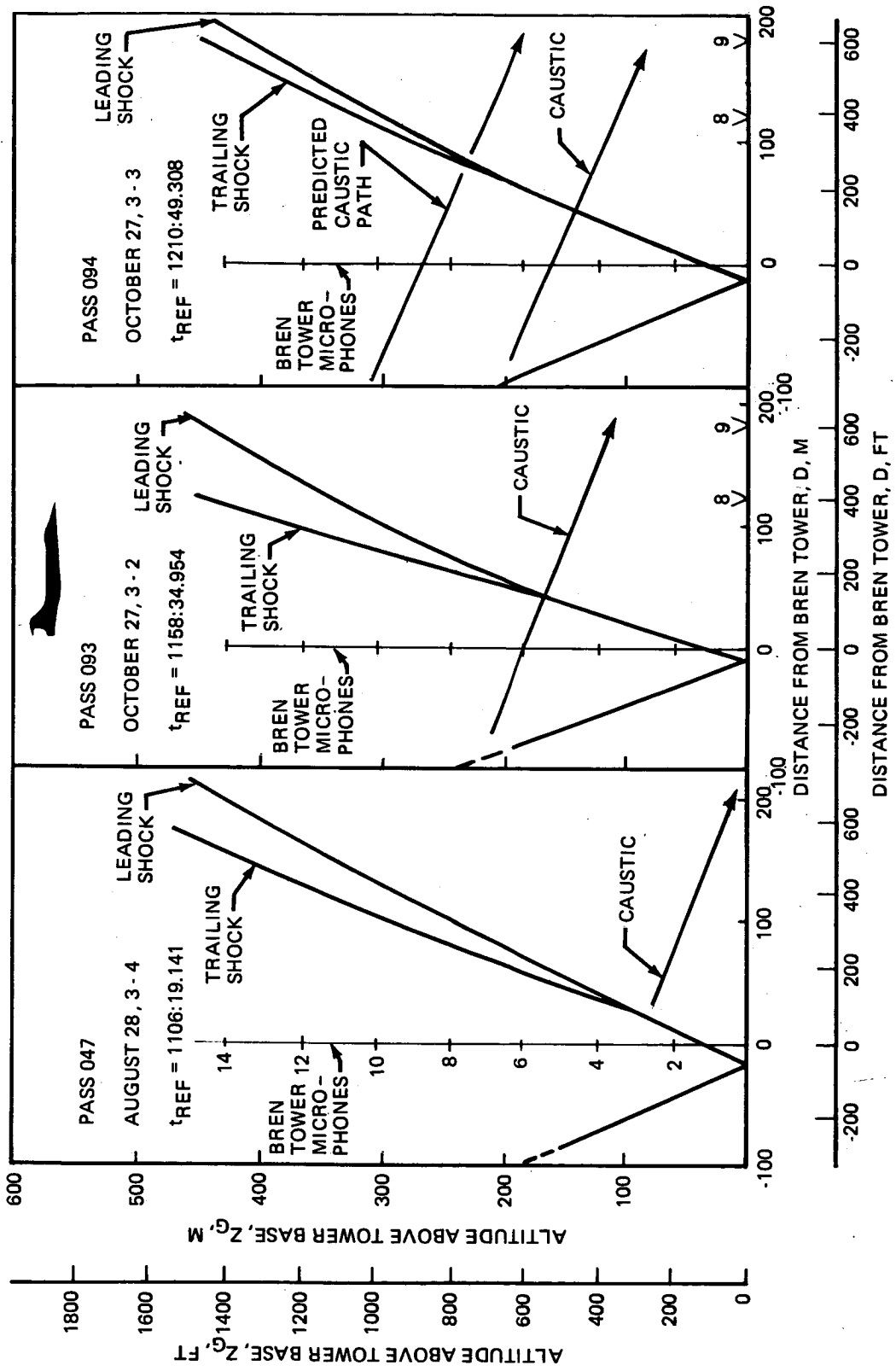


FIGURE 43.—SHOCK WAVE SYSTEM FOR PASSES 047, 093, 094

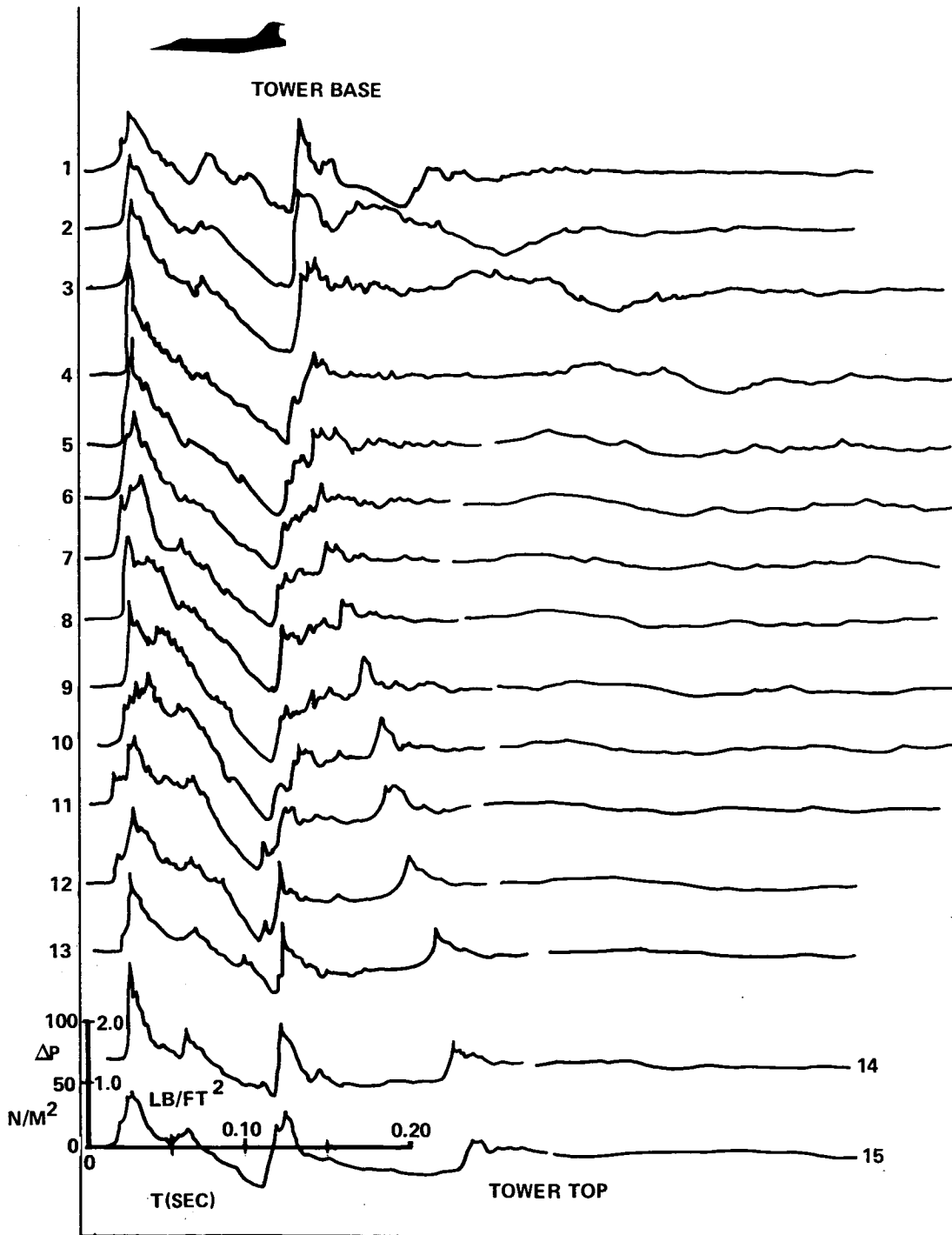


FIGURE 44.— TOWER PRESSURE SIGNATURES NEAR CAUSTIC-GROUND INTERSECTION—
PASS 047, AUGUST 28, 3-4

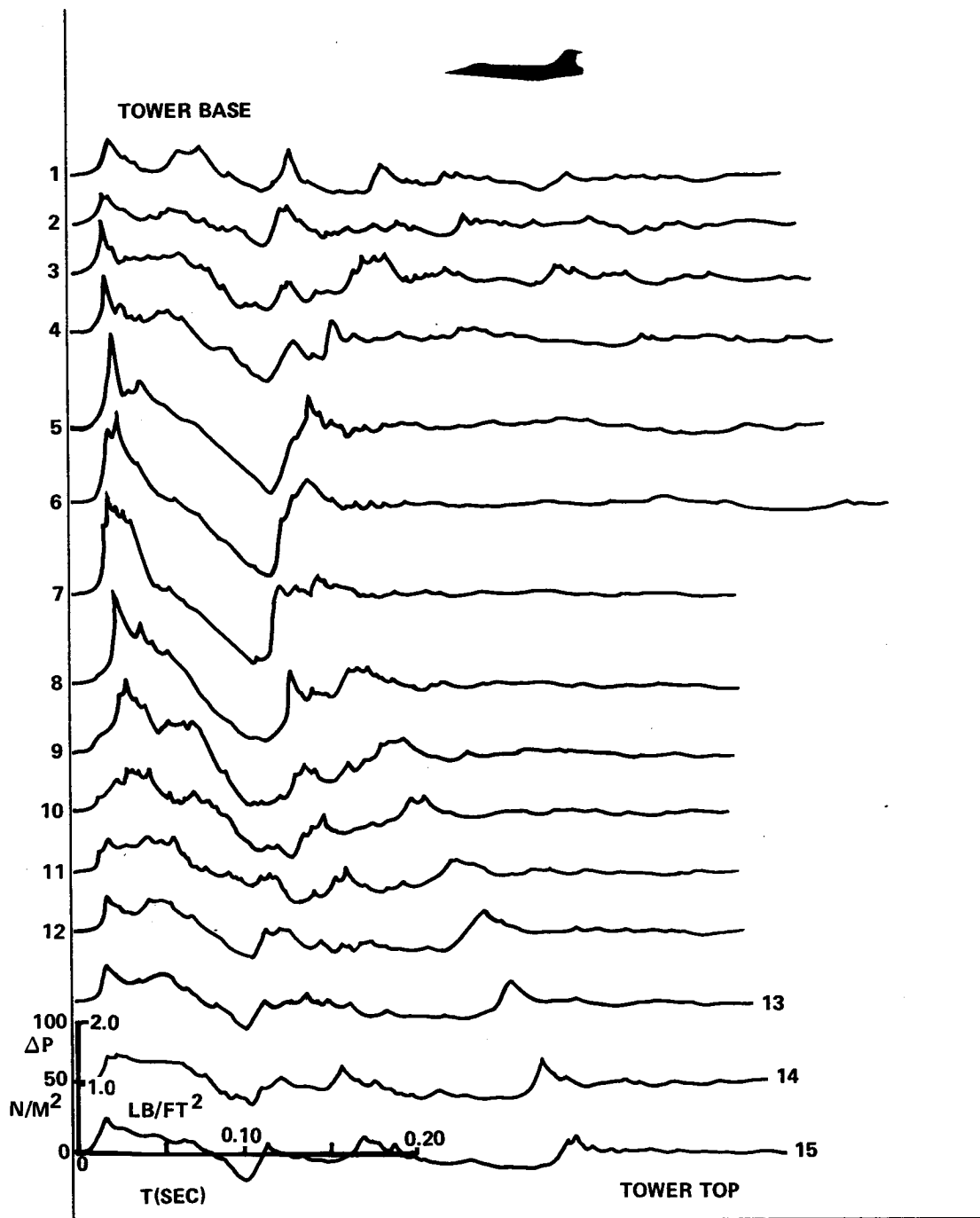


FIGURE 45.—TOWER PRESSURE SIGNATURES NEAR CAUSTIC-GROUND INTERSECTION—PASS 093, OCTOBER 27, 3-2

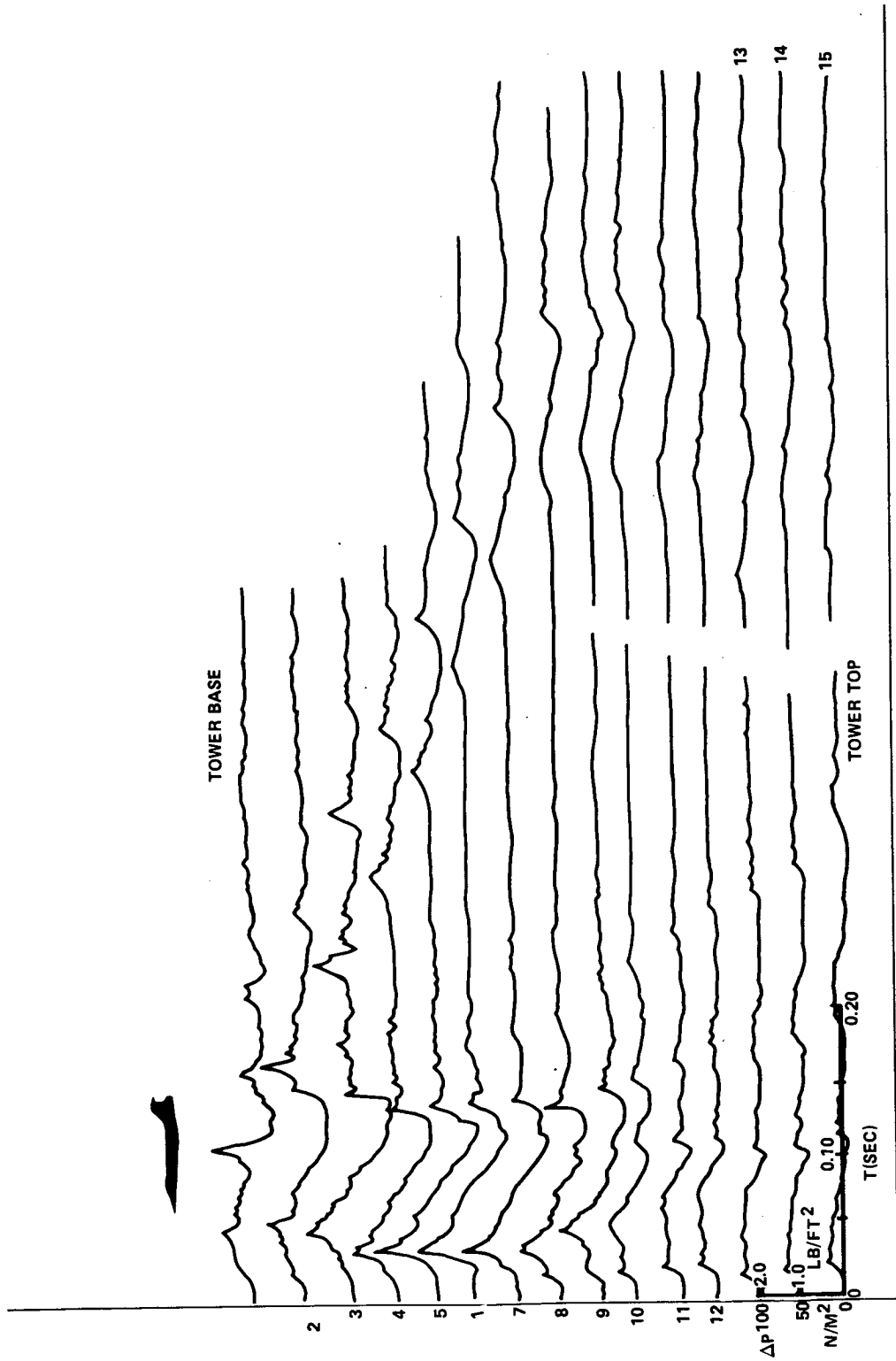


FIGURE 46.—TOWER PRESSURE SIGNATURES NEAR CAUSTIC-GROUND INTERSECTION—PASS 094, OCTOBER 27, 3-3

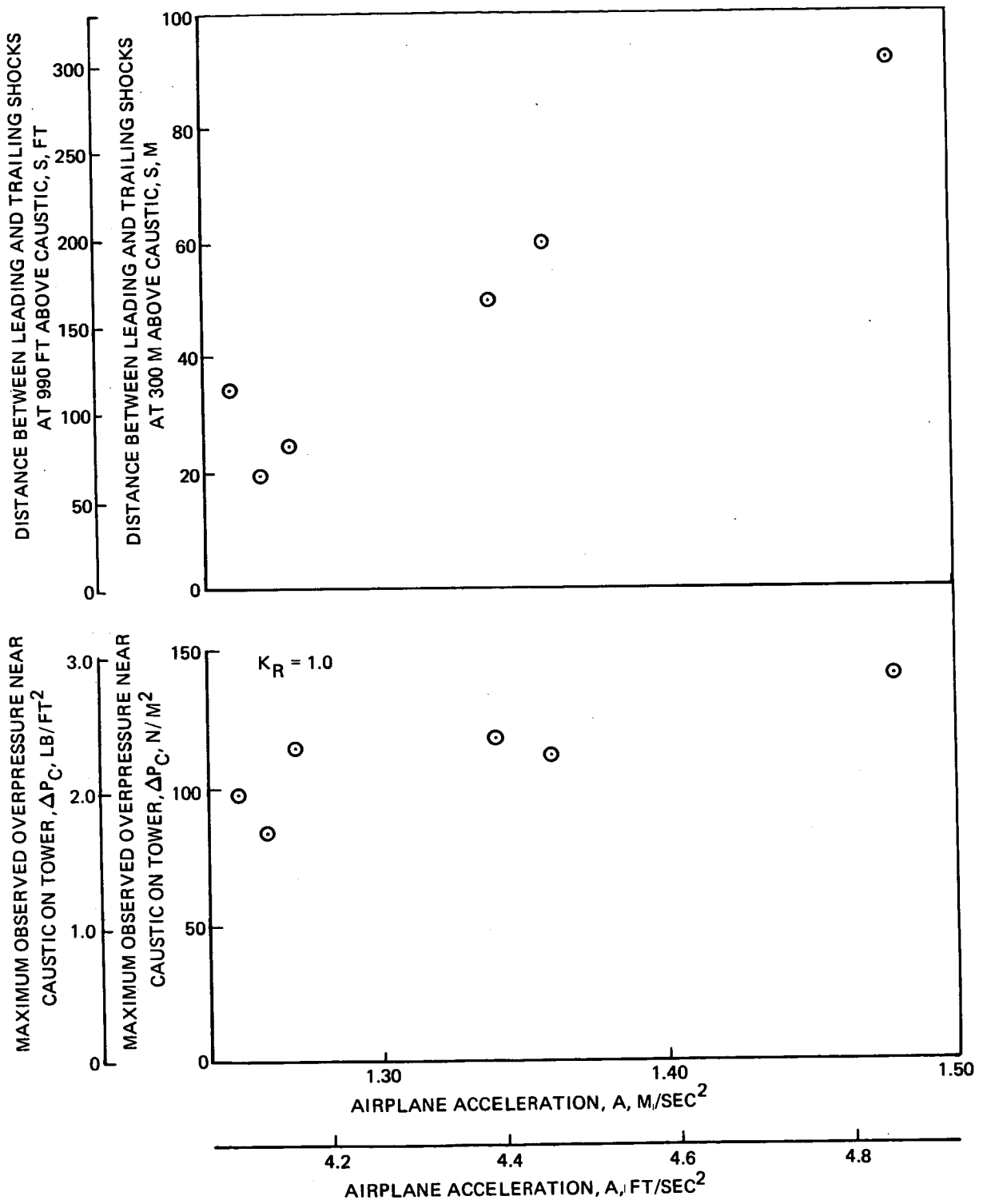


FIGURE 47.—EFFECT OF AIRPLANE ACCELERATION MAGNITUDE ON CAUSTIC INTENSITY AND DISTANCE BETWEEN LEADING AND TRAILING SHOCKS

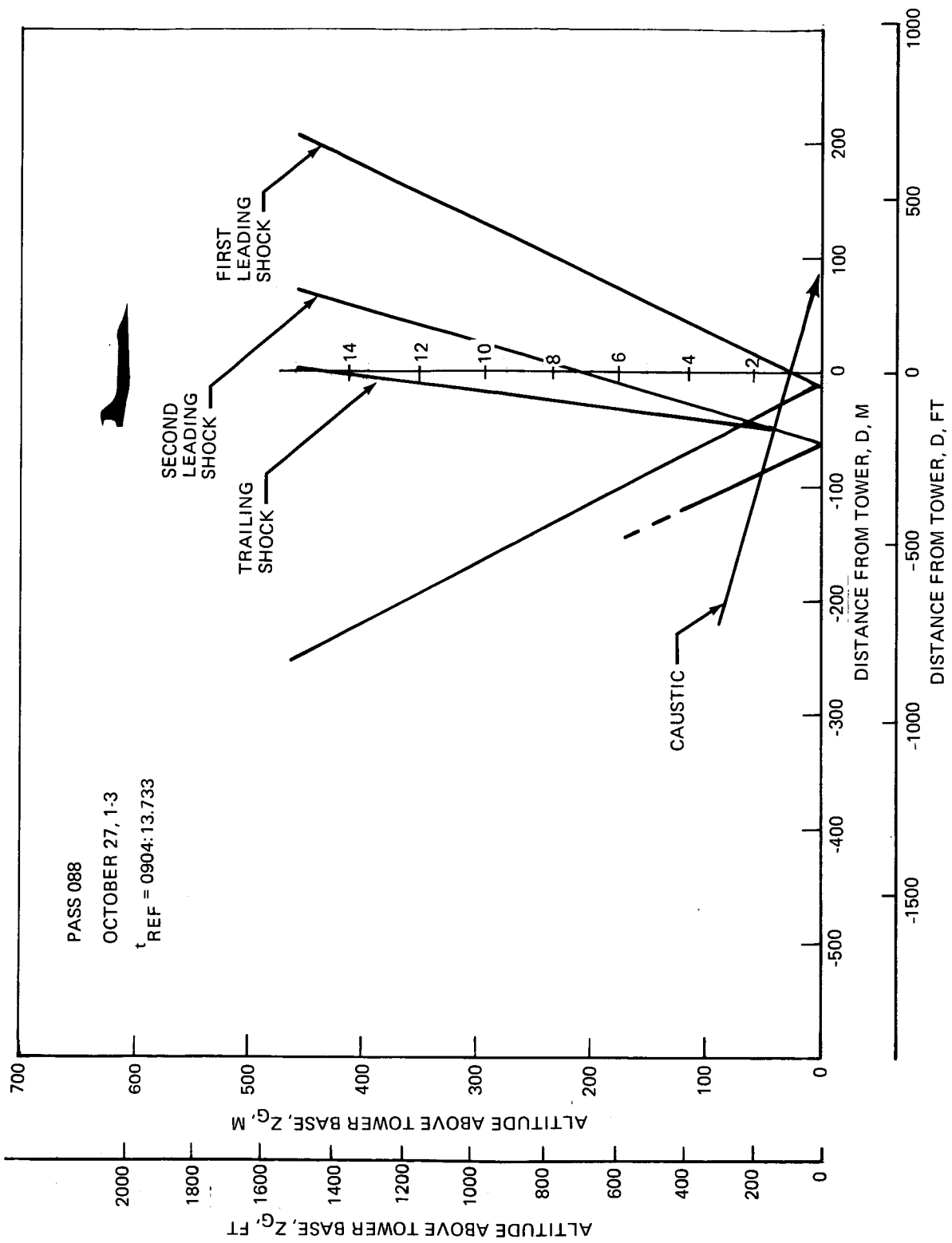


FIGURE 48.—SHOCK WAVE SYSTEM PROFILE FOR PASS 088

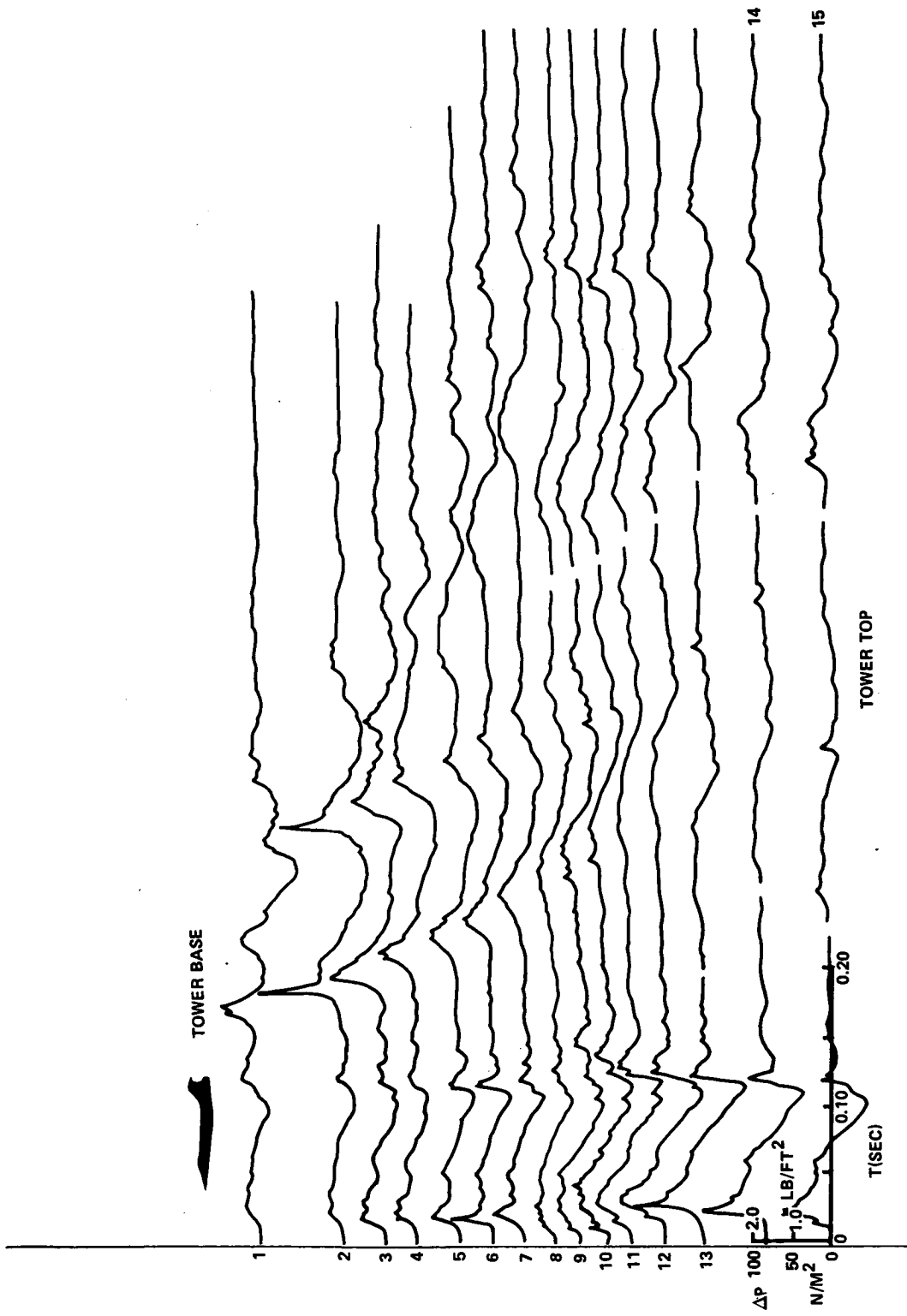


FIGURE 49.—TOWER PRESSURE SIGNATURES NEAR CAUSTIC-GROUND INTERSECTION—PASS 088, OCTOBER 27, 1-3

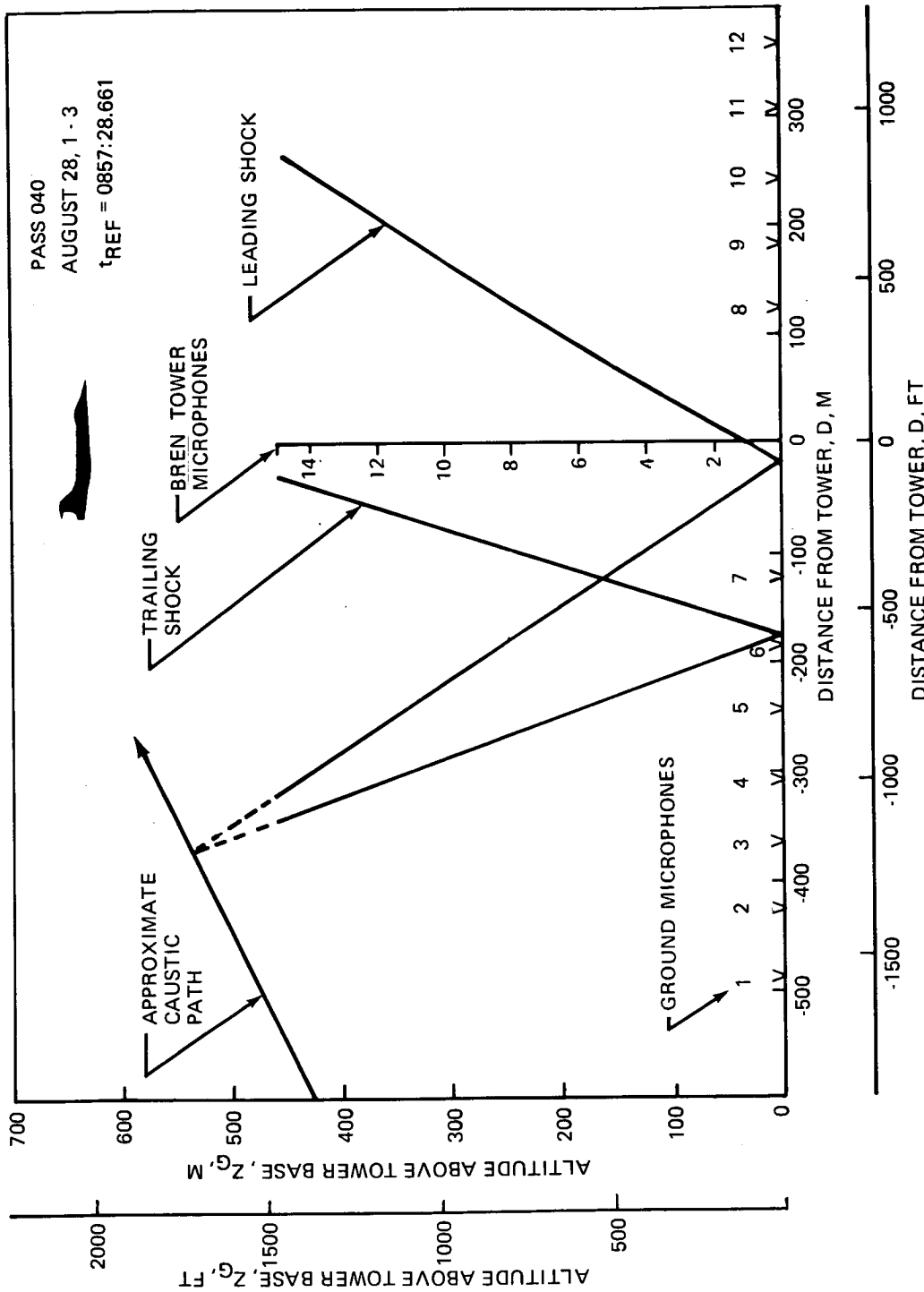


FIGURE 50.—SHOCK WAVE SYSTEM PROFILE FOR PASS 040

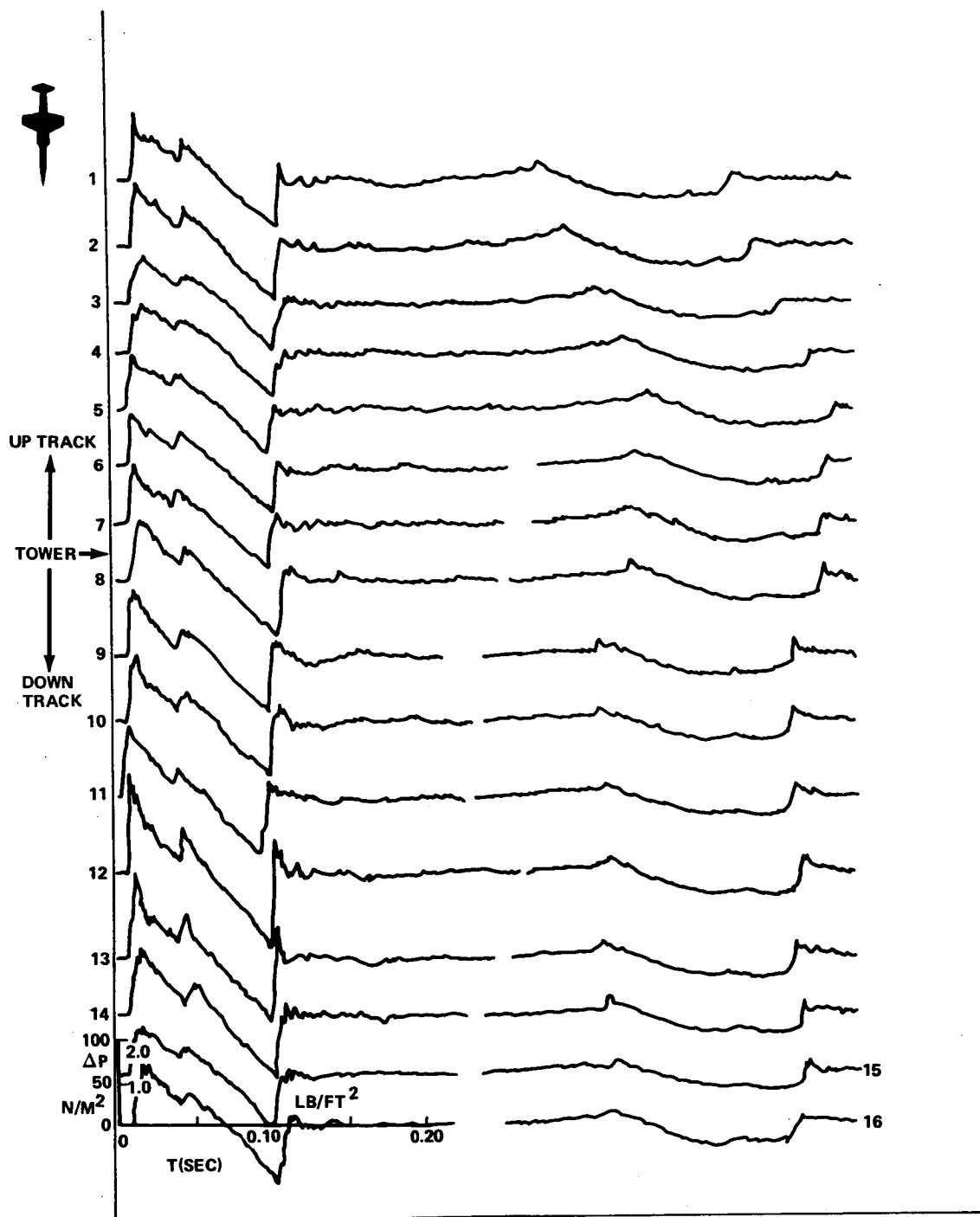


FIGURE 51.— GROUND PRESSURE SIGNATURES DOWNTRACK FROM CAUSTIC-GROUND INTERSECTION— PASS 040, AUGUST 28, 1-3

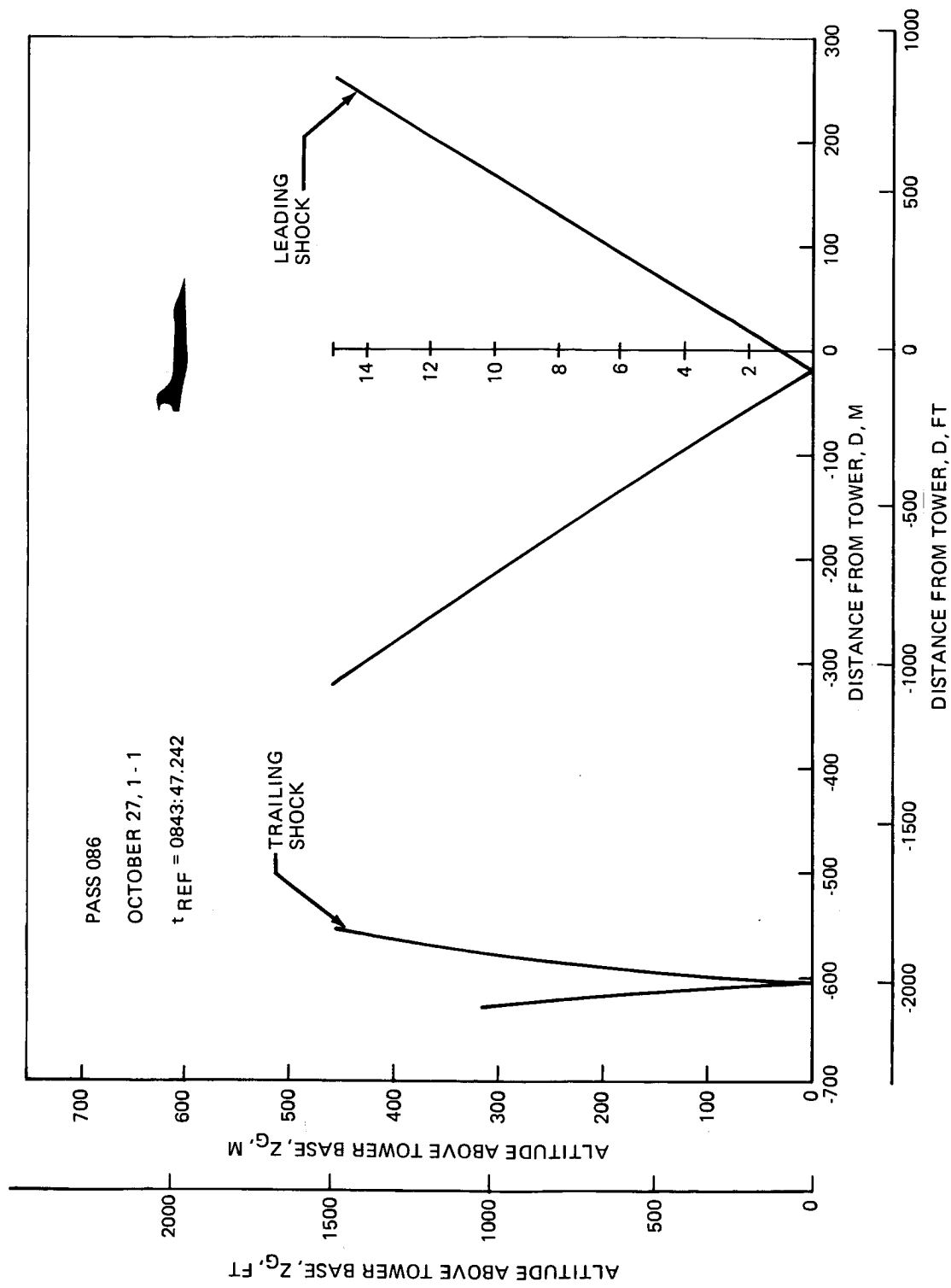


FIGURE 52.—SHOCK WAVE SYSTEM PROFILE FOR PASS 086

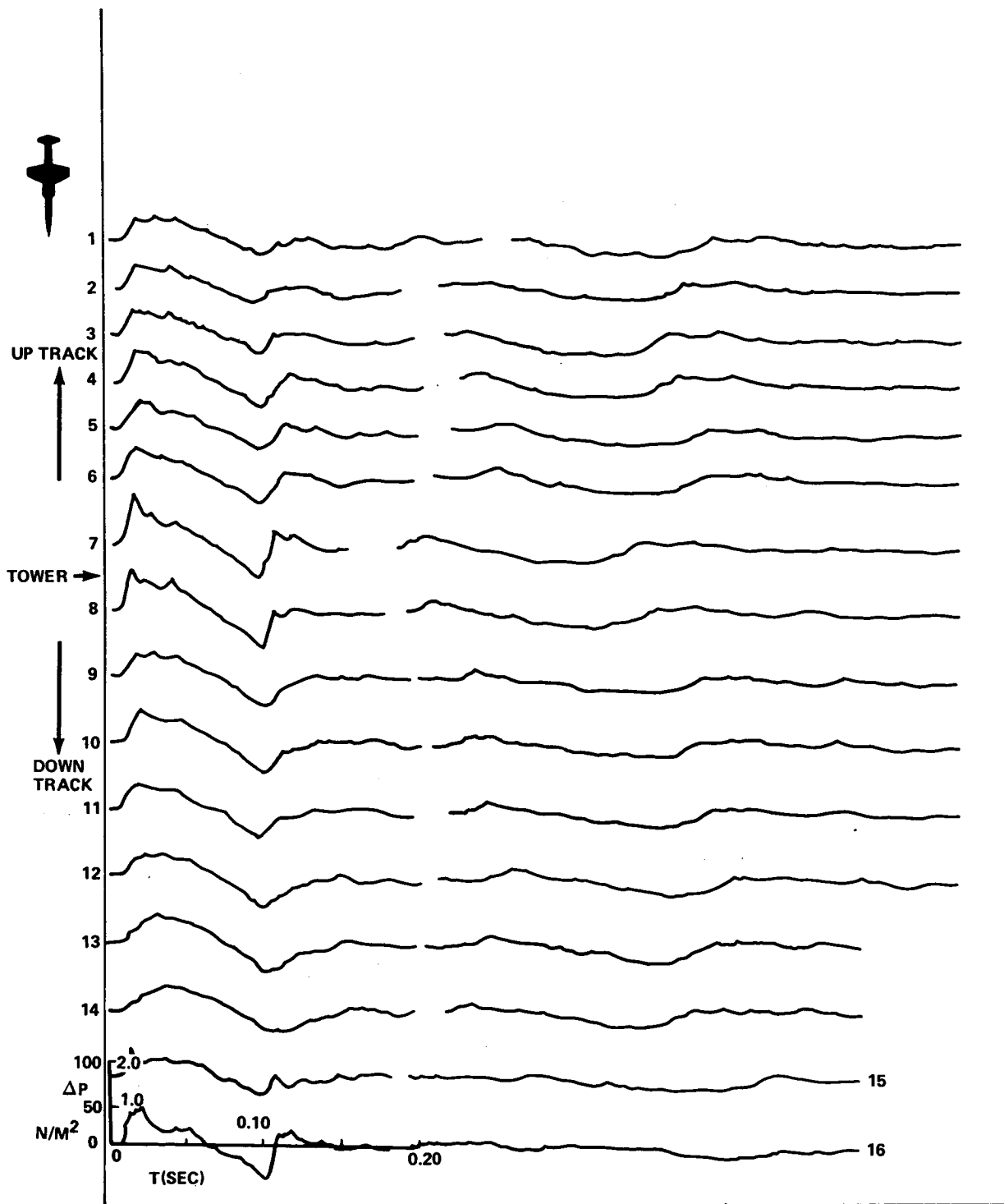


FIGURE 53.—GROUND PRESSURE SIGNATURES DOWNTRACK FROM CAUSTIC-GROUND INTERSECTION—PASS 086, OCTOBER 27, 1-1

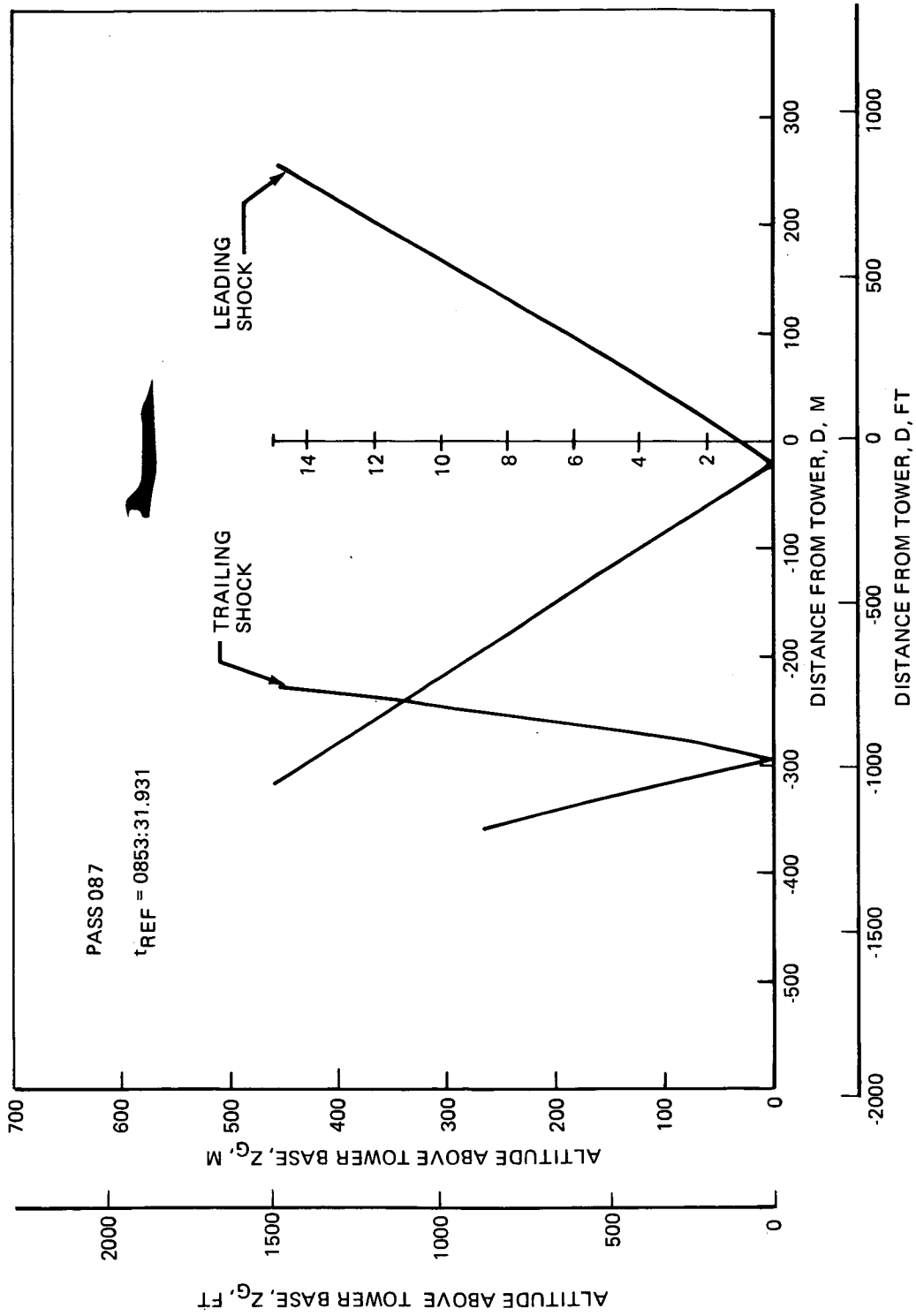


FIGURE 54.—SHOCK WAVE SYSTEM PROFILE FOR PASS 087

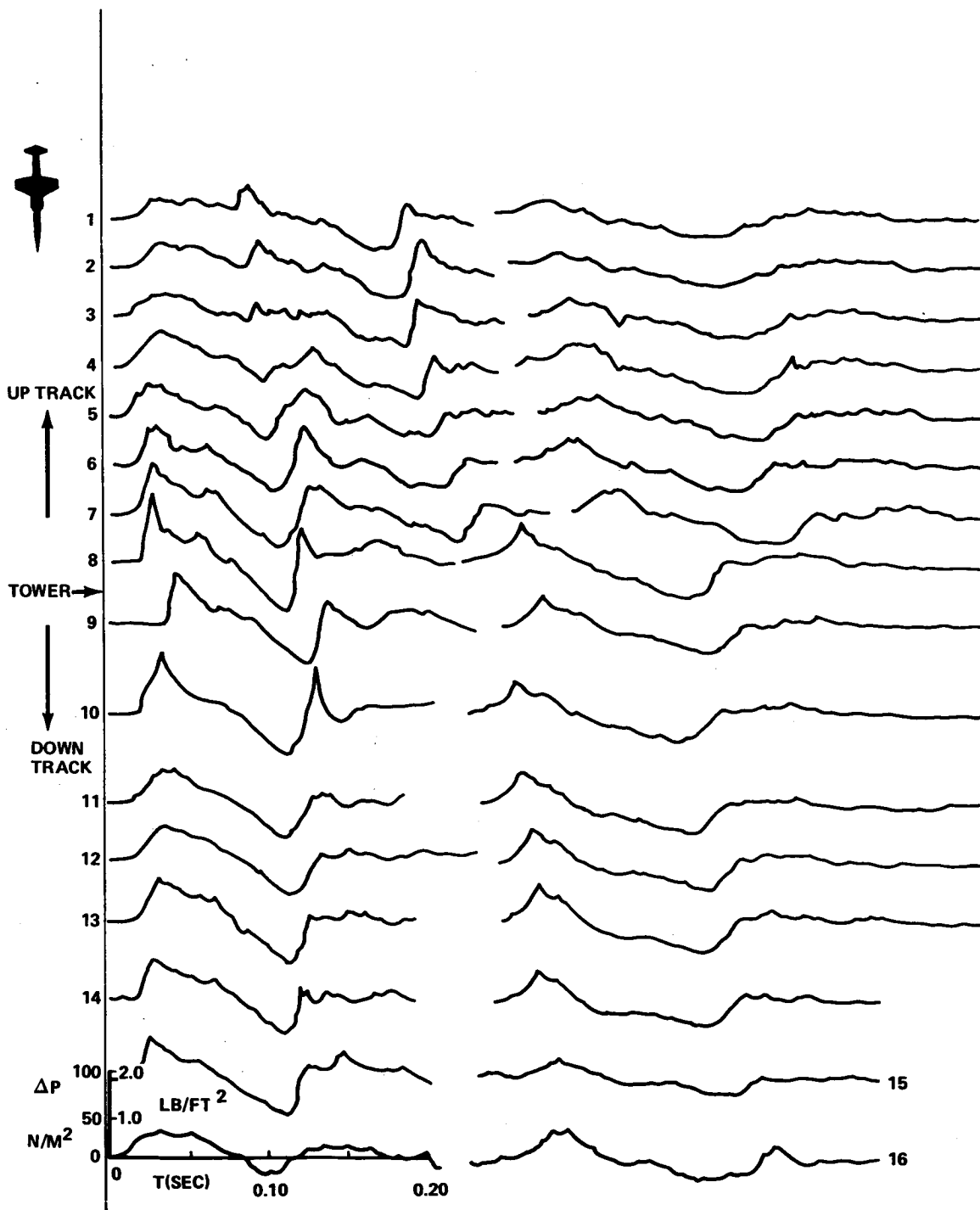


FIGURE 55.— GROUND PRESSURE SIGNATURES DOWNTRACK FROM CAUSTIC-GROUND INTERSECTION— PASS 087, OCTOBER 27, 1-2

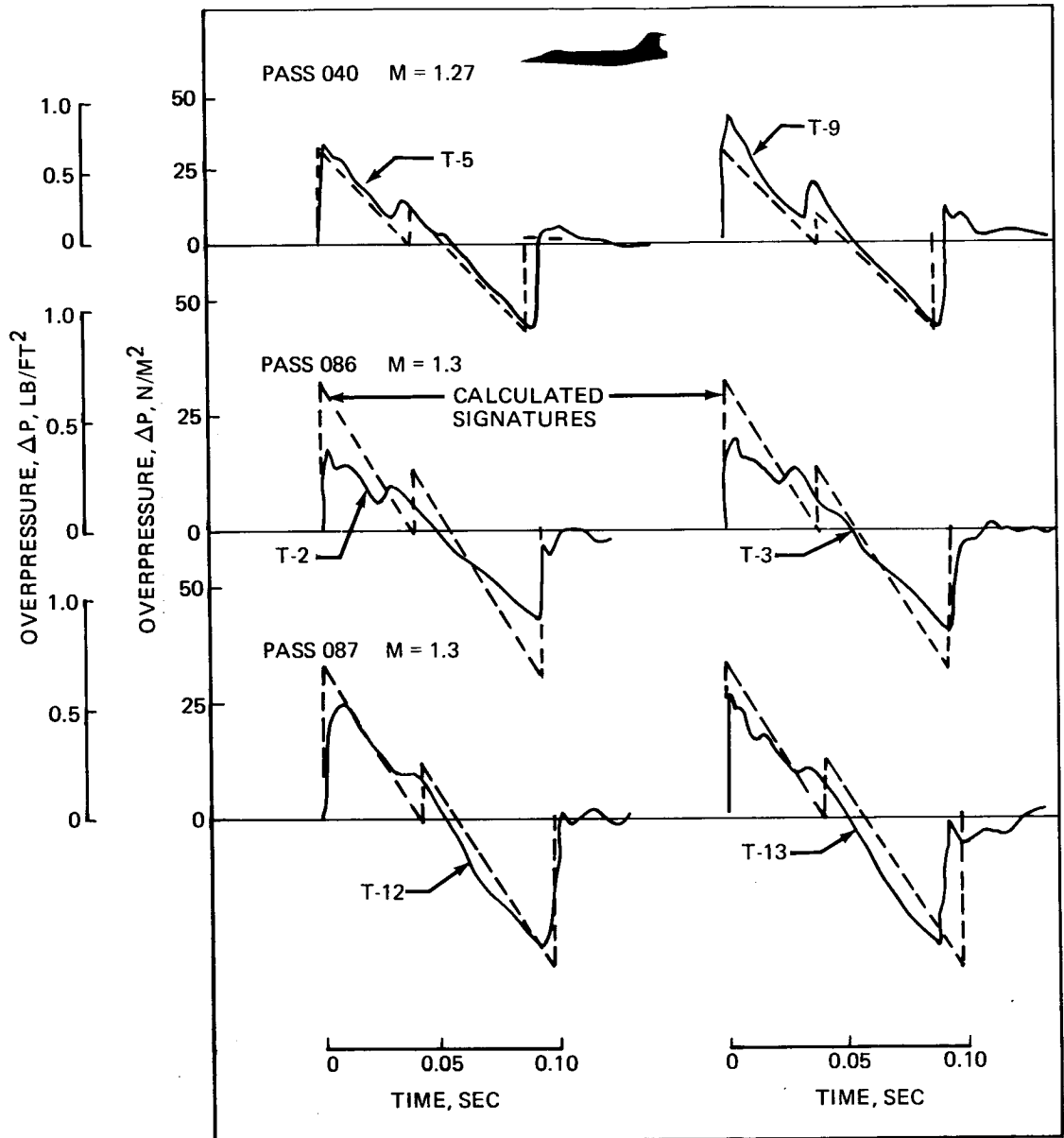


FIGURE 56.—CALCULATED AND OBSERVED PRESSURE SIGNATURES—PASSES 040, 086, 087

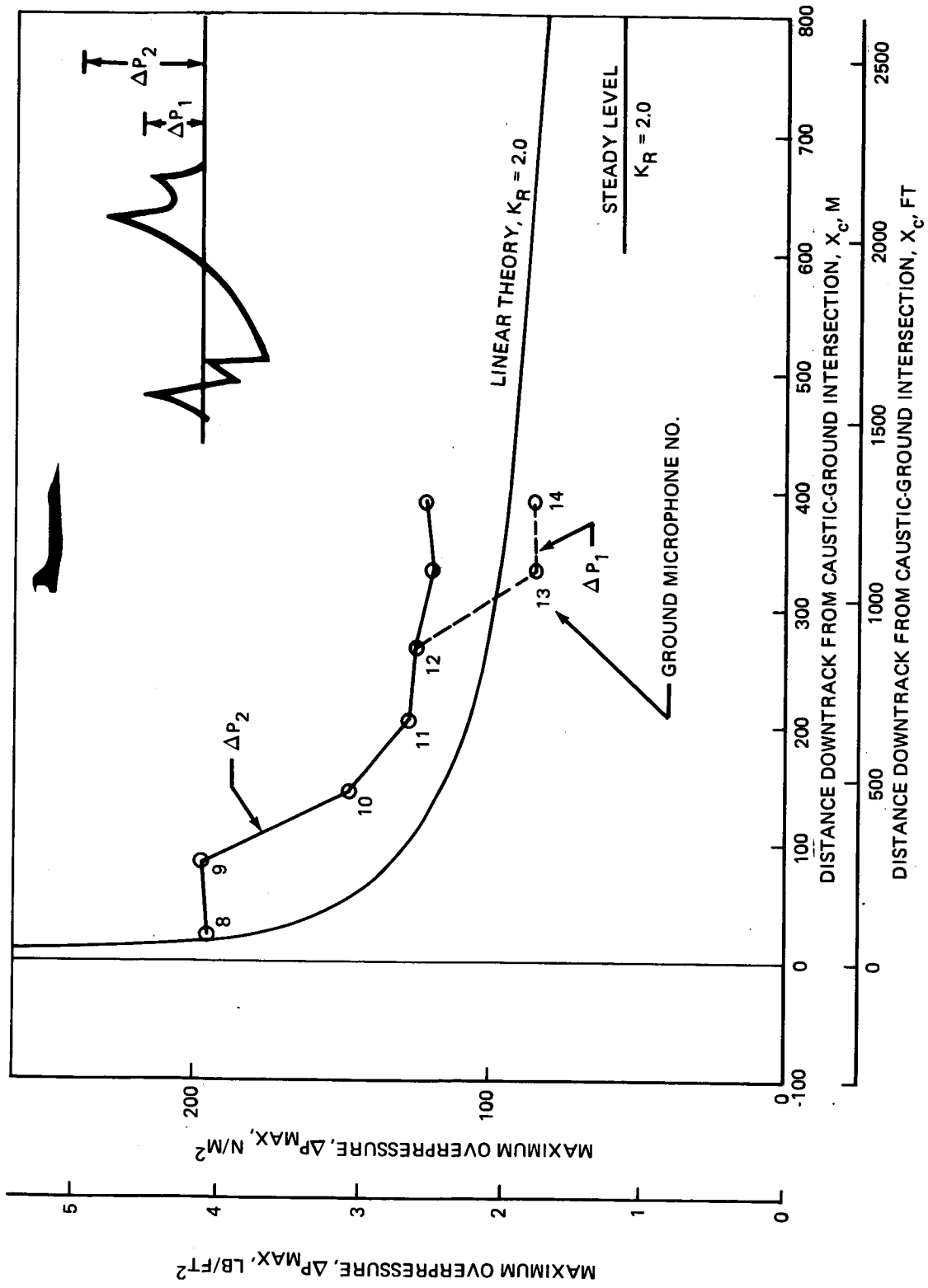


FIGURE 57.--VARIATION OF OVERPRESSURE NEAR CAUSTIC--THEORY AND EXPERIMENT--PASS 045

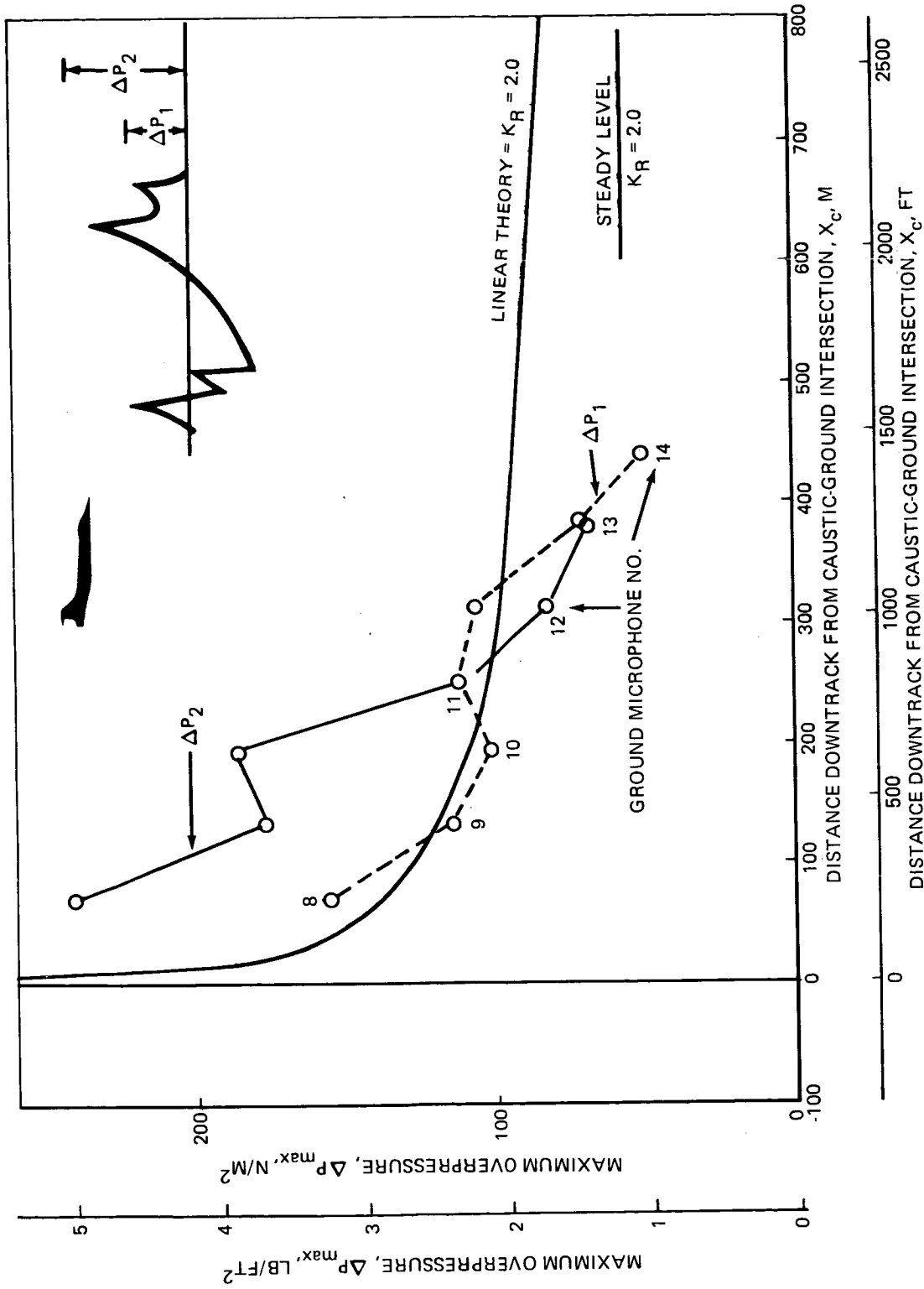


FIGURE 58.—VARIATION OF OVERPRESSURE NEAR CAUSTIC—THEORY AND EXPERIMENT—PASS 046

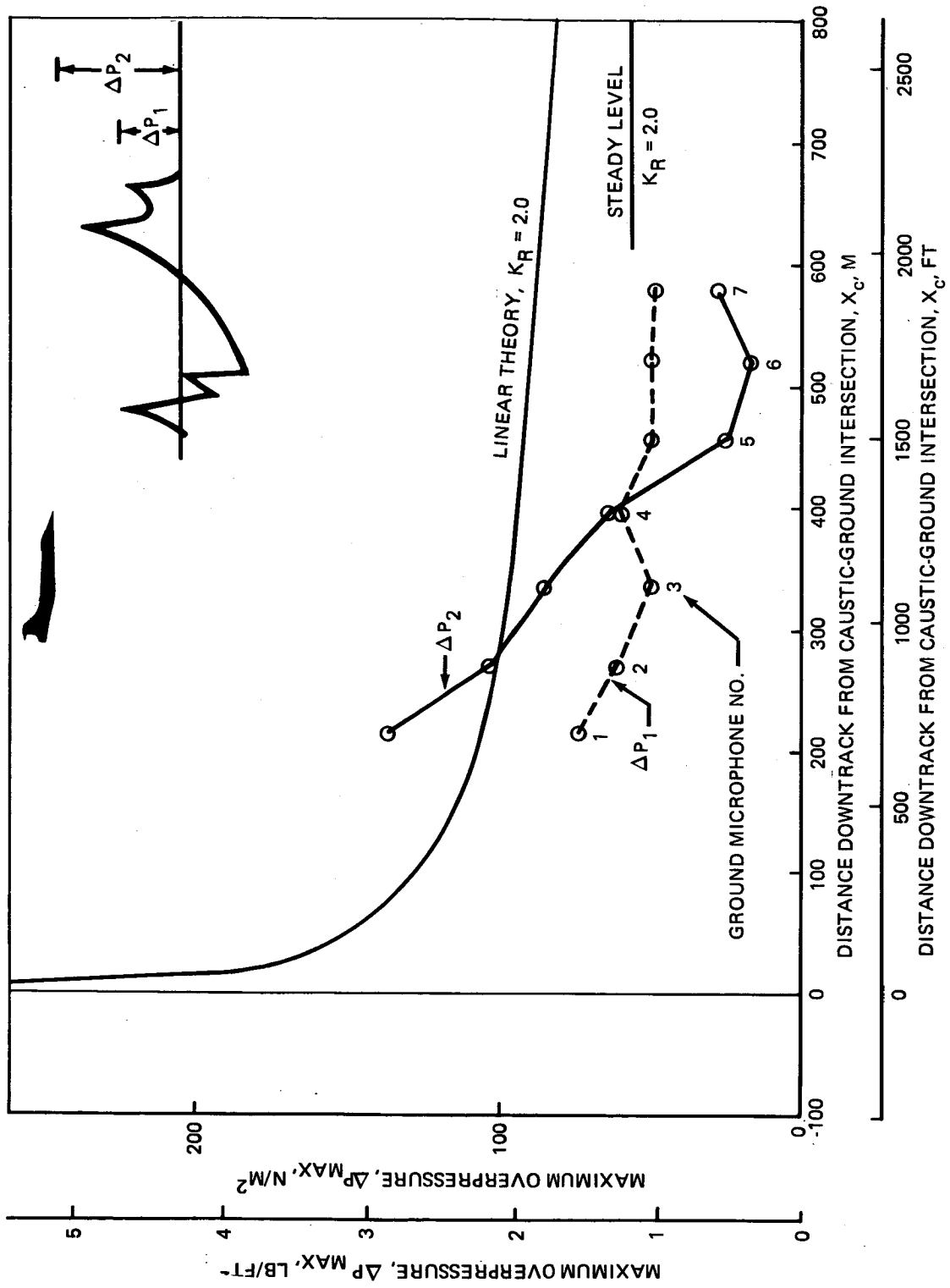


FIGURE 59.—VARIATION OF OVERPRESSURE NEAR CAUSTIC—THEORY AND EXPERIMENT—PASS 092

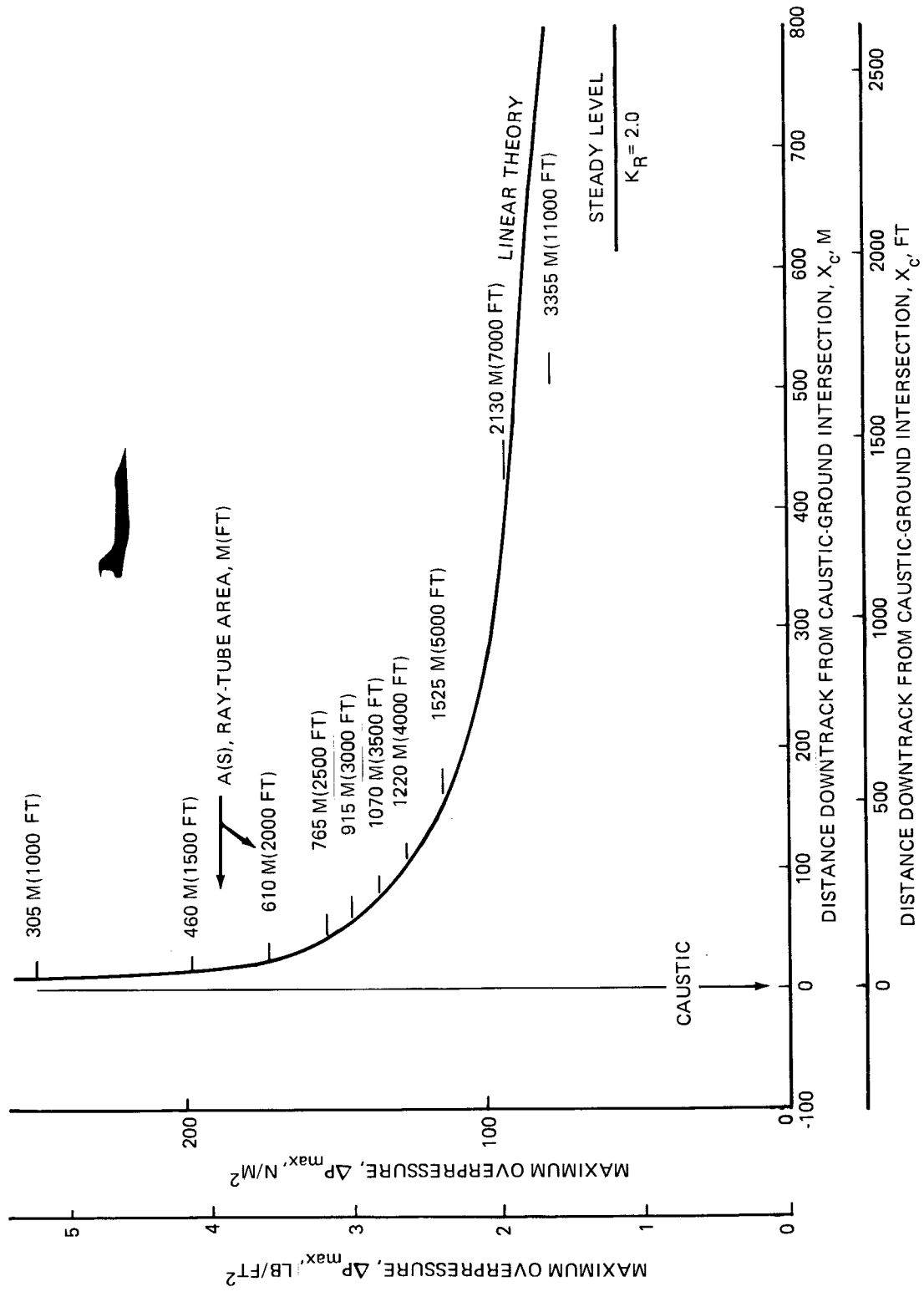


FIGURE 60.—LINEAR THEORY, RAY-TUBE AREA VARIATION NEAR ACCELERATION CAUSTIC

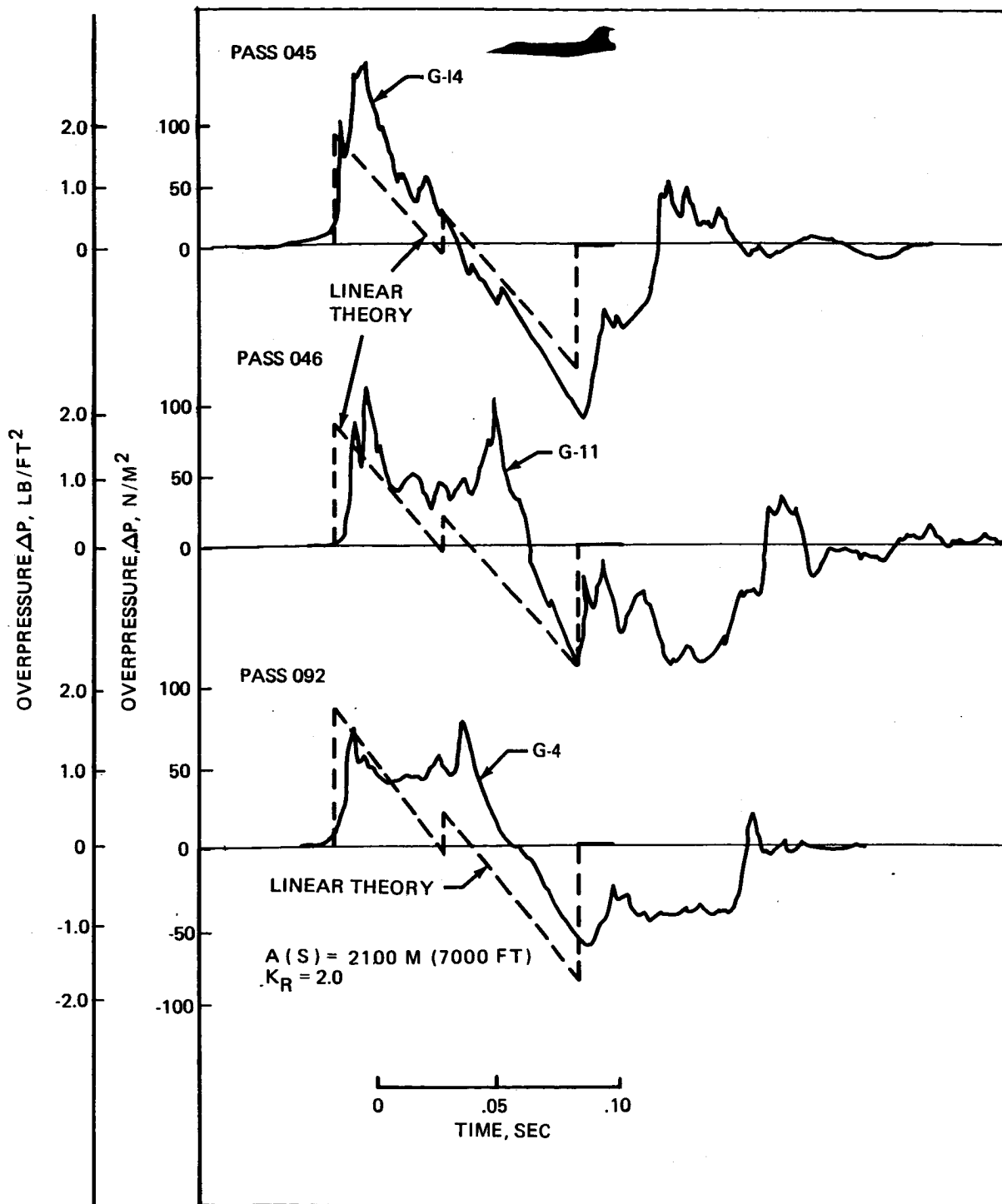


FIGURE 61.—LINEAR THEORY PRESSURE SIGNATURES AT 400 M (1300 FT) COMPARED WITH OBSERVATIONS

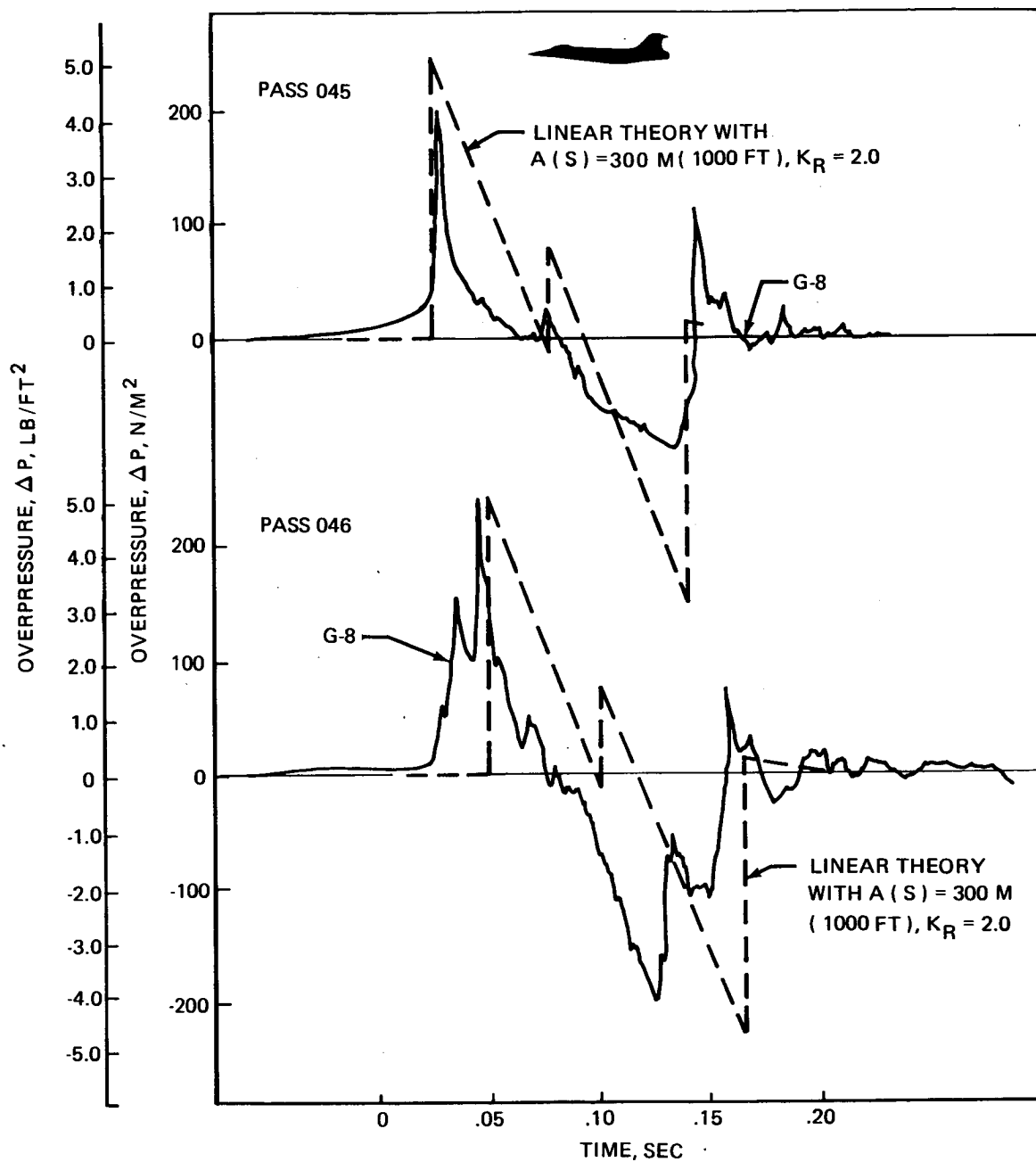


FIGURE 62.—LINEAR THEORY PRESSURE SIGNATURE WITH RAY-TUBE AREA LIMIT COMPARED WITH CAUSTIC SIGNATURES

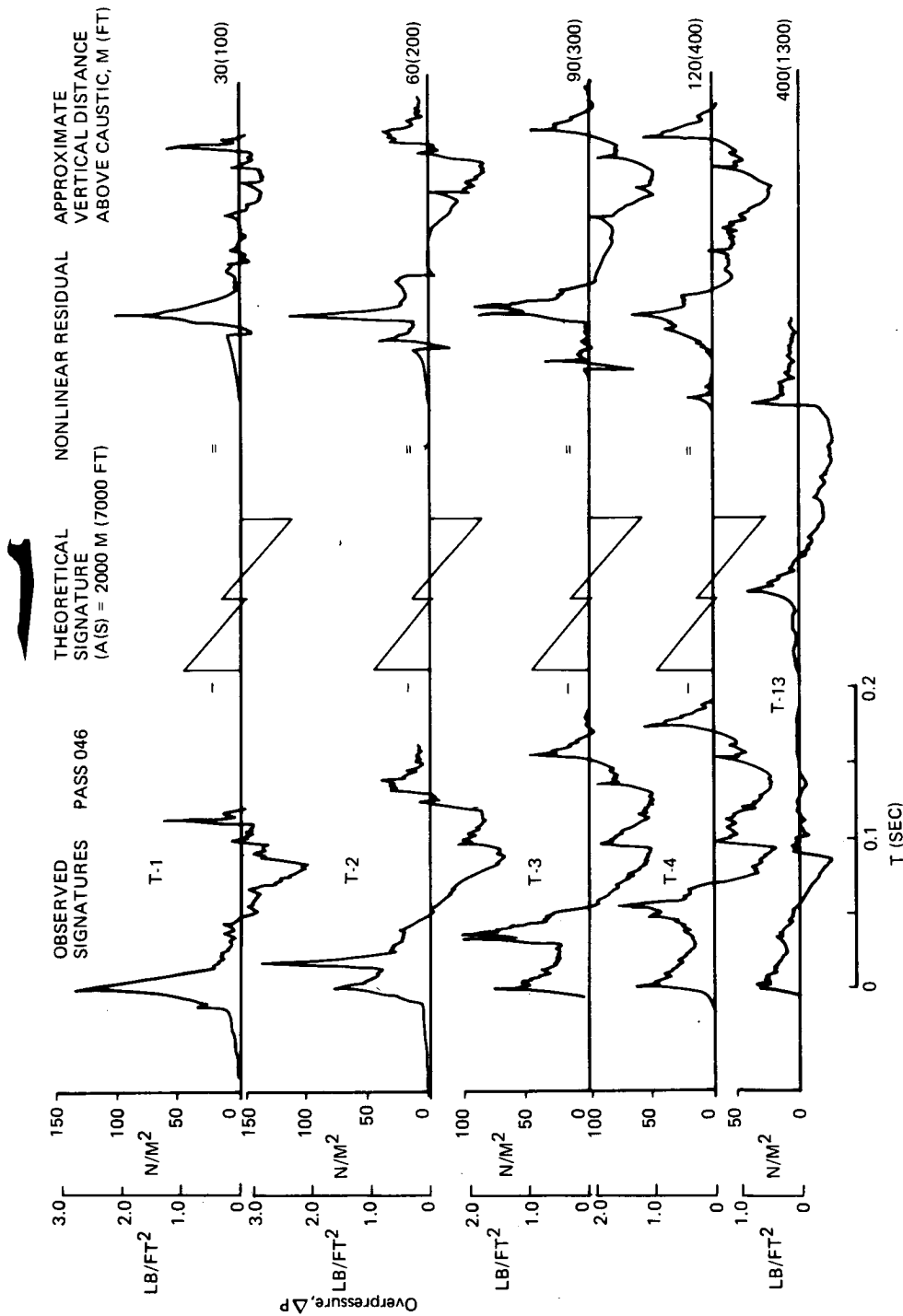


FIGURE 64.—SEPARATION OF OBSERVED PRESSURE SIGNATURES NEAR THE ACCELERATION CAUSTIC INTO LINEAR AND NONLINEAR COMPONENTS, PASS 046, AUGUST 28, 3-3

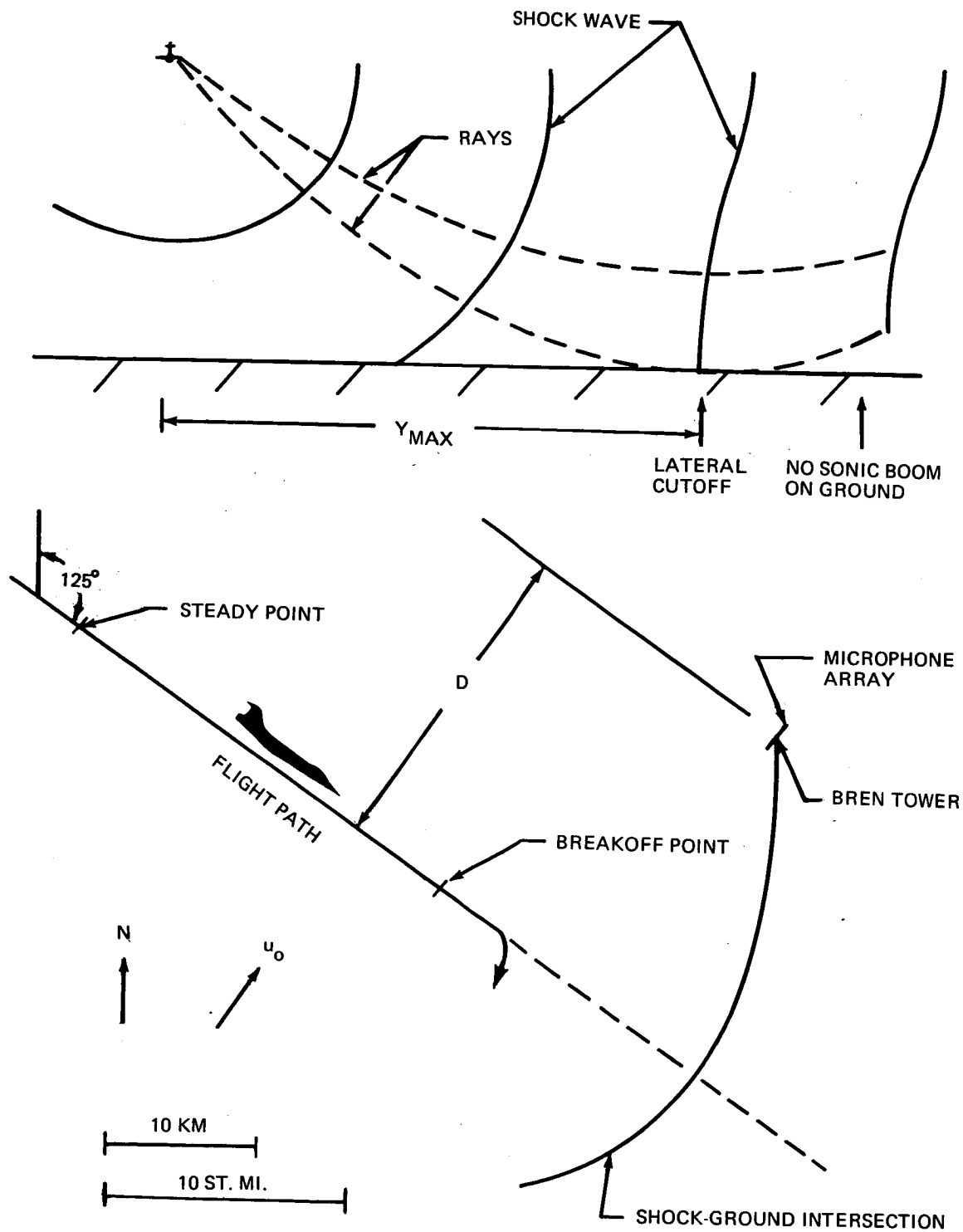


FIGURE 65.—EXPERIMENTAL SETUP FOR THE LATERAL CUTOFF FLIGHTS

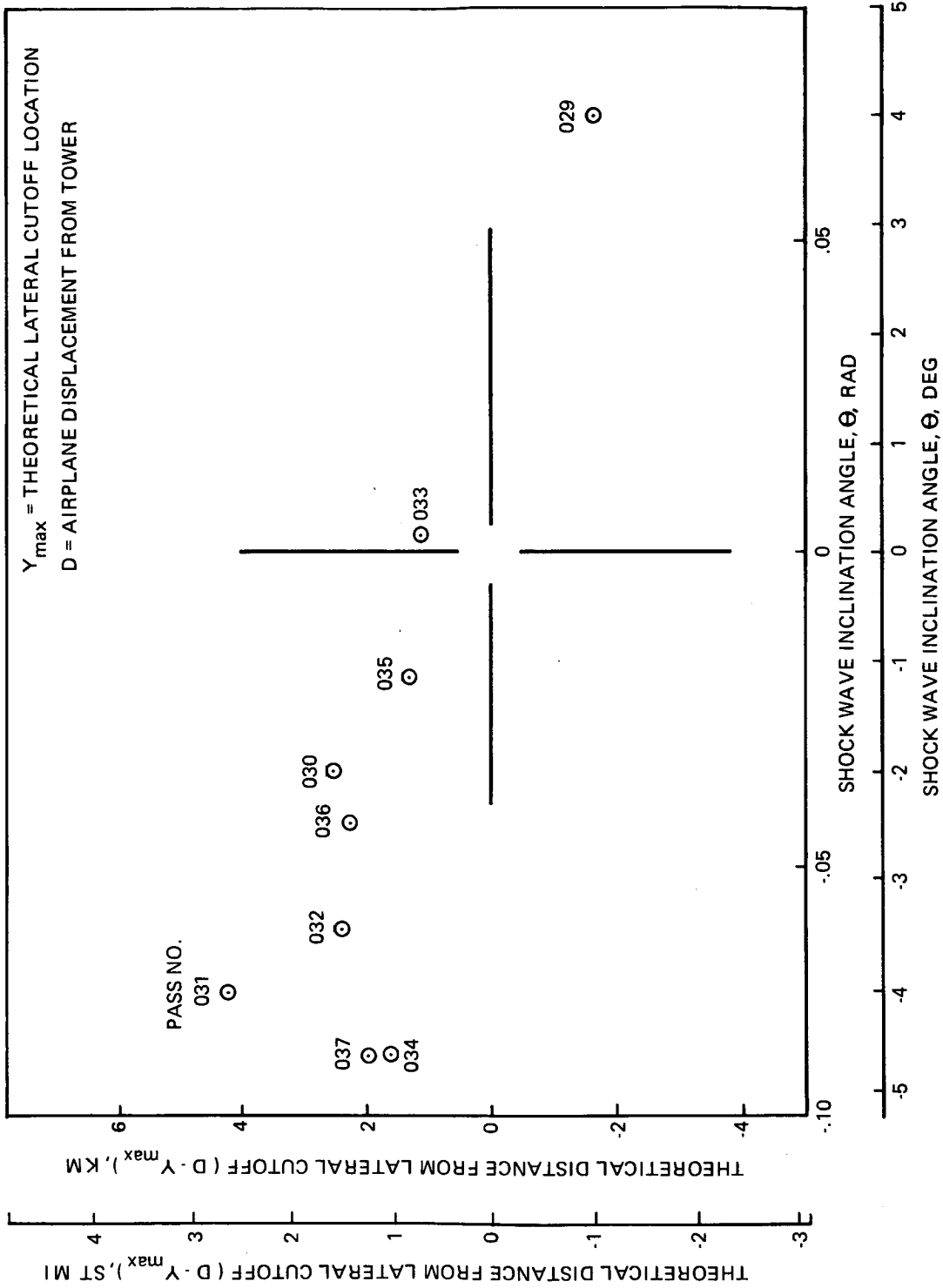


FIGURE 66.—COMPARISON OF OBSERVED LATERAL CUTOFF LOCATION WITH THEORY

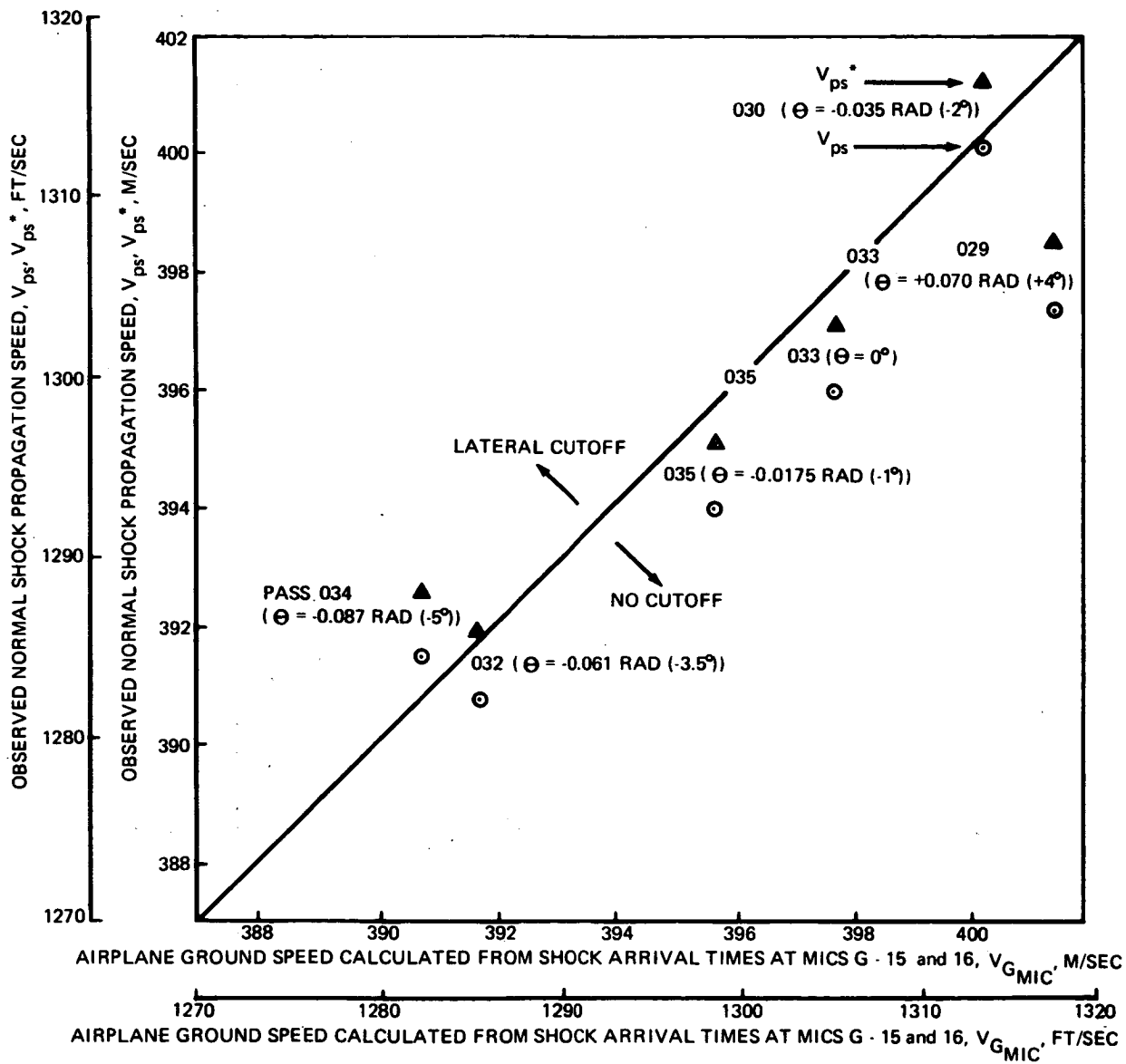


FIGURE 67.—NORMAL SHOCK PROPAGATION SPEED NEAR LATERAL CUTOFF

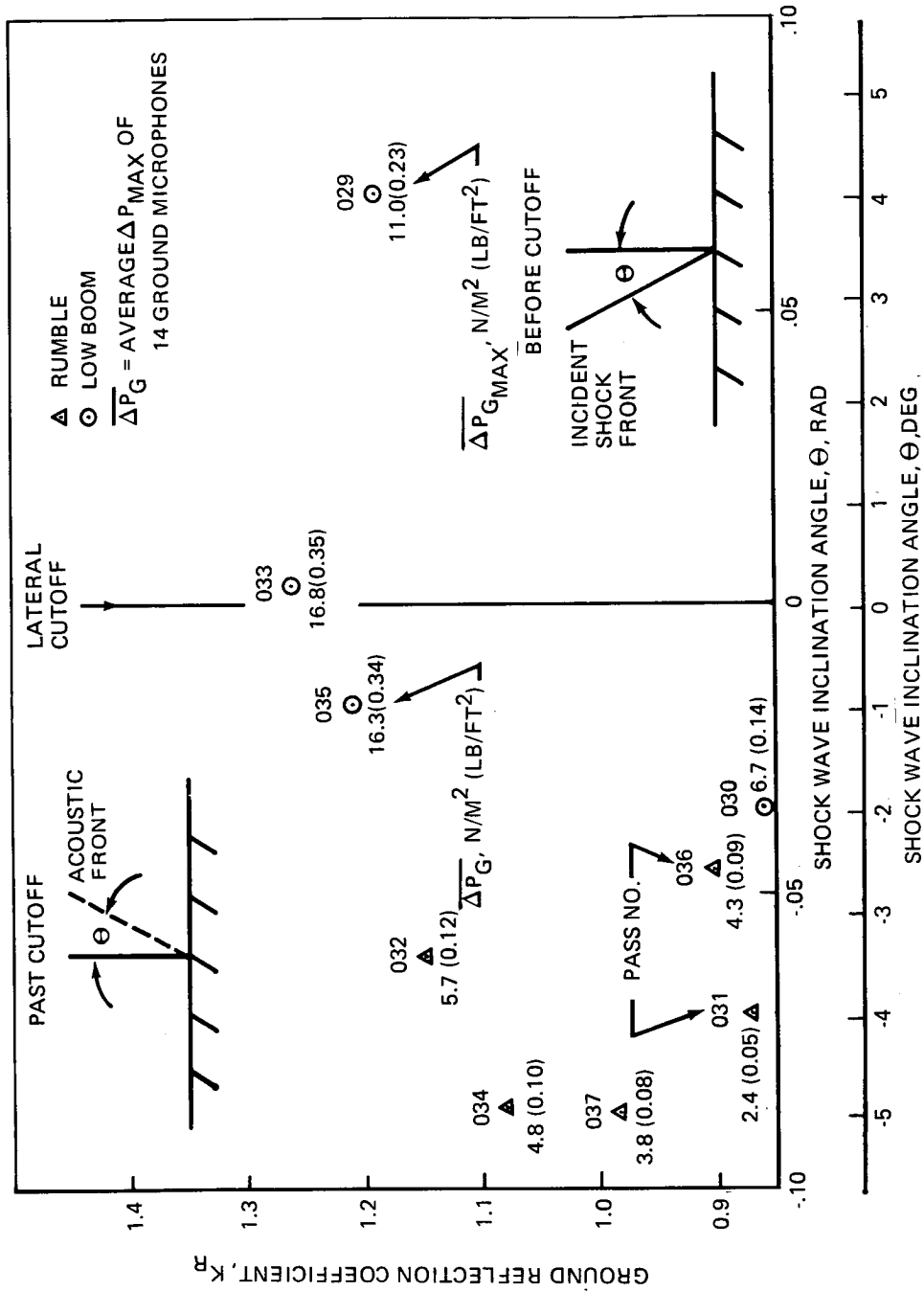


FIGURE 68.—VARIATION OF GROUND REFLECTION COEFFICIENT, K_R , NEAR LATERAL CUTOFF

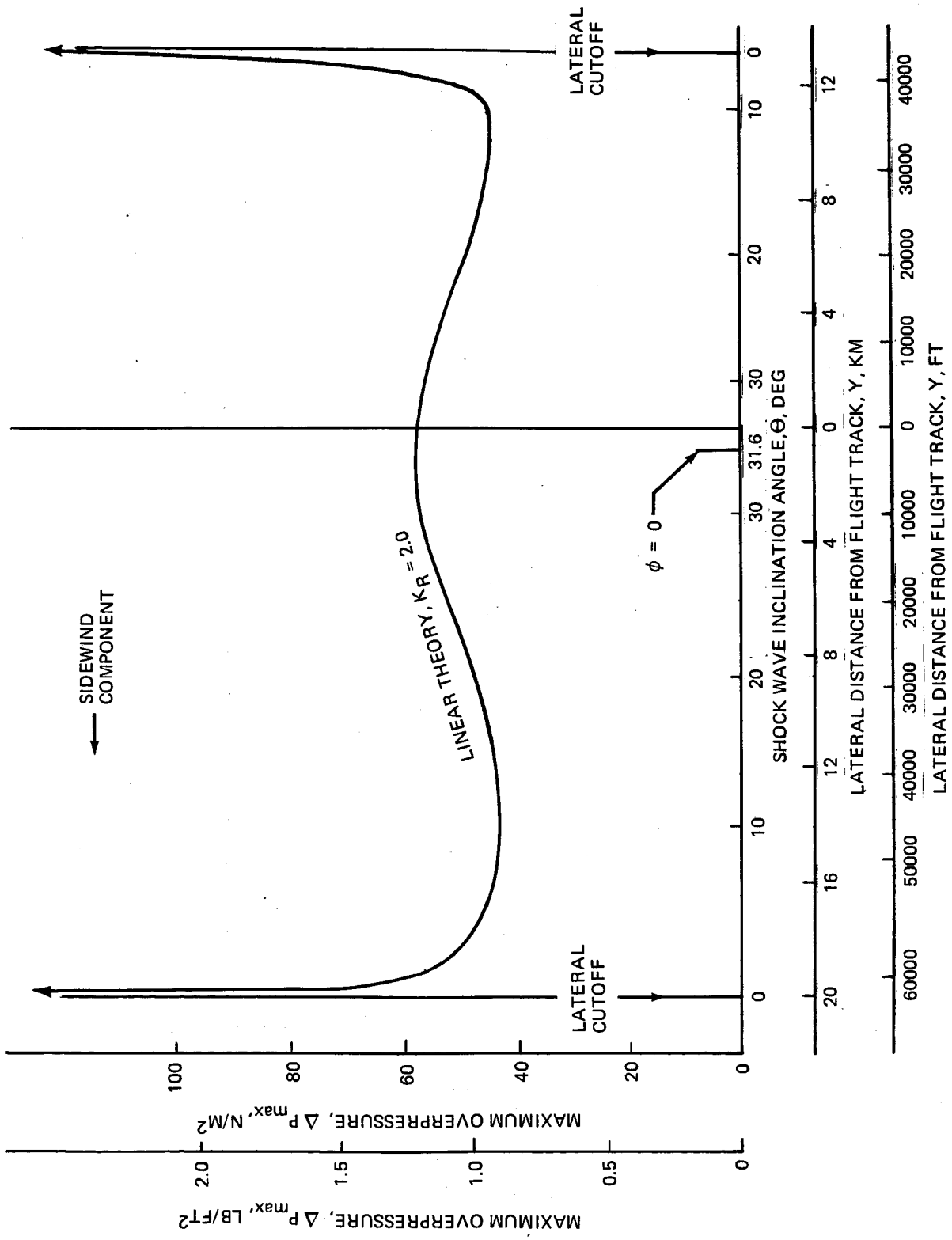


FIGURE 69.—LINEAR THEORY VARIATION OF OVERPRESSURE WITH LATERAL DISTANCE

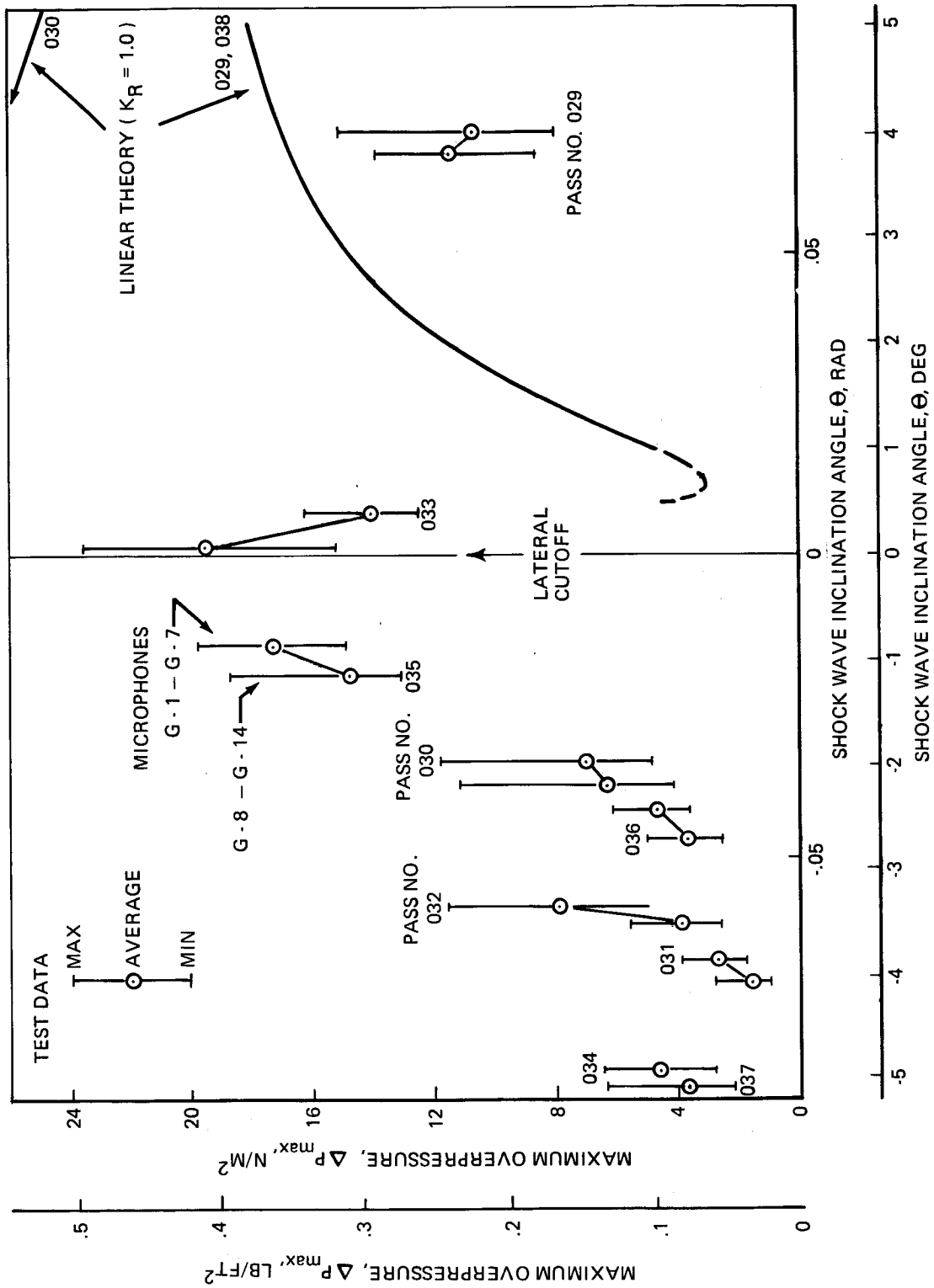


FIGURE 70.—VARIATION OF MAXIMUM OVERPRESSURE ON GROUND NEAR LATERAL CUTOFF

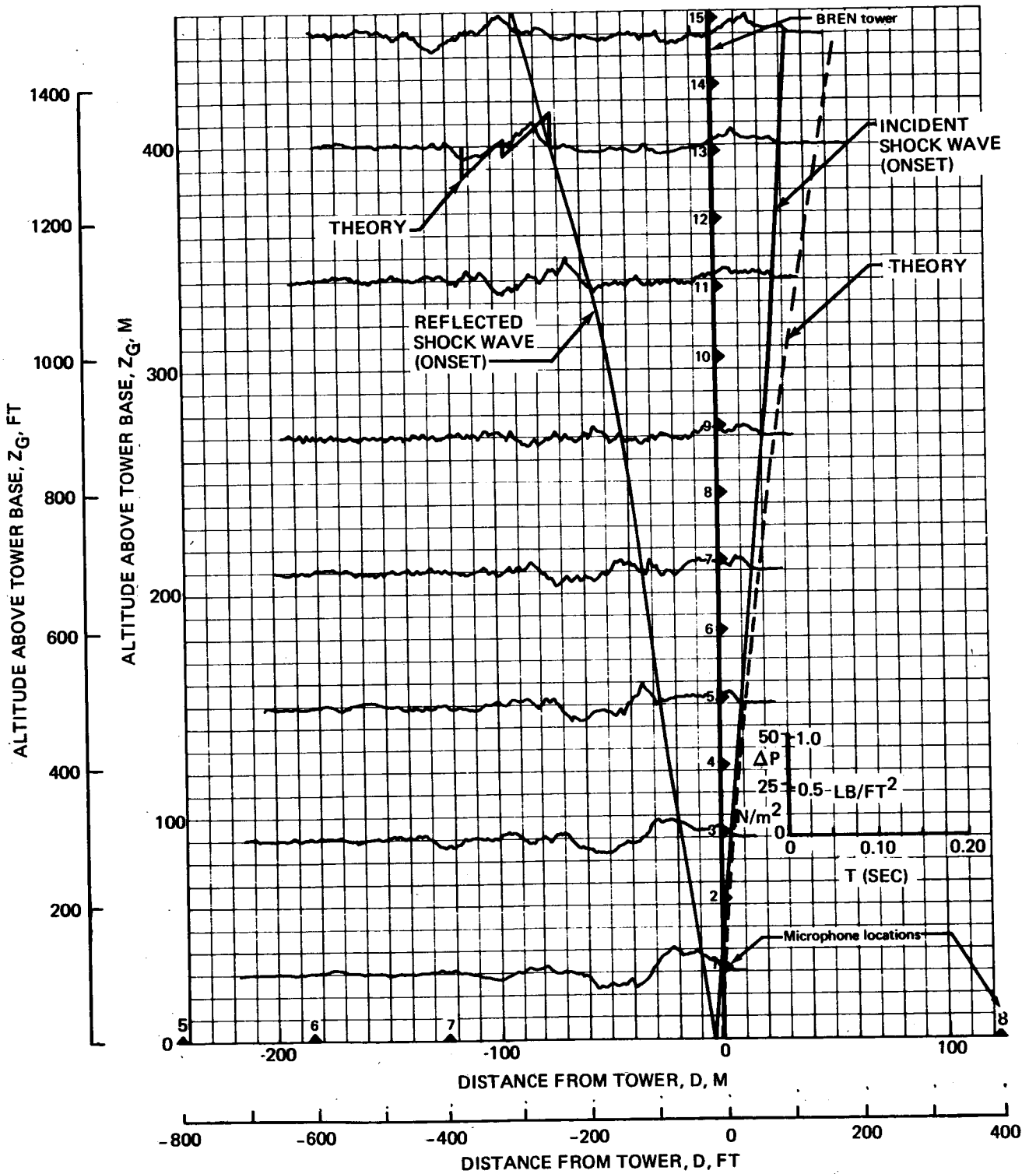


FIGURE 71.—SHOCK WAVE PROFILE AND TOWER PRESSURE SIGNATURES BEFORE LATERAL CUTOFF—PASS 029, AUGUST 27, 1-1

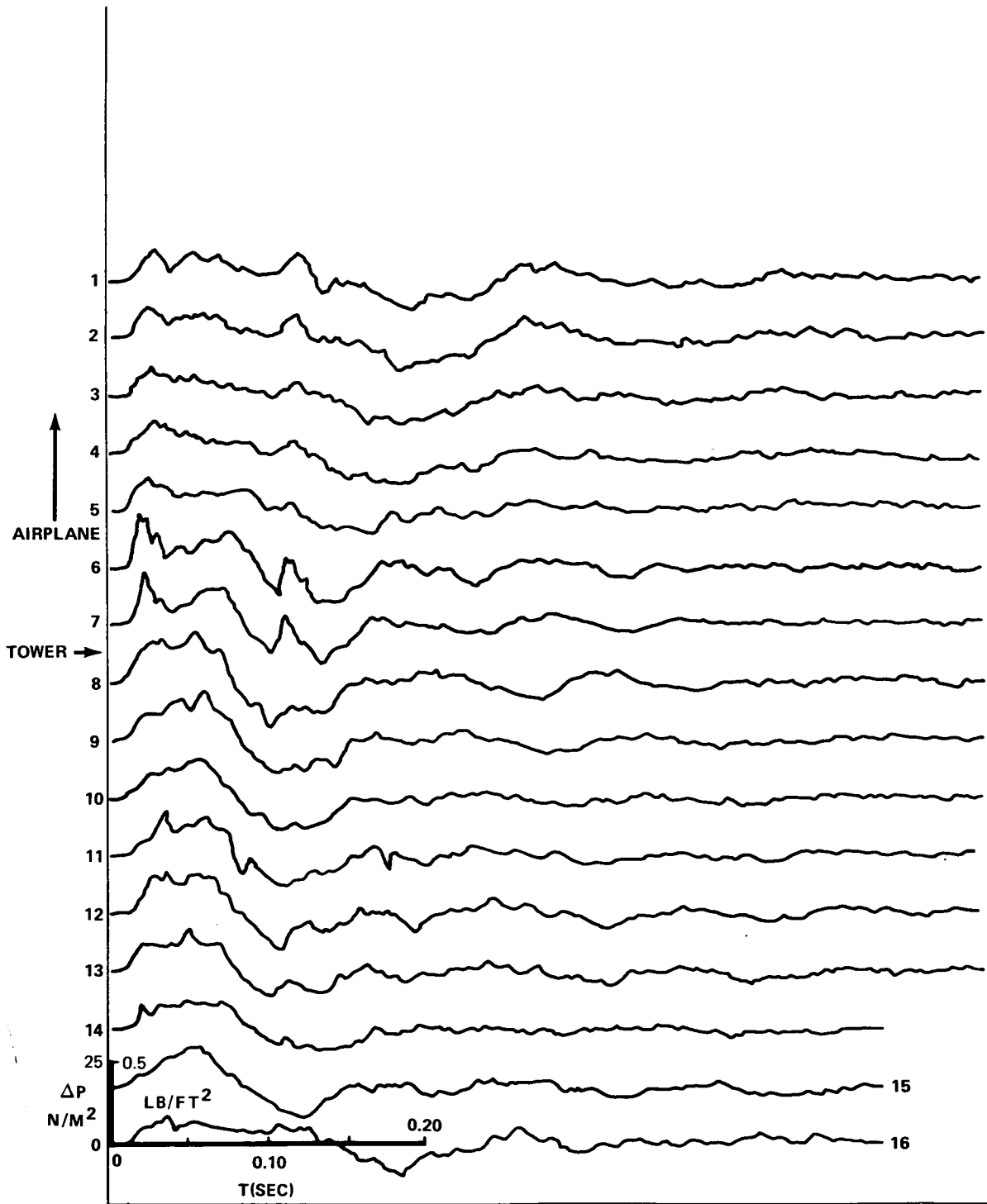


FIGURE 72.— GROUND PRESSURE SIGNATURES BEFORE LATERAL CUTOFF—PASS 029, AUGUST 27, 1-1

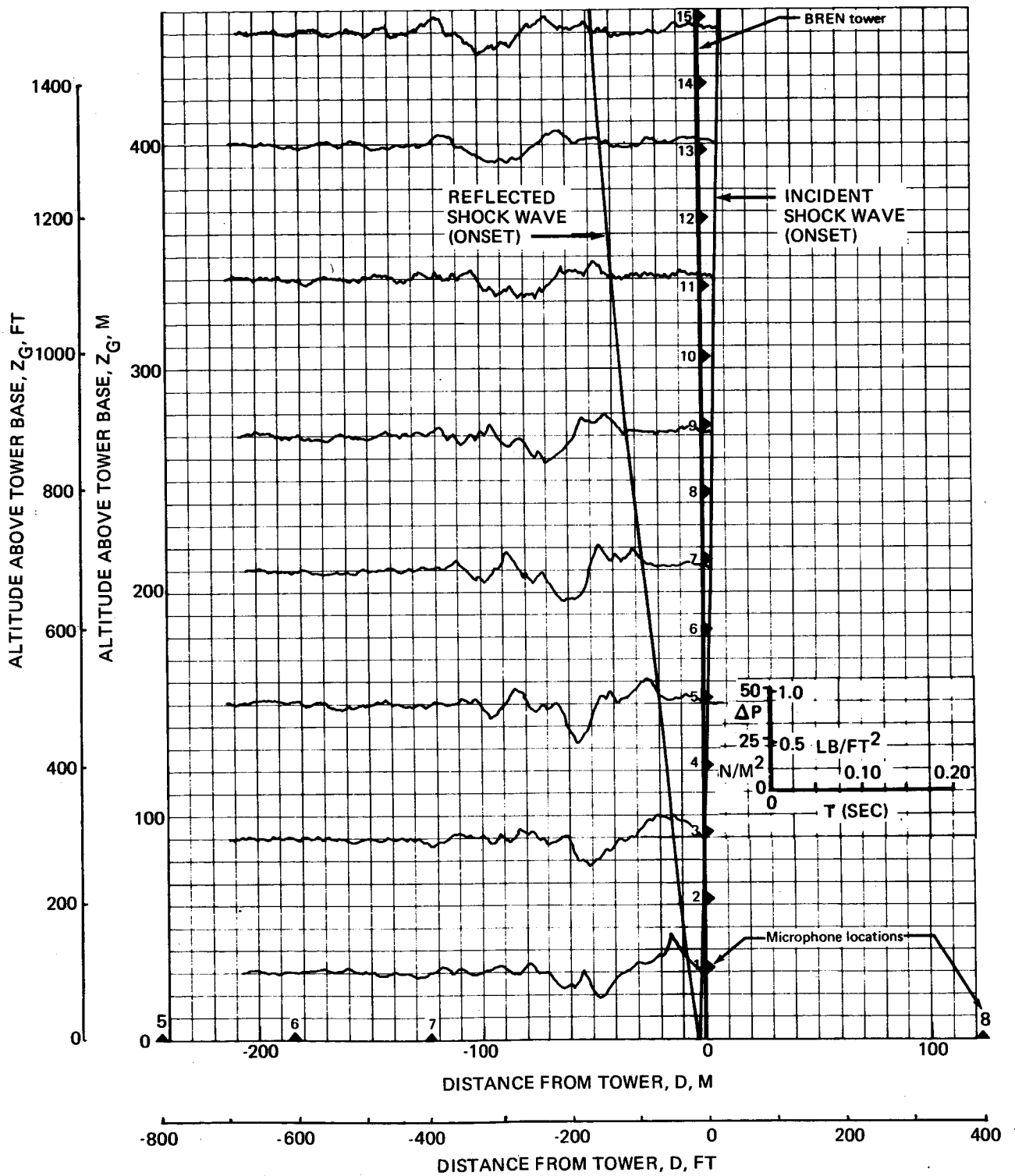


FIGURE 73.—SHOCK WAVE PROFILE AND TOWER PRESSURE SIGNATURES NEAR LATERAL CUTOFF—PASS 033, AUGUST 27, 2-2

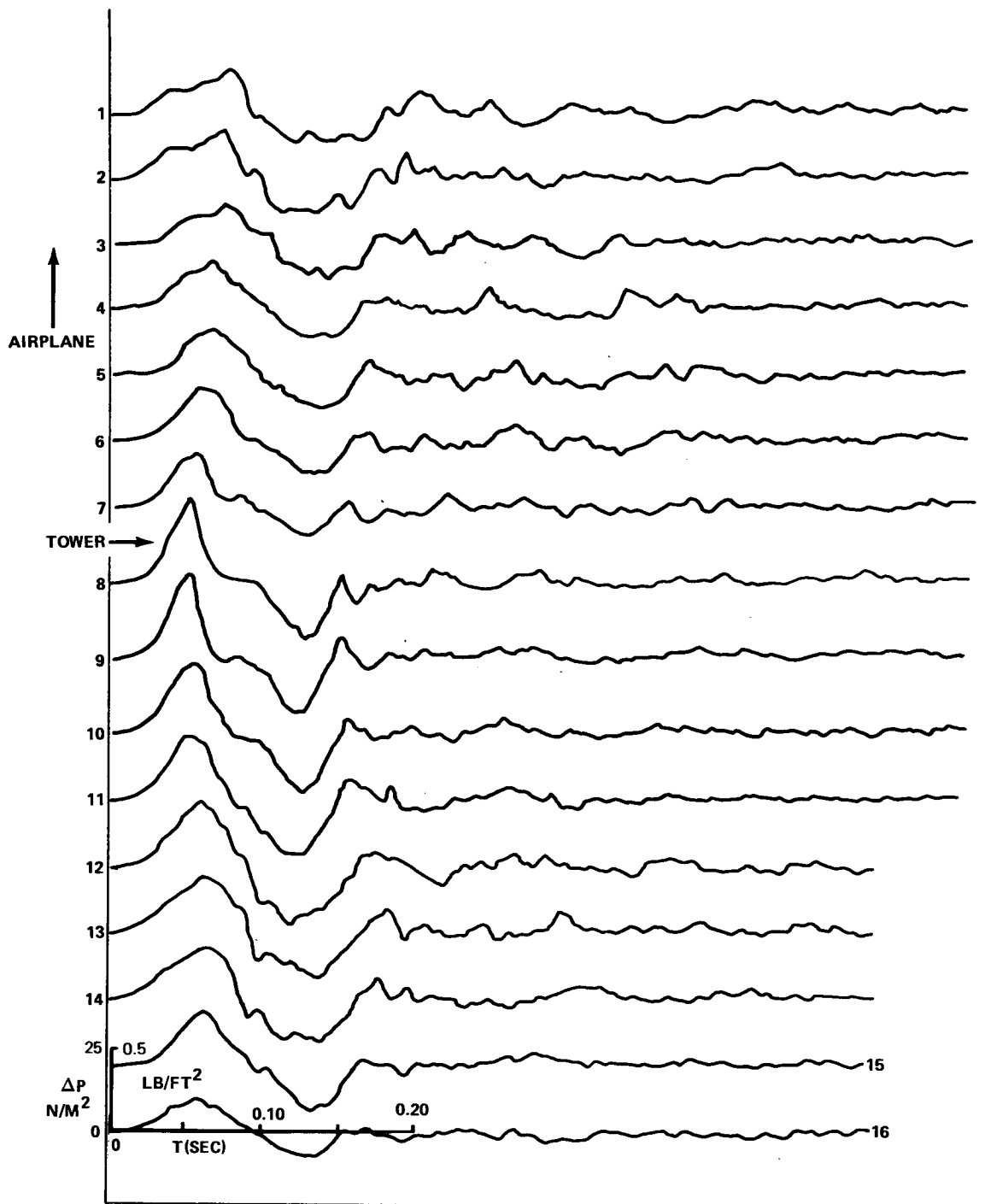


FIGURE 74.— GROUND PRESSURE SIGNATURES NEAR LATERAL CUTOFF—PASS 033, AUGUST 27, 2-2

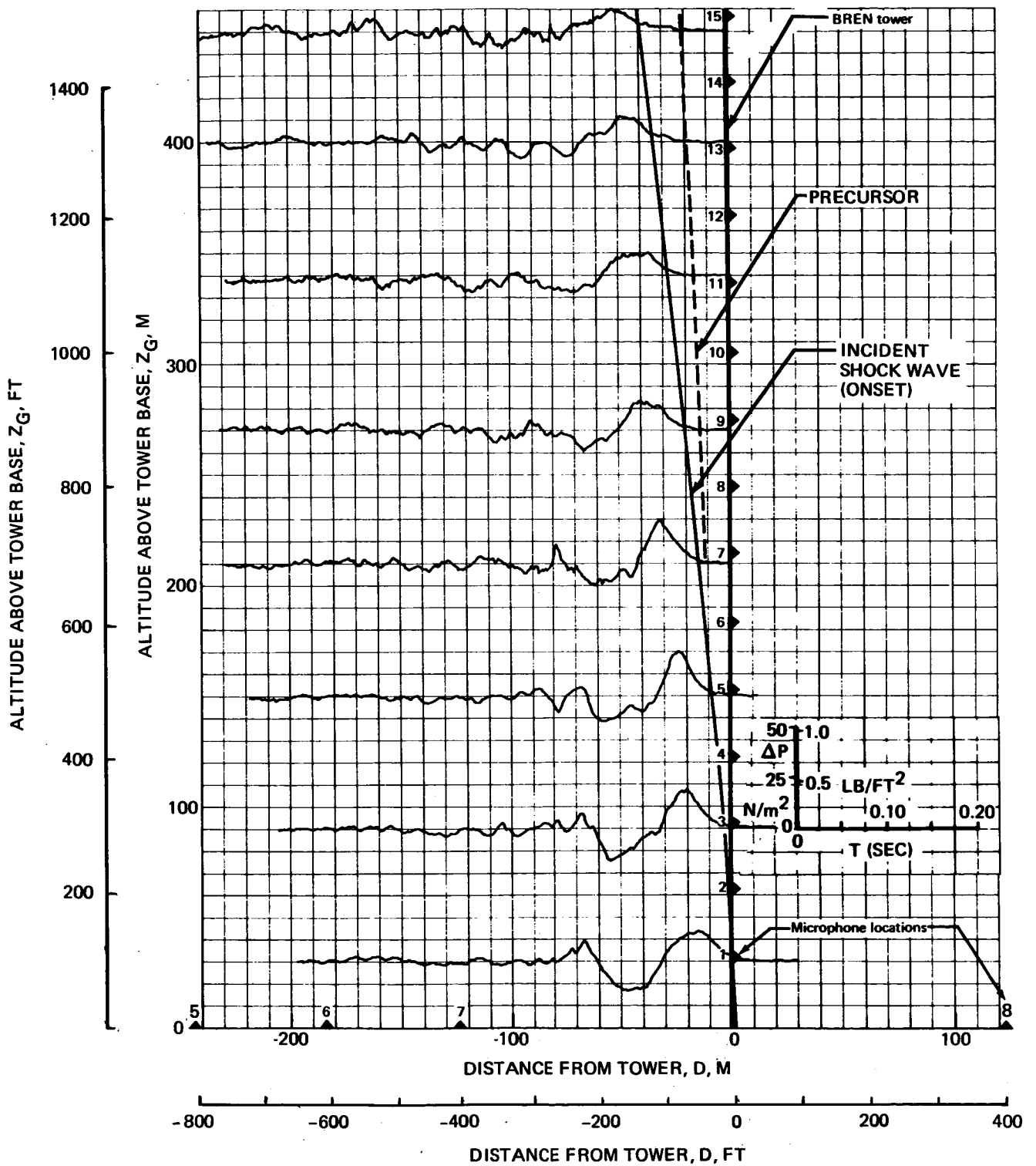


FIGURE 75.—SHOCK WAVE PROFILE AND TOWER PRESSURE SIGNATURES NEAR LATERAL CUTOFF—PASS 035, AUGUST 27, 3-1

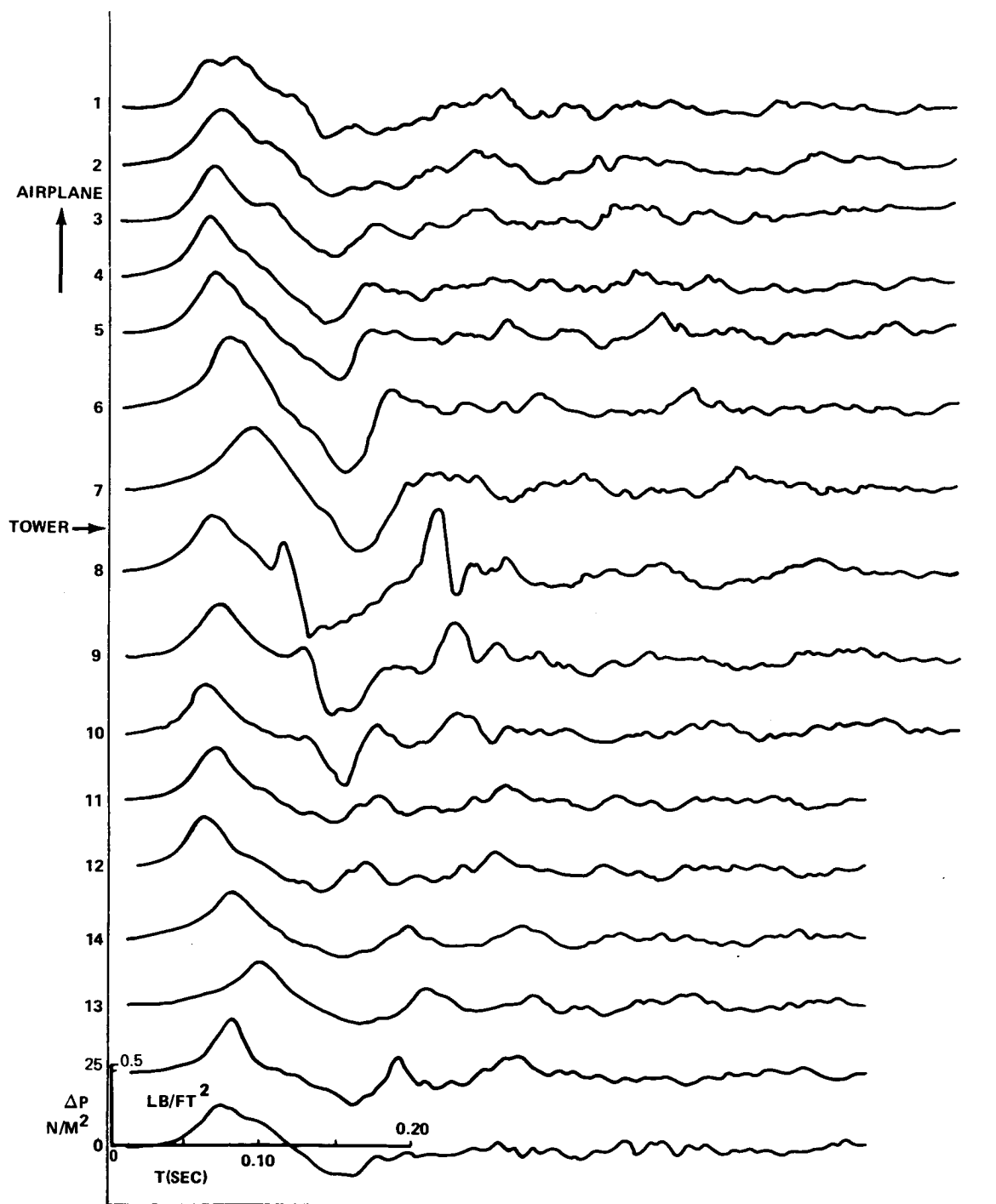


FIGURE 76.— GROUND PRESSURE SIGNATURES NEAR LATERAL CUTOFF—PASS 035, AUGUST 27, 3-1

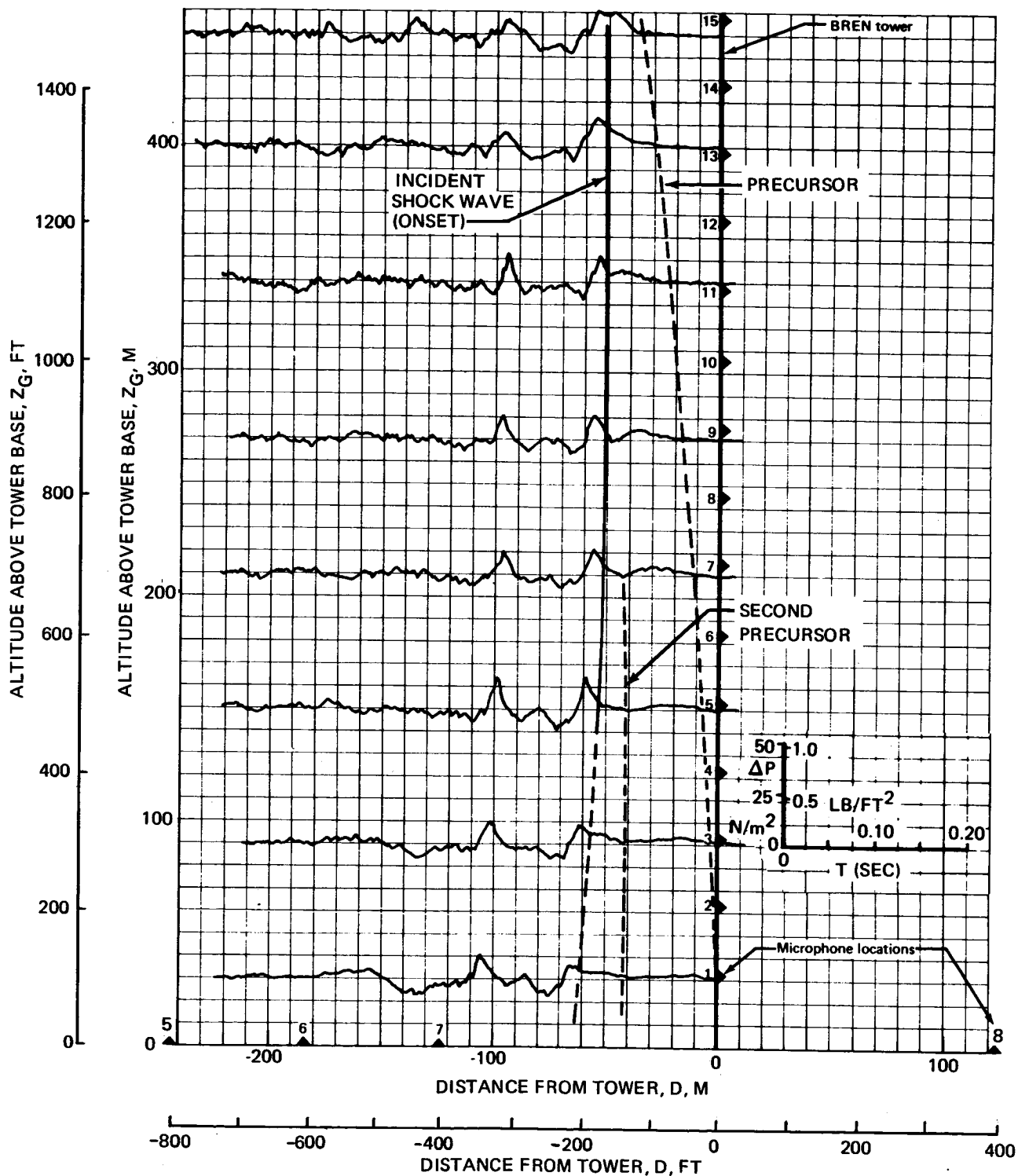


FIGURE 77.—SHOCK WAVE PROFILE AND TOWER PRESSURE SIGNATURES NEAR LATERAL CUTOFF—PASS 030, AUGUST 27, 1-2

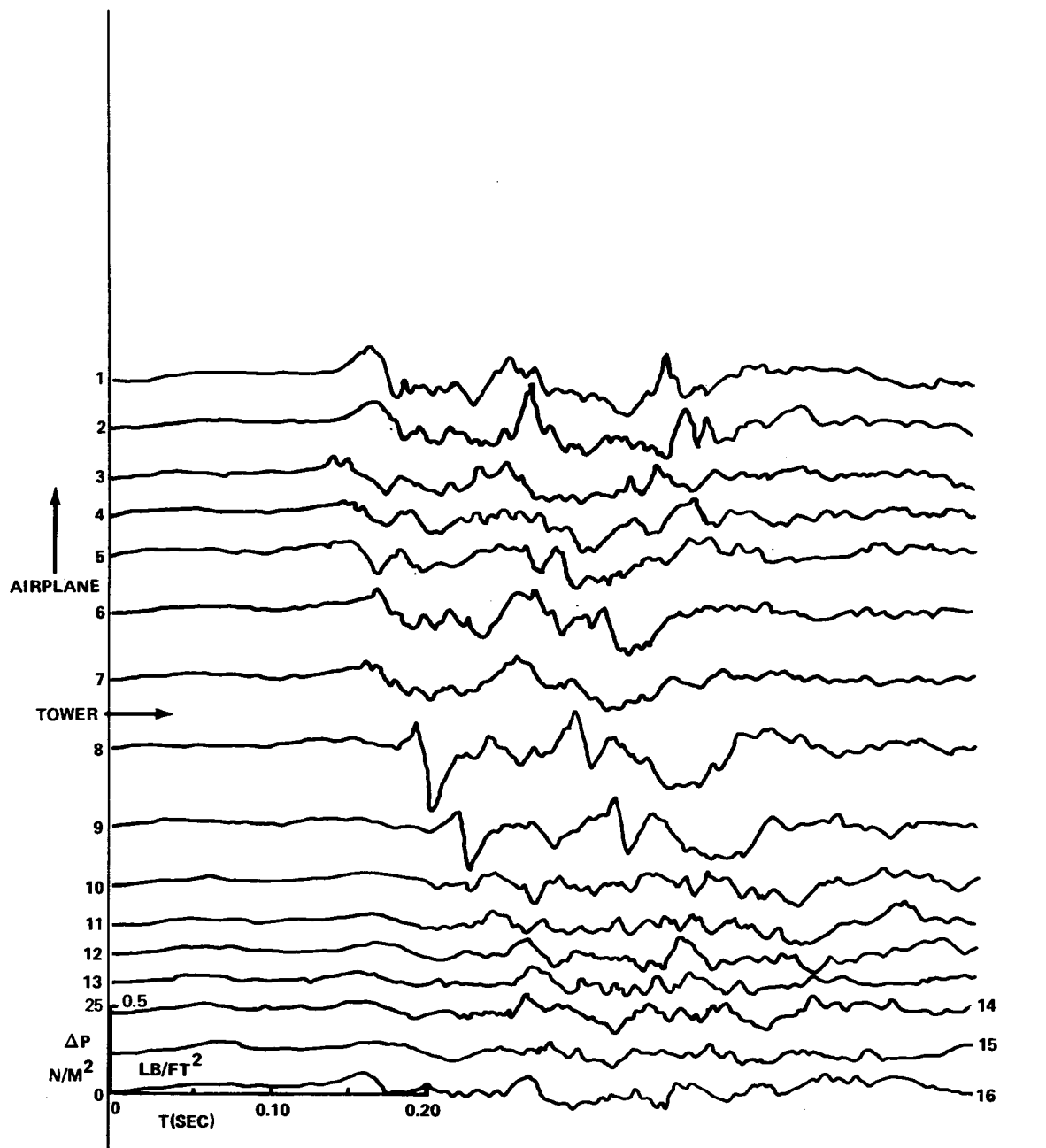


FIGURE 78.— GROUND PRESSURE SIGNATURES NEAR LATERAL CUTOFF
 —PASS 030, AUGUST 27, 1-2

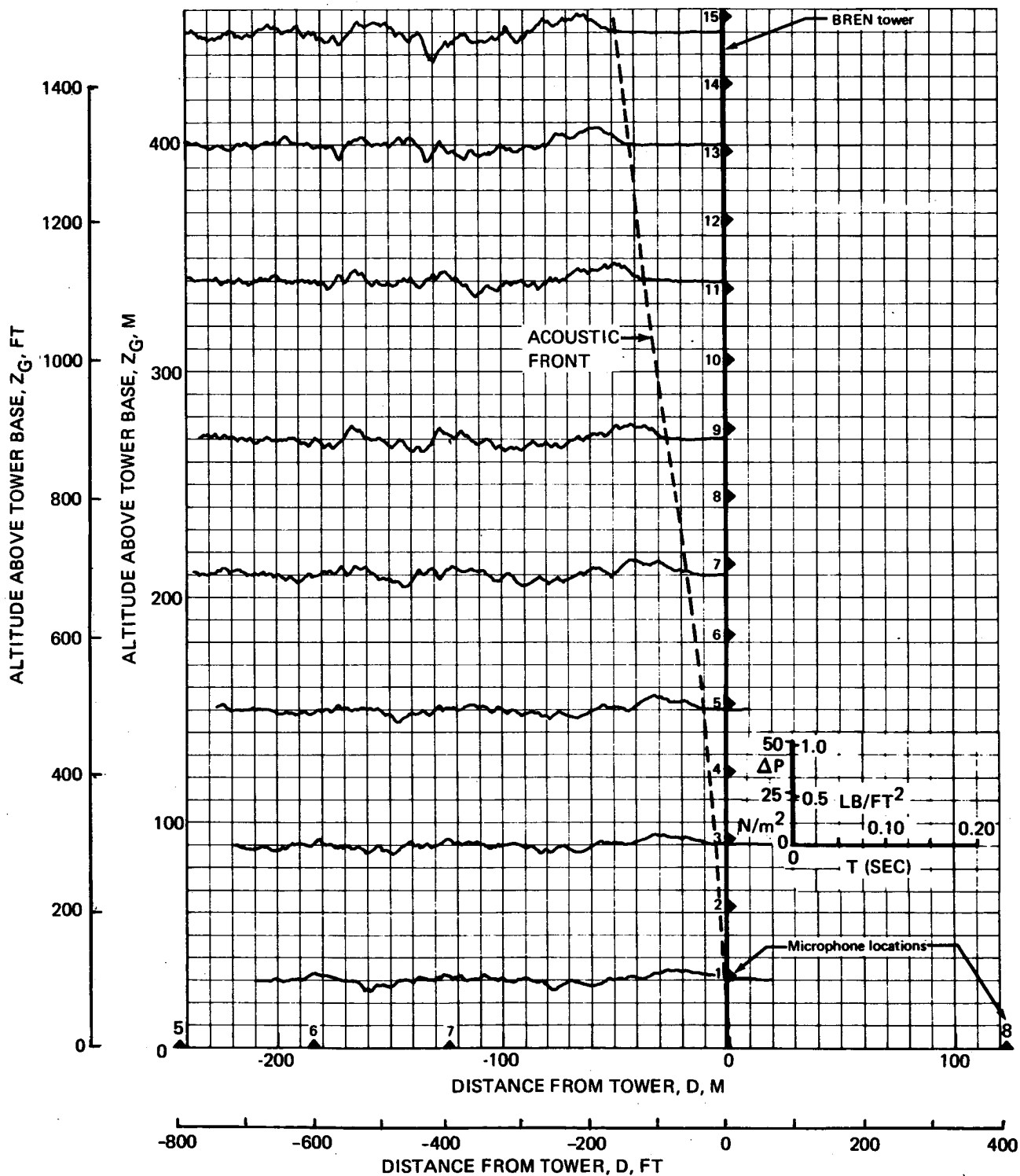


FIGURE 79.—ACOUSTIC WAVE PROFILE AND TOWER PRESSURE SIGNATURES PAST LATERAL CUTOFF—PASS 032, AUGUST 27, 2-1

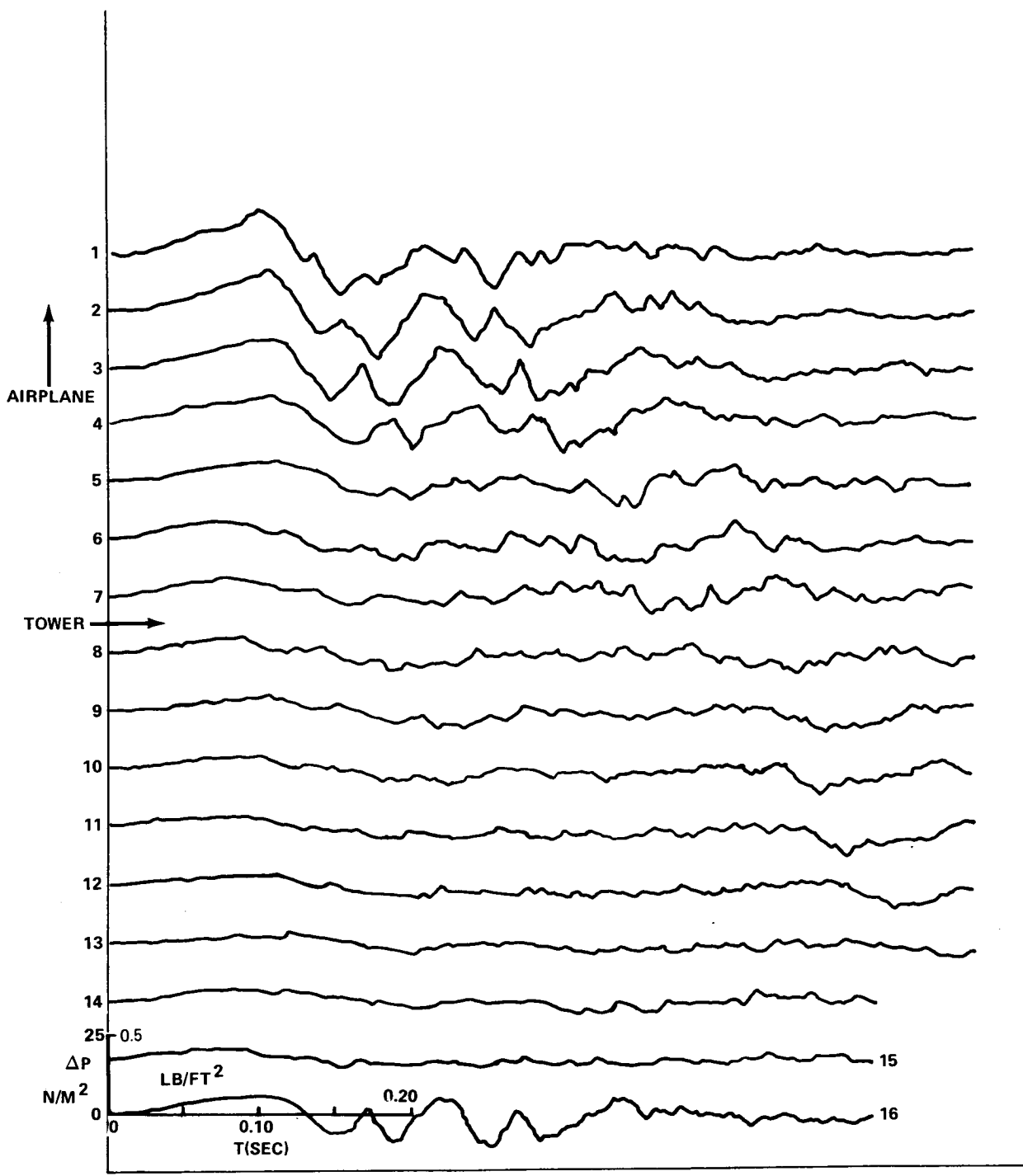


FIGURE 80.— GROUND PRESSURE SIGNATURES PAST LATERAL CUTOFF
 —PASS 032, AUGUST 27, 2-1

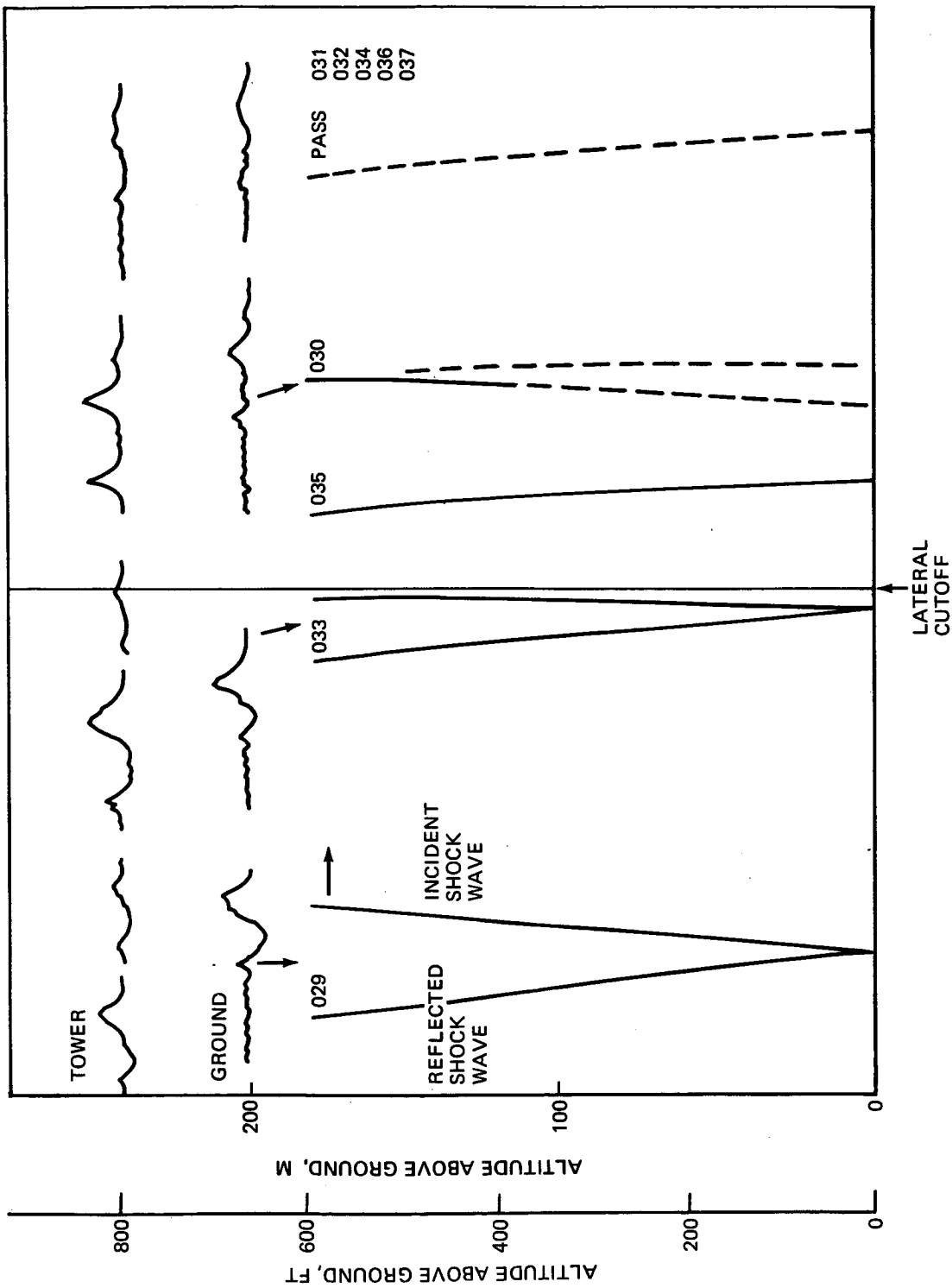


FIGURE 81.—SUMMARY OF SIGNATURES AND SHOCK WAVE PROFILES NEAR LATERAL CUTOFF

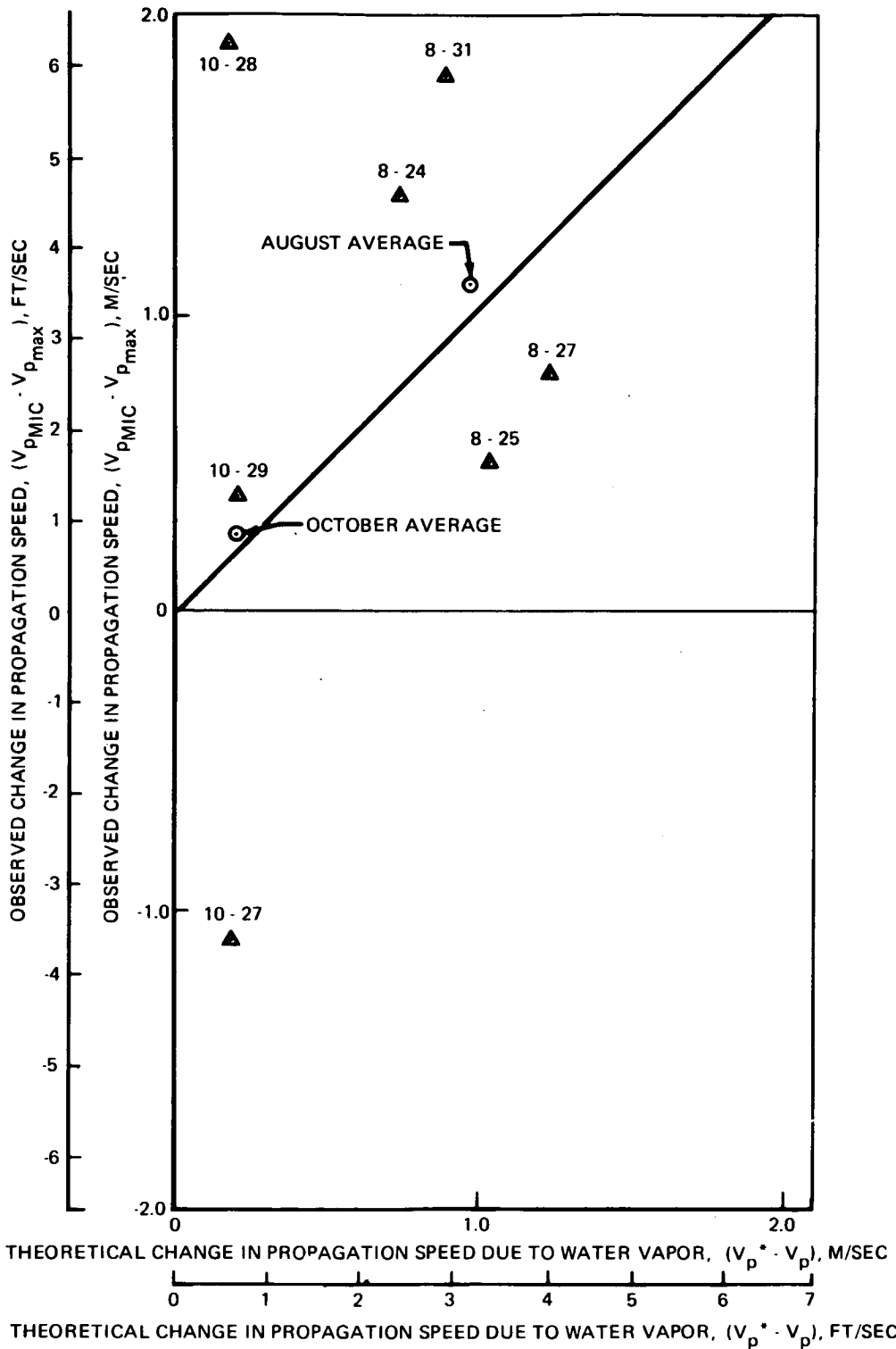


FIGURE 82.—CHANGE IN PROPAGATION SPEED DUE TO WATER VAPOR—THEORY AND EXPERIMENT

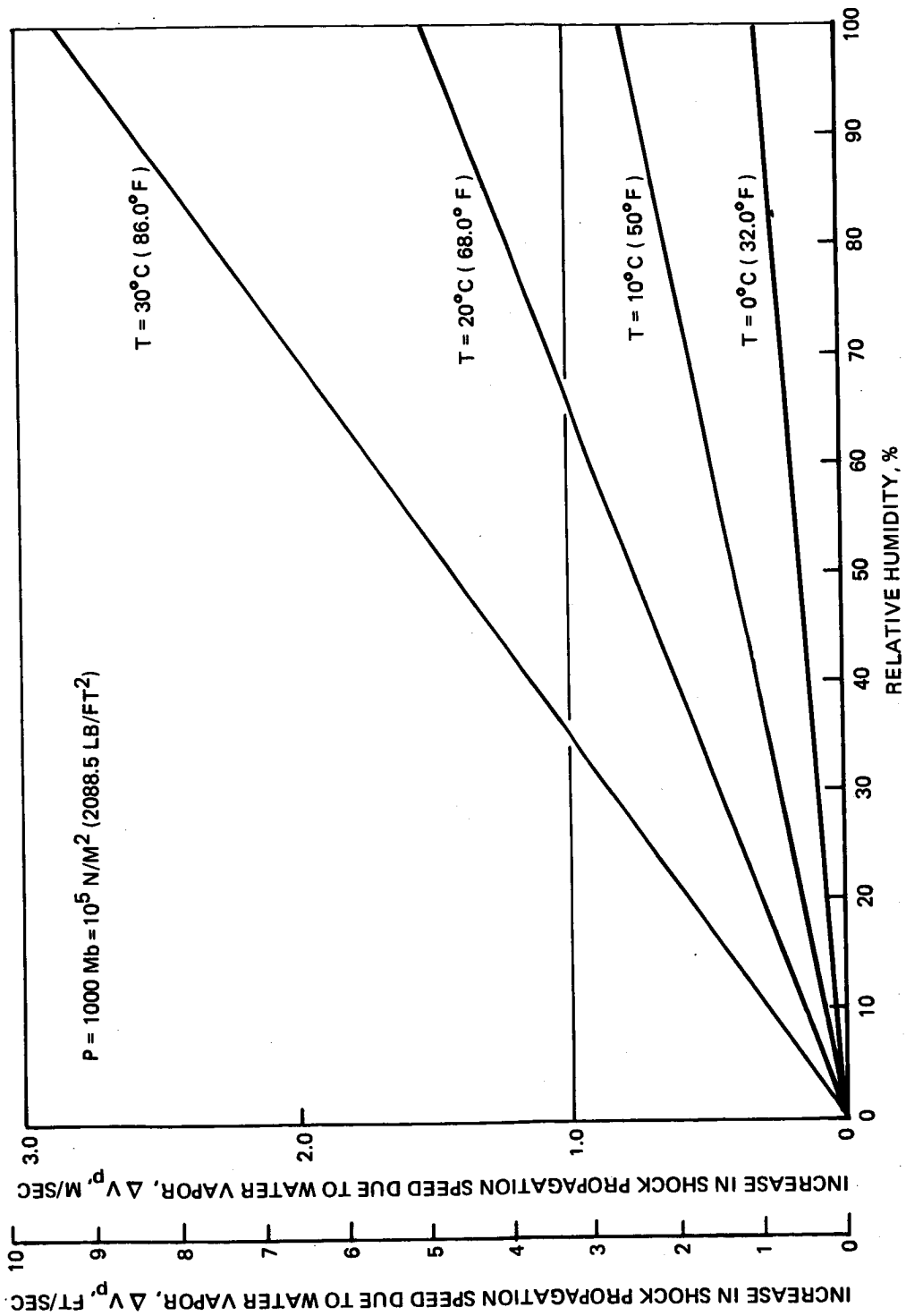


FIGURE 83.—INCREASE IN SHOCK PROPAGATION SPEED DUE TO WATER VAPOR—THEORY

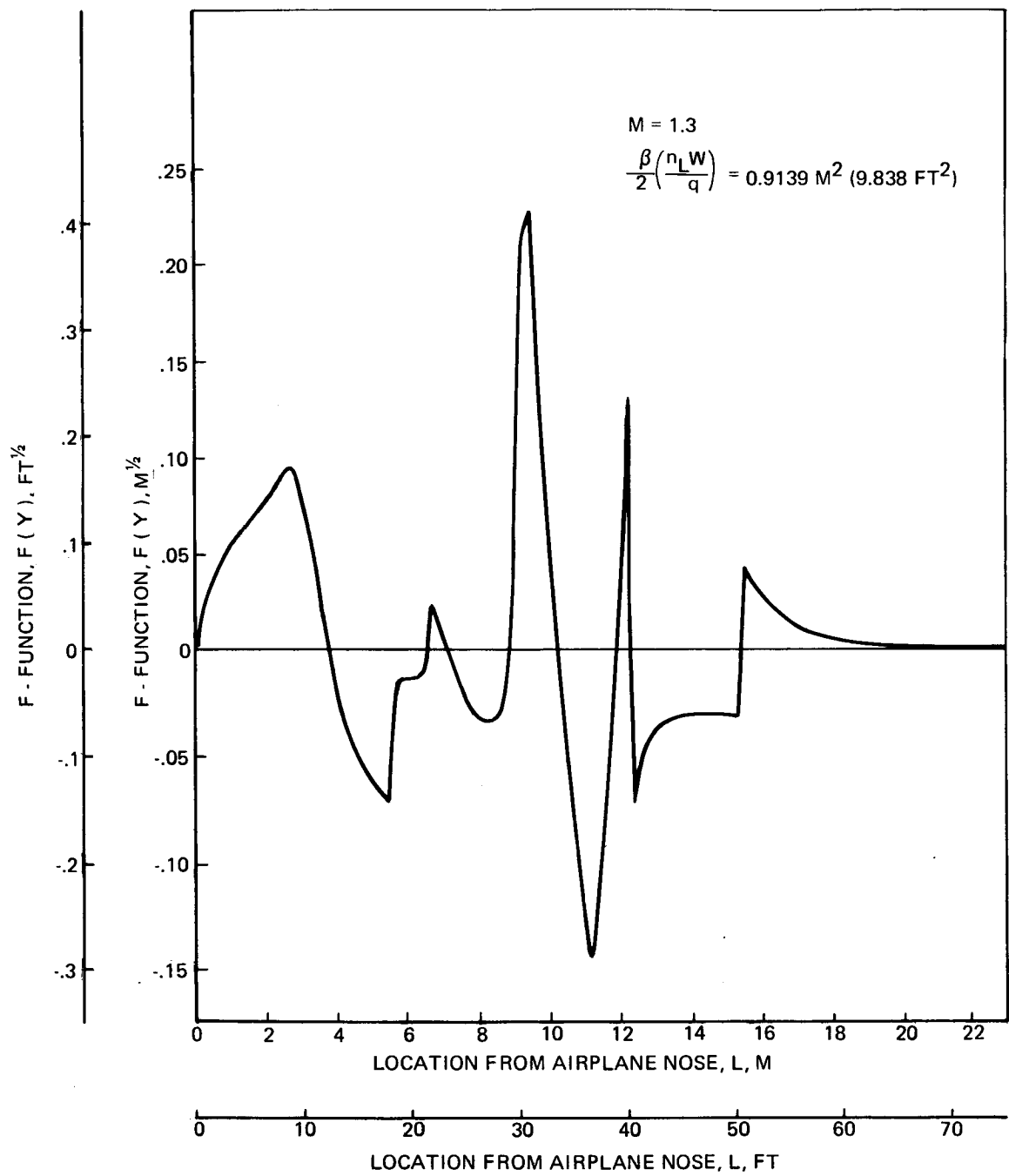


FIGURE 84.—F-FUNCTION FOR F-104 AIRPLANE, M = 1.3

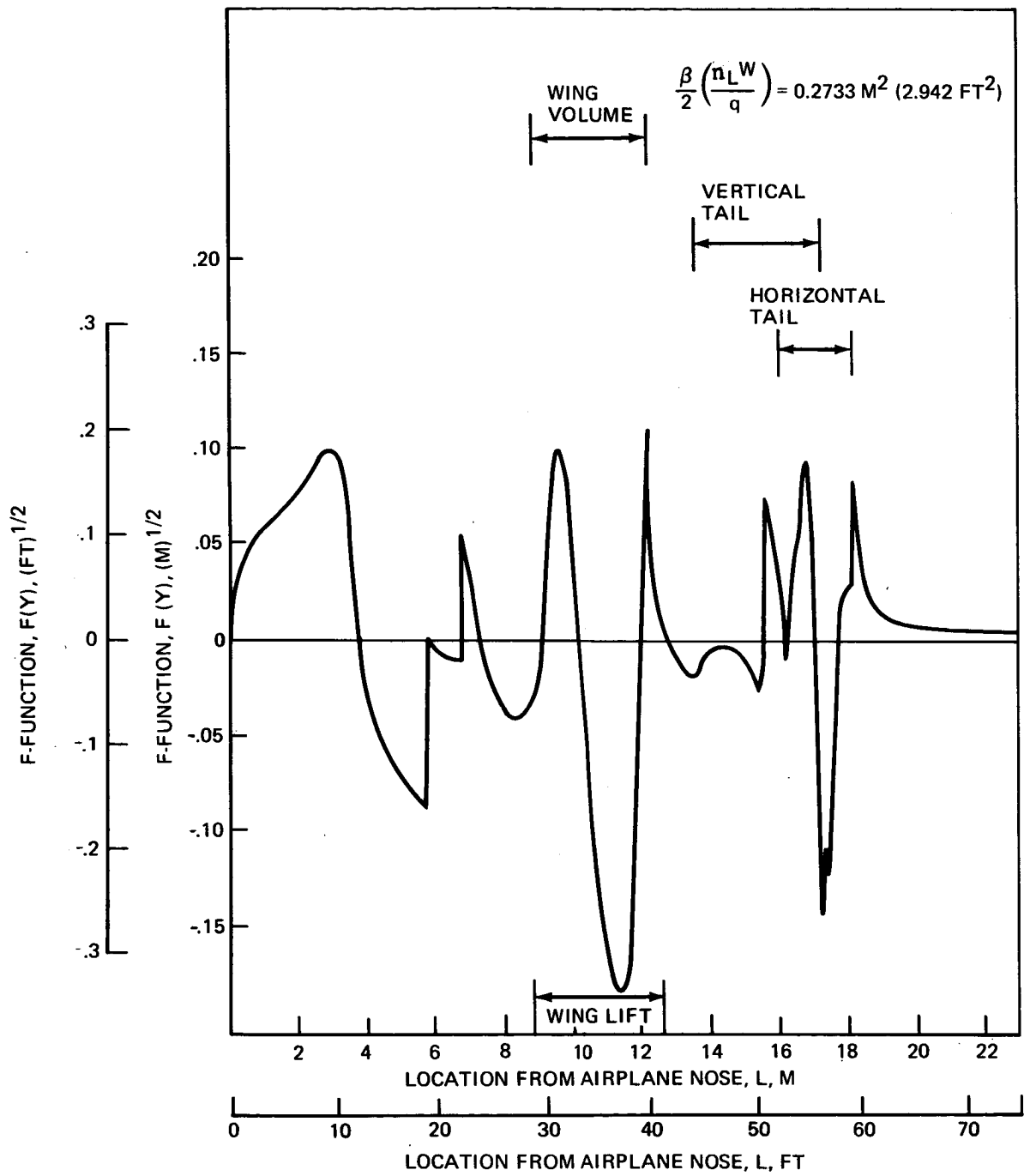


FIGURE 85.—F-FUNCTION FOR F-104 AIRPLANE, M = 1.10